pennsylvania
DEPARTMENT OF TRANSPORTATION

Corrosion Repair Strategies for Steel Girder Ends Using High Performance and Traditional Materials

FINAL REPORT

1 August 2022

By Kent A. Harries, PhD, PEng
University of Pittsburgh

University of Pittsburgh

COMMONWEALTH OF PENNSYLVANIA
DEPARTMENT OF TRANSPORTATION

CONTRACT # 4400018535 / 511801
WORK ORDER # PIT 002

DEPARTMENT OF TRANSPORTATION
UNITED STATES OF AMERICA

FINAL REPORT

Corrosion Repair Strategies for Steel Girder Ends Using High Performance and Traditional Materials

Kent A. Harries, PhD, FASCE, FACI, FIIFC, P.Eng.

Jason A. Mash, P.E. PLS

Chase Rogers

University of Pittsburgh

Civil and Environmental Engineering

1 August 2022

Disclaimer

Acknowledgements

This work was sponsored by the Pennsylvania Department of Transportation and the U.S. Department of Transportation Federal Highway Administration.

The authors wish to acknowledge the in-kind support of Mr. Ronnie Medlock at High Steel Structures and Dr. Brandon Chavel, formerly of AISC.

Technical Report Documentation Page

1. Report No. FHWA-PA-2022-006-PITT WO 002	**2. Government Accession No.**	**3. Recipient's Catalog No.**
4. Title and Subtitle Corrosion Repair Strategies for Steel Girder Ends using High Performance and Traditional Materials		**5. Report Date** 1 August 2022 **6. Performing Organization Code**
7. Author(s) Kent A. Harries, PhD, FASCE, FACI, FIIFC, P.Eng. Jason A. Mash, P.E. Chase Rogers		**8. Performing Organization Report No.**
9. Performing Organization Name and Address University of Pittsburgh, Civil and Environmental Engineering 742 Benedum Hall Pittsburgh PA 15260		**10. Work Unit No. (TRAIS)** **11. Contract or Grant No.** 4400018535
12. Sponsoring Agency Name and Address The Pennsylvania Department of Transportation Bureau of Planning and Research Commonwealth Keystone Building 400 North Street, 6th Floor Harrisburg, PA 17120-0064		**13. Type of Report and Period Covered** Final Report 20 April 2020 – 1 August 2022 **14. Sponsoring Agency Code**

15. Supplementary Notes

none

16. Abstract

This project investigated practical repair methods using high performance and traditional materials which can be applied to corroded and/or damaged steel girder ends in their in-situ state. Observed corrosion damage follows well known patterns: beam end corrosion is associated with leaking expansion joints and is most prevalent at bottom flange-to-web interfaces where debris accumulates, trapping moisture. The current state of practice for structural repair of beam ends is the complete replacement of the affected region. For localized damage, bolted or welded steel patches and/or doubler plates are used. An experimental study involving static tests of corrosion-damaged beam ends to failure is reported. End A tests were conducted without conditioning and End B tests were conducted following one million cycles of fatigue conditioning. Two control (undamaged Girder 1A and corrosion damaged Girder 2A) and four repair techniques (Girders 3-6) were tested: conventional bolted steel repair; ultra-high performance concrete (UHPC) encasement; normal strength reinforced concrete (RC) encasement; and adhesively bonded glass fiber reinforced polymer (GFRP) plates, respectively. All methods but GFRP performed well, restoring the undamaged strength and stiffness of the steel girder regardless of fatigue conditioning. GFRP repairs were unsuccessful. An extensive finite element modeling campaign was conducted and validated based on the experimental program. The modeling of the test specimens proved to be robust and captured observed behavior well. Recommendation for appropriate means of repairing corrosion damaged beam ends are provided.

17. Key Words bolted steel plate repair; conventional concrete repair; experimental evaluation; fatigue; finite element method evaluation; FRP repair; girder end region; repair; steel bridges; UHPC repair;	**18. Distribution Statement** No restrictions. This document is available from the National Technical Information Service, Springfield, VA 22161

19. Security Classif. (of this report)	**20. Security Classif. (of this page)**	**21. No. of Pages**	**22. Price**
Unclassified	Unclassified	168	

Form DOT F 1700.7 **(8-72)** **Reproduction of completed page authorized**

Executive Summary

The objective of this project was to investigate practical repair methods using high performance and traditional materials which can be applied to corroded and/or damaged steel girder ends in their *in-situ* state. Observed corrosion damage follows well known patterns: beam end corrosion is associated with leaking expansion joints and is most prevalent at bottom flange-to-web interfaces where debris accumulates, trapping moisture.

A review of damage studies from the literature and of a non-random sample of Pennsylvania bridges illustrated the proliferation of such beam end damage. In most cases, damage is generally confined to the lower third of the web. Many beam ends were reported to have 100% section loss at some locations and girder section distortion resulting from this was identified in some Pennsylvania structures.

Having established relatively consistent patterns of beam end corrosion damage, the residual capacity of the bearing region must be established. Web shear, web yield due to bearing, and web crippling are the primary limit states of concern. Other limit states identified – in particular flange distortion – result from the loss of web bearing capacity and are therefore not primary limit states.

There is limited experimental and some analytical study of the behavior of corroded beam end regions. Due to the nature of corrosion damage, the utility of studies that assume essentially uniform [machined] damage is limited and difficult to generalize. Nevertheless, the existing studies largely validate the limit states described above. Given the typical damage being more severe at the lower web-flange junction, web yield tends to dominate behavior. Such behavior, if extreme, can result in distortion of the girder and will result in the affected bearing region carrying essentially no load. The key to a good prediction is a good record of section loss.

The current state of practice for structural repair of beam ends is the complete replacement of the affected region. For localized damage, bolted or welded steel patches and/or doubler plates are used. Extended encasement of beam end regions in conventional concrete has also been observed for beams having embedded bearings.

Reported in Section 1.8, an extensive study, demonstrated the efficacy of partially encasing damaged beam ends in ultra-high performance concrete (UHPC) and proposed recommendations for such UHPC encasement. Alternate encasement materials, including normal strength reinforced concrete are also described. Additionally, considerations for transfer of beam forces to the encasing concrete using shear connectors are presented.

The use of fiber reinforced polymer (FRP) materials to address various aspects of steel degradation are also described (Section 1.11). In terms of beam end repair, using adhesively bonded FRP plates or sections is analogous to welded or bolted patch repairs. Such repairs can strengthen and provide stability to a deteriorated steel web. Despite some advantages and one successful laboratory installation, the difficulty in developing and maintaining an adequate bond was demonstrated in the present study and the use of FRP is not advised as a means of repairing beam end damage.

Experimental Program

An experimental study involving static tests of corrosion-damaged beam ends to failure is reported in Chapter 3. End A tests were conducted without conditioning and End B tests were conducted following one million cycles of fatigue conditioning. Two control (undamaged Girder 1A and corrosion damaged Girder 2A) and four repair techniques (Girders 3-6) were tested: 3) conventional bolted steel repair; 4) ultra-high performance concrete (UHPC) encasement; 5) normal strength reinforced concrete (RC) encasement; and 6) adhesively bonded glass fiber reinforced polymer (GFRP) plates, respectively. The following conclusions are drawn:

1. Each of repairs 3A (steel), 4A (UHPC) and 5A (RC) effectively restored the load bearing capacity of corrosion-damaged 2A to that of the undamaged girder 1A.

2. Each of 3A, 4A and 5A also achieved comparable stiffness to 1A.
3. Each of the repairs 3B (steel), 4B (UHPC) and 5B (RC) exhibited little deterioration associated with the one million cycles fatigue conditioning performed. 5B exhibited minor cracking.
4. Following fatigue conditioning, each of 3B, 4B and 5B, exceeded the load bearing capacity of 1A.
5. The stiffness of 3B, 4B and 5B exceeded that of the End A tests and 4B and 5B exceeded that of 1A, confirming the 'shakedown' effect of the fatigue conditioning.
6. GFRP-repaired 6A exhibited a catastrophic debonding failure at 42% of the load bearing capacity of 1A. Up to this debonding, behavior was comparable to 1A. Subsequently, 6B was not tested.

Numerical Program

An extensive finite element modeling campaign was conducted and validated based on the experimental program. The modeling of the test specimens proved to be robust and captured observed behavior well. Once the test specimen modeling was "benchmarked" against the observed behavior, the models were expanded to archetypal plate girders to verify the validity of the repair methods. The following conclusions are drawn from the numerical modeling:

1. The modeling approach was sufficiently robust to capture behaviors of interest. Apart from the need for good geometric modeling of section loss, the models required little special calibration.
2. The models confirmed the validity of adopting AASHTO prescribed equations for estimating residual capacity of damaged girder ends.
3. Development of tension field action was observed in the steel repair and UHPC repair. Such behavior requires stiff end bearings.
4. Stability of the steel web through encasement was achieved in the UHPC and reinforced concrete repairs.

Recommendations of Practical Means of Repairing Corrosion-damaged Girder Ends

A qualitative assessment of the repair techniques tested was undertaken. Based on this and the results of the experimental and analytical programs, recommendations for practical means of repairing corrosion-damaged girder ends are made. These include recommendations for:

Conventional bolted steel repairs including details for bearing stiffener replacement and web patches. Such repairs are preferable to other methods considered.

UHPC Encasement was also found to be a viable means of repairing corrosion-damaged girder ends. However, UHPC is expensive and requires specialized equipment for mixing and monitoring the batch sizes needed for beam end repairs. If UHPC is already being deployed on a project, its use for girder end repair may be found to be appropriate. It is unclear that UHPC provides any improvement in performance or long-term behavior over conventional methods of repair. Recommendations for UHPC encasement are presented.

RC Encasement is also a viable means of repairing corrosion-damaged girder ends especially in cases were large shear stresses are not anticipated. Recommendations for reinforcing details are provided.

For both UHPC and RC encasement, alternative shear connector details – particularly using bolted, rather than welded studs, is described and recommendations presented.

The importance of detailing and inspection to ensuring the durability of repairs is highlighted.

Contents

List of Figures

List of Tables

Notation

a	shear span length
a	empirical parameter defined in Table 2 used for Equation 7
a_{max}	maximum out of plane distortion of web
A_b	area of concrete in bearing
A_g	gross area of bearing
A_{hole}	area of 100% section loss
A_{pn}	the area of the stiffener bearing upon the flange
A_s	area of steel reinforcing
A_{sc}	area of shear stud
b	empirical parameter defined in Table 2 used for Equation 7
b	width of flange
b_f	width of flange
b_{sb}	bearing stiffener width
C	ratio of shear buckling resistance to the shear yield strength
C_c	volume of the corroded web panel
COV	coefficient of variation
C_s	volume of the uncorroded web panel
CTE	coefficient of thermal expansion
d	total depth of the steel section
d'	height of shear reinforcement within the girder depth
d_o	stiffener spacing
D	depth of web plate
e	eccentricity of connection
E	Young's modulus of elasticity
E_L	elastic modulus in longitudinal direction of FRP plate
E_T	elastic modulus in transverse direction of FRP plate
f_c'	compressive strength of concrete
f_{ct}	direct tensile strength of concrete
f_{fu}	tensile strength of FRP
f_r	modulus of rupture of concrete
f_t	tensile cracking strength of concrete
f_u	ultimate tensile strength of reinforcing bar steel
f_y	yield strength of reinforcing bar steel
F_L	strength in longitudinal direction of FRP plate
F_{LT}^{cr}	critical buckling stress of FRP plate
F_T	strength in transverse direction of FRP plate
$(\Delta F)_{TH}$	threshold stress for infinite fatigue life
F_y	yield strength of steel
F_u	ultimate tensile strength of steel
G_{LT}	in plane shear modulus of FRP plate
G_s	shear modulus of steel
h	depth of web for rolled shape
h	empirical parameter defined in Table 2 used for Equation 7

I	moment of inertia
k	initial stiffness of beam in terms of shear stress
k	stiffened web panel factor
k	stiffness of 'softened contact' (ABAQUS)
K	distance from the outer face of the flange to the web toe of the fillet
K	initial stiffness of beam
K_s	surface condition factor for slip critical connections
L_a	anchorage length of FRP
m	empirical parameter defined in Table 2 used for Equation 7
M	applied moment
M_n	nominal moment capacity
M_p	plastic moment capacity
M_y	moment capacity at yield
n	number of anchors
N	in situ capacity of a single anchor
N	length of the bearing
N	number of fatigue cycles
P	applied load
P_{sb}	axial capacity of bearing stiffnener
Q_n	nominal shear capacity of single shear stud
r	radius of gyration
$R_{n,crip}$	web crippling capacity due to bearing
$R_{n,yield}$	web yield capacity due to bearing
R_{sb}	capacity of fitted end of bearing stiffener
s	spacing of anchors
s	spacing of reinforcing steel
S	elastic section modulus
t_f	thickness of flange
t_{FRP}	thickness of FRP plate
t_{sb}	bearing stiffener thickness
t_w	average thickness of the web accounting for loss of section due to corrosion
t_w	thickness of web
t_{wc}	average thickness of the web in the bottom 4 in. of the web height over the length $2.5K + N$
t_{wcc}	average remaining thickness of the web in the bottom 4 in. of the web height over the length $md + N$
t_{web}	uncorroded thickness of web
T_g	glass transition temperature
v	shear stress in web
v_{max}	maximum applied shear stress
V	applied shear
V_c	concrete component of shear capacity
V_{cr}	shear capacity of web
V_{max}	maximum applied shear
V_n	nominal shear capacity

V_s	reinforcing steel component of shear capacity
Z	plastic section modulus
α	proportion of section loss
γ_{36kips}	maximum shear strain measured at 36 kips shear
γ_{max}	maximum shear strain
δ_1, δ_2	measured displacements
ε_0	concrete strain at peak stress
$\varepsilon_a, \varepsilon_a, \varepsilon_a$	measured strains from shear gage
ε_c	concrete strain
ε_{cu}	ultimate concrete strain
ε_{max}	maximum principal strain
ε_{min}	minimum principal strain
θ	angle of maximum principal strain
ρ_c	density of concrete
σ_c	concrete stress
$\sigma_{engineering}$	engineering stress
σ_{true}	true stress
$\sigma_{true}^{plastic}$	plastic component of true stress
σ_u	ultimate stress
τ_a	shear strength of adhesive
φ	material reduction factor

1 Introduction and Literature Review

1.1 Objective and Description of Problem

The purpose of this research project is to investigate practical repair methods using high performance and traditional materials which can be applied to corroded and/or damaged steel girder ends in their *in-situ* state. The focus of the study is on girder end repairs typically associated with leaking joints.

The focus of this study is on the type of corrosion and damage shown schematically in Figure 1. Such corrosion is relatively common and is primarily associated with leaking deck and abutment joints. The problem has been associated with many different joint types. Resulting corrosion damage patterns are similar and may be exacerbated or mitigated by other local details such as the presence of stiffeners or the nature of the bearing provided. Effects and extent of the corrosion are also affected by the bridge environment and (sea or road) salt exposure. Lack of adequate air circulation in the vicinity of girder bearings and the accumulation of debris (trapping moisture) also effect the extent and pattern of damage. In the context of this report, such damage will be collectively referred to as 'beam end corrosion'. Typical examples of beam end corrosion found in the literature, illustrating the spectra of damage possible, are shown Figure 2. A review of beam end corrosion examples in Pennsylvania is provided in Section 1.6 with multiple images provided in Appendix A.

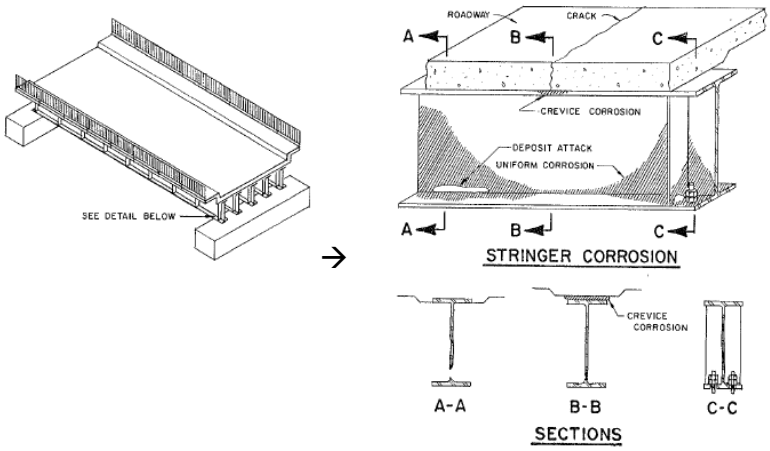

a) description of stringer corrosion in NCHRP Report 333 (1990)

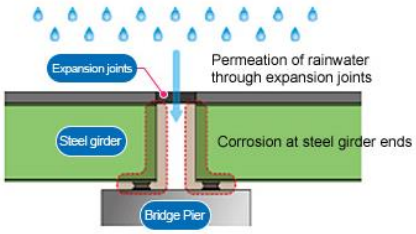

b) description of expansion joint leaking (Hanshin Expressway 2020)

Figure 1 National and international descriptions of beam end corrosion.

PennDOT DM-4 §5.5.2.6b states in part: "Deteriorated steel beam ends shall be cleaned, strengthened if needed, painted and protected from future deterioration by providing continuity or leakproof joints." The scope of this project is *structural strengthening*. Strengthening involves the assessment of extant conditions, particularly the residual capacity that may be relied upon following strengthening – this will be described in Section 1.3. Subsequently, the strengthening scheme is designed and implemented as described throughout this report.

It should be clear that any strengthening should be accompanied by the mitigation of deleterious actions. This will often involve – as DM-4 §5.5.2.6b states – painting and repairs to the deck and/or joints. These are beyond the scope of this project although will be addressed when they are integral to a strengthening scheme.

Connecticut
(Zmeta et al. 2017)

Connecticut
(McMullen and Zaghi 2020)

Nebraska
(Al Badran 2003)

Web failure, Korea
(Ahn et al. 2013)

New York
(Bao et al. 2018)

Japan
(Liu et al. 2011)

Figure 2 Examples of beam end corrosion.

1.2 Characterizing Beam End Corrosion

Gerasimidis and Brena (2019) report a review of 168 bridges in Massachusetts. From this, 808 corroded beam ends were reviewed, and a method of categorizing beam end damage was established. This characterization is shown in Table 1 and will be adopted (with some revision) in the present study to describe beam end corrosion damage. In addition to the beam end corrosion pattern, the degree of section loss must also be reported. Damage may also be characterized as a combination of the patterns shown. For example, the image accompanying M1 shows a through hole (M1) surrounded by a generally triangular corroded area (W5). Multiple holes are also common (e.g., M1+M3).

Patterns W1 and W3 were most commonly observed (84% of observed cases for beams with end diaphragms and 76% for cases without). In most cases (59%), the vertical extent of the corroded region (C_H) was less than 20% of the overall beam depth. Nonetheless, 18% of cases extended the full beam depth (Gerasimidis and Brena 2019). Furthermore, Gerasimidis and Brena reported 15% of beam ends reviewed had through-web holes (M1 – M4).

Flange corrosion was characterized by Gerasimidis and Brena by its length along the flange and section loss (an example is seen in the image accompanying W1). Flange section loss was assumed to extend across the entire flange width.

Gerasimidis and Brena were silent on damage to bearing stiffeners. Considering that the role of a bearing stiffener is the same as that of the web at a bearing, the same damage patterns can be used. For bearing stiffeners, Patterns W1 and M1 are typical and should be reported.

Table 1 Beam end corrosion pattern characterization (adapted from Gerasimidis and Brena 2019).

Pattern	Drawing	Representative image
W1 Rectangular shape corrosion pattern at the beam end above the bearing.	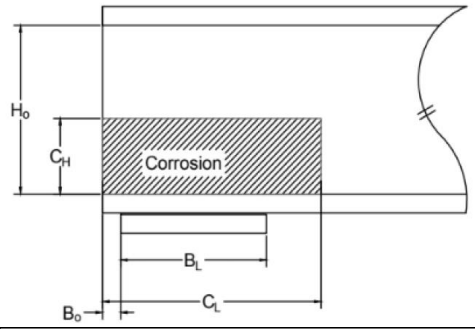	
W2 Similar to W1, with the addition of a triangular-shaped corrosion area at the end of the rectangular shape.	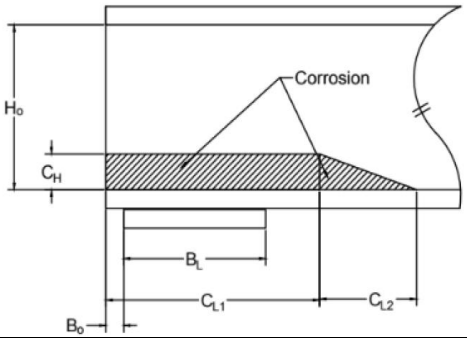	
W3 More complex shape generally described by three areas of corrosion.	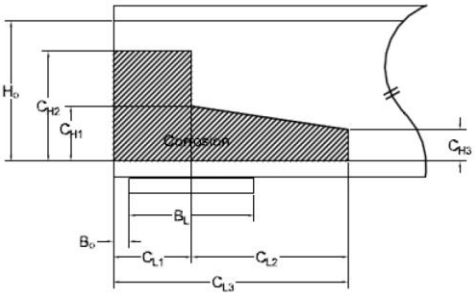	
W4 Modification of W3 to having variation of complex shape.	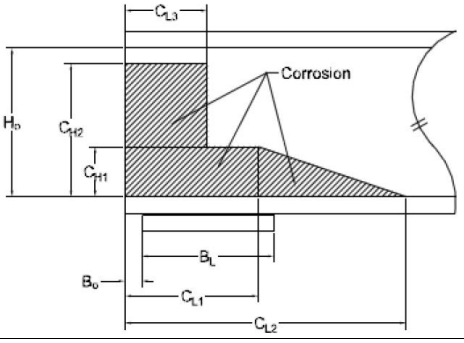	
W5 Triangular shape corroded area.	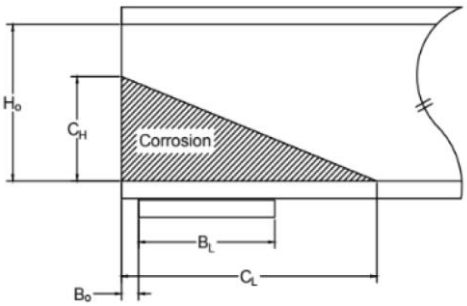	

Pattern	Drawing	Representative image
W6 Corrosion above welded [repair] plate.	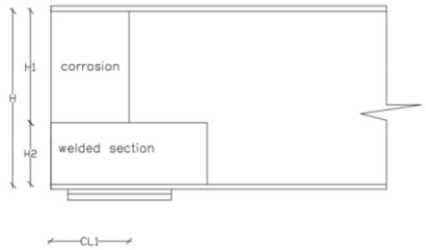	
M1 Hole through lower part of web over bearing.	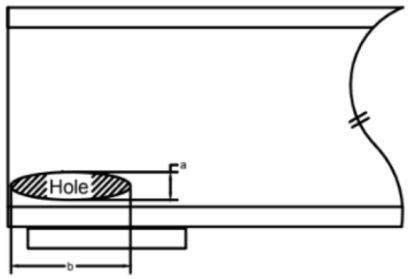	
M2 Hole below diaphragm.	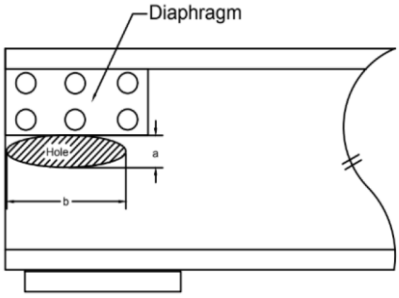	
M3 Hole through top part of beam.	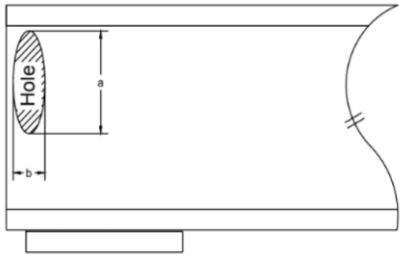	
M4 Hole through lower part of beam away from bearing.	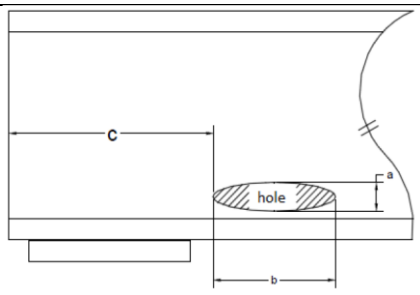	
E-W1 Rectangular shape corrosion pattern at the face of the beam embedment into the diaphragm. Adding **E-** to all other patterns shifts point of reference to face of embedment.	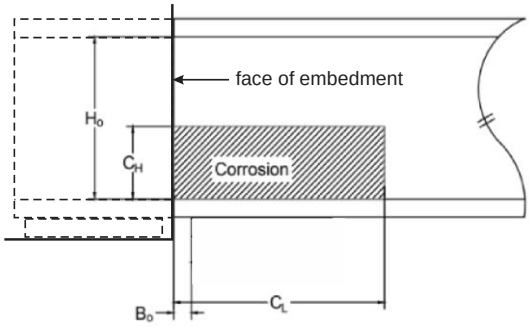	

1.3 Residual Capacity of Bearing Regions Exhibiting Beam End Corrosion

The following three subsections report the capacity calculations for web shear buckling, bearing-induced web yielding and bearing-induced web crippling, respectively. To rate an existing structure having beam end corrosion, these equations are applied using the corroded web geometry as described.

1.3.1 Web Shear

The shear capacity of an end panel of a stiffened web is given by AASHTO LRFD (2020) Eq. 6.10.9.2-1 as:

$$V_{cr} = \varphi C[0.58F_yDt_w] \quad [1]$$

Where F_y = yield strength of web;

D = depth of the web plate of the section;

t_w = average thickness of the web accounting for loss of section due to corrosion; and,

φ = 1.0 for shear.

Collectively, the term in brackets in Equation 1 is the web shear plastic capacity. Web instability is accounted for using the coefficient C, the ratio of shear buckling resistance to the shear yield strength (AASHTO LRFD Eqs 6.10.9.3.2-4 to 6.10.9.3.2-6):

$$C = 1.0 \qquad \text{for } \frac{D}{t_w} \le 1.12\sqrt{\frac{Ek}{F_y}} \quad [2a]$$

$$C = \frac{1.12}{D/t_w}\sqrt{\frac{Ek}{F_y}} \qquad \text{for } 1.12\sqrt{\frac{Ek}{F_y}} < \frac{D}{t_w} \le 1.40\sqrt{\frac{Ek}{F_y}} \quad [2b]$$

$$C = \frac{1.57}{(D/t_w)^2}\frac{Ek}{F_y} \qquad \text{for } \frac{D}{t_w} > 1.40\sqrt{\frac{Ek}{F_y}} \quad [2c]$$

Where E = Young's modulus for steel = 29,000 ksi = 200 GPa; and,

$k = 5 + 5/(d_o/D)^2$ for stiffened web panels having stiffener spacing d_o; or,

$k = 5$ for unstiffened web panels.

AASHTO LRFD does not permit accounting for 'tension field' behavior in an end panel. If a suitably stiff bearing stiffener is provided, tension field behavior can develop in the end panel, as is permitted by ANSI/AISC 360 (2016).

NCHRP *Report 333* states that buckling capacity of corroded webs may be assessed using Equation 1 (with t_w taken as the nominal *uncorroded* web thickness, t_{web}) and applying a factor related to the ratio of corroded web thickness to nominal web thickness:

$$\varphi = (t_w/t_{web})^3 \quad [3]$$

Similarly, Ahn et al. (2013) reported a reduction factor for accounting for web corrosion which is applied to the nominal shear capacity of the section; i.e., Equation 1 with t_w taken as the nominal *uncorroded* web thickness (t_{web}). The strength reduction factor is given as a function of affected web volume:

$$\varphi = 0.7368 + \left[0.2859/\left(1 + e^{-\left(\frac{C_c/C_s - 8.8318}{-3.4666}\right)}\right)\right] \quad [4]$$

Where C_c = volume of the corroded web panel; and,

C_s = volume of the uncorroded web panel.

1.3.2 Web Yield due to Bearing

AASHTO LRFD (2020) Eq. D6.5.2-3 prescribes the yield capacity of webs at beam ends subject to concentrated compressive (or tensile) loads as:

$$R_{n,yield} = \varphi_b(2.5K + N)F_y t_{wc} \quad [5]$$

Where K = distance from the outer face of the flange to the web toe of the fillet;

N = length of the bearing;

t_{wc} = average thickness of the web within the bottom 4 in. of the web height over the length $2.5K + N$ (Gerasimidis and Brena 2019); and,

φ_b = 1.0 for bearing.

In applying Equation 5, through web holes (M1 in Table 1) are accounted for in the calculation of t_{wc} by including regions of zero thickness in the calculation of average thickness. It is noted that in the calculations presented by Gerasimidis and Brena, N is reduced to account for through web holes and t_{wc} is calculated based on remaining steel. While mathematically the same, the presentation adopted here results in a slightly less complex calculation.

1.3.3 Web Crippling due to Bearing

The web crippling (local instability) capacity at a girder bearing is given by AASHTO LRFD (2020) Eqs D6.5.3-3 and D6.5.3-4):

for $N/d > 0.2$: $$R_{n,crip} = \varphi_w 0.4 t_{wc}^2 \left[1 + \left(\frac{4N}{d} - 0.2\right)\left(\frac{t_{wc}}{t_f}\right)^{1.5}\right]\sqrt{\frac{EF_y t_f}{t_{wc}}} \quad [6a]$$

for $N/d \leq 0.2$: $$R_{n,crip} = \varphi_w 0.4 t_{wc}^2 \left[1 + 3\left(\frac{N}{d}\right)\left(\frac{t_{wc}}{t_f}\right)^{1.5}\right]\sqrt{\frac{EF_y t_f}{t_{wc}}} \quad [6b]$$

Where d = total depth of the steel section;

t_f = thickness of the flange subject to bearing; and,

φ_w = 1.0 for web crippling.

For interior pier reactions and beams having an extension beyond the bearing greater than or equal to $d/2$, $R_{n,crip}$ is found as twice that calculated using Equation 6b. Once again, crippling is affected only immediately above the bearing and the calculation of t_{wc} is the same as that given for Equation 5.

Gerasimidis and Brena (2019) recognize that non-uniform web corrosion results in 'amplitude imperfections'; i.e., the load path through the web is no longer planar due to material loss. Real out-of-plane distortions of the web may also exist *in situ*. Such imperfections will further reduce the web crippling capacity. Based on regression analysis of hundreds of corrosion scenarios, Equations 6a and 6b are modified as follows:

for $N/d > 0.2$: $$R_{n,crip} = \varphi_w \left[a\sqrt{EF_{yw}t_f}\,t_{wcc}^{1.5} + b^{\left(\frac{d}{3N}\right)}\left(\frac{4N}{d} - 0.2\right)\sqrt{EF_{yw}t_f}\left(\frac{t_{wcc}^2}{t_f}\right)^{1.5}\right]\left(\frac{CL}{N+md}\right)^h \quad [7a]$$

for $N/d \leq 0.2$: $$R_{n,crip} = \varphi_w \left[a\sqrt{EF_{yw}t_f}\,t_{wc}^{1.2} + b\left(\frac{N}{d}\right)\sqrt{EF_{yw}t_f}\left(\frac{t_{wcc}^2}{t_f}\right)^{1.5}\right]\left(\frac{t_{wcc}}{t_{web}}\right)^h \quad [7b]$$

Where t_{wcc} = average remaining thickness of the web within the bottom 4 in. of the web height over the length $md + N$;

t_{web} = nominal uncorroded web thickness; and

the remaining empirically-derived parameters are given in Table 2:

Table 2 Values of parameters required for Equations 7a and 7b.

	for $N/d > 0.2$			for $N/d \leq 0.2$		
imperfection amplitude →	t_{web}	$0.5t_{web}$	$0.1t_{web}$	t_{web}	$0.5t_{web}$	$0.1t_{web}$
a	0.37	0.32	0.57	0.33	0.32	0.38
b	0.17	0.50	0.23	0	0.17	0
h	0.10	0.40	0.40	0.40	0.20	0.15
m	0.20	0.20	0.10	0.10	0.10	0

1.3.4 Bearing Stiffeners

The presence of adequate bearing stiffeners mitigates the web yield and crippling limit states (see AASHTO LRFD (2020) §6.10.11.2). The capacity of the fitted ends of a bearing stiffener is (AASHTO LRFD Eq. 6.10.11.2.3-2):

$$R_{sb} = \varphi_b 1.4 A_{pn} F_y \quad [8]$$

Where A_{pn} = the area of the stiffener bearing upon the flange; and,

φ_b = 1.0 for bearing.

The axial resistance of a bearing stiffener arrangement is given by AASHTO LRFD (2020) §6.9.4 as:

$$P_{sb} = \varphi_c \pi^2 E A_g / (0.75D/r)^2 \leq A_g F_y \quad [9]$$

Where $\varphi_c = 0.95$ for compression.

For a conventional arrangement having b_{sb} x t_{sb} bearing stiffeners on both sides of the web, A_g and r may be [conservatively] approximated as: $A_g = 2b_{sb}t_{sb}$ and $r = 0.289(2b_{sb})$. Corrosion of bearing stiffeners is captured by reducing the thickness t_{sb} to account for partial section loss and reducing b_{sb} for instances of 100% loss of stiffener section.

As a result of section loss, corroded bearing stiffeners may fall below the AASHTO-prescribed slenderness limit intended to prevent local buckling of the stiffener and therefore become inadequate to serve their intended role. To adequately behave as a bearing stiffener (AASHTO LRFD Eq. 6.10.11.2.2-1):

$$b_{sb} \leq 0.48 t_{sb} (E/F_y)^{0.5} \quad [10]$$

1.4 Experimental Study of Capacity of Bearing Regions Exhibiting Beam End Corrosion

Gerasimidis and Brena (2019) and subsequently Tzortzinis et al. (2019) report tests of six corroded beam end specimens obtained from two decommissioned bridges (Table 3). The unstiffened beam segments were tested over simple spans of 25 feet (Specimens 1-3) or 20 feet (Specimens 4-6) with the load applied 5 feet from the tested end in all cases. This results in different shear span-to depth ratios of 1.8 and 2.9 for Specimens 1-3 and 4-6, respectively. All beams had extensive section loss at the bearings and many had significant holes leading to very low predicted capacities (Table 3).

Table 3 Experimental results reported by Gerasimidis and Brena (2019).

Specimen	1	2	3	4	5	6
shape	33WF125			21WF73		
bearing failure load (kips)	99.1	67.6	84.3	42.8	30.9	40.9
predicted bearing failure load (Eq. 5) (kips)	38.3	102.2	0	91.5	17.6	6.1

Specimens 3 and 6 were both reported to have large holes over the bearing resulting in the very low predicted capacities in Table 3. When tested, these holes ‘collapsed’ and the residual capacity

reported resulted from the edges of the holes coming into contact and subsequently transmitting bearing forces.

In this study, only bearing failures (i.e., web yield and crippling) were considered. However, the authors report that the failures of Specimens 1 and 5 were "characterized by a buckling wave appearing in the web" and Specimen 4 exhibited a "long wave instability" which interacted with web crippling.

The low capacity of Specimen 2 was affected by a significant web imperfection which initiated the authors' development of Equations 7a and 7b to account for this. Subsequent recalculation of the capacity of this specimen reduced the predicted capacity 21% to 81.2 kips.

Although not discussed by the authors, the relatively high degree of variability and unpredictable behaviors of the heavily damaged decommissioned beam ends suggests that residual capacity of the steel section may be unreliable in repair scenarios.

Kim et al. (2013) report five large scale tests of specimens having a depth of 31.5 in. The 15/64 in. webs had artificially induced (machined) uniform section loss of 5/64 in. or 10/64 in. over the lower 4 in. or 8 in. of the web (Table 4). The specimens were tested in a simple span arrangement such that each half of the beam represented a single shear panel. Bearing stiffeners were used to mitigate local failures and thus, in this study, only the web shear (Equation 1) is assessed. Results and predicted capacities are summarized in Table 4.

Table 4 Experimental results reported by Kim et al. (2013).

Specimen	00T6	10T4	20T4	10T2	0'T6
thickness lower portion of web (in.)	15/64	10/64	10/64	5/64	15/64
height of lower portion of web (in.)	0	4	8	4	0
uncorroded volume ratio	1.00	0.96	0.92	0.92	1.00
shear buckling strength (kips)	289.2	286.8	259.1	266.7	228.7
predicted shear buckling strength (Eq. 1) (kips)	151				

The results presented by Kim et al. illustrate the relatively conservative nature of shear buckling provisions in the absence of local effects such as web crippling. The relatively small amount of uniform and controlled 'damage' in these specimens resulted in quite uniform behavior that may not be representative of the kind of variability likely in the field. The results reported by Kim et al. were subsequently used by Ahn et al. (2013) in their development of Equation 4.

1.5 Analytical Study of Capacity of Bearing Regions Exhibiting Beam End Corrosion

A number of studies have reported finite element (FE) simulations of beam end corrosion behavior; these are summarized in Table 5. All studies report quasi-static nonlinear analyses. All but Gerasimidis and Brena (2019) focus on web buckling and generally provide model details that will mitigate local bearing effects. With a focus on web buckling behavior, bilinear (including elastic-plastic) material properties are likely adequate as reported in most studies. To accurately capture buckling effects, the effects of residual stress should also be modeled although this is only done in half of the available studies.

Most studies take a similar approach of using shell elements with reduced thickness to model corrosion damage and removing elements entirely to simulate holes. Khurram et al. (2014) report using a coupled shell-solid element utilizing multi-point constraints to reduce the integration. This is thought to be necessary due to the small mesh size used (0.1 in.) which is only a fraction of the 0.5 in. web thickness. Curiously, only Gerasimidis and Brena (2019) report having conducted a convergence study to determine mesh size.

Table 5 Summary of analytical studies of beam end corrosion.

citation	Liu et al. (2011)	Ahn et al (2013)	Yamaguchi et al. (2014)	Khurram et al. (2014)	Bao et al. (2018)	Gerasimidis and Brena (2019)
behavior considered	web buckling of beam in flexure	web buckling of beam in flexure	web buckling of beam in flexure	web buckling of vertical stub test	web buckling of vertical stub test	web yield and crippling of beam in flexure
instability analysis	Programmed distortion	eigenvalue	eigenvalue	eigenvalue	not reported	Programmed distortion
FE program	DIANA 9.3	MARC 2010	ABAQUS	ABAQUS	ABAQUS	ABAQUS
element type	8-node shell (CQ40S)	4-node shell	4-node shell	coupled shell-solid element	not reported [appear to be 3D brick elements]	4-node shell (SR4)
mesh size in critical area	2.0 in.	0.40 in.	not reported	0.1 in.	3.0 in.	0.50 in.
corrosion simulation	element thickness reduction	element thickness reduction	element thickness reduction	element thickness reduction	element thickness reduction	element thickness reduction
hole simulation	no holes	no holes	no holes	no holes	elements removed	elements removed
material	elastic-plastic	elastic-plastic	bilinear (0.01E)	measured nonlinear	bilinear [assumed]	measured nonlinear
residual stress	yes	no	yes	yes	no	no
validated	single uncited prototype	Kim et al. (2013)	no	Khurram et al. (2014)	1:10 scale vertical stub test	Gerasimidis and Brena (2019)
parameters considered in parametric study	• corrosion pattern and thickness	• corrosion thickness • corrosion volume • bearing support condition	• corrosion pattern and thickness	• corrosion height and thickness • stiffener damage	• hole size • area loss	• corrosion topology • beam geometry • material properties • boundary conditions • web distortion

To date, no analytic study has addressed the complete behavior of a corroded beam end. Most studies have focused on web buckling neglecting local effects. As described below, Gerasimidis and Brena (2019) focused on local effects, neglecting buckling. Khurram et al. (2014) and Bao et al. (2018) base their models and experimental validation on vertical stub tests. These are short sections of beams tested in vertical compression. While such tests may be conducted rapidly and can theoretically capture all behaviors of interest depending on support conditions provided, they do not simulate realistic *in situ* boundary conditions of beam ends.

The results of the studies reported in Table 5 are all quite similar: shear capacity is reduced in the presence of corrosion. In general, the results presented are limited by chosen specimen geometry and extrapolation to other geometries is inappropriate. The results generally confirm well-established shear buckling behavior as described by Equations 1 to 3.

1.5.1 massDOT Report 19-008

In their extensive study, Gerasimidis and Brena (2019) validate a high-fidelity FE model of their test specimens (Table 3), providing an excellent basis for modelling beam end corrosion; some critical aspects of their modeling campaign are summarized here.

Gerasimidis and Brena implemented a quasi-static analysis using ABAQUS, a general-purpose FE program that engages the nonlinear analysis routines necessary for failure and instability analysis of the corroded beam ends. The beam end models were implemented using mid-surface shell elements (S4R) having specifically assigned thickness based on detailed corrosion mapping of the test

specimens (Figures 3a and 3b). In subsequent parametric analyses, reduced element thickness was assigned uniformly in deteriorated regions. Holes were simulating by removing elements.

A mesh convergence study led to using 2 in. elements over the span of the beam and a denser 0.5 in. mesh at the corroded beam end. The denser mesh was extended 5 in. beyond the modeled corrosion. The mesh and transition can be seen in Figure 3d.

Interaction between the bottom flange and bearing (Figure 3c) was modeled using 'softened contact' in the normal direction in which contact interaction is defined using a linear contact pressure-overclosure relationship. This was calibrated to experimental results which were found to have a stiffness of approximately 20 kips/in. In the transverse directions, a frictional interaction was applied. Following calibration with experimental results, a coefficient of friction of 0.74 was selected. The sensitivity of model results to this parameter is reported to be negligible – maximum divergence was 1.2%.

When holes were modeled at the flange-web interface, 'hard contact' interaction in the normal direction was implemented, eliminating the penetration of web slave nodes into flange master nodes (Figure 3d) and permitting the holes to "close" and transmit load. Finally, the use of mid-surface shell elements permits plate distortions to be modelled directly (Figure 3e).

Gerasimidis and Brena (2019) report an extensive parametric study of over 2000 cases which were used to calibrate Equation 7. Parameters considered in the study included: a) beam type; b) material; c) presence or absence of stiffener; d) beam length; e) boundary condition (bearing type); f) corrosion topology (Table 1); g) presence of holes; and, h) initial distortion magnitude.

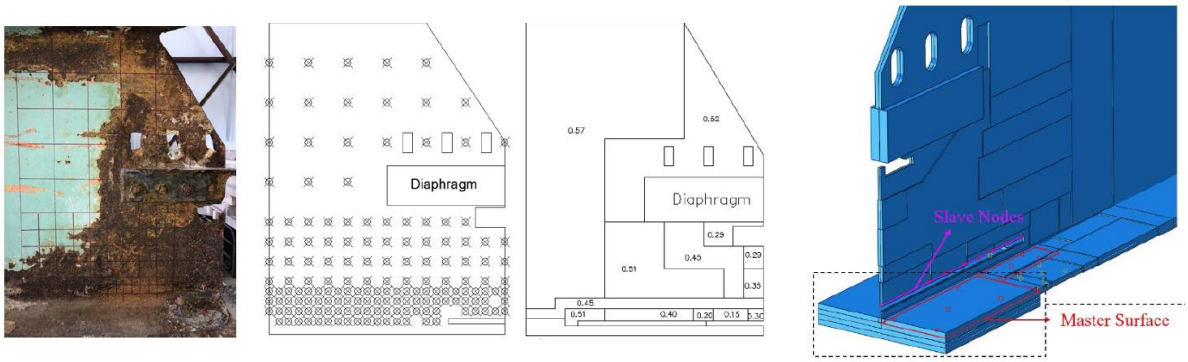

a) corrosion mapping (note horizontal hole at web-flange interface at end of girder)

b) FE model

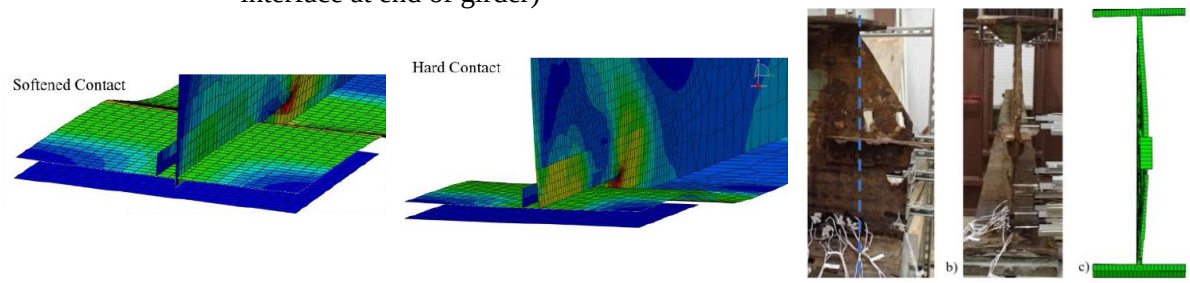

c) softened contact of flange to bearing (note resulting variation of flange stress)

d) hard contact following hole closure

e) initial distortion of web

Figure 3 Details of FE model of Specimen 1 reported by Gerasimidis and Brena (2019).

1.6 Condition Review of Pennsylvania Bridges

In order to establish a snapshot of conditions in Pennsylvania, a review of bridge inspection reports was undertaken. Reports were provided by District Bridge Engineers based on a request for such information. Not all districts responded, and the reports provided were selected by the Engineers. Thus, this review is a snapshot rather than a representative picture of the state of Pennsylvania bridges affected by beam end corrosion. The reviews undertaken by the Research team are detailed in Appendix A and summarized in this section.

Table 6 summarizes fifteen bridges (labeled A through O in no particular order) distributed geographically across the state (Figure 4) that were reviewed. The bridges range in size from short single lane bridges on rural roads (e.g., Bridges C, G and H) to bridges carrying interstate traffic (L, M and N). Eight bridges (B, D, I, J, K, L, M and N) were multiple span structures. The review included 145 beam ends over the 15 bridges. The focus of this study is end bearing regions which includes non-continuous beam supports at intermediate piers. Minor damage of continuous girders over pier supports was noted in Bridge L.

Table 6 Condition Review Summary

Bridge	Girder	Span	Bearing type	NBI condition[a]	Load rating	End region damage[b]
A	9-W18x60 @ 4ft	23 ft	encased in concrete	3	15 ton	E-M3, E-W3, E-W1
B[c]	4-W24 @ 8ft	4 spans, noncomposite	steel plate	3	not posted	M1, W1
C	5-S12x31.8 @ 4.25 ft	12 ft	steel plate	4	not posted	W2, W3, W5
D	5 – 54 in. plate girders @ 8ft	4 spans, composite	sliding plates, rocker bearings	4	not posted	M1, M3, W1, W4
E[c]	5-W30 @ 8ft	1 span, noncomposite	rocker bearings	4	not posted	W1
F[c]	12-W14x38 @ 4ft	1 span, noncomposite	encased in concrete	4	not posted	E-W1, E-W5, M1
G[c]	8-W24 @ 4ft	1 span, noncomposite	encased in concrete	2	closed	E-W1, M1
H[c]	9-W24 @ 4ft	1 span, noncomposite	encased in concrete	5	closed	M1,
I[c]	7-18” I x 47# @ 4ft	2 spans, noncomposite	none (bear on substructure)	5	not posted	E-W1, E-M3
J[c]	5-48 in. plate girders @ 10ft	13 spans, composite	sliding plates	5	not posted	M1, M3, W1, W2
K[c]	5-60 in. plate girders @ 10ft	3 spans, noncomposite	rocker bearings	5	not posted	M1
L[c]	14-W30 @ 8ft	3 spans, composite	rocker bearings	5	not posted	W1, W2, W3
M[c]	14-W24x76 @ 10ft	3 spans, composite	steel plates, rocker bearings	5	not posted	M1, M3
N[c]	12-33 WF 130 @ 10ft	4 spans, composite	sliding plates	5	not posted	M1, M3, W5
O[c]	10-W24 @ 8ft	1 span, noncomposite	encased in concrete	4	not posted	W3

[a] National Bridge Inventory Rating
[b] see Table 1
[c] girder section or spacing estimated from inspection report

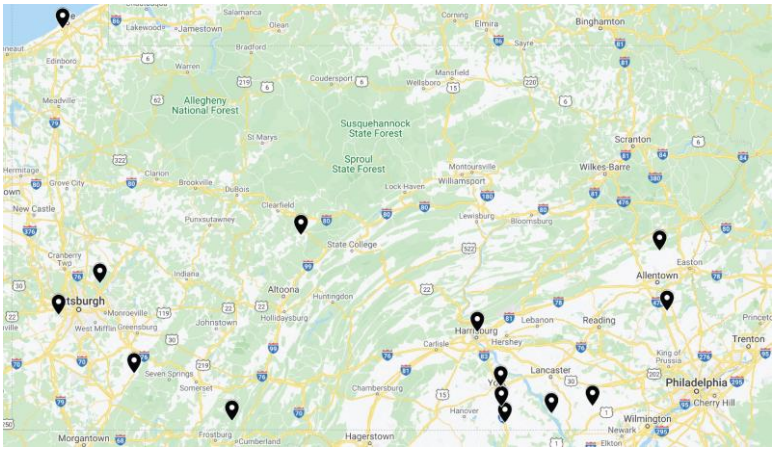

Figure 4 Geographic distribution of 15 bridges reviewed.

As can be seen in Appendix A, the degree of section loss (or remaining plate thickness) reported varies from very minor superficial corrosion to 100% section loss. Indeed, all but three bridges (C, E and L) exhibited some degree of complete web section loss (holes through web). Many of the beams also exhibited notable bottom flange section loss. Where bearing stiffeners are present, these exhibit essentially the same damage as the web to which they are attached.

The observed corrosion damage follows the patterns described previously: beam end corrosion is associated with leaking expansion joints and is most prevalent at bottom flange-to-web interfaces where debris accumulates, trapping moisture. The presence of a bearing stiffener may make this problem worse, although the stiffener also provides greater capacity to the bearing region.

1.6.1 Girder Section Distortion

A few reports identified distortion of the corroded girders at the end bearings. Bridge B exhibits an extreme example of M1 damage – the complete loss of the web section above the bearing extending approximately one bearing length into the span (Figure 5a). This bearing region also has what appears to be a cut through the entire flange just inboard of the bearing (Figure 5b). The combination of the loss of web section, the absence of a bearing stiffener, and the now nonsymmetric section results in a lateral displacement of the web as seen in Figure 5c. It should be clear from Figure 5 that without a bearing stiffener, this girder end is presently carrying no appreciable load. Bridge B has only four girders and therefore a considerable incremental load has been redistributed to the remaining three girders at this pier support. Although not noted and not seen in Figure 5, one expects a distortion of the flange to accompany this damage.

a) Pattern M1 damage (b = 17 in.; a = 1.5 in.) b) apparent cut through bottom flange c) lateral distortion of web

Figure 5 Lateral distortion of web accompanying significant Pattern M1 damage (Bridge B)

The loss of web support at the bearing – particularly associated with Pattern M1 damage – leads to the lower flange being placed in flexure about its own weak axis as long as some bearing resistance remains. Bridge J, shown in Figure 6, has bearing stiffeners. In this case, the loss of web section has resulted in an unsupported flange as shown by the obvious flexural distortion seen in Figure 6.

a) Pattern M1 damage (b = 10 in.; a = 2 in.)

b) flexural distortion of bottom flange

Figure 6 Flexural distortion of flange accompanying significant Pattern M1 damage (Bridge J)

1.6.2 Bearings Embedded in Diaphragm

Six of the reviewed structures were relatively short span structures having their beam ends and bearings fully embedded into concrete end diaphragms (A, F, G, H and O). Although the condition of the bearing itself and the beam immediately above this is unknown, it is likely – provided the diaphragm remains in good shape – that this region will be relatively undamaged. Thus most of the damage is concentrated immediately inboard of the bearing. The damage classification described in Table 1 does not specifically account for this case. In this study, therefore, we have adopted the addition of **E-** to each damage pattern designation to indicate an embedded bearing. In these cases, the damage is identified not relative to the end of the beam (as in Table 1) but from the face of the diaphragm. A representative example of pattern **E-W1** is shown at the end of Table 1. Such embedded beam ends represent a special case of beam end corrosion and will require additional considerations for repair[1].

Each of the bridges having embedded bearings exhibited significant damage at the face of the embedment, up to and including complete loss of the web section. Figure 7 shows the spectra of such damage observed in single structure (Bridge O).

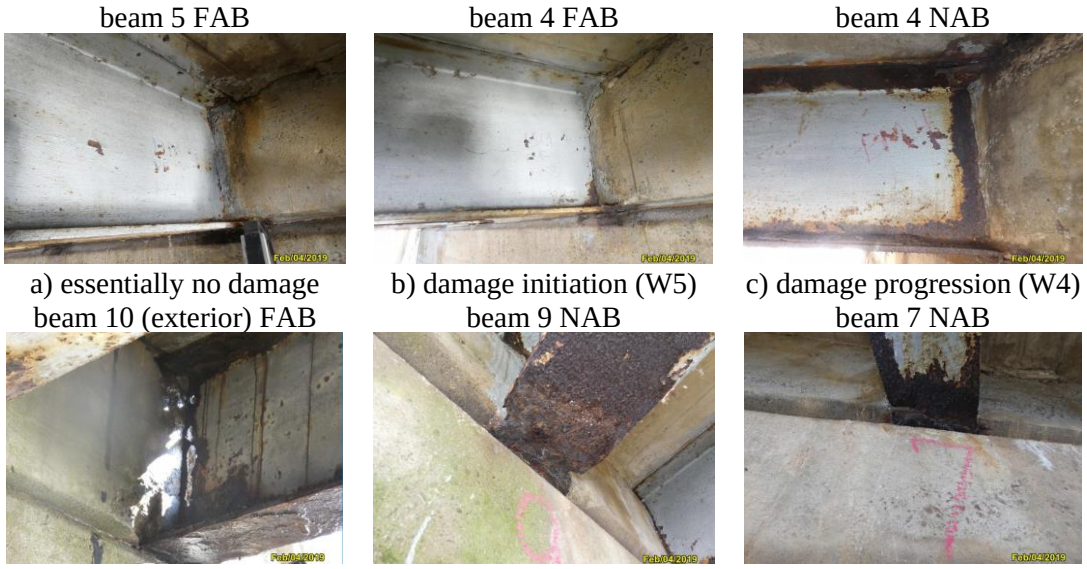

beam 5 FAB — a) essentially no damage

beam 4 FAB — b) damage initiation (W5)

beam 4 NAB — c) damage progression (W4)

beam 10 (exterior) FAB — d) complete loss of web

beam 9 NAB — e) partial loss of flange

beam 7 NAB — f) complete loss of flange

Figure 7 Spectra of damage at embedded beam ends of single bridge (Bridge O)

[1] Embedded beam ends are beyond the scope of this project, however in the interest of completeness, they will be addressed in some of the discussion presented.

1.6.3 Previous Repairs

Three of the bridges investigated show evidence of previous repairs. Bridge A, which exhibited relatively significant web section loss at the face of all embedded connections had been retrofit with 2x4 timber frames (Figure 8a). These frames will maintain the support of the top and bottom flanges lost due to web deterioration but will not improve the shear capacity of the girders in the manner that they are installed. This bridge is posted (15t) and it is likely that the slab is resisting most of the shear in this structure. Bridge D appears to show small regions of welded patches made to the web plates immediately above the bearings at Pier 3 (Figure 8b).

a) timber retrofit to replace continuity provided by web (Bridge A)

b) Welded patch web plates above bearings at spans 3 and 4 over pier 3 (Bridge D)

Figure 8 Previous repairs identified in review of bridge inspection reports.

Finally, Bridge I has a steel-formed concrete encasement at the far abutment (Figure 9). This encasement, built in early 2020, was provided to address significant deterioration of the steel grid deck and top of the far abutment (PennDOT *personal correspondence* 2020); it was not provided to address beam end corrosion. The embedded girder ends at the near abutment show significant deterioration including instances of complete web loss and near total flange plate loss (see Appendix A). However, the 2018 inspection report does not identify a similar level of damage at the far abutment. The encasement is constructed of [stay-in-place] vertical and horizontal steel plate forms spanning between girder webs into which normal strength (Class AA) concrete is placed. The new concrete is made composite with existing abutment with four #5 dowels in each 42 in. bay. Six #5 bars are places transversely along the new diaphragm through holes in the interior girders. To some extent, these will ensure that the beam is engaged in the concrete diaphragm (as shear studs would). It is unclear why steel stay-in-place forms were used as these are not shown in the detail (Figure 9b).

a) condition of far abutment prior to encasement (pre 2020)
note relatively little beam end corrosion compared to near abutment shown in Appendix A.

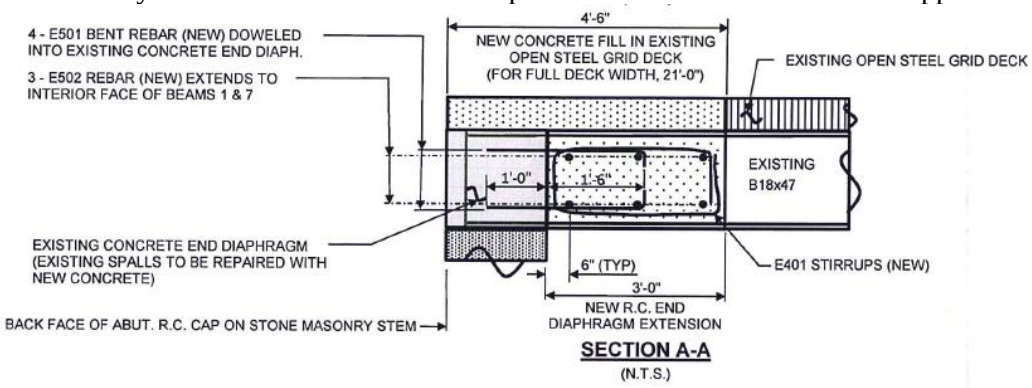

b) detail of steel-formed encasement

c) steel-formed concrete encasement at far abutment (post 2020)

Figure 9 Steel-formed concrete encasement of bridge having embedded beams (Bridge I).

During the review of Bridge I repairs, an additional apparent repair of girder end corrosion at the near end abutment was identified; this is shown in Figure 10. The repair appears to be a bolted steel web plate anchored to the abutment with a bolted and anchored clip angle. It is unclear whether this repair is one or two sided; no details of this repair are available to the research team.

a) beams 4 to 7 reported April 2018 b) beams 3 to 6 reported June 2019

Figure 10 Steel-formed concrete encasement of bridge having embedded beams (Bridge I).

1.7 'Conventional' Structural Repair of Beam End Corrosion Damage

For the purposes of this discussion, 'structural repair' is load bearing and is provided to stabilize, restore or improve the capacity of the beam end region. The repair measures may resist some of the load, relying on residual capacity of the existing beam end, or the repair measures may entirely

replace the load carrying capacity of the beam end. Repairs can also be envisioned that do not augment the strength of the beam end, but enhance its stability, permitting greater loads to be carried.

The current state of practice for structural repair of beam ends is the complete replacement of the affected region as shown schematically in Figure 11a. This approach requires the girder to be temporarily supported ('jacked') away (inboard) from the beam end. This will often require modification of the beam (addition of bearing stiffener(s), for instance) to accept the jacking loads in addition to erection of temporary supports. The damaged beam end region is cut out and a new section (often a WT to replace the bottom flange without the need for additional fabrication) is installed with full penetration groove welds all around (Figure 11a). Figure 11b shows an example of a bolted installation in which the web and flange splices can be seen. A variation of this approach may see only the web replaced with a new plate. The new section is finally sand-blasted and painted. Clearly this operation requires the bridge to be closed to traffic and will impact carriageways under the bridge.

It is reported (Stratton et al. 2021) that the AASHTO/NSBA Steel Bridge Collaboration has proposed that this repair will be included in a proposed guide document. The proposed Guide G14.2 will provide guidance for making this type of repair including issues arising when existing structures are fabricated of historic shapes or materials.

In some cases of relatively minor or localized damage to the web, other viable steel-based repairs may include the addition of web doubler plates (patches seen in Figure 8b), web-flange stiffening, or replacing or providing new/additional bearing stiffeners (Figure 12b). These methods still require field welding or bolting (Figure 12) but can often be accomplished with only lane closures on the bridge.

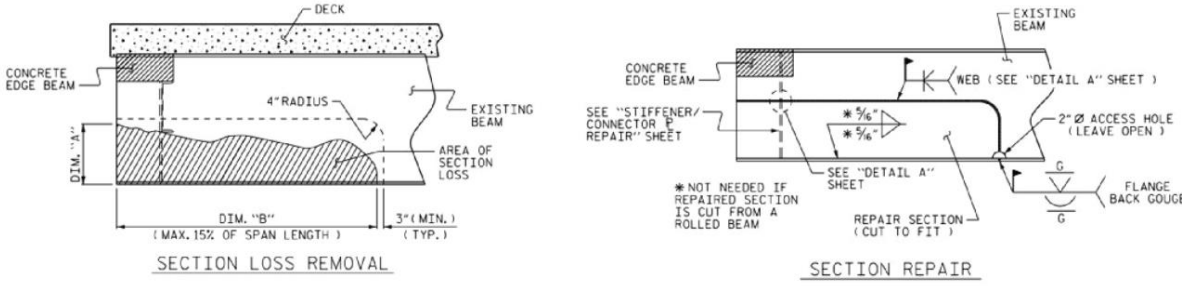

a) schematic representation (Stratton et al. 2021)

b) bolted beam end replacement (Wakabayashi et al. 2013)

Figure 11 Steel beam end repair – replacing deteriorated region.

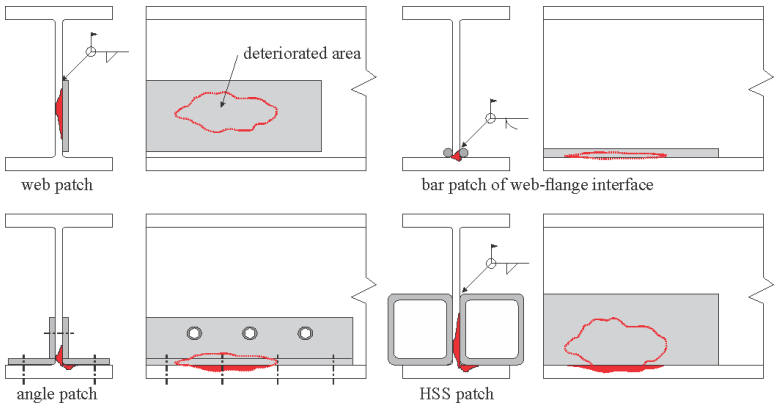

a) schematic examples of patch repairs

b) bolted repair of web-flange region and bearing stiffener (Wakabayashi et al. 2013)

Figure 12 Steel patch repairs of deteriorated beam end regions.

Addition of corbels (or shelves) and new bearings 'inboard' of existing deteriorated beam ends may also be feasible in some cases – most typically at interior pier locations where 'balanced corbels' can be post-tensioned to cap beams. This method is similar to that used to enhance the length of bearing regions to accommodate [seismic] movement. Such an approach may also be feasible for simple span bridges having their bearings embedded in concrete diaphragms.

The focus of this study, however, is the investigation of alternate methods of beam end strengthening. These methods may leverage high-performance materials and the intent is that they may be implemented without the need to provide temporary support for the bridge and preferably that they may be installed without closing the bridge to traffic.

1.7.1 Temporary Support During Repair

The objective of not requiring temporary support has an inherent implication that the existing structure is adequate to resist whatever loads are present during the repair (and subsequent curing, if applicable) procedure. Without pre-loading, prestressing or post-tensioning of some kind, any repair scheme is only able to partially resist loads applied after its installation. Repairs that are called upon to resist any portion of the bridge self-weight, for instance, must have this load relieved during installation.

Preloading during repair installation may be effectively used on continuous structures but is not an option available for simple spans. The research team is unaware of any post-tensioning technology suitable for beam end repairs. While some potentially applicable prestressed technology has been proposed, none has been demonstrated at full scale and none – to the authors' knowledge – in any application similar to the repair of deteriorated beam ends.

1.8 Partial Encasement of Damaged Beam End in High Performance Concrete

Considerable interest has recently developed in the use of ultra-high performance concrete (UHPC) as a means of steel beam end repair. Reported in McMullen and Zaghi (2020), and Zmerta et al. (2017), this work was conducted primarily at the University of Connecticut (UConn) and is represented by the doctoral theses of Zmerta (2015), Kruszewski (2018) and McMullen (2019). The UConn work is summarized in Section 1.8.3.

1.8.1 Ultra High Performance Concrete

Ultra high performance concrete (UHPC) is a "cementitious composite material composed of an optimized gradation of granular constituents, a water-to-cementitious materials ratio less than 0.25, and a high percentage of discontinuous internal fiber reinforcement". Today, a variety of UHPC

products are available on the market, most provided as premixed 'powders' to which fibers, water and liquid admixtures are added. The preblended mixes typically contain a proprietary blend of cement (≈30-40% by weight), silica sand (≈35-40%), silica fume (≈10-15%) and ground quartz (≈10%) having a relative uniform grading between 0.1 and 1000 μm. To obtain such grading, components are often ground finer than for other applications resulting in components being referred to as silica 'flour' or nanosilica. UHPC contains no coarse aggregate and will not intentionally include particle sizes exceeding 2000 μm.

UHPC exhibits compressive strength greater than 21.7 ksi (150 MPa) and sustained postcracking tensile strength greater than 0.72 ksi (5 MPa). UHPC has a discontinuous pore structure that reduces liquid ingress, enhancing durability compared to conventional and high-performance concretes (Graybeal 2014). Table 7 contrasts typical material properties of UHPC with those of high strength concrete (HSC) and conventional normal strength concrete (NSC). In terms of mechanical behavior, although considerably stronger, UHPC does not differ considerably from conventional concrete. Due to the lack of large aggregate, UHPC has a proportionally lower modulus when estimated using compression strength. Although initial tensile strength is also similar, UHPC – due to the inclusion of a high volume of fibers – exhibits significant post cracking tensile strength.

Table 7 Typical properties of UHPC, HPC and NSC (equations express f_c' in ksi units)

	UHPC	**HSC**	**conventional concrete (NSC)**
primary citation	Russell and Graybeal (2013)	ACI 363R-10 & Burg and Ost (1994)	AASHTO LRFD
density, ρ_c	150 to 156 pcf	150 to 156 pcf	≈ 145 pcf
compressive strength, f_c'	20 to 30 ksi	10 to 17 ksi	4 to 8 ksi
tensile cracking strength, f_t	0.9 to 1.5 ksi	0.7 to 1.0 ksi	0.4 to 0.7 ksi
direct tensile strength, f_{ct}	$f_{ct} \approx 0.25(f_c')^{0.5}$	$f_{ct} \approx 0.24(f_c')^{0.5}$	$f_{ct} \approx 0.23(f_c')^{0.5}$
modulus of rupture, f_r	$f_r \approx 0.25(f_c')^{0.5}$ [no fibers] $f_r \approx 0.44(f_c')^{0.5}$ [with fibers]	$f_r \approx 0.24$ to $0.37(f_c')^{0.5}$	$f_r \approx 0.23(f_c')^{0.5}$
elastic modulus, E_c	6000 to 10,000 ksi	7200 to 8200 ksi	3600 to 5200 ksi
elastic modulus estimate	$E_c = 1460(f_c')^{0.5}$	$E_c = 1260(f_c')^{0.5} + 1000$ ≈ 1500 to $1570(f_c')^{0.5}$	$E_c = 1820(f_c')^{0.5}$
Poisson's ratio	0.20	0.20	0.20
CTE	5.5 to 8.5 x 10^{-6}/ºF	5 to 7 x 10^{-6}/ºF	≈ 6 x 10^{-6}/ºF
specific creep	0.04 to 0.3 x 10^{-6}/psi	0.2 to 0.4 x 10^{-6}/psi	0.1 to 1.0 x 10^{-6}/psi
total shrinkage	up to 900 x 10^{-6}	up to 750 x 10^{-6}	up to 800 x 10^{-6}

Durability of UHPC is typically quantified as being very good to excellent. Haber et al. (2018) reports tests of six UHPC mixes. All exhibit "very low" (<1000 Coulombs passing) chloride permeability and "very low" (>37 kΩcm) surface resistivity. Both results indicating impermeable mixes that will be resistant to corrosion of internal reinforcement. Haber also reports negligible mass loss and change in relative dynamic modulus following 600 freeze-thaw cycles, once again indicative of very durable mixes.

Russell and Graybeal (2013) summarize the four primary characteristics that distinguish UHPC from conventional concrete as: a) higher compressive strength; b) higher tensile strength with ductility; c) increased durability; and d) higher initial unit cost. Early studies of UHPC focused on utilizing its high compression strength and improved tensile behavior to optimize material use for superstructure elements. More recently, UHPC is recognized as a material suited to durability-driven applications including repair. In particular, UHPC is increasingly specified for field-cast closure pours or as grout material in prefabricated superstructure elements (often those used in accelerated bridge construction (ABC) projects) (Graybeal 2014). UHPC is also being investigated for a variety of other applications including: precast concrete piles, seismic retrofit of substandard bridge substructures, thin-bonded overlays on deteriorated bridge decks, and security and blast mitigation applications (FHWA 2019)

1.8.2 Implementation of UHPC

Bridge owners perceive one of the primary advantages of UHPC to be its long-term durability – presumably resulting in structures with a longer service life and reduced life-cycle costs compared with structures built with conventional concrete (Russell and Graybeal 2013). However, Russell and Graybeal point out that "no studies were identified [for their 2013 report] to show that this is the case." They go on to suggest that UHPC may not prove to be cost-effective for large superstructure elements due to its high differential cost.

Russell and Graybeal, identify scenarios in which UHPC can be used to address performance issues without a major cost impact. They cite the use of UHPC as cast-in-place connections between prefabricated elements (likely the most common use of UHPC today). In this application, the incremental cost of using UHPC is small while the improved performance (eliminating cracking and leaking that occurs when conventional concretes or grouts are used) is significant. UHPC is also potentially beneficial for producing simplified connection details having shorter reinforcement splice lengths and fewer conflict points (Russell and Graybeal 2013).

Today, few producers or contractors have experience with UHPC. In general, UHPC requires specialized mixing equipment or longer mixing times in conventional concrete mixers, longer set times, and more rigorous curing regimes. Quality control methods and tolerances are significantly different. For example, the use of small-size cylinders for measurement of compressive strength is required in order that tests may be conducted using available machines.

As of the 6.21.20 version, there are no UHPC products included in PennDOT Bulletin 15. Furthermore, the only products listed under "Steel Fibers for Fiber-Reinforced Concrete (ASTM A820)" specifically state: "Not for use with Ultra High Performance Concrete."

1.8.3 University of Connecticut study

As part of a multi-phase project, the University of Connecticut (UConn) investigated the use of UHPC as a repair method to recover beam end bearing capacity, which was reduced due to beam end corrosion. The repair takes the form of a UHPC panel formed against the girder web and connected using headed shear studs welded to the undamaged portions of the girder web.

1.8.3.1 Zmerta (2015)

Zmerta (2015; summarized in Zmerta et al. 2017), as a proof-of-concept, reports tests of three W21x55 girders. The girders were tested over a span of 12 feet with the load placed 32 in. from the test end (resulting $a/d = 1.5$) to simulate the shear critical condition for the girder (Figure 13a). Although additional stiffeners were provided for the test, the "studied end", shown in Figure 13a, remained unstiffened. The compression flange was braced laterally along the longer shear span to prevent lateral buckling. The nominal bearing capacity of a W21x55 loaded in the manner tested is 123 kips, governed by web crippling (Eq. 6; the length of the bearing was reported to be N = 5.625 in.) as indicated in Table 8. Despite the short span, flexural capacity (525 kip-ft = 197 kip bearing capacity for geometry tested) of the section controls the response and crippling can be mitigated (using a bearing stiffener, for instance).

An undamaged control specimen and two specimens having artificial corrosion damage (Figures 13b and c) – produced by thinning the web using a milling machine – were tested. The rectangular damaged region extended 19 in. along the girder and extended 3.75 in. up the web (i.e., Pattern W1 with C_L = 19 in. and C_H = 3.75 in.). A portion of the flange was also removed as seen in Figures 13b and c. The resulting plate thickness of each damaged girder is given in Table 8. The nominal residual capacity of this damaged girder based on web crippling capacity (Eq. 6) is only 18.4 kips (the other capacities will not fall as dramatically). A quirk of this study is that in order to produce the damage, a tee-section was cut from the original girder, the damaged simulated on this, and then the tee was replaced into the girder using full-penetration groove welds. The cut-line is shown in Figure 13b and only the tee is shown in the left image in Figure 13b. A second concern that must be noted is that the

measured flange and web dimensions of the undamaged W21x55 girders are well out of expected rolling tolerance.

The undamaged girder behaved largely as expected, exhibiting a web crippling failure (Figure 13d) at an applied bearing load of 180 kips, demonstrating considerable reserve capacity. The damaged girder exhibited a web crippling failure at an applied bearing load of 43.4 kips. This failure is characterized by a 'kink in the web at the top of the damaged region (i.e, at the change in section) as seen in Figure 13e. The damaged girder exhibited considerably greater residual capacity than predicted although it only achieved about 35% of its nominal capacity exhibiting about 66% web material loss.

Table 8 Girder geometry and test results reported by Zmerta (2015)
[nominal capacities calculated by present authors]

girder	plate thickness (in.) (% remaining)				bearing capacity (kips)	limit state
	undamaged flange	damaged flange	undamaged web	damaged web		
W21x55 nominal capacity	0.522	n.a.	0.375	n.a.	226 **123** 154 197	web shear (Eq. 1) **web crippling** (Eq. 6) web bearing (Eq. 5) flexure: $M_n = ZF_y$
undamaged	0.558	n.a.	0.339	n.a.	180	web buckling
damaged	0.558	0.325 (58%)	0.335	0.113 (34%)	43.4	web crippling
repaired	0.504	0.271 (54%)	0.383	0.102 (27%)	35 69 176	first crack of UHPC shear crack in UHPC flange flexure

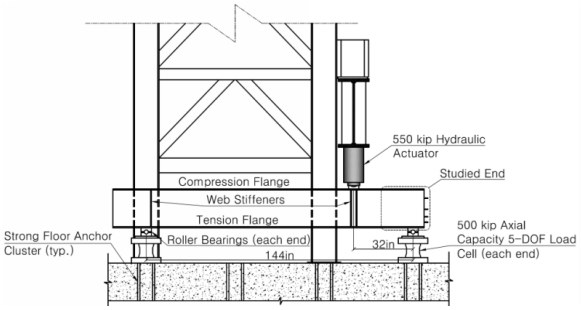

a) test set up

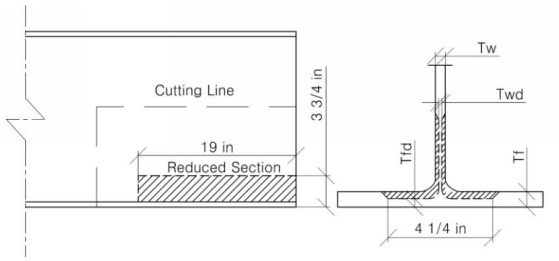

b) simulated damage

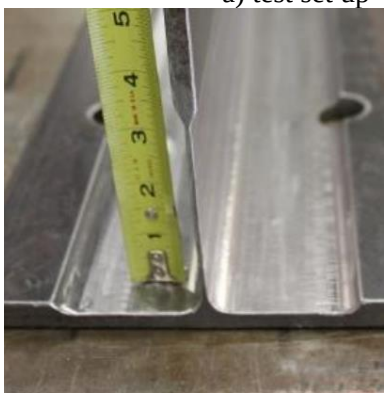

c) simulated damage

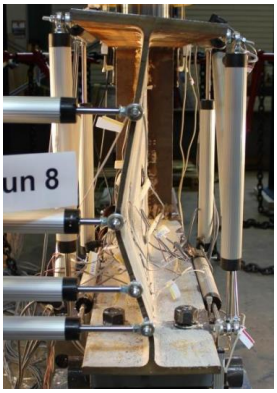

d) crippling of undamaged web

e) crippling of damaged web

Figure 13 Test set-up and damaged girders reported by Zmerta (2015)

The second damaged specimen was repaired using UHPC. The repair, shown in Figure 14, consisted of 1.75 in. thick UHPC panels on both sides of the web extending 25 in. along the beam and 13 in. (about two-thirds) up the web. Forty-eight 3/8 in. diameter by 1.25 in. long headed shear studs were applied to both sides of the undamaged region of the girder web (96 studs in all). Twelve additional studs were applied to each bottom flange outstand (24 in all). All studs were applied on a 2 in. pattern

as shown in Figure 14a. The stud patterns were offset 1 in. on either side of the web. 'Bulb-shaped' UHPC panels were installed as shown in Figure 14b; the single-use forms were reportedly milled from 2 in. foam insulation boards.

Commercially available Ductal® UHPC was used. This UHPC mix is reportedly capable of achieving 12 ksi compressive strength in 12 hours if cured at 120°F and 90% relative humidity. The strength evolution of the UHPC reported by Zmerta was only 4 ksi at 12 hours but 16 ksi at the time of girder testing (96 hours).

As reported in Table 8, the UHPC-repaired girder exhibited the first cracks in the UHPC at a bearing load of 35 kips. Shear cracks appeared at 69 kips and the girder exhibited evidence of web yielding (circled regions in Figures 14c and d) at an applied bearing load of 176 kips when the test was stopped. The observed cracking of the UHPC was relatively well distributed and minor (Figures 14c and d). The inclination of the cracks suggest a compressive strut developed in the UHPC resisting the bearing force. The UHPC prevented the web from buckling and/or crippling.

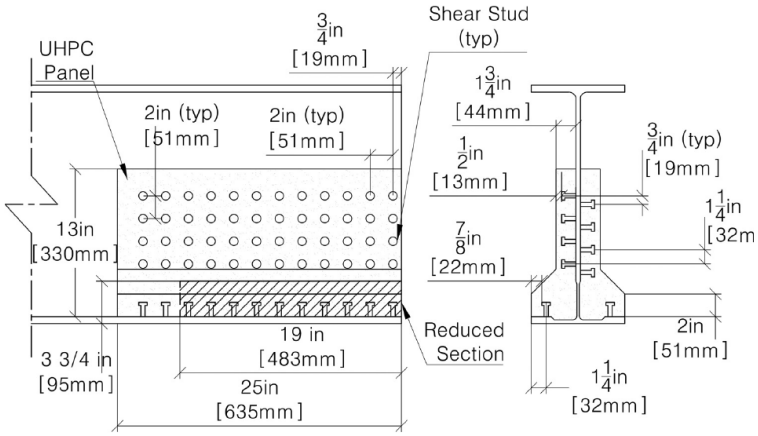

a) headed stud and UHPC layout

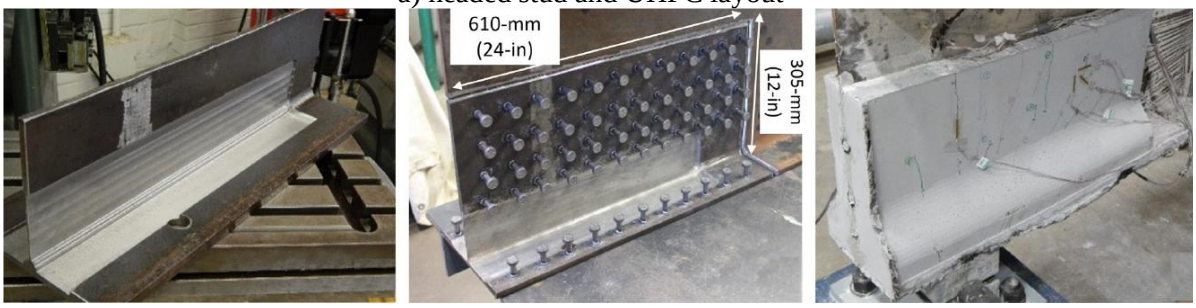

b) progression or repair [note that left image shows only damaged tee region prior to being rewelded into girder]

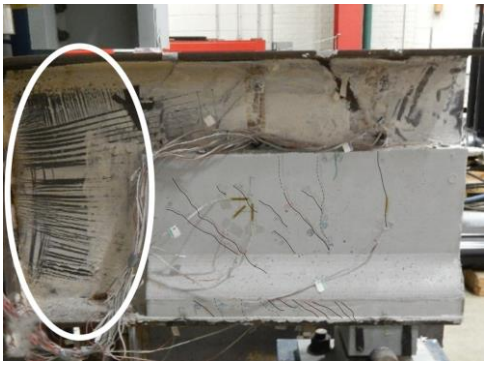

c) cracking of near side of UHPC panel (end of girder at right)

d) cracking of far side of UHPC panel (end of girder at left)

Figure 14 UHPC repaired girder reported by Zmerta et al. (2017)

Zmerta (2015) also reports an analytical study. Finite element (FE) simulations of the test girders were developed using LS-Dyna. Four-node shell elements were used to model the steel girders, solid elements to model the UHPC and beam elements were used to model the studs. The models were validated using the experimental results (Figure 15) prior to being extended to investigate other girder repair geometries. Figure 15b shows the test girder models with a composite concrete deck added. The addition of the deck has little effect on girder predictions since behavior was driven by web crippling in each case.

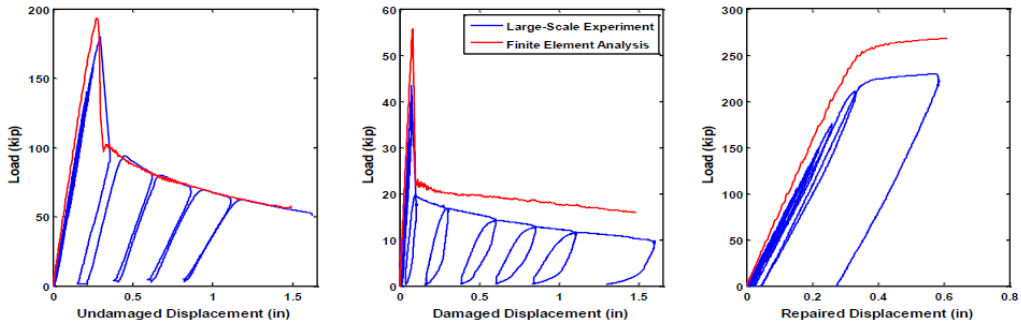

a) FE-predicted (red) and experimental (blue) bearing load versus displacement curves

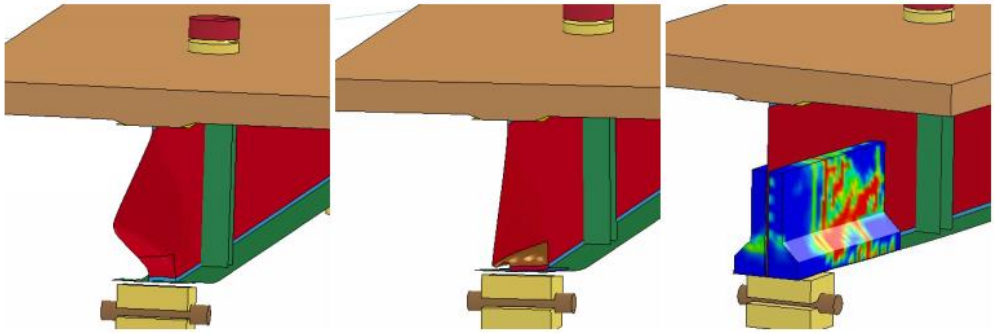

b) FE-predicted failure modes in presence of composite deck

Figure 15 FE models of test girders reported by Zmerta (2015).
left to right: undamaged girder, damaged girder, repaired girder.

The analytical program reported by Zmerta was extended to consider different girder geometries as summarized in Table 9. W36x160 rolled sections were considered with and without the presence of 0.5 in. bearing stiffeners. Additionally, a 54 in. deep plate girder having a 3/8 in. web was considered. This section had 1 in. bearing stiffeners and 5/16 in. 'first interior stiffeners'. Each prototype was subject to corrosion damaged in a W2 pattern (see Table 1). Web and bearing stiffener thickness was reduced 75% and flange thickness was reduced 48% (W36) and 38% (plate girder). Based on the FE modeling, the residual girder capacities varied from 33% to 8% of the nominal section flexure capacity (see Table 9).

Three variations of UHPC encasement repairs were modeled: full web height; partial web height and L-shaped; these are shown in Table 9. Each was predicted to fully restore the undamaged bearing capacity of the prototype. The W36 beams were restored to being flexure critical. Because the UHPC should constrain web instability, the tension field behavior of the 54 in. plate girder was enhanced by the presence of the UHPC (AASHTO does not permit the inclusion of tension field behavior in the end shear panel).

The simulated UHPC encasement repairs contained fewer studs anchored to the web than the experiments (compare Figure 14a to those in Table 9). The models appear to suggest that anchoring the UHPC between the flanges (full height) is equally – if not more – efficient as providing a relatively dense array of studs on the web. The L-shaped (matching the damage pattern) repair was also adequate for the rolled shape that is flexure-critical without damage.

Table 9 FE models of UHPC-repaired girder end regions (after Zmerta 2015).

girder	W36x160	W36x160	54 in. plate	
bearing stiffener	none	0.5 in.	1.0 in.	
	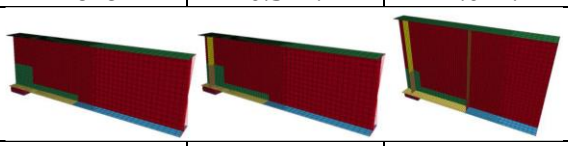			
nominal capacity (kips)	234	243	475	
nominal limit state	flexure	flexure	tension field	
damage pattern (in.)	W2 C_{L1} = 16.25 C_{L3} = 51.25 C_{H2} = 14.57 C_{H1} = C_{H3} = 3.65		W2 C_{L1} = 12.53 C_{L3} = 51.50 C_{H2} = 17.18 C_{H1} = C_{H3} = 4.90	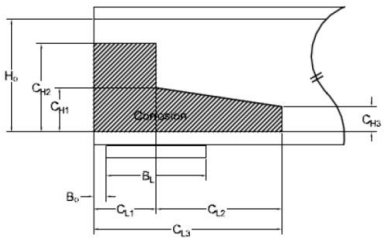
damaged capacity (kips)	18	80	98	
damaged limit state	web crippling	web/stiffener crippling	web/stiffener crippling	
	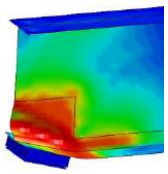	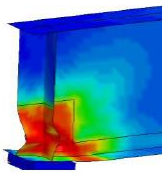	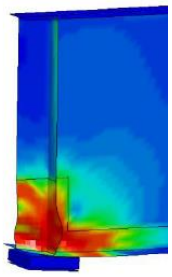	
full height repair capacity (kips)	277	278	649	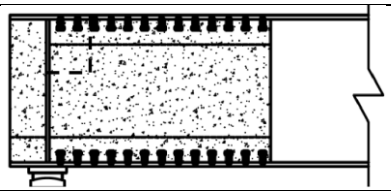
full height repair limit state	flexure	flexure	tension field	
partial height repair capacity (kips)	274	272	504	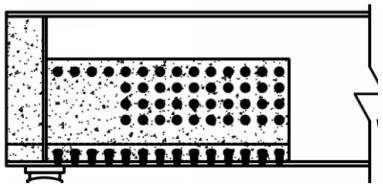
partial height repair limit state	flexure	flexure	tension field; UHPC compression	
L-shaped repair capacity (kips)	271	269	not modeled	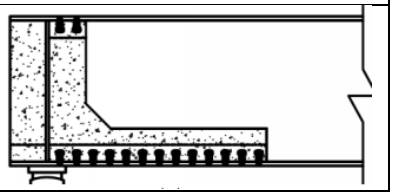
L-shaped repair limit state	flexure	flexure		

1.8.3.2 McMullen (2019)

McMullen (2019; summarized in McMullen and Zaghi 2020) extended Zmerta's proof of concept to full-scale tests having [perhaps] more realistic simulated corrosion damage. McMullen ultimately proposes design and construction recommendations as described below.

McMullen tested four (one control and three repaired) 54 in. deep plate girder sections loaded in three-point flexure such that the shear span was 64 in. (a/d = 1.18). The damaged end panel was spliced to a longer test beam which was reused in each test (Figure 16). In the test configuration used, the nominal bearing capacity of the end region is 212 kips, representing tension field failure (Eq. 1). Due to the presence of a bearing stiffener, crippling (Eq. 6) and bearing (Eq. 5) limit states are significantly higher. Based on the bearing stiffener geometry, the nominal bearing capacity of the girder is 495 kips.

Corrosion was simulated by a combination of grinding and sandblasting resulting in the localized damage shown in Figure 16b. Simulated damage was targeted at 66% of web and stiffener plate loss and 50% of flange plate loss concentrated in a region at the end of the girder. The damage pattern was W1 with C_L = 8 in. and C_H = 5 in. As seen in Figure 16b, small regions of 100% section loss were simulated immediately above the bearing (Pattern M1: a ≈ 2 in.; b ≈ 4 in.). The bearing capacity of the damaged girder was 95.3 kips (Table 10) controlled by crippling of the reduced web and stiffener as seen in Figure 16c. Another important observation made by McMullen is that the failure of the specimen having more realistic, non-uniform damage exhibited more gradual reduction of stiffness than observed for the very uniform artificial damage reported by Zmerta (2015) and Kim et al. (2013).

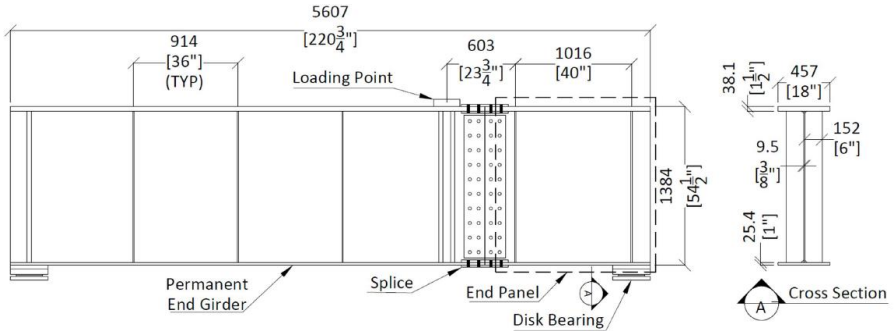

a) test arrangement showing test panel at right of slice and reused girder element to left

b) specimen with damaged end region

c) end region of damaged specimen following testing showing crippling of web and stiffeners

Figure 16 Test set up and damage reported by McMullen and Zaghi (2020)

UHPC encasement, shown in Figure 17, was limited to a 'stub column' immediately above the bearing, encasing the bearing stiffener region only. Two repairs extended the full height of the 52 in. web while the third extended 26 in. Two commercially available UHPC mixes having strengths exceeding 20 ksi were used (see Table 10). Ductal® JS1212 is a high early-strength mix (intended to

achieve 12 ksi in 12 hours) whereas JS1000 has a higher ultimate strength but a retarded initial set (intended to achieve 14 ksi in 96 hours).

During UHPC placement and the initial 6 hours of cure of full height specimen 2, field-derived vibrations were applied to simulate traffic loads[2]. No deleterious effect of these vibrations, having maximum acceleration of 0.002g, were observed.

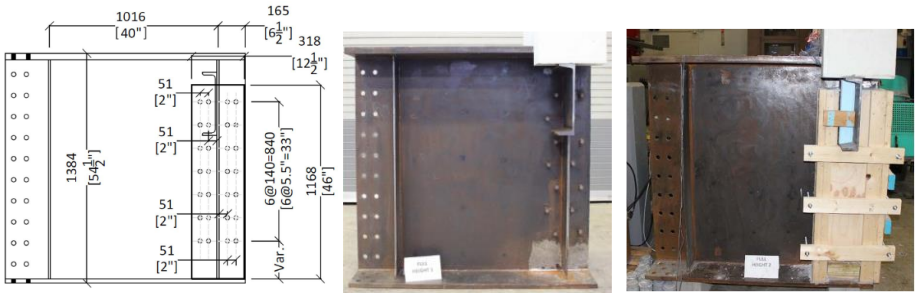

a) full height repair

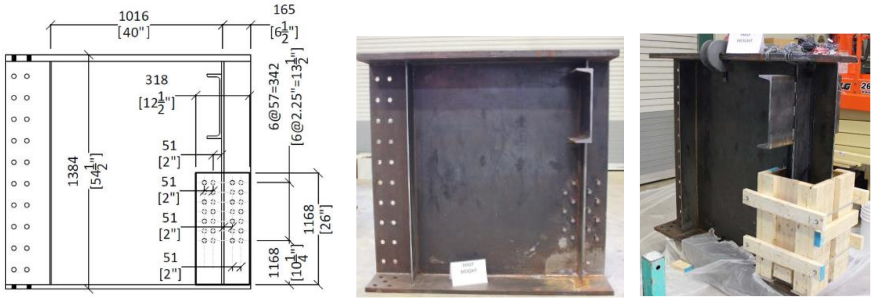

b) partial height repair

Figure 17 UHPC repairs reported by McMullen and Zaghi (2020)

Test results of the UHPC repaired girders are provided in Table 10. Both full-height repairs behaved similarly, achieving the nominal capacity of the undamaged girder (495 kip bearing capacity) and exhibiting a tension field buckling failure in the web panel immediate adjacent the repair. The failures are shown in Figure 18. The partial height repair exhibited some tension field behavior but ultimately, the web crippled immediately at the top of the UHPC (Figure 18c). Because tension field behavior was engaged, all repaired girders exhibited post-peak residual capacity exceeding 85% through displacements exceeding twice those at the ultimate capacity.

Table 10 Test results reported by McMullen (2019)

	damaged girder	full height repair 1	full height repair 2	partial height repair
UHPC	n.a.	JS1000	JS1212	JS1212
strength at 24h (ksi)		[a]	≈ 8	≈ 8
strength at 48h (ksi)		≈ 11	≈ 16	≈ 16
strength at test (ksi)		29.3	25.3	23.3
bearing capacity (kips)	95.3	527	497	472
limit state	web/stiffener crippling	web buckling (tension field)	web buckling (tension field)	web crippling immediately above UHPC
residual capacity		85%	90%	85%

[a] Ductal® JS1000 is a retarded set product not expected to have significant strength at 24h

[2] It is important to distinguish that these were vibrations applied using a shaker on top of the specimen (located on top of the white box shown in Figure 17a). This in no way duplicates the cyclic strains associated with actual traffic loads.

a) full height 1 b) full height 2 c) partial height

Figure 18 Failure modes of UHPC encased girders reported by McMullen and Zaghi (2020)

Like Zmerta (2015), McMullen (2019) presented a finite element (FE) based verification of the experimental results. The FE simulation modeled uniform, rather than actual damage. The degree of uniform section loss simulated in the FE model was adjusted to calibrate the model with experimental results. The web, which had about 66% section loss and a small region of 100% loss was modelled as having 80% uniform loss. The stiffener, also having 66% section loss was modeled as having 60% section loss. Modeled flange section loss was not reported although considering the shear-critical behavior of the girder, the model is not likely sensitive to this. Once calibrated, unsurprisingly, the model replicated the experimental data well.

McMullen (2019) provided recommendations for such UHPC encasement repairs. These (greatly paraphrased) are as follows:

1. Headed stud capacity in UHPC may be conservatively estimated using conventional stud capacity calculation. Given the high concrete strength, stud capacity will typically govern. This recommendation is limited to the use of 0.5 in. studs as investigated.
2. Studs should only be welded to undamaged portions of the girder. The recommended surface preparations is “power tool clean and free of loss material” (SSPC SP3). Studs placed on opposite sides of the web should be staggered.
3. Stud spacing, clear cover, edge distance, and distance to the deteriorated area should be four stud diameters ($4d_b$).
4. UHPC should have a 28 day strength exceeding 18 ksi.
5. Full-height encasement is preferable although half-height encasement is acceptable to improve constructability (place UHPC from below the deck, rather than through holes drilled through the deck).
6. Watertight forms are required for UHPC placement and forms should have a non-absorbing (hydrophobic) surface in contact with the UHPC.
7. UHPC may be placed with the bridge in operation (vibration is acceptable).
8. The capacity of the UHPC encased girder bearing may be taken as the nominal capacity of the repaired girder. Any increase in original capacity should be assessed on a case-by-case basis.

The present authors provide the following commentary on these recommendations.

Recommendations 1 and 3: As described Section 1.10, stud capacity, particularly when placed in clusters, is likely affected (Provine et al. 2019). Neither McMullen (2019) nor Zmerta (2015) provide any justification for the need for such dense stud patterns. Indeed, the analytical study presented by Zmerta (Table 9) appears to disavow this need in full-height repairs.

Recommendation 4: Neither McMullen (2019) nor Zmerta (2015) provide any justification for a minimum UHPC strength. Sections 1.8.5 and 1.9 further explore the effects of concrete properties in relation to an encasement repair.

Recommendation 7: Ignores entirely the nature of [non prestressed] repair as discussed in Section 1.7.1. The conclusions of this study, therefore, are limited to ultimate limit state [overload] performance.

In summary, the UConn study of UHPC encased beam ends illustrates the efficacy of this method of repair but provides no comparison to alternatives.

1.8.4 Field Applications of UHPC Repair

Hain and Zaghi (2021) report a field implementation repairing 45 beam ends on a bridge carrying I-91 over a rail corridor in New Haven Connecticut. The UHPC repair method was reportedly selected due to the complexity of the site and logistics (Figure 19a): the skewed bridge had variable beam sizes and bearing and stiffener details. Additionally, the piers provided little lateral clearance to both electrified (Amtrak) and freight rail lines. UHPC was placed from above the deck through cored holes connected to a PVC-pipe distribution system below the deck (Figure 19b) and the girder end region was heated to promote curing (enclosure seen in Figure 19a). A view of the final repair is seen in Figure 19c. Initial data reported at 2 months after placement indicated that the web shear in the end region was being shared with the UHPC in a ratio of about 2:1 (steel strain to UHPC strain). After four days and through at least 28 days, the incidence of low-probability, high-strain events was also reduced by the presence of the UHPC.

a) I-91 bridge over rail corridor b) PVC distribution of UHPC c) completed repair

Figure 19 Field implementation of UHPC repair reported by Hain and Zaghi (2021)

Texas DOT (TxDOT 2021) reports a similar repair on the Sidney Sherman Bridge serving the Port of Houston (Figure 20a). A UHPC encasement was selected to provide a 20-year life extension and due to the unacceptable cost of traffic closures that may otherwise be required. Figure 20b shows the UHPC encasement of a transverse steel diaphragm.

a) Sidney Sherman Bridge b) completed repair of diaphragm

Figure 20 Field implementation of UHPC reported by TxDOT (2021)

FHWA (2021) reports other field implementations as follows (as of December 2019):

- I-95 in Jacksonville, Florida (2017)
- Route 6/10 over I-95, Providence, Rhode Island (2018)

- Masters Road over Belle River, St. Clair County, Michigan (2018). This 55 foot long bridge, erected in 1934, is listed on the National Register of Historic Places (Figure 21)

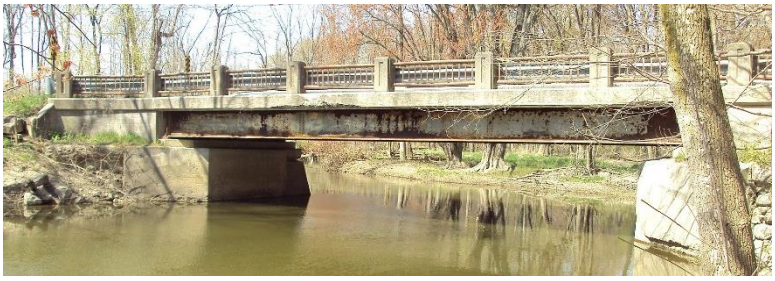

Figure 21 Masters Road-Belle River Bridge (Wikipedia.com; CC BY-SA 3.0)

1.8.5 UHPC versus Conventional Concrete

In the entire UConn study, only Kruszewski (2018) makes a limited comparison of UHPC to conventional concrete. Kruszewski conducts a series of 'push-out' tests intended to evaluate the behavior of studs welded to the beam web. The performance of four UHPC mixes (one without fiber) are compared to a HSC mix having 28-day compression strength of 8 ksi. The HSC push-out specimens are shown in Figure 22a; one specimen is tested with internal reinforcement (shown) and one without. None of the UHPC specimens have internal reinforcement beyond the steel fibers in the mix; all have the same dimensions and stud details shown in Figure 22.

The 0.5 in. diameter studs are 2 in. long and welded to a 0.375 in. web at a spacing (pitch) of 2 in. along the line of loading. The concrete and UHPC panels are 10 in. wide and 2.75 in. thick resulting in 5 in. side cover and 0.75 in. top cover over the studs. The benchmark single stud capacity, Q_n, for all tests is reported as 14.7 kips, governed by fracture of the stud ($A_{sc}F_u$ term in Eq. 11; see Section 1.10). As described in Section 1.10 however, Provine et al. (2019) recommend reducing the stud capacity by a factor of 0.7, reducing the benchmark capacity to 10.3 kips.

It is important to note that the test arrangement does not comply with AASHTO LRFD §6.10.10.1 requirements for stud pitch (greater than 6 stud diameters = 3 in.) or top cover (greater than 2 in.). Provines et al. propose that the minimum pitch can be safely reduced to 4 stud diameters. The 2 in. top cover requirement, on the other hand, is presumed to address durability (corrosion) rather than stud capacity. For interior exposure, ANSI/AISC 360-16 requires only 0.5 in. top cover. Nonetheless, reduced cover with no additional reinforcement may be expected to split, especially when a cluster of studs is called upon to transfer large loads in a small area (ACI 318 2019).

As should have been expected, the unreinforced HSC push-out test split along the line of studs in a brittle manner (Figure 22b). The ultimate capacity was reported to be 10.4 kips/stud although the slip before failure was only 0.04 in. The reinforced HSC specimen (Figure 22c) remained intact, exhibiting a ductile failure with 0.37 in. of slip although the capacity was only 10.6 kips/stud. The comparable UHPC specimens achieved capacities ranging from 15.3 to 17.0 kips/stud at slip values on the order of 0.17 in. and all exhibited stud shear failures (Figure 22d). Without fiber, however, the UHPC split longitudinally at a capacity of 11.6 kips/stud and a slip of only 0.1 in. (Figure 22e).

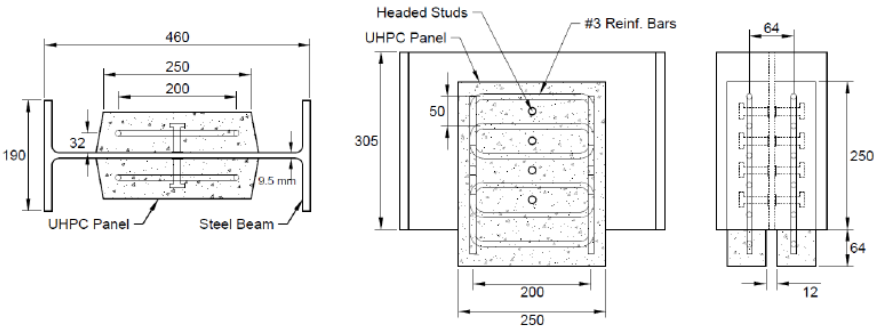

plan web elevation flange elevation

a) push out specimen showing reinforcement detail

b) HSC with no reinforcement
10.4 kips/stud

c) HSC with reinforcement
10.6 kips/stud

d) UHPC
>15.3 kips/stud

e) UHPC with no fibers
11.6 kips/stud

Figure 22 Push out tests of HSC and UHPC (Kruszewski 2018).

Kruszewski (2018) concludes that concrete failure governs behavior of studs in HSC and UHPC without fibers and does not recommend the use of either. However, taking into consideration the clustered stud tests and the recent work of Provines et al. (2019), this conclusion should be reconsidered. The reduced benchmark stud capacity (10.3 kips/stud) was [barely] achieved in all cases. Furthermore, the reinforced HSC specimen achieved the recommended (EC4 2005) minimum slip to provide ductility (0.24 in.). Kruszewski, somewhat inexplicably, defines ductile failure of UHPC-embedded studs as "sustaining 90% of the capacity over a slip range of [0.16 in.]". This criterion appears to have been selected to satisfy the results of the testing conducted.

Without question, splitting must be mitigated. Internal reinforcement in HSC and fibers in UHPC were shown to accomplish this. It is hypothesized that greater top cover may also accomplish this objective and it is noted that the 0.5 in. top cover provided was too small to provide adequate durability in a bridge application.

1.9 Other Materials for Concrete Encasement

While UHPC may work well for deteriorated beam end repair, it is cost-prohibitive and may prove difficult to implement without specialized equipment and contractors. Other variations of high-performance concrete (HPC), however may be viable replacements. In general, these are better established in industry and represent only a marginal cost premium over conventional concrete.

1.9.1 Nano-modified Concrete

UHPC (described above) is a subset of a larger class of materials: nanoconcretes. Nanoparticles are characterized by having large surface area ratios and thus outstanding chemical reactivity. As a filler in concrete, nanoparticles provide additional nucleation sites and seeds that accelerate hydration and result in concrete having increased strength and durability (Nguyen-Tri and Nguyen 2020). A large number of nano-reinforcements and fillers are reported in the literature including nanosilica, nano-Al_2O_3, tetra ZnO whiskers (T-ZnO), nano-ZnO, ZrO_2, Cr_2O_3, CuO, $CaCO_3$, nano-TiO_2, Cu nanomaterial, graphene, carbon nanotubes, carbon nanofibers, nano boron nitride, etc. Like UHPC, nanomodified concrete mixes require special mixing controls to reduce agglomeration and ensure uniform dispersion of nanoparticles (Yu et al. 2014).

In general, the denser packing and reactivity of nanoconcrete results in higher strength (e.g., Rupasinghe et al. 2017 reporting a study incorporating nanosilica) and reduced chloride permeability (e.g., Balapour et al. 2018, also reporting nanosilica). The inclusion of nanoparticles in a variety of adhesives is known to improve adhesive bond (Taylor 2011). Nanosilica (SiO_2) and nano-Al_2O_3 has been shown to enhance the adhesive component of concrete to plain (undeformed) reinforcing bars (Ismael et al. 2016). No studies directly considering the interface of nanoconcrete with steel plate are known.

1.9.2 High Strength Concrete (HSC)

High-strength concrete (HSC) is essentially a conventional concrete – having coarse and fine aggregate and a higher cement content than normal strength concrete (NSC) (ACI 363R-10). Coarse aggregate will typically be granitic, have a relative uniform grading, and have a smaller top size than NSC. Although definitions vary, HSC most often refers to concrete having design strength exceeding 6 ksi (although in practice, this is typically much higher). Typical properties of HSC are reported in Table 7. AASHTO LRFD presently recognizes the use of HPC having strengths up to 15 ksi. 91-day strengths as high as 20 ksi are reported regularly in the literature and practice (e.g., in 1988, concrete having 91-day strength of 21 ksi was achieved for the construction of Two Union Square in Seattle). The performance of HSC is very sensitive to coarse aggregate properties and often trial batches with available aggregate are required to achieve strengths at the higher range of what is shown in Table 7.

1.9.3 Fiber Reinforced Concrete (FRC)

Fiber-reinforced concrete (FRC) is conventional or high-strength concrete having discrete short reinforcing fibers added into the mix. Typical fiber materials include steel, glass, and organic polymers (synthetic fibers). Naturally occurring asbestos fibers and vegetable fibers, such as sisal and jute, may also be used. The inclusion of fibers helps to control micro and macro cracking behavior resulting in improved long-term serviceability of the FRC structure or product (ACI 544.5R-10). As in UHPC, fibers improve the modulus of rupture and impart some residual post-cracking capacity to the concrete.

1.9.4 Fabric Reinforced Cementitious Matrix (FRCM)

Fabric-reinforced cementitious matrix (FRCM) (also known as textile-reinforced concrete (TRC) or mortar (TRM)) products combine high-performance sprayable or trowelable mortar with open grid or mesh reinforcement to create thin-walled reinforced mortar shells. Reinforcement may be a variety of materials although carbon fiber grid and steel wire mesh are most commonly reported. FRCM is used almost exclusively for strengthening applications of concrete and masonry (ACI 549.4-20) and is seen as an alternative to FRP repairs (see Section 1.11) particularly where sensitivity to elevated temperature (fire rating or resistance) is a concern.

There is no known study or application of FRCM to deteriorated steel infrastructure. In such an application, FRCM would not differ substantially from FRC and may be considered a hybrid of FRC – using prefabricated fiber grid/mesh, rather than distributed fibers in the mix.

1.9.5 Latex-modified Concrete (LMC)

Latex-modified concrete (LMC) is defined as “hydraulic cement and aggregates combined at the time of mixing with organic polymers that are dispersed or redispersed in water.” (ACI 548.4-11). LMC is used extensively in deck overlays as protection against chloride ion penetration (e.g. Harries et al. 2013). Reviews of field performance of LMC overlays indicate that LMC has “excellent” resistance to chloride ion penetration, freeze-thaw durability, and resistance to scaling. LMC also exhibits “excellent” bond to the concrete substrate (Bertrand 2012; Bertrand and Sprinkel 2009; Sprinkel 2003 and 2009). LMC is a ‘mature technology’; the main body of knowledge was developed in the 1980’s and 1990’s and now resides in specification documents such as ACI 548.4-11, ACI 548.3R-09, FHWA Report RD-78-35 (1978) and DOT specifications.

In the only known study of its kind, Nakayama and Beaudoin (1987) assessed the bond of six different LMC mixes to a steel plate substrate. The only preparation of the smooth steel substrate was to be cleaned in advance with acetone (degreased). The inclusion of EVA[3], SBR[4] and PVA[5] latex polymers at varying dosages was shown to improve the bond between mortar and steel over a non-modified control mortar. Failure occurred at the interface about 5-10 μm into the mortar. The enhancement of bond was attributed to the presence of a latex film at this interface and the dominance of C-S-H[6] and CH[7] hydration products at the interface. Addition of two anionic latexes, AVA[8] and V-V[9], demonstrated no improvement in bond.

1.9.6 Magnesium Phosphate Cement

Magnesium phosphate cement (MPC) is a water hardening inorganic cementitious material which offers very high early strength, low drying shrinkage, excellent adhesion, good resistance to frost damage and improves the corrosion resistance of embedded steel (Jia et al. 2019). It is commonly used in bridge deck patching operations. One-hour compression strength can exceed 7 ksi and 28-day strength can approach 12 ksi and more. Tensile strength is *proportionally* greater than Portland cement concrete, although modulus is a marginally less. MPC, being a mortar, is easily prepared on site. There are commercial formulations of MPC intended for wall repairs that are in 'putty' form and exhibit initial set in minutes, therefore requiring no formwork even for vertical surfaces.

1.10 Shear Stud Capacity

Using any encasement material requires force transfer to the existing steel. This is conventionally accomplished with shear studs. Single stud capacity, Q_n, is given by AASHTO LRFD (2020) Eq. 6.101.10.4.3-1 as:

$$Q_n = 0.5 A_{sc} \sqrt{f_c' E_c} \leq A_{sc} F_u \qquad [11]$$

Where A_{sc} = area of stud;

f_c' and E_c = strength and modulus (see Table 7) of concrete; and,

F_u = tensile strength of stud.

Using the AASHTO-prescribed relationship between f_c' and E_c (Table 7) and F_u = 75 ksi, it is easily shown that the right-hand term of Eq. 11 – the stud tension capacity – will govern capacity for concrete having f_c' greater than 5.3 ksi. For the sake of the foregoing discussion, we will assume that $f_c' > 5.3$ ksi and the right-hand term of Eq. 11 governs capacity.

The $A_{sc}F_u$ term implies that the full tensile capacity of the stud may be developed. If the stud were loaded in "pure" shear, its capacity would be assumed to be $0.58A_{sc}F_u$. The reality lies between these extremes. Embedded in concrete, the stud behavior is complex: it crushes into the concrete and the local stress transfer between stud and concrete results in a complex combination of shear, flexure and tension in the stud. To account for this, both Eurocode (EC4 2005) and Australian (AS 2004) standards factor the right-hand term in Eq. 11 as $0.8A_{sc}F_u$.

Additionally, Eq. 11 is associated with stud dimension, spacing and detailing requirements. As is the case for other embedded anchors (see for example ACI 318-19 Chapter 17), clustering anchors close together in concrete reduces their individual capacity (capacity of the cluster is lower than the sum of the individual stud capacities). In a recent study focusing on AASHTO practice, Provines et al. (2019)

[3] poly(ethyl-vinyl acetate); two different EVA products were tested
[4] styrene butadiene rubber
[5] poly(vinyl acetate)
[6] calcium-silicate-hydrate is the main product of hydration of Portland cement.
[7] calcium hydroxide (Portlandite) – $Ca(OH)_2$
[8] poly(acrylic-vinyl acetate)
[9] poly(vinylidene chloride-vinyl chloride)

address cases in which studs are 'clustered' and make a number of recommendations pertinent to AASHTO practice and relevant to the objective of the present study:

1. reduce minimum pitch of studs from six to four stud diameters in AASHTO LRFD 6.10.10.1.2.
2. reduce minimum transverse spacing from four to three stud diameters in AASHTO LRFD 6.10.10.1.3.
3. revise existing AASHTO LRFD Eq. 6.10.10.4.3-1 (Eq. 11, above) as follows:

$$Q_n = 0.5A_{sc}\sqrt{f_c{}'E_c} \leq 0.7A_{sc}F_u \quad [12]$$

4. revise shear stud fatigue requirements to be provided in terms of stress rather than force. Adopt a value of $(\Delta F)_{TH}$ = 7 ksi for infinite fatigue life and the following for finite fatigue life:

$$(\Delta F)_n = (32{,}800x10^6/N)^{1/6.3} \quad [13]$$

Recommendations 1 and 2 will allow tighter clusters of studs on a beam web, offsetting the loss of capacity associated with Recommendation 3. Since beam end repairs will primarily carry live load, Recommendation 4 will be critical to and may ultimately control the stud design for such a repair. It appears as though Eq. 13 results in considerably lower stud fatigue capacity than is presently permitted by AASHTO LRFD 6.10.0.2.

1.10.1 Other Shear Connectors

Shear studs are simply mechanical connectors 'rigidly' attached to a steel substrate. Studs are welded to one side of a plate in a single-step process using a 'stud gun'. One limitation of the stud welding process is that the substrate needs to have a uniform thickness and be relatively smooth. According to the American Welding Society Structural Welding Code (AWS D1.1 2015), to avoid burn-through or distortion of the substrate, the substrate plate thickness must be at least one-third the stud diameter. Similarly, and more conservatively, AISC 360 states the stud diameter shall not be greater than 2.5 times the thickness of the base metal. Thus, according to AWS D1.1, a 0.5 in. stud should not be used on a plate less than 0.17 in. thick. Additionally, according to AWS D1.1, the surface preparation of the plate needs to conform to SSPC SP2 (2018) – "hand tool cleaning at least 2 in. from the weld" – to ensure uniform arcing of weld current. In new construction, these requirements are trivial, although in a beam end repair it may be necessary to weld a stud to a portion of web that has experienced section loss and/or is pitted due to corrosion. Welded shear studs, therefore, may not be a practical option for beam end repairs.

When studs are required on both sides of a plate, such as in the proposed beam end repair application, alternative shear connectors may prove equally efficient (Figure 23). High strength threaded rods or structural bolts, inserted through the plate and nutted on both sides of the plate to maintain their 'rigid' attachment are preferable in repair scenarios. Such an approach avoids hot-work and having to shoot shear studs onto a vertical surface (which requires special ferrules and more care to be taken in the welding process to ensure correct alignment of the ferrules and stud itself). Pavlovic et al. (2013) reported that 0.625 in. diameter high strength bolts achieve 95% of the capacity of 0.625 welded studs although the slip at service loads is greater. To mitigate these reductions, the bolted stud can be designed using a value of A_{sc} calculated based on the net area of the bolt[10]. Additionally, since alignment tolerance is not a concern for single bolts, oversized holes are not required: a bolt acting as a stud may be placed into a hole of the same diameter. This minimizes slip and affects bearing at initial loading.

Kruszewski (2018) conducted push-off tests of conventional welded shear studs and bolted threaded rods in UHPC. The same diameter stud and rod were used, meaning the net area of the rod was about 70% that of the stud and its flexural stiffness was about 50% that of the stud. The tensile strength of

[10] This can also be accomplished using the gross area of the bolt and the nominal tensile strength of the bolt, F_{nt}, defined by AISC 360-16. F_{nt} is calibrated to account for net area through the threads of structural bolts.

the rods, however, was higher than that of the studs. Although the initial yield of the push-off tests having the threaded rods was lower, the ultimate capacities and slips of both rods and studs were comparable, a result confirmed by Pavlovic et al (2013).

Bolted shear studs are commercially available from suppliers such as Tension Control Bolts, Ltd (TCB). The TCB bolted shear stud was evaluated at the University of Manchester (Tension Control Bolts 2022). The bolted shear studs were found to exceed the strength requirements for the European standard for high strength structural bolted assemblies (EN 14399-1). The study was silent on the issue of ductility.

In other applications, 'concrete dowels' are used to affect shear transfer. In this case larger holes are drilled through the steel web and concrete is allowed to flow through these producing a dowel. This approach is commonly used for steel embedments in composite construction where the concrete dowel typically includes a reinforcing bar through the web hole. (e.g., El-Tawil et al. 2009). Kruszewski (2018) demonstrated this approach in push off tests using UHPC. 1.5 in. diameter holes through a 0.375 in. thick web developed 19.9 kips (shear stress on UHPC dowel = 11.2 ksi); 2 in. holes developed 25.4 kips (8.1 ksi).

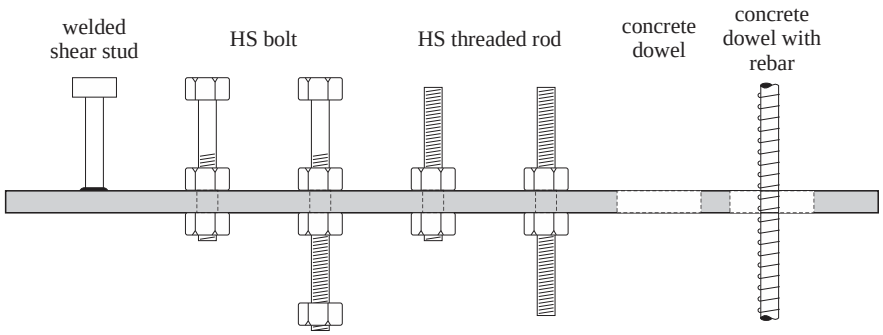

Figure 23 Variations of shear connectors.

1.11 FRP Based Repairs

1.11.1 FRP Materials

Fiber reinforced polymer (FRP) composite materials combine high-modulus and/or high strength fibers in a low-modulus polymeric matrix which ensures load transfer between the fibers. The strength and stiffness of an FRP composite is determined by the fiber type, fiber volume and fiber architecture while the in-service performance is influenced both by the fiber and matrix material. Orientation of the fibers is controlled so that the resulting FRP system is anisotropic and may be tailored to suit the local structural demands in the component to which it is applied.

Carbon (CFRP) and glass (GFRP) FRP materials are ubiquitous in the field of structural repair. CFRP may be high strength (hsCFRP), high modulus (hmCFRP) or ultra-high modulus (uhmCFRP) (Table 11). GFRP (today, most typically based on ECR-glass[11] fibers) have a much lower modulus than CFRP but are typically less expensive on a unit stiffness basis. To be effective in strengthening applications, the modulus of the FRP selected for a particular application should be compatible with the substrate material. For this reason, CFRP materials are most often used with a steel substrate.

A polymeric matrix binds and protects the fibers of an FRP, transferring force into, and between, fibers through interfacial shear. The matrix also provides stability and environmental protection to the embedded fibers. Epoxy resin systems are most commonly used as the matrix in hand lay-up

[11] Electrical/Chemical Resistance glass with high acid resistance

applications and as the adhesive in plate bonding techniques. Polyester resin systems are often used as the matrix material in precured composite materials such as those used for plate bonding applications.

In terms of ease of handling, installation and quality control, precured CFRP plates or strips are rapidly becoming the preferred products for structural repair. The exception is that wet lay-up fabrics remain appropriate for applications involving irregular shapes or forming around corners. In either case the resulting system has a steel-adhesive-FRP interface region. Table 11 provides a summary of representative basic material properties for each layer in the system. The FRP properties are given for the composite strip product rather than for the raw fibers. Hand lay-up products will typically have lower strengths and stiffnesses than those shown since the resulting fiber volume ratio is typically lower than in precured systems.

Table 11 Typical properties of steel-adhesive-FRP systems.

	Mild Steel	Precured FRP Strips				Adhesive	
		hsCFRP	hmCFRP	uhmCFRP	GFRP	high modulus	low modulus
tensile modulus, ksi	29,000	24,100	30,000	44,100	6100	700	58
tensile strength, ksi	40-70	442	420	210	130	3.6	0.6
ultimate strain, %	18-25	1.8	1.4	0.5	2.2	1.0	>10
density, lb/ft^3	470	~100	~100	~100	~135	~75	~75
CTE, $10^{-6}/^oF$	12	~0	~0	~0	4.9	90	n.r.
T_g[a], ^oF	-	300	300	300	resin	145	-
shear strength, ksi	-	-	-	-	-	3.6	1.3
bond strength, ksi	-	-	-	-	-	~3	~0.7
[a] T_g = glass transition temperature – associated with vitrification of polymer matrix							

A great deal of work has been conducted on the use of externally bonded FRP systems for structural strengthening of building and bridge systems and components. The overwhelming majority of this work has focused on the retrofit of concrete structures (ACI 440.2R-17). In virtually all existing applications, FRP materials are used to supplement steel reinforcement. Indeed, early FRP external bonding applications were developed as an alternative to heavy and awkward steel plate bonding techniques. Provided adequate quality control is executed, the behavior of externally bonded FRP is largely governed by the substrate concrete and the bond of the FRP thereto. The bond of FRP to concrete can only be as strong as the substrate concrete and may fail through a variety of mechanisms, some associated with classical debonding mechanisms and others associated with the behavior and condition of the concrete substrate. This will not be the case for a stronger steel substrate, allowing more conventional bond mechanics to be used to describe debonding behavior (Harries and Dawood 2012).

1.11.2 Repair of Steel Members with FRP

There is comparatively little work investigating the use of bonded FRP materials for the repair of steel members. Teng et al. (2012), Harries and El-Tawil (2008), and Zhao and Zhang (2006), all provide overviews of the state-of-the-art. Most available research and guidance focuses on the use of FRP for flexural strengthening: applying FRP materials to the tensile flange of a section to increase its capacity. Cadei et al. (2004), CNR (2007) and Schnerch et al. (2007) are all prepared as design and installation guidelines for FRP-based strengthening of steel structures.

Two NCHRP-IDEA projects, IDEA-011 (Mertz and Gillespie 1996) and IDEA-051 (Mertz et al. 2002) focused on the flexural strengthening of corroded bridge girders and addressed the use of bonded FRP materials on the tension flange of simple span girders. The rationale was that the bottom flanges of bridge girders typically see the greatest level of corrosion, largely due to debris accumulation. Mertz and Gillespie (1996) report six small scale tests of 60 in. long W8x10 members repaired with five different adhesively bonded schemes shown in Figure 24 (the fifth scheme was similar to that shown in Figure 24a using a different CFRP material.) All specimens demonstrated an

increase in flexural stiffness and strength compared to the un-strengthened control specimen. As might be expected, the "sandwich-reinforced" specimen (Figure 24b), having the FRP material located a distance below the flange (thereby increasing the effective section depth) showed the greatest improvement in stiffness and elastic strength (although the second CFRP strip technique (Figure 24a) was comparable in terms of both parameters). The composite-wrapped specimen (Figure 24c) showed the greatest increase in ultimate capacity since the composite wrap surrounding the foam core provided better shear transfer through higher loads than the aluminum honeycomb. All specimens tested failed in a debonding mode of failure, with the CFRP peeling from the flange at its ends. The second CFRP strip specimen, and the specimen having a pultruded channel (Figure 24d), were able to restore the unstrengthened beam capacity prior to debonding.

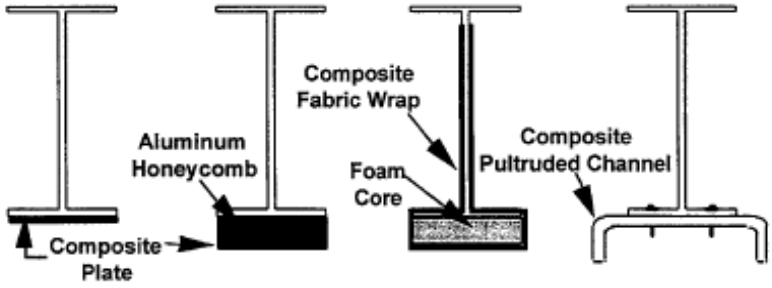

a) FRP plate reinforced | b) sandwich reinforced | c) FRP wrapped | d) pultruded section

Figure 24 Small scale specimens tested by Mertz and Gillespie (1996).

Two corroded 24 in. deep girders (similar to W24x84 but with tapered flanges), recovered from a 1940-era Pennsylvania bridge, were tested using a strengthening scheme similar to that shown in Figure 24a: having CFRP strips applied to both the top and bottom sides of the tension flange (Mertz and Gillespie 1996). The CFRP strengthening was able to increase the stiffness and moment capacity of the corroded girders. The first girder was deteriorated such that its stiffness and strength was approximately 87% of that expected for a new, uncorroded girder; the second girder had a residual stiffness and strength of about 62%. Strengthening the first girder restored the uncorroded stiffness and exceeded the uncorroded strength. The repair to the more severely damaged second girder significantly improved behavior but was unable to restore the uncorroded stiffness or strength. The ultimate capacity of both specimens was controlled by buckling of the compression flange which was not addressed in the strengthening scheme. Nonetheless, the tension flange did yield and no debonding of the CFRP was observed in either specimen.

Having demonstrated the viability of strengthening steel with CFRP strips, Mertz et al. (2002) extended their initial work with pilot studies investigating the transfer length of bonded CFRP and the fatigue performance of FRP strengthened girders. Simple steel tensile specimens having CFRP strips bonded to both faces were used to investigate the force transfer between steel and CFRP. In all specimens, regardless of load level considered, approximately 99% of the total force transfer occurred within the first 3 to 4 in. of the bonded reinforcement. This result is consistent with typical calculations of 'effective bond length' which is considered to be a characteristic property of thin bonded FRP systems (Teng et al. 2002). Mertz et al. recognized the importance of a thin adhesive layer in facilitating stress transfer between the steel substrate and CFRP. However, an efficient stress transfer exacerbates debonding stresses. Despite this, Mertz et al. only report debonding in one tension specimen at strains corresponding to yield of the underlying steel specimen. They attribute the lack of debonding in the other specimens to the use of adhesive having a low shear modulus and high elongation properties. Fatigue performance of CFRP bonded to the tension flange of simply supported specimens revealed little degradation of specimen stiffness or strain carried by the CFRP and no apparent debonding after several million cycles of loading.

Mertz et al. (2002) and Miller et al. (2002) report a field installation on a single girder of a bridge carrying I-95 Southbound over Christina Creek outside Newark Delaware. This installation was a demonstration of the techniques developed in the IDEA projects. A single W24x84 girder spanning 24.6 ft was repaired with CFRP on the bottom of the tension flange. Load tests indicated a reduction in tension flange steel strains of 11.4% under a vehicle load approximately equivalent to AASHTO H32 loading. Chacon et al. (2004) report a related demonstration project involving the strengthening of two W24x100 floor beams of the Ashland Bridge carrying State Route 82 over Red Clay Creek in Delaware. In this application a decrease in tension flange steel strain of 5.5% was observed under service load conditions. Neither of these demonstration strengthening projects were strictly necessary – the strengthened girder and floor beams did not require strengthening. Rather, the projects were intended to serve as test beds to investigate the long-term performance and durability of CFRP strengthening techniques for steel bridge girders. Regrettably, no such follow-on studies have been reported.

Patnaik and Bauer (2004) report an experimental program of flexural strengthening by adhering CFRP strips to the tension flange of steel beams. As expected, the moment capacities of the beams were increased - in this case by about 14%. Both strengthened beams are reported to have failed due to lateral torsional buckling, however the authors report a final failure involving rupture of the CFRP. This latter observation demonstrates that in this application, the bond strength of the CFRP to the steel substrate was substantial.

A second series of tests reported by Patnaik and Bauer (2004) involved 14 in. deep beams having intentionally slender – 0.12 in. wide by 13 in. tall (d/t_w = 108) – webs intended to investigate shear strengthening with CFRP. As expected, the unstrengthened beam failed due to elastic web buckling prior to flexural yielding. The application of vertically oriented, unidirectional CFRP to both sides of the web is reported to have allowed the section to yield prior to the onset of inelastic web buckling. Furthermore, although significant debonding of the short CFRP strips was evident, the failure is reported to have been ductile and "it was possible to sustain the load for a short time even after the initiation of web shear buckling."

Al-Saidy et al. (2004) investigated the effect of CFRP plates on the behavior of composite steel-concrete beams. The investigation focused on the behavior of beams damaged intentionally at their tension flange to simulate corrosion and then repaired with CFRP plates. Damage varied between no damage and a loss of 75% of the bottom flange. The test results showed that the elastic flexural stiffness of damaged beams can be partially restored (up to 50%); whereas the strength of damaged beams can be fully restored to their original, undamaged state using the CFRP plates investigated. Similarly, Photiou et al. (2006) reported a series of tests on artificially degraded flexural beams in which the failure load for all specimens exceeded the plastic collapse load of the undamaged beam. Furthermore, by using U-shaped FRP applications extending up the web to the neutral axis, composite action was provided between the steel member and fiber layer leading to better performance and mitigating debonding even at failure levels.

Other similar investigations of the use of CFRP strips attached to the tension flange of I-girders have demonstrated generally improved flexural capacity – proportional to the CFRP applied – although little improvement to girder stiffness (Sen et al. 2000; Tavakkolizadeh and Saadatmanesh 2003a; Lenwari et al. 2005). In such applications, Lenwari et al. (2006) demonstrated that the stress intensity at the ends of CFRP plates governs the debonding strength and that this region is critical for the initiation of debonding. Colombi and Poggi (2006a) observed similar behavior but also demonstrated a substantial increase in the post-yield stiffness provided CFRP debonding could be mitigated.

Schnerch et al. (2004) investigated resin and adhesive selection for wet lay-up of carbon fiber sheets and bonding of pre-cured laminate plates used to enhance the flexural behavior of a steel monopole. Resin selection for the wet lay-up process was determined through testing of double lap shear coupons using ten different resins. Test results showed a 25% increase in the elastic stiffness of the steel monopole resulting from the application of a limited number of CFRP sheets.

1.11.3 Mitigation of Fatigue Damage with FRP

FRP materials, particularly CFRP, exhibit excellent performance when subject to fatigue loads. In conditions of tension fatigue where environmental effects are not affecting behavior, CFRP behavior is dominated by the strain-limited creep-rupture process. Plotted on a semi-log S-N curve, CFRP composites exhibit strength degradation on the order of 5% to 8% per decade [of logarithmic cycles] (Curtis 1989). For comparison, steel degrades at approximately 20% per decade and the AASHTO LRFD (2020) fatigue curves are even steeper than this.

Jones and Civjan (2003) used ASTM A36 steel fracture specimens to evaluate the ability of a CFRP overlay to enhance fatigue performance. Center-hole specimens with crack initiators and edge-notched specimens were used. Increases in fatigue life were reported for all specimens tested, although the effectiveness of the CFRP (and thus the fatigue life enhancement) was dominated by adhesive behavior.

Tavakkolizadeh and Saadatmanesh (2003b) presented the results of a study of notched steel beams with CFRP patches subject to medium cycle fatigue loading. Twenty-one S5x10 ASTM A36 steel beams were prepared and tested under four-point bending. The number of cycles to failure, changes in the stiffness and crack initiation and growth in the specimens were compared to unretrofitted specimens. The authors concluded that the CFRP patches not only extended the fatigue life of the notched detail more than three times, they also decreased the crack growth rate significantly.

Harries et al. (2010) report similar tests of W6x12 beams having a notch compromising 100% of the tension flange. In monotonic tests, bonded CFRP strips increased the residual capacity of the notched section 150%, restoring about 67% of the unnotched beam capacity. At fatigue loads representing 70% (essentially 100% of the notched capacity), 40% and 20% of the unnotched beam capacity, crack initiation (beyond the existing notch) was retarded from 5000 cycles (70% load) to 50,000 cycles (40%) and 225,000 cycles (20%). Similarly, fatigue life was increased from 20,000 cycles when loaded at 70% unnotched capacity, to 152,000 cycles at 40%, and 1,703,000 cycles at 20%.

Nozaka et al. (2005) report a fundamental study of the use of CFRP strips for the repair of fatigue-damaged tension flanges of steel I-girders. The focus of this study was to establish appropriate values for the effective bond length for such repairs. A variety of repair configurations were tested including providing a gap (bonded and unbonded), no gap, and fully bonded or partially bonded CFRP in the region of the existing fatigue crack. Two CFRP systems and five adhesive systems were tested. The results reported the greatest increase in strength resulting from the system using both the CFRP and adhesive with the lowest moduli of elasticity of those considered.

Liu et al. (2006) report a study of the direct tension fatigue behavior of bonded CFRP sheets used to create “strap joints” between two steel plates. This study reported an apparent fatigue limit of 40% of the ultimate static strength of the strap joint specimens. Below this limit specimen failure and steel-CFRP bond behavior was not affected by the applied fatigue loads.

1.11.4 Enhancing Stability of Steel Elements with FRP

FRP materials have been demonstrated to enhance the stability of steel members (Harries 2014). In this application, the high stiffness and linear material behavior of the unidirectional FRP materials are utilized to provide “bracing” that improves the buckling and post buckling behavior of steel components. Recent research has demonstrated that the application of FRP reinforcement can lead to improvements in the flange local buckling (FLB), web local buckling (WLB) and flexural torsional buckling (FTB; often referred to as lateral torsional buckling) behaviors of steel members. This application is not aimed at increasing the load carrying capacity of the steel section, *per se*. Rather, the approach is aimed at providing stability (in the sense of bracing) to the steel section. The FRP application is intended to enforce nodal lines in a plate element for the purposes of increasing its critical load and constraining plastic flow. The member becomes, in effect, an FRP-stabilized steel section.

El-Tawil et al. (2011) demonstrated the use of CFRP wraps to enhance the plastic hinge behavior of double-channel members subjected to reversed cyclic flexural loads. Two cases are considered, one in which the entire gross cross section is wrapped, the second where only the extending flanges are wrapped; both methods exhibited improved behavior of the hinge as compared to unwrapped specimens. El-Tawil et al. report that the presence of the CFRP wrap increased the size of the plastic hinge region, inhibited the occurrence of local buckling and delayed the onset of lateral torsional buckling. These effects resulted in reduced steel strain demands, increased rotational capacity, and improved energy dissipation in the plastic hinge region.

In a study investigating the use of CFRP to strengthen hollow structural square (HSS) columns, Shaat and Fam (2006) report on concentric axial load tests of squat HSS sections wrapped with both longitudinal and transversely oriented CFRP sheets. Axial compression strength increases on the order of 8% to 18% are reported. Similarly, axial stiffness increases, resulting from the longitudinally oriented CFRP, of between 4% and 28% are reported. The authors suggested that the transverse CFRP helps to restrain outward directed local buckling of the HSS walls affecting the improved behavior observed.

Harries et al. (2009) reported an experimental study demonstrating the premise of an FRP stabilized steel section. Concentric axial compression tests of both long and "stub" WT6x7 sections were carried out to investigate the ability of an FRP retrofit to affect FTB and WLB behavior, respectively. Short stub specimens were dominated by web (stem) local buckling (WLB). The presence of the FRP increased the axial load carrying capacity between 4% and 14%. And bifurcation loads were increased as much as 17%. The improved response correlated with the effective increase in radius of gyration affected by the repair. In all specimens the presence of the FRP served to mitigate the 'kink' associated with inelastic buckling (Bruneau et al. 1998). In no case was FRP debonding observed until the post-peak applied load had fallen below 80% of the peak load attained and the lateral deflections of the stem tip exceeded 0.6 in. The slenderness of a compression member is a function of member length and radius of gyration. In Harries et al., the stem of the WT section is locally very slender and presents a specific region at which to concentrate the FRP retrofit application. Considering only the WT stem, the increase in weak-axis radius of gyration due to the application of the FRP ranged from 12% to 35%. This suggests the prospect of increasing stability on a local level.

Ekiz and El-Tawil (2008) demonstrated the use of a hybrid FRP system to inhibit inelastic buckling of a steel plate. In this study, the plate is first 'built out' with mortar, PVC or honeycomb core materials and then wrapped with CFRP. Cores ranging from 0.25 in. to 0.75 in. thick were used, effectively increasing the 0.25 in. steel plate thickness between 3 and 7 times. The performance of the strengthening scheme depended upon the strength and stiffness of the core material. Mortar performed best as it was less compressible than the PVC and honeycomb materials used. Provided the steel did not crush into the core material, improved performance was obtained when there was no bond between the core material and steel plate, allowing a strain discontinuity at this interface. This behavior is analogous to a buckling restrained brace in which the brace is debonded from the restraining shell (Black et al. 2004 and Xie 2004).

1.11.5 Mitigating Crippling Induced by High Local Stresses

FRP 'patches' have been demonstrated to reinforce thin-walled (thin-webbed) steel structures against the crippling effects of concentrated transverse and axial loads (Zhao et al. 2006; Fernando et al. 2009). Zhao et al. investigated the use of CFRP wraps and plates to improve the web crippling behavior of cold-formed rectangular steel sections subject to end crushing (Figure 25a). The specimens had 4 in. tall webs having thicknesses of 0.08 in., 0.12 in. and 0.20 in. resulting in web slenderness ratios, d/t_w, ranging from 50 to 20. The CFRP plates used had a thickness of 0.05 in. and a modulus of 23,900 ksi. Thus the effect of the bonded CFRP on the slenderness was equivalent to adding 0.04 in. of steel per CFRP plate[12]. The presence of the CFRP plates increased the crippling

[12] t_{FRP} *x* (E_{FRP}/E_{steel}) = 0.05 in. x 23900 ksi/29000 ksi = 0.04 in.

loads, however not to the same extent as simply increasing the steel web thickness. Importantly, Zhao et al. concluded that the presence of CFRP sufficiently mitigated web buckling to permit web yield and, in some cases, strain hardening behavior to develop. Based on the limited available research and the related research on inelastic buckling, it is felt that the effectiveness of such 'in plane' FRP patches is limited, most likely to cold-formed steel applications where the addition of the FRP represents a significant effect on local slenderness.

Okeil et al. (2009) proposed the use of adhesively bonded pultruded FRP sections as stiffeners for slender plate elements (Figure 25b). Okeil et al. focus on stiffeners for thin-webbed built-up steel sections and demonstrated that these may be designed in a manner similar to conventional steel stiffeners to control tension field action in such sections. Such adhesively bonded FRP stiffeners are common in both new design and repair applications in aerospace and marine applications.

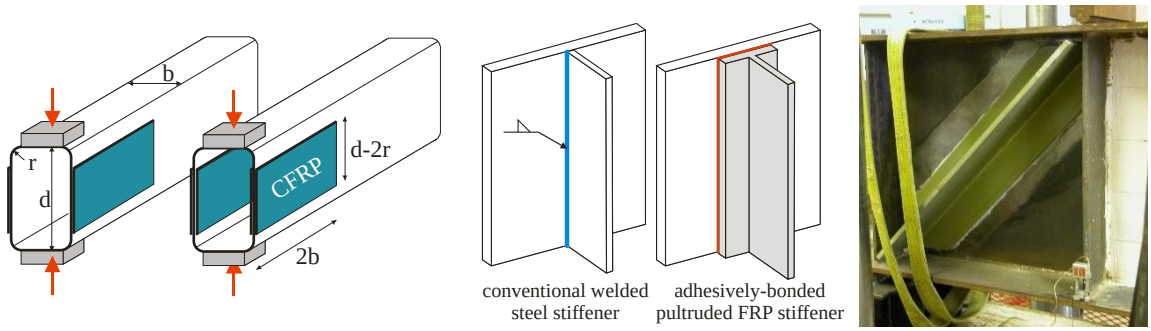

a) methods for mitigating crippling in thin-walled rectangular sections (after Zhao et al. 2006)

b) adhesively bonded FRP stiffeners (adapted from Okeil et al. 2010) (photo courtesy of Dr. Ayman Okeil)

Figure 25 Use of FRP to mitigate crippling associated with local loads and stress fields.

Thin-walled circular steel tubes and structures such as tanks subject to transient axial load, often resulting from seismic effects, are susceptible to so-called "elephant-foot buckling". Studies (Teng and Hu 2007; Nishino and Furukawa 2004; Haedir and Zhao 2011 and Bhetwal and Yamada 2012) have demonstrated that external FRP wraps can mitigate this mode of failure and enhance the ductility of the structure. Batikha et al. (2009) propose a method of reinforcing thin-walled cylindrical structures using adhesively-bonded FRP 'rib' stiffeners. Similar to the work of Okeil et al. (2009), such an approach is aimed at controlling tension field behavior.

1.11.6 Bond of FRP to Steel

An in-depth review and discussion of the bond behavior of FRP to steel is provided in Harries and Dawood (2012). A primary limit state in FRP-strengthened steel members is debonding of the FRP laminate. The thickness of the adhesive layer plays a significant role in the debonding failure as reported by Xia and Teng (2005) based on Mode II[13] tests. Typically, a thin uniform adhesive layer is desirable. Such adhesive layers of reasonable thickness (say less than about 0.08 in. thick) will generally debond in a relatively ductile manner. These relatively thin bond lines can be easily achieved in wet lay-up type applications due to the low viscosity of the adhesives used to impregnate the dry fibers. On the other hand, when using prefabricated plates or strips, more viscous adhesives are typically used and the need for clamping and bond line spacers should be considered. Thicker adhesive layers generally exhibit brittle delamination failures along the steel-adhesive interface. Xia and Teng have also shown that FRP-steel interfacial behavior with thin adhesive layers is accurately

[13] Reference to Modes is in terms of fundamental fracture mechanics. At a crack, Mode I is an opening displacement normal to the crack (peeling) and Mode II is a shear displacement along the crack (sliding). Mode III is out-of-plane tearing and will not be discussed.

modeled using a bilinear load-slip relationship. Additionally, debonding behavior for thin adhesive layers is closely related to adhesive tensile properties and is relatively independent of adhesive layer thickness.

Interfacial stress discontinuities occur at the termination of the adhesive layer. A variety of termination details, shown in Table 12, may be used to reduce these discontinuities (Stratford and Chen 2005). The use of a fillet, regardless of geometry, reduces Mode I stresses at the termination of the adhesive layer to approximately 60% of those present when no fillet is used. Mode II stresses are reduced to about 75%. Similarly, stepping multiple FRP plates has been shown to reduce both the Mode I and II stresses to about 80% of those resulting from not stepping the FRP layers. Finally, tapered plates result in Mode I and II stresses approximately 60% and 80%, respectively, of those of untapered plates. Plates having a reverse taper (i.e., increasing adhesive thickness at end) perform even better, having Mode I and II stresses, respectively, approximately 25% and 50% of those of untapered plates (Stratford and Chen 2005).

Table 12 Details at termination of adhesive layer and approximate stress concentrations.

Description	square	fillet			step	taper	
		straight	convex	concave		standard	reverse
Geometry							
Normalized Mode I stress	1.00	0.60	0.60	0.60	0.80	0.60	0.25
Normalized Mode II stress	1.00	0.75	0.75	0.75	0.80	0.80	0.50

Dawood et al. (2009) tested a series of spliced high-modulus CFRP laminates with different plate termination details. The test results indicated that providing a 20-degree reverse tapered plate end with a spew fillet approximately doubled the capacity of the spliced joint compared to a square plate end detail. Finite element analysis indicated that the reverse tapered detail essentially eliminated the Mode I stresses near the plate end, but had little effect on the magnitude of the Mode II peak stresses. Increasing the taper angle from 20 to 80 degrees increased the magnitude of the peak principal stresses by approximately 75%. The finite element analysis also indicated that the magnitude of the peak stresses is sensitive to the stiffness and thickness of the adhesive layer with stiffer and thinner adhesive layers exhibiting higher stresses.

1.11.7 Steel Substrate Preparation

Steel substrates generally form weakly adhered oxide layers (rust) which, if not removed, can be deleterious to adhesive bond performance. Effectively bonding to steel requires a clean and sound substrate. A typical application involves abrasive (grit) blasting – typically to SSPC-SP5 standard (2006) – followed within a few hours with a primer or conditioner to ensure that corrosion product does not reform and contaminate the newly exposed ‘white’ steel. Since epoxy adhesives are often used, the primer will typically be a compatible silane-based adhesion promoter.

Bourban et al. (1994), McKnight et al. (1995), and Karbhari and Shulley (1995) recommend the use of a silane primer; although no specific mechanical surface preparation was recommended. The results from this research are inconclusive as to whether the silane primer itself improved bond performance – it is possible that the primer enhanced bond performance simply by inhibiting the formation of corrosion product between the time of surface preparation and that of CFRP application. Dawood and Rizkalla (2010) demonstrated that the use of an organosilane primer improved bond durability in specimens exposed to severe environmental conditions for up to 6 months. Bond capacity after conditioning was improved up to 50% over unprimed control specimens.

Several studies have shown that a properly selected silane pretreatment can significantly enhance the moist durability of the interface between steel and epoxy adhesives (Gettings and Kinloch 1977; Gledhill et al. 1990; Walker 1991; West 2001; Sizemore et al. 2011). The effectiveness of a given

silane primer is sensitive to the silane concentration, nature of the solvent, pH, nature of the adherends, surface preparation, and chemistry of the adhesive. Previous studies generally indicate that a specific class of silanes, known as γ-GPS[14], are effective in enhancing the moist durability of the interface between grit-blasted steel surfaces and epoxy adhesives.

Sizemore et al. (2011) clearly showed the ability of an organosilane primer to improve the performance of CFRP-to-steel bond using an epoxy adhesive. The use of 0.5% silane in aqueous solution improved bond performance – measured by CFRP strain at debonding and steady state strain energy release rate (toughness) – by about 20% over control specimens having the same surface preparation without a primer. The aqueous solution provides the water necessary to hydrolyze the silane into its intermediary silanol form permitting the immediate formation of the polysiloxane film (Harries and Dawood (2012) provide a description of the chemistry of the reactions). Sizemore et al. also investigated the use a commercially available degreasing agent chosen because of its corrosion inhibiting properties. Specimens cleaned with this degreaser following surface preparation exhibited poor bond performance of only about 85% of that of the unprimed control specimens. Garden (2001) reports an *in situ* curved I-girder completely wrapped in CFRP; in this case no primer was used. Rather, silica gel packs were used to protect the prepared surface from moisture and corrosion following preparation and prior to FRP installation.

Preparation of the FRP substrate is typically less involved requiring only light abrasion (sanding) to provide a textured surface and cleaning with a mild solvent to remove dust and contaminants from the surface. In wet lay-up applications, the fiber fabrics should be kept clean and dry until they are impregnated with a saturating resin.

1.11.8 Environmental Exposure

Moisture, humidity and elevated temperature can all affect the behavior of a bonded FRP system, regardless of the substrate material to which it is applied. Moisture can enter a bonded joint by diffusion through the adhesive, wicking along the interfaces between dissimilar materials, capillary action along cracks or voids, or absorption through porous adherends. The presence of moisture can lead to degradation of the adhesive/adherend interface, or degradation of the bulk adhesive (Kinloch 1983). Some FRP materials are additionally susceptible to creep due to sustained loads and adhesive bondlines are susceptible to damage from cyclic (fatigue) loads (Harries 2005). Due to the electrical potential difference between steel and carbon, the presence of moisture can also drive galvanic corrosion of the steel. Glass fibers are not electrically conductive and may be used to mitigate galvanic corrosion when provided as a protective layer between the steel surface and CFRP layers (Miller et al. 2002, Cadei et al. 2004; Photiou et al. 2006). When used in conjunction with a steel substrate, some additional environmental protection may be accorded the FRP by the presence of a topcoat or finishing system.

1.11.8.1 Interfacial Attack

The theory of adhesion by physical adsorption (Owens 1970) suggests that adhesive bond is unstable in the presence of water. A number of studies (see previous section) have shown that a properly selected silane pretreatment can significantly enhance the moist durability of the interface between steel and epoxy adhesives. In general, no single set of parameters can be universally recommended to yield optimum durability for all types of bonded joints. Nonetheless, the use of γ-GPS has been shown to be, effective in enhancing the moist durability of the interface between grit-blasted steel surfaces and epoxy adhesives (Dawood and Rizkalla 2020; Sizemore et al. 2011)

1.11.8.2 Adhesive Degradation

Cured adhesives are generally porous, hydrophilic materials that are susceptible to significant moisture uptake in moist or humid conditions. Long-term exposure to moisture can lead to swelling (Hand et al. 1991), reduction of ultimate strength (Hand et al. 1991; Knox and Cowling 2000) and

[14] γ-glycidoxypropyltrimethoxy = $CH_2OCHCH_2O(CH_2)3Si(OCH_3)_3$

elastic modulus (Know and Cowling 2000; Lapique and Redford 2002), and depression of the glass transition temperature (De Neve and Shanahan 1992) of many common adhesives. Moisture absorption can also lead to increased toughness (Crasto and Kim 1996), ductility, and ultimate strain capacity (Lapique and Redford 2002). Exposure to elevated temperatures may lead to further cross-linking of polymeric adhesives (so-called 'post cure') which can increase the strength, stiffness, and glass-transition temperature of the adhesive.

The properties of the adhesive in the highly stressed regions near FRP termination points are particularly important to the overall performance of FRP strengthening systems. Under constant strain conditions, swelling of adhesives can lead to relaxation of stresses of up to 90% (Hand et al. 1991). Additionally, the reduction of the elastic modulus of the adhesive in this region can lead to redistribution of stresses thereby reducing the magnitude of stress concentrations. These potentially beneficial effects can be offset by the reduction of adhesive ultimate strength. The complex nature of adhesive aging under environmental exposure leads to increased uncertainty in the adhesive properties and the state of stress at critical locations. Consequently, it is preferable to prevent moisture absorption into the adhesive to the extent possible.

1.11.8.3 Galvanic Corrosion

Galvanic corrosion is the accelerated corrosion of a less noble material (anode - steel) when coupled with a more noble material (cathode - carbon). Steel and carbon are sufficiently separated in the galvanic series to drive a galvanic current (Francis 2000). In order to minimize the potential for galvanic corrosion it is necessary to prevent exposure to moisture and/or to electrically isolate the carbon and the steel from one another.

Mechanically fastened connections between steel and CFRP have exhibited notable corrosion with obvious localized build-up of corrosion product around the edges of the CFRP (Brown 1974). Painting the assemblies with epoxy paint reduced but did not eliminate the corrosion of the joints. In contrast, adhesive-bonded joints – providing electrical isolation between the two materials – did not exhibit any localized accelerated corrosion. Subsequent testing of mild structural steel coupled to carbon fibers representative of those used in structural applications indicated that the corrosion rate was sensitive to the thickness of the adhesive coating (Tavakkolizadeh and Saadatmanesh. 2001). Other researchers suggest that embedding a thin layer of glass fiber within the adhesive layer can provide a more reliable electrical barrier (Miller et al. 2002, Cadei et al. 2004; Photiou et al. 2006). Test results also indicate that embedding a glass fiber layer within the adhesive helped to increase the initial strength of CFRP-to-steel bonded joints (Dawood and Rizkalla 2010). However, after six months of accelerated environmental degradation, joints with and without embedded glass fibers exhibited comparable levels of strength degradation. Furthermore, few materials retain their insulating properties after exposure to environmental conditions for more than a few years (Sloan and Talbot 1992).

1.11.8.4 Temperature Effects on Bond Behavior

Relatively little research has been conducted to evaluate the effect of thermal variations on the behavior of steel structures strengthened with FRP materials. Elevated temperatures can reduce the stiffness and strength of adhesive materials. In contrast, extremely low temperatures can increase the stiffness of typical adhesives and may also result in embrittlement. Several analytical studies indicate that the magnitude of thermally induced bond stresses can exceed the stresses induced by mechanical loading (Schnerch 2005; Stratford and Cadei 2006). It has been shown that short-term exposure to freezing temperatures has little effect on the tensile response, ultimate strength, and failure mode of CFRP-to-steel bonded joints (Al-Shawaf et al. 2006). In contrast, short-term thermal cycling between -4°F and 122°F) followed by short-term exposure to salt spray markedly reduced the ductility of bonded joints although little effect on the ultimate strength was observed (Colombi et al. 2005).

1.11.8.5 Fatigue Performance of Bond

O'Neill et al. (2007) investigated the behavior of typical adhesive systems subject to fatigue conditioning. The adhesives considered all had measured monotonic shear capacities between 1750 and 2320 psi although their shear stiffnesses differed by a factor of twenty. Fatigue conditioning consisted of 1000 cycles at a stress range from 10% to 60% of the monotonic shear capacity followed by a monotonic test to failure. Degradation of the ultimate shear stress was apparent for all adhesive types tested. O'Neill et al. conclude that for relatively low fatigue stress ranges, a stiffer adhesive will exhibit minimal degradation. At higher stress ranges, however, degradation should be expected and a softer adhesive will provide greater ductility and may be expected to behave in a more predictable manner. In general, the fatigue resistance of steel beams repaired with CFRP plates has been found to be at least equal to that of plain steel beams (Miller et al 2001; Dawood et al. 2007; Harries et al. 2010).

1.11.9 FRP Repair of Corroded Beam Ends

In the only known study of its kind, Wakabayashi et al. (2013) proposed and demonstrated a CFRP repair of corroded beam ends. The proposed system is shown schematically in Figure 26. Two repair scenarios were demonstrated. The first, shown in Figure 27 involved restoring the bearing capacity of corroded bearing stiffeners. The design (uncorroded) capacity of the specimen was 431 kips. Artificially induced (machined) corrosion reduced this to 377 kips. The CFRP repair shown in Figure 27 restored the capacity to 448 kips.

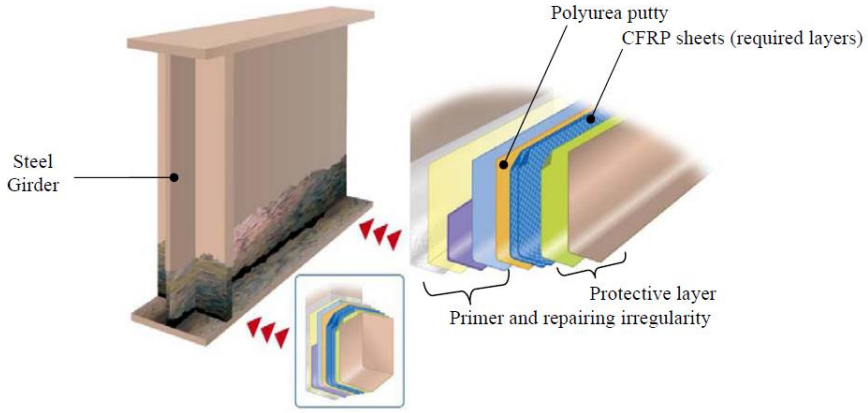

Figure 26 Schematic representation of CFRP repair of corroded beam end (Wakabayashi et al. 2013).

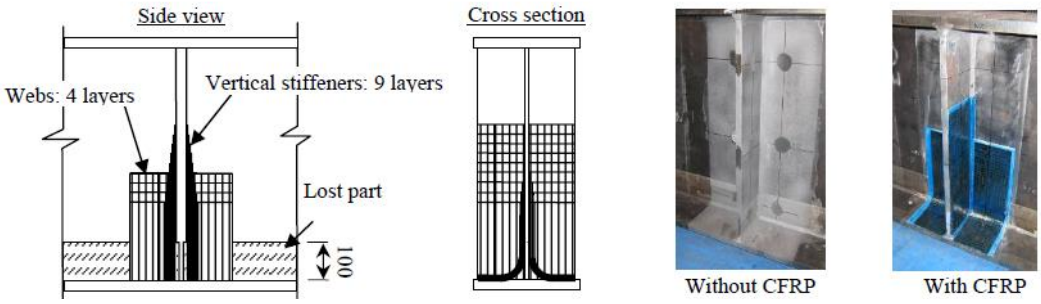

Figure 27 CFRP repair of corroded bearing stiffener arrangement (Wakabayashi et al. 2013).

The second scenario demonstrated by Wakabayashi et al. is the loss of shear capacity resulting from a corroded hole at the web-bottom flange interface (Figures 28a and b). The repair is seen in Figure 28c and the details shown in 28d. The section is 51.2 in. deep having a 0.32 in. thick web. The beam was tested with a 51.2 in. shear span over a 25.6 ft simple span. The resulting load displacement curves of

the uncorroded, deteriorated and repaired girders are shown in Figure 28e. The shear buckling capacity of the undamaged section was 312 kips. The damage shown in Figure 28b resulted in a reduced capacity of 262 kips. The repair restored the capacity to 332 kips.

a) prototype corrosion damage

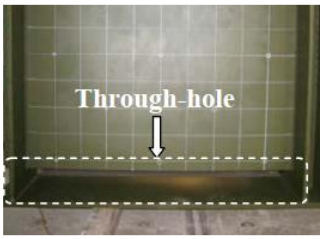

b) simulated test girder

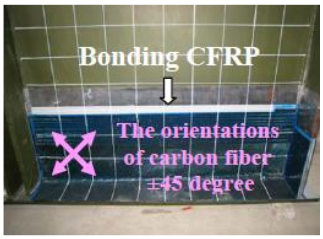

c) CFRP repair

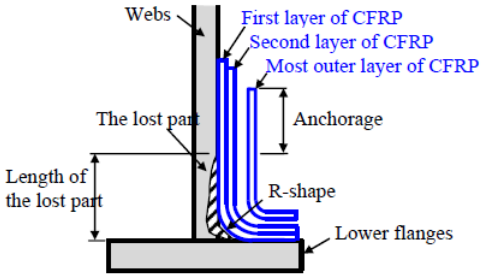

d) details of CFRP repair

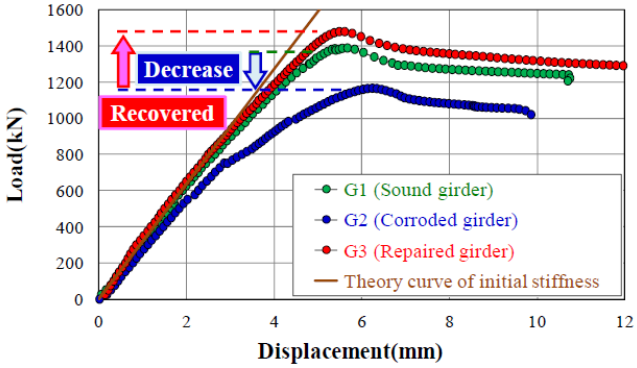

e) load displacement relationships

Figure 28 Shear repair of corroded beam end using CFRP (Wakabayashi et al. 2013).

1.11.10 Stay-in-Place FRP Forms

The constructability of concrete encasement applications may be improved using stay-in-place forms. Such forms may permit simpler installation (since they do not need to be removed) and eliminate the step of stripping the forms. Stay-in-place forms also enhance the durability of the encased concrete (Ringelstetter et al. 2006). Such an approach has been seen in Pennsylvania applications (see Figure 9c). Steel plate stay-in-place forms are not recommended as these corrode and do not permit any inspection of the encased concrete. Light-weight glass fiber panels may provide an alternative. These will serve as forms, are noncorrosive and can be sufficiently 'transparent' to reflect or make visible significant distress in the encased concrete.

1.12 Summary of Key Findings of Literature Review

This section summarizes key findings of the literature review in the context of the objective of this project. That is, to investigate practical repair methods using high performance and traditional materials which can be applied to corroded and/or damaged steel girder ends in their *in-situ* state.

1.12.1 Scope of the Issue and Extant Conditions.

Observed corrosion damage follows well known patterns: beam end corrosion is associated with leaking expansion joints and is most prevalent at bottom flange-to-web interfaces where debris accumulates, trapping moisture.

Gerasimidis and Brena (2019) report an extensive review of 164 bridges (808 damaged beam ends) in Massachusetts. This dataset is used to characterize beam end damage as described in Table 1. With some modification, this characterization is adopted in the present study. In the large dataset reported by Gerasimidis and Brena, the damage was dominated by patterns W1 and W2 and the extent of the

damage generally confined to the lower third of the web. Only 15% of samples are reported to have 100% section loss at some locations.

A non-random sample of 15 Pennsylvania bridges (145 beam ends) was reviewed for this study. 100% section loss was common and girder section distortion resulting from this was identified. The proliferation of embedded bearing regions having significant damage at the face of the embedment was also noted. The embedded bearing detail, however, is limited to short span structures having relatively shallow rolled girders. The concerning condition of some of the Pennsylvania bridges reported in this study is reflective of the request for examples made by the research team rather than of the overall condition of steel bridges.

Having established relatively consistent patterns of beam end corrosion damage, the residual capacity of the bearing region must be established. Web shear (Eq. 1), web yield due to bearing (Eq. 5), and web crippling (Eq. 6) are the primary limit states of concern. The residual capacities in each case are found using the AASHTO-prescribed equations and the existing (reduced) web plate thickness, t_w, or t_{wc} as defined for Eq. 1 or Eq 5 (and 6), respectively. Other limit states are evident in the review – in particular flange distortion – although these result from the loss of web bearing capacity and are therefore not primary limit states.

There is limited experimental and some analytical study of the behavior of corroded beam end regions. Due to the nature of corrosion damage, the utility of studies that assume essentially uniform [machined] damage is limited and difficult to generalize. Nevertheless, the existing studies largely validate the AASHTO-prescribed limit state equations described above. Given the typical damage being more severe at the lower web-flange junction, web yield (Eq. 5) tends to dominate behavior. Such behavior, if extreme, can result in distortion of the girder as described in relation to Figures 5 and 6 and will result in the affected bearing region carrying essentially no load. The key to a good prediction is a good record of section loss.

1.12.2 Analytical Modeling Beam End Regions

A number of studies have reported finite element (FE) simulations of beam end corrosion behavior. All studies report quasi-static nonlinear analyses and focus on web buckling behavior. In general, the models reported in the literature provide details (or restraints/constraints) that will mitigate local bearing effects. The latter, however, are critical to corroded end region behavior, resulting in most extant studies having little relevance to the present study. Gerasimidis and Brena (2019), however, report an extensive validation and parametric study focused on local effects, neglecting buckling (Section 1.5.1). The development and details of this model are most relevant to the present study. The modeling effort conducted for the present study (Chapter 4) will leverage the extensive validation provided by Gerasimidis and Brena.

1.12.3 State of Practice of Structural Repair of Beam End Corrosion Damage

The current state of practice for structural repair of beam ends is the complete replacement of the affected region as shown schematically in Figure 11. For localized damage, bolted or welded steel patches and/or doubler plates, as shown in Figure 12, are used. Extended encasement of beam end regions in conventional concrete has also been observed for beams having embedded bearings. This latter approach is, in many ways, analogous to adding a corbel although within the depth of the beam.

1.12.4 Partial Encasement of Beam End Corrosion Damage

Reported in Section 1.8, an extensive study (Zmerta 2015, Kruszewski 2018 and McMullen 2019), demonstrated the efficacy of partially encasing damaged beam ends in ultra-high performance concrete (UHPC). McMullen proposes recommendations for such UHPC encasement; although in some cases, provides no justification for the details proposed. There are two significant limitations of this series of studies: a) conclusions are limited to ultimate limit state (overload) performance; and b) the study makes no comparison with other methods of repair or other encasement materials.

Encasement relies on transfer of beam forces to the encasing concrete using shear connectors (studs or similar connections as shown in Figure 23). Considering the confined region over which this transfer takes place and the necessary use of small stud diameters, the recommendations of Provines et al (2019) are very relevant to beam end region repair. In particular, adoption of Eq. 12 is recommended. The consideration of non-welded shear connectors should also be made to avoid the need for applying a large number of welded studs in a relatively confined space. Finally, it is noted that due to the nature of welding shear studs to the thin webs of damaged girders, quality control testing of the studs is likely impractical.

Section 1.9 summarizes other materials that may be equally as efficient as UHPC in partial encasement applications. These include: a) high strength concrete (HSC); b) fiber reinforced concrete (FRC); c) fabric-reinforced cementitious matrix (FRCM); and d) latex-modified concrete (LMC). EVA, SBR and PVA latex polymers at varying dosages in LMC have shown promise by enhancing the bond between the concrete and steel plate. Such adhesion will be critical for the long term durability of encasement repairs.

1.12.5 Fiber Reinforced Polymer Repair of Beam End Corrosion Damage

The use of fiber reinforced polymer (FRP) materials to address various aspects of steel degradation have been demonstrated (Section 1.11). In terms of beam end repair, using adhesively bonded FRP plates or sections (see Figure 25) is analogous to welded or bolted patch repairs. Such repairs can strengthen and provide stability to a deteriorated steel web. The advantages of FRP over steel repairs are that FRP repairs are a) corrosion resistant; b) lighter; c) easier to rapidly customize in the field using hand tools; and d) require no hot-work in a confined area. With proper adhesive selection and substrate preparation, the durability of the interface between FRP and steel is enhanced. There is only one known study demonstrating CFRP (carbon FRP) repair of a corroded beam end: Wakabayashi et al. (2013) demonstrated the complete restoration of capacity of a bearing region having 100% section loss along the web-to-flange interface.

1.12.6 Effect of Existing Load

The objective of providing a repair without requiring temporary support has an inherent implication that the existing structure is adequate to resist whatever loads are present during the repair (and subsequent curing, if applicable) procedure. Without pre-loading, prestressing or post-tensioning of some kind, any repair scheme is only able to partially resist loads applied after its installation. Repairs that are called upon to resist any portion of the bridge self-weight, for instance, must have this load relieved during installation.

2 Archetypal Damage and Repair Strategies

2.1 Selection of Archetypal Damage

Section 1.6 and Appendix A provide a snapshot of beam end corrosion conditions in Pennsylvania. Bridges ranging in size from short single lane bridges on rural roads to bridges carrying interstate traffic were reviewed taking in 145 beam ends over the 15 bridges. The degree of section loss reported varies from minor superficial corrosion to 100% section loss. Indeed, all but three bridges exhibited some degree of complete web section loss (holes through web). Many of the beams also exhibited notable bottom flange section loss. Where bearing stiffeners were present, these exhibit essentially the same damage as the web to which they are attached. The observed corrosion damage follows the expected patterns: beam end corrosion is associated with leaking expansion joints and is most prevalent at bottom flange-to-web interfaces where debris accumulates, trapping moisture. The presence of a bearing stiffener may make this problem worse, although the stiffener also provides greater capacity to the bearing region.

Six of the reviewed structures were relatively short span structures having their beam ends and bearings fully embedded into concrete end diaphragms. In these cases, it is likely that most of the damage is concentrated immediately inboard of the bearing. Such embedded beam ends represent a special case of beam end corrosion and will require additional considerations for repair.

A few reports identified distortion of the corroded girders at the end bearings. This is a special case that may accompany relatively severe section loss. Any structural repair undertaken of a distorted girder should first correct the distortion.

Three archetypical damage cases were selected from the review of Pennsylvania data. The cases were also selected to capture the range of girder dimension and end region details present in the data. Two conventional bearing regions – one stiffened plate girder (case I) and one unstiffened rolled section (case II) – were selected. Each of these had 25% loss of section damage over the bearing and extending about 36 in. from the girder end. For simplicity, the assumed loss of section is best described as Pattern W3 (see Table 1). Additionally, a region of 100% web loss above the bearing (Pattern M1) is also provided. A single embedded beam end (case III) is considered. This girder has 25% section over most of its depth at the face of the embedment (Pattern E-W5) and 100% web loss near the bottom of the section (Pattern E-M4). It is assumed that the 25% section loss penetrates into the embedment about 2 in. but that the bearing area itself is unaffected. Although the consideration of embedded bearings (case III) is beyond the experimental and analytical scope of this project, they are discussed in this chapter in the context of potential repair strategies.

Each damage archetype is based on a Pennsylvania example reported in Appendix A and is shown in Figure 29. The damage is intended to be representative of severe – although potentially repairable – damage. Additionally, consideration is given to the ability to physically scale the archetypes for later laboratory investigation. Table 13 summarizes the as-built (i.e., uncorroded) and as-is (i.e. residual corroded) capacity of the girder ends. Details of the calculations are provided in the Section 1.3.

A few behaviors should be noted in Table 1.

a) Bearing stiffeners (see Section 1.3.4) mitigate web yield and crippling but may, themselves by damaged. In such a case, web yield and crippling may become relevant limit states.
b) Similarly, embedment of the end region provides lateral support for the web and mitigates web crippling. Embedment may also enhance the web yield capacity although this is less clear.
c) The bearing of embedded end regions is believed to be relatively unaffected by corrosion; therefore, bearing capacity at the location of the as-built bearing is unaffected by damage.

I
stiffened
plate
girder

Bridge D

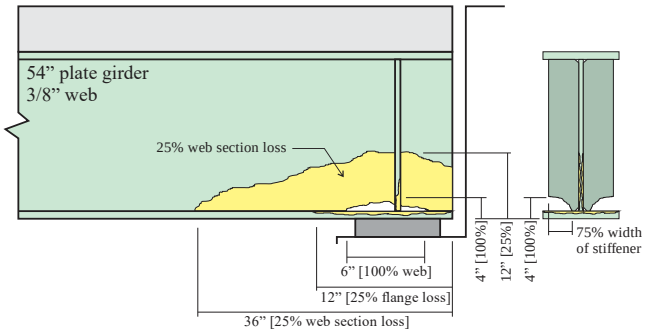

II
W24x76

Bridge M

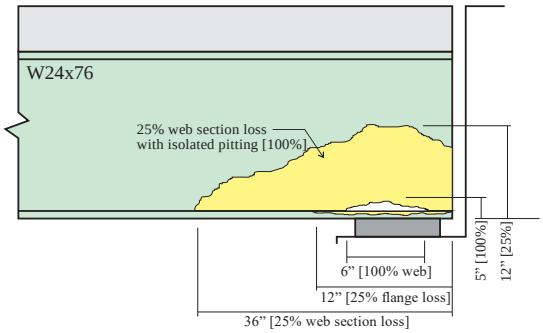

III
embedded
W18x60

Bridge A

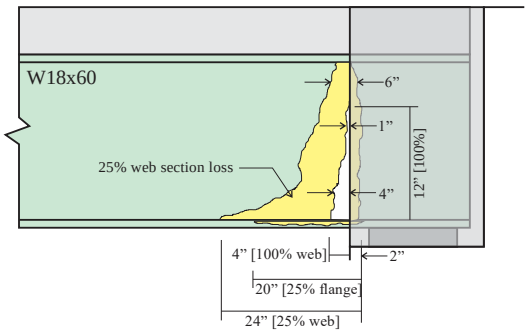

Figure 29 Archetypal damage cases.
(see Appendix A for bridge details)

Table 13 Bearing region capacities of archetypal damage cases
(values in bold indicate limiting capacity; those in parentheses indicate normalized residual capacity)

			I (54" plate girder)		II (W24x76)		III (18x60)	
			as-built	as-is	as-built	as-is	as-built	as-is
web shear (Eq. 1)	F_y	ksi	36[a]		50[a]		50[a]	
	D	in.	54	50	23.9	19	18.2	6
	t_w	in.	0.375	0.28	0.44	0.33	0.415	0.31
	k		5		5		5	
	C		0.49	0.36	1.00	0.83	1.00	1.00
	V_{cr}	kips	**186**	80 (0.43)	305	182 (0.60)	219	**54** (0.25)
web yield (Eq. 5)	N	in.	10		8		6	
	K	in.	1.25[a]		1.18		1.15	
	t_{wc}	in.	0.375	0.21	0.44	0.22	0.415	0.22[d]
	$R_{n,yield}$	kips	177[b]	99[b] (0.56)	241	120 (0.50)	**184**	98[d] (0.53)
web crippling (Eq. 6)	d	in.	56		23.9		18.2	
	t_f	in.	1.0[a]	0.75	0.68	0.51	0.695	0.52[d]
	N/d		0.14		0.33		0.33	
	$R_{n,crip}$	kips	106[b]	37[b] (0.35)	**185**	**47** (0.25)	163[c]	47[c,d] (0.29)
bearing stiffeners (Eq. 7 and 8)	b_{sb}	in.	7	1.75	-		-	
	t_{sb}	in.	0.625	0.47	-		-	
	R_{sb}	kips	394	**47 (**0.12)	-		-	
	P_{sb}	kips	315	59 (0.19)	-		-	
retrofit capacity required assuming **NO** load sharing		kips	186		185		184	
retrofit capacity required assuming load sharing		kips	V_{cr}: +87 R_{sb}: +139		V_{cr}: +3 $R_{n,yield}$: +65 $R_{n,crip}$: +138		V_{cr}: +130 $R_{n,yield}$: +86 $R_{n,crip}$: likely OK	

[a] assumed value
[b] bearing stiffeners mitigate this limit state
[c] embedment mitigates this limit state
[d] calculation based on bearing at the damaged region; typically the bearing region is relatively unaffected; therefore bearing capacity at the location of the as-built bearing is unaffected.

2.2 Sample Designs

It is not possible to assess the demand on the bearing region without *in situ* bridge context. Where bearing stiffeners have been provided, it may be reasonable to assume that the demand is close to the as-built capacity of the beam. In any case, assuming correct original design, it is conservative to take the controlling as-built capacity as the demand on the bearing region; this is done here. In many cases, this may be remarkably conservative since the selection of the beam is likely driven by flexural demand at midspan and the as-built shear capacities shown in Table 13 are not required to restore the capacity of the bridge structure itself. Thus, the calculation presented in this Chapter are 'worse case scenarios'.

Some repair approaches will permit a degree of load sharing between the as-is structure and the retrofit provided. In such a case, the demand on the retrofit is the difference between the residual as-is capacity and as-built capacity. Retrofit demand can become unclear when different limit states control capacity in the as-built and as-is condition. Once again, conservatively, the retrofit can be designed to carrying 100% of the as-built capacity. In this instance, all actions are considered.

The efficacy of the retrofit and its degree of load sharing are also functions of the *in situ* loading *during* the retrofit installation. For the examples presented in this Chapter, it is assumed that the beam end is entirely relieved during retrofit. Thus 100% of the combined residual and retrofit capacity of

the beam is available post-retrofit. Furthermore, the calculations provided consider only the ultimate limit state (typically the AASHTO STRENGTH I load combination).

The following sections present illustrative examples of repairs of the damage cases presented in Figure 29. A summary of damage-repair pairs is summarized in Table 14. The calculations presented in the following sections are incomplete and simplified. They are not intended to provide definitive designs but to assess the viability and limitations of each repair scenario while highlighting some key issues.

Table 14 Example repairs and the section number in which they are presented.

	repair technique								
Section	2.3.1	2.3.2	2.3.3	2.3.7	2.3.8	2.3.9	2.3.11	2.3.11	2.3.11
archetypal damage	conventional bolted steel	UHPC encasement	normal strength concrete encasement	adhesively bonded FRP	bonded wet lay-up FRP	adhesively bonded steel plate	corbel repair of embedded bearing	embedded repair of embedded bearing	steel splice repair of embedded bearing
I	2.3.1.1	2.3.6	2.3.6	2.3.7.1	r.n.a.		r.n.a.	r.n.a.	r.n.a.
II				2.3.7.2	r.n.a.		r.n.a.	r.n.a.	r.n.a.
III		r.n.a.	r.n.a.		r.n.a.		2.3.11.1	2.3.11.2	2.3.11.3
membrane only					2.3.8.1		r.n.a.	r.n.a.	r.n.a.
r.n.a.: repair technique not applicable to damage case									

2.3 Repair Strategies

A number of potential strategies were identified in Chapter 1. In this section, these are introduced in relation to the three archetypal damage cases. Not all strategies will be applicable to each case.

The following assumptions are made in this Chapter:

Assumption 1: The proposed structural repairs presuppose mitigation of the primary source of damage: leaking joints. All repairs have 'boundaries' with the existing steel. Regardless of material or detail, these are regions of potential crevice corrosion. The source of water and debris must be mitigated for any repair to have a reliable performance and lifespan. It is understood that the 'microclimate' occurring near the bearing regions of some bridges cannot typically be mitigated.

Assumption 2: Physical distortion of the beam end web (an example is shown in Figure 5) should be corrected prior to strengthening. Distortion is especially expected if web crippling is dominating behavior. Flexural distortion (Figure 6) must be considered as to its effect on the repaired beam end and corrected as required.

Assumption 3: Prior to repair installation, all corrosion product is removed. This is typically specified as "power tool clean and free of loss material" [SSPC-SP3]. If adhesives are to be used, "white metal blast cleaning [SSPC-SP5] is typically required.

Assumption 4: Although this assumption will be discussed in greater depth in Sections 2.4 and 2.5, typically it is assumed that beam end repair will accompany bearing replacement. This being the case, it is assumed that the girder may be lifted in order to permit some transfer of self-weight to the repair material upon lowering the girder back into place.

2.3.1 'Conventional' Bolted Steel Repair

A 'conventional' repair of beam end corrosion damage involves welding or bolting steel plates or sections (typically angles) to the existing section. This is summarized in Section 1.7.

Considering the capacities shown in Table 13, it is clear that providing a new bearing stiffener, or restoring the capacity of an existing bearing stiffener, will restore considerable capacity to the beam end primarily by mitigating the web yield and crippling limit states. Considering Case II, the residual shear capacity (190 kips) exceeds the as-built limiting capacity (web crippling = 185 kips). This suggests that the addition of an effective bearing stiffener may be sufficient to restore the capacity of this girder.

Conventional steel repair is well suited for small localized damage as the attached plates can span the damage. Larger regions of deterioration, however, require consideration as to whether the remaining sound steel substrate is suitable for bolting or welding.

The Research Team is aware of the repair conducted for Case I[15] – this is shown in Figure 30. This repair is well suited to the deep exterior girders of this bridge (Figure 29).

2.3.1.1 Pros of Conventional Bolted Repairs

In most cases, new member thicknesses are matched to existing member thicknesses and conventional grades of structural steel (36 ksi and 50 ksi) are adequate, greatly simplifying the design process. Plate bending and hole drilling are common fabrication processes which require no specialized tooling and can be done in a fabrication shop, reducing field work. Contractors are familiar with this type of repair method and no specialized tooling or labor are required. Design bases for steel are well established permitting quantitative designs to be executed.

2.3.1.2 Cons of Conventional Bolted Repairs

Field drilling or welding existing members *in situ* is required and may be affected by limited access. Bolting or welding to existing reduced sections needs to be considered and, particularly, the amplitude of the steel surface may affect the efficacy of connections. Optimally, connections should be made to sound steel and the repair designed to span the damaged region. This may lead to the need for heavier plates or stiffened repair elements.

Steel-to-steel joints must be properly sealed to avoid future issues with crevice corrosion (pack rust). Once again, if the cleaned steel does not have a typically 'smooth' surface, sealing this joint becomes more critical and more difficult.

Handling and inserting larger steel elements in the confined space of a beam end region may pose a challenge in some instances.

2.3.1.3 Conventional Bolted Steel Repair of 54-in. Deep Plate Girder (Case I)

This is perhaps the simplest retrofit. It is clear that the bearing stiffener must be replaced and the corroded web reinforced to safely resist 208 kips shear. With an adequate bearing stiffener, web yield and crippling limits states may be neglected.

Upon removal of the existing damaged bearing stiffeners, new angle stiffeners may be bolted to the section. Using the selection tables in the AISC *Steel Construction Manual* (SCM), A pair of L6x4x$^{7}/_{8}$ SLBB will resist 220 kips and provide ample room to bolt to the web. The new stiffeners must bear on the flange above the bearing and may therefore require an end plate. This detail is shown in Figure 30c which shows a pair of L9.5x5x$^{3}/_{4}$ SLBB stiffeners having a much greater capacity. Similarly, the damaged web and bottom flange can be 'patched' using a pair of $^{3}/_{8}$ in. plates (one on each side of web) bent into an angle as shown in Figure 30b. The repair shown in Figure 30 uses ½ in. plates, again highlighting the ease in which these repairs can be made to be conservative in nature.

[15] Jason Mash designed this repair in his role as a consulting engineer.

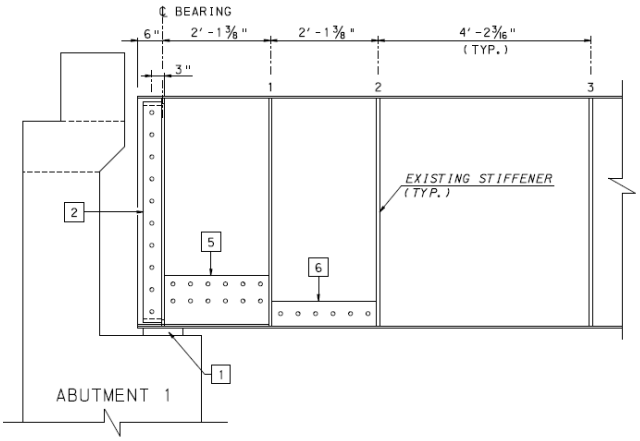

a) bearing region repair

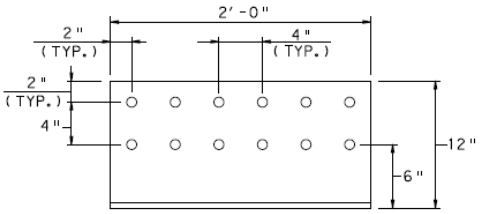

b) Repair 5 shown in Figure a

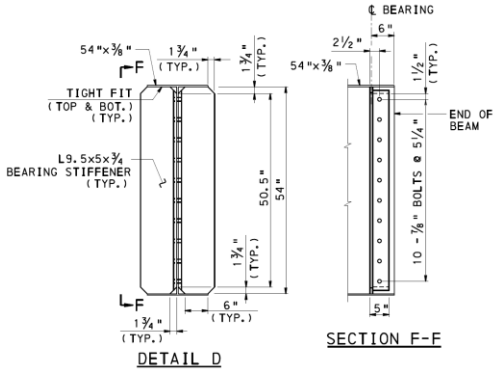

c) Repair 2 shown in Figure a

Figure 30 'Conventional' steel repair for damage Case I.

2.3.2 UHPC Encasement

This method has been demonstrated by McMullen and Zaghi (2020), and Zmerta et al. (2017) and is described at length in Sections 1.8. UHPC encasement simultaneously provides a compressive strut to resist shear at the beam end and provides stability to the web. The method, shown in Figure 14 applied to a W21x55 section, involves partially (typically) or fully encasing the girder web in ultra-high performance concrete (UHPC). Composite behavior is assured by the use of shear studs located in sound regions of the web. McMullen and Zaghi (2020) report that partial depth repairs may be susceptible to web crippling at the edge of the repaired region (see Figure 18c).

2.3.2.1 Pros of UHPC Encasement

The durability of UHPC is greater than conventional concrete and realistically no cracking of the fiber-reinforced UHPC should be expected. McMullen (2019) reports that vibrations do not affect UHPC compressive strength[16]. Although not demonstrated, it is easy to envision how such UHPC encasement can address both girder and bearing deficiencies in a single operation. McMullen (2019) provides design recommendations for UHPC encasement repairs; these are reported in Section 1.8.3.2.

2.3.2.2 Cons of UHPC Encasement

Hot work is required to weld the shear studs to the existing girders (see Section 1.10.1 for alternatives). UPHC is a proprietary product: it is expensive, and requires special handling during

[16] The Research Team disputes the validity of this conclusion. A single girder tested by McMullen was subject to vibrations having a maximum acceleration of 0.002g for the initial six hours of cure. Such vibratory loading fails to duplicate the cyclic *strains* associated with actual traffic loads.

mixing and placement. Potentially complex (Figures 14b and 19b) and water proof formwork is required and all but partial encasement of deep webs will likely require top-down access through the bridge deck to place UHPC. Design recommendations are prescriptive, providing no means of calculating the effect(s) of strengthening.

2.3.3 Concrete Encasement

While UHPC may work well for deteriorated beam end repair, it is expensive and may prove difficult to implement without specialized equipment and contractors. Other variations of high-performance concrete (HPC), however may be viable alternatives; these are described in Section 1.9. Encasement in concrete materials other than UHPC differs only in that a reinforcing bar cage is likely required to provide adequate crack control (Kruszewski (2018); see Section 1.8.5). For this reason, full depth encasement is likely necessary.

The Research Team contends that encasement with a good quality concrete (say a AAA mix having specified strength equal to 5 ksi) will be adequate to restore strength and stability to damaged beam ends. Durability can be enhanced using modified mix designs and/or adding fiber.

2.3.3.1 Pros of Concrete Encasement

High-performance [non UHPC] materials, such as fiber-reinforced, latex-modified, or hybrid concrete materials are often better established in industry and represent only a marginal cost premium over conventional concrete [and a considerable savings compared to UHPC].

2.3.3.2 Cons of Concrete Encasement

Providing shear studs (Section 1.10), reinforcing bar cages and potentially complex formwork is required. Full depth encasement will likely require top-down access through the bridge deck to place. Once again, design will be largely prescriptive in nature.

2.3.4 Stay-in-place Forms

The constructability of concrete encasement applications may be improved using stay-in-place forms. Such forms may permit simpler installation (since they do not need to be removed) and eliminate the step of stripping the forms. Stay-in-place forms are discussed in Section 1.11.10.

2.3.5 Shear Studs for Concrete Encasement Repairs

Encasement repairs require shear studs. For a beam end repair, this requires ‘hot’ work on a vertical surface in a confined space. Additionally, studs need to be installed on sound steel; their capacity will be significantly affected if applied to uneven surfaces such as are likely in corroded end regions.

Bolted shear studs (Figure 23) mitigate the need for hot work and are equally effective provided net section through the root of the thread is used as the stud area, A_{sc} (Kruszewski 2018; Pavlovic et al. 2013). Since web plates are typically relatively thin, installation can be made with a hand drill; for larger installations, a small magnetic-base drill can be used. Holes for bolted studs should not be over-sized.

Although concrete-dowel connections have been demonstrated, their efficacy for thin webs is uncertain. However, a concrete dowel is naturally formed in regions of full section loss. Placing a small diameter reinforcing bar through larger web holes should enhance continuity over larger areas of section loss (Figure 23, right side).

2.3.6 Concrete Encasement Repairs of 54-in. Deep Plate Girder (Case I)

Since the bearing stiffener requires replacement, a full-depth encasement is proposed. The concrete must be sufficiently strong to replace the stiffener and should be similarly stiff. It will be easiest to form the encasement against the beam flanges making a ‘stub column’ over the bearing, thus it will be assumed to be 16-in. wide and the length of the bearing (8-in.) long; making 128 in^2 of concrete. This replaces a pair of 7 x $^5/_8$ stiffeners.

The existing stiffeners have a capacity of 315 kips although only 186 kips is required. To achieve the former with the concrete stub column acting in bearing, a concrete compression capacity of only 2.5 ksi is needed. Furthermore, the concrete area is 14 times that of the steel it is replacing and thus will be axially stiffer. The typical ratio of $E_{steel}/E_{concete}$ is 7 to 8 and falls for higher strength mixes.

Assuming a full depth concrete encasement, the shear stress resisted by the concrete is 186/(16 x 54) = 0.22 ksi. Neglecting the presence of confining reinforcement, and assuming the shear strength of concrete to be $0.06\sqrt{f_c'}$ [ksi][17], a very high strength concrete, having $f_c' > 14$ ksi is required. This would suggest the need for UHPC encasement.

However, the large flange width should easily accommodate the inclusion of internal shear reinforcement and permit more refined design calculations. For instance, including #3 closed hoops on each side of the beam web spaced at 6 in. provides a shear component, V_s = (4 x 0.11 x 60 x 50/6) = 220 kip[18], making conventional concrete practical.

Finally, the concrete encasement and steel beam must be made composite. The shear carried by the beam web must be redistributed to the encasing concrete. This will be partially accomplished through concrete strut action anchored by the flanges but will also require studs be located along the web. Assuming the use of $^5/_8$-in. bolts (Figure 23) having a net section area of 0.22 in^2 and using a rupture strength of 75 ksi, the capacity of a single stud is 11.5 kips (Eq. 12); requiring only 20 studs to develop the required shear force.

Schematic examples of the resulting encasement details are shown in Figure 31. Because complete encasement is needed, top-down concrete placement is not possible. Figure 31 shows one approach that may be used to place concrete with a pump. In this arrangement, vibration of the concrete can be made through the formwork, using a form vibrator. The use of self-consolidating concrete (SCC) is also a promising approach for such applications.

Finally, the design of the embedment region may be better suited to a strut and tie approach. In this case, some additional efficiencies may be realized.

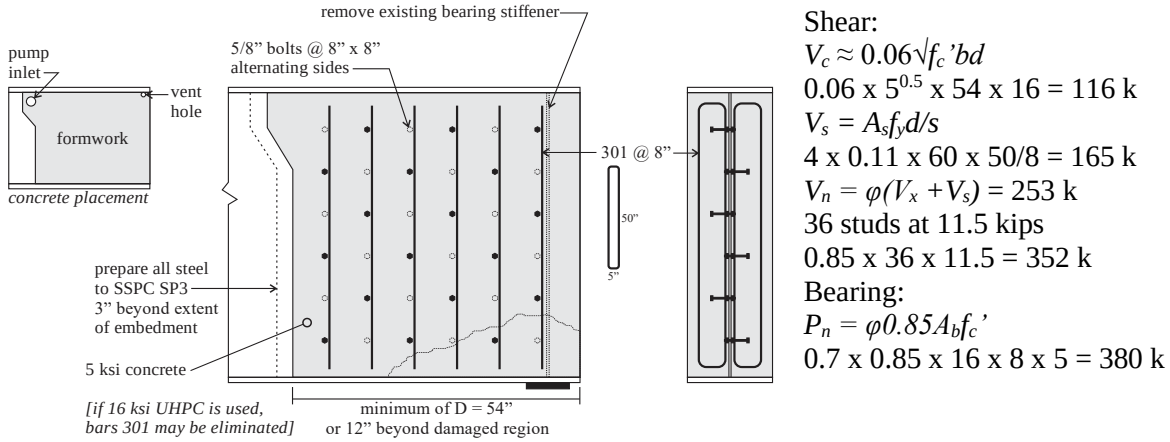

Figure 31 Conceptual representation of concrete encasement repairs

2.3.7 Adhesively Bonded FRP Plate Sections

Section 1.11 describes the use of fiber-reinforced polymer (FRP) materials for infrastructure repair. For beam end repairs to be effective, the repair must restore both strength and stiffness of the beam end region. The most commonly available and least expensive FRP materials are glass-fiber based (GFRP). GFRP has a lower modulus than steel and therefore proportionally more material is required

[17] AASHTO LRFD (2020) Eq. 5.7.3.3-3
[18] AASHTO LRFD (2020) Eq. 5.7.3.3-4

to provide the stiffness required for load sharing. Nonetheless, pultruded FRP plate 'patches' have been demonstrated to improve crippling resistance of slender steel sections (Zhao et al. 2006; Fernando et al. 2009). For larger loads or for use as bearing stiffeners, pultruded FRP sections (typically similar in form to rolled steel sections) may be preferable (Okeil et al. (2009). Figure 25 shows examples of each application.

2.3.7.1 Pros of FRP Repair

FRP materials are light weight and corrosion resistant. They are easily handled and can be cut and shaped on site with hand tools. Structural adhesive preparation and application is well known to contractors. Quantitative design is possible.

2.3.7.2 Cons of FRP Repair

Susceptibility to effects of poor surface preparation or adhesive application – this is discussed at length in Section 1.11. Bridge contractors may not be familiar with material and adhesive handling.

2.3.7.3 Bonded GFRP Repair of 54-in. Deep Plate Girder (Case I)

Bonded GFRP repairs take a similar design approach to conventional steel repairs. It is necessary to replace the functionality of the damaged steel with bonded GFRP. Since the repair is replacing steel, the expected behavior of the beam should remain essentially unchanged; thus, we must consider strength *and* stiffness. For this example, 'off-the-shelf' pultruded GFRP components are used. All material and geometric data has been obtained from a Pennsylvania-based manufacturer's[19] current catalog and design guide.

For a bearing stiffener, a WT section is proposed; this provides a large area for bonding to the existing web (flange width b) and reasonable axial compression capacity. The bearing stiffener will be fully supported over its length and therefore only local buckling of the outstanding web is a concern. BRP *Design Guide* (2012) provides allowable bearing stress based on slenderness: for a W shape having *b/t* = 6/0.5 = 12, the permitted bearing stress is 3.3 ksi. The area of the WT is 8.75 in^2 making the permitted axial capacity 8.75 x 3.3 = 29 kips (58 kips for double-sided stiffeners), well below what is required (208 kips).

Pultruded GFRP is easily built-up using adhesive bonding techniques. Fabricating a WT having similar dimensions from a pair of back-to-back 6x6x½ angles increases the area of the stiffener to 2 x 5.75 = 11.5 in^2 and reduces the slenderness of the stem to *b/t* = 6 permitting a bearing stress of 6 ksi to be used (BRB 2012)[20]. The axial capacity becomes 11.5 x 6 = 69 kips (138 kips for double-sided stiffeners). The addition of a web plate underlying the angles will also contribute as described below.

To reinforce the web, GFRP flat sheet is used. Because the pultrusion process varies, GFRP sheet material properties are marginally lower than those of pultruded shapes and are a function of plate thickness. The approach for the shear design is to assume the web to be entirely GFRP and calculate the capacity based on the total thickness of GFRP provided. Thus the plate is designed to span regions of 100% section loss.

The critical shear buckling stress for an unstiffened pultruded GFRP plate is (ASCE FCAPS):

$$F_{LT}^{cr} = \left(2.67 + 1.59\frac{G_{LT}}{\sqrt{E_L E_T}}\right)\frac{\sqrt[4]{E_L E_T^3}}{(d/t)^2} \qquad [14]$$

[19] *Bedford Reinforced Plastics* in Bedford PA; there are other similar manufacturers in Pennsylvania (*Creative Pultrusions* in Alum Bank) and across the country (e.g., *Strongwell* in Virginia).

[20] When arranged as back-to-back angles with the 'flange' fully supported it is believed that the allowable stress per BRB (2012) could be increased to 10 ksi as is used for W sections. We have continued to use the value of 6 ksi in these illustrative calculations.

The required thickness of GFRP can be found by solving for t such that the required shear capacity, V_{cr} = 0.8 x F_{LT}^{cr} x d x t (the 0.8 is the recommended value for material reduction factor, φ).

For the plate assumed, E_L = 1800 ksi, E_T = 1400 ksi, and G_{LT} = 425 ksi. Providing two 54-in. deep, ¾-in. flat sheets (t = 1.5 in.) gives a shear capacity of 231 kips. Adhesive bond stress is 0.5 x 231/54 = 2.2 kips/vertical inch which will easily be developed using a conventional structural adhesive[21].

The ¾-in. plates will be bonded beneath the bearing stiffeners (see Figure 32) allowing them to contribute to the capacity of the bearing stiffener. Using a permitted bearing stress of 8 ksi for the flat sheet (BRP 2012), the additional bearing capacity is 12 x ¾ x 8 = 72 kips, increasing a single bearing stiffener capacity to 141 kips. Assuming the flange is fully bonded, the shear that must be transferred by the adhesive bond is: 141/(12 x 54) = 0.22 ksi.

The repair calculations shown are for replacement of steel with GFRP. These were conducted to illustrate the viability of the method. In this case, it appears that the 54-in. deep section considered may be close to an upper limit on the utility of bonded GFRP sections.

Refining this approach for the archetypal damage assumed in Case I could result in a thinner web plate being used over the damaged region having partial section loss. The region of total web loss would be reinforced with an additional angle as shown in Figure 32, resulting in more than the full ¾-in. GFRP thickness at this location. The entire GFRP assembly would be fabricated in the shop and adhesive bonded only to the steel on site. Care needs to be taken with fillet detail; a reverse taper fillet should be used at all joints if possible (see Section 1.11.6 and Table 12).

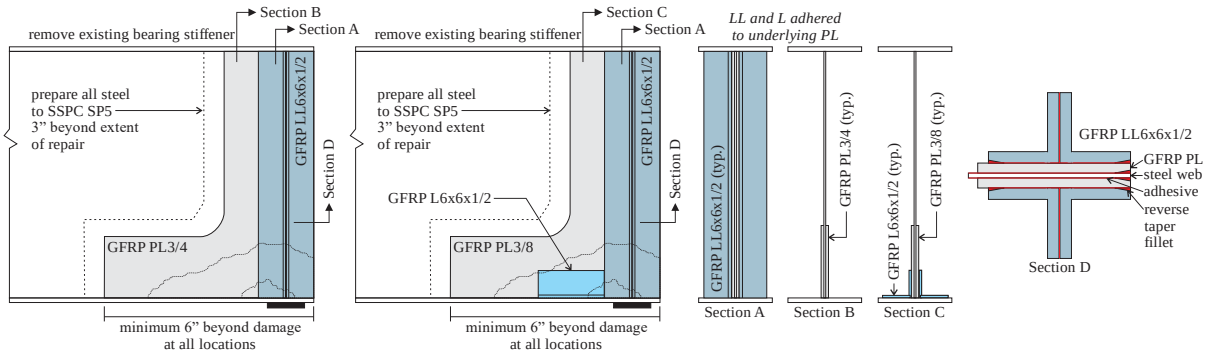

Figure 32 Conceptual representation of adhesive-bonded FRP repairs for plate girder

2.3.7.4 Bonded GFRP Repair of Unstiffened W24x76 (Case II)

Case II requires repair to establish web yield and crippling capacity; web yield capacity is 98% of that required. In such an instance, providing a bearing stiffener that effectively mitigates these limit states is likely most efficient. The stiffener design would be very similar to that described in the previous section although the available flange width in this case is b = 9 in.

The allowable stress limits given by BRB (2012) can be shown to be conservative (Cardoso et al. 2014), especially for the cases in which one flange is fully supported as it is adhered to the web of the girder. BRB (2012) permits allowable bearing stress up to 10 ksi for all sections except angles. The lower 6 ksi limit for angles is understood to be based on the complex interaction of local, global and torsional buckling behavior exhibited by angles. Since the angles are fully adhered to the girder web, these behaviors are mitigated in the present application and increasing the allowable bearing stress to 10 ksi is believed to be acceptable. In such a case, the capacity of the LL4x4x½ bearing stiffener is 75 kips (150 kips total). Like the repair shown in the previous section, an additional web plate may be used to increase the capacity of the stiffener.

[21] SikaDur30, used as reference, has a 14-day shear strength of 3.6 ksi.

Another method of increasing the bearing capacity of the back-to-back angles is to bond an additional GFRP plate between the back-to-back legs of the angles (analogous to a gusset plate). This also reduces the slenderness (*b/t*) of the stem of the double angle assembly which increases the local buckling capacity and may permit a greater stress to be used. For the case shown in Figure 33, adding a 1-in. GFRP plate between angles increases the bearing capacity to 190 kips.

If additional web shear capacity is also required, an inclined bearing stiffener arrangement could be adopted. As shown schematically in Figure 33b, such an approach requires a 'drag strut' angle along the bottom flange to better anchor the diagonal shear strut. An additional flat plate is installed beneath the double angle to provide a uniform bonding plane (Figure 33b).

Although the assembly shown in Figure 33b appears cumbersome, this would be fabricated in the shop. In most cases the tolerance available through the adhesive glue line will be adequate to assure full bearing. If bearing is needed at top and bottom flanges, the assembly would be made slightly long in the shop and trimmed to fit in the field.

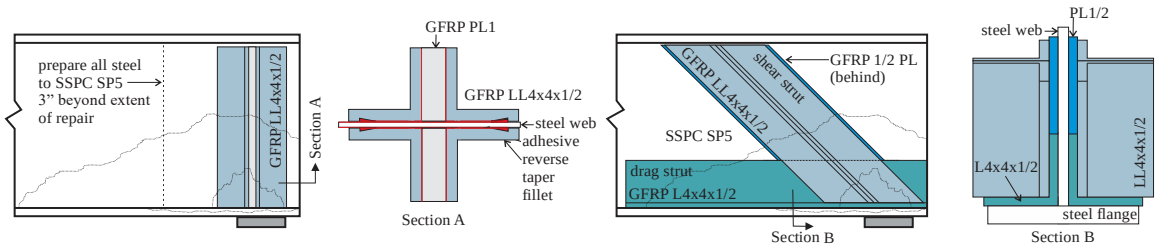

a) vertical bearing stiffener b) inclined bearing stiffener

Figure 33 Conceptual representation of adhesive-bonded FRP repairs for rolled shape.

2.3.8 Wet lay-up FRP Repairs

Wakabayashi et al. (2013) demonstrated the efficacy of wet lay-up carbon fiber reinforced polymer repairs (CFRP) shown in Figures 27 and 28. CFRP has stiffness approaching that of steel and therefore relatively thin repairs are possible. However, wet lay-up FRP materials are suited only to resisting membrane forces. Additionally, these materials rely on their substrate to provide stability. As a result, they are well suited to concrete repair but often ill-suited to steel repair where the restoration of stability may be a key requirement. Although Wakabayashi et al. illustrated a repair in which CFRP spanned a region of 100% section loss, the design was executed based on providing an amount of CFRP equivalent to the steel lost. This results in a large number of plies. Furthermore, the need to anchor the plies introduces a reentrant corner at the web-to-flange junction that could lead to adhesive peeling. The present research team believes that this repair would perform very poorly under repeated loads.

Thus, it is believed that wet lay-up CFRP is only suited to restoring shear capacity to webs exhibiting partial section loss. Wet lay-up is unlikely to be effective in improving web yield or crippling capacity. Lack of out-of-plane anchorage (as would be required near a web-flange interface) could result in debonding of the CFRP especially under the effects of repeated loads.

2.3.8.1 Pros of Wet lay-up FRP Repair

Wet lay-up CFRP repairs will be durable and have been demonstrated in countless bridge applications on concrete substrates. Wet lay-up applications are well suited to complex or variable geometry (although reentrant corners lead to debonding) and are relatively easily executed even in confined spaces as they require no machinery or clamping.

2.3.8.2 Cons of Wet lay-up FRP Repair

Susceptibility to effects of poor surface preparation or adhesive application – this is discussed at length in Section 1.11. Wet lay-up application of CFRP requires trained and certified contractors.

2.3.8.3 Example of Wet lay-up FRP repair

Wet lay-up FRP is a very thin application (design thickness on the order of 0.04 in. per FRP ply) suited for developing membrane forces. As described above, such a thin application is not well suited to spanning large regions of 100% section loss or for restoring section loss in compression elements (e.g., bearing stiffeners).

Wet lay-up CFRP can be used for restoring web capacity. If a web exhibits section loss α, it has a remaining steel thickness $(1-\alpha)t_w$. To restore the web capacity, CFRP equivalent to αt_w must be provided. The resulting design thickness of CFRP is:

$$t_{FRP} = \alpha t_w (G_s/E_{FRP,\pm 45}) \quad [15]$$

Typically, a so-called "high modulus" carbon fiber reinforced polymer (CFRP) product will be used; these are often characterized in terms of their dry-fiber areal weight. For large strengthening applications, typically fabrics weighing about 18 oz/yd^2 are selected. These will minimize the number of plies required while still being sufficiently pliable to form to complex geometries and not sag upon application. The uniaxial design tensile strength and modulus of these products[22] are $f_{fu} \approx 160$ ksi and $E_f \approx 10{,}000$ ksi with a design thickness of $t_f = 0.04$ in/ply. For shear, the unidirectional fabric will be oriented at ±45 degrees to the longitudinal axis of the beam (Figure 34). The resulting modulus of the CFRP in a ±45 degree orientation is approximately equal to the shear modulus of steel ($G_s \approx 11{,}400$ ksi), thus the CFRP replaces the steel in an essentially 1:1 ratio. Considering the design thickness of a single ply of CFRP is on the order of 0.04 in., multiple plies are required to restore even relatively minor plate thickness loss. The use of heavier CFRP sheets is possible although issues of sag of the material upon application may be an issue. This design approach is the same as proposed by Wakabayashi et al. (2013).

The ultimate strength of the CFRP patch is considerably greater than the steel it is replacing; nonetheless, this strength must be developed through adhesive bond. Typically, the CFRP patch will be 'developed' as shown in Figure 34. The anchorage length, L_a, should be based on the established capacity of the adhesive bond to steel and should include some allowance for positioning error/variability. Cadei et al. (2004) recommends a minimum anchorage length of $72t_{FRP}$. Typical values of adhesive shear strength are in the range of $\tau_a = 3.6$ ksi [4]. Thus:

$$L_a > f_{fu}t_{FRP}/\tau_a \geq 72t_{FRP} \quad [16]$$

It is noted that in wet lay-up applications, a design FRP thickness, t_f, is provided and $t_{FRP} = t_f \, x$ *number of plies*. The actual *in situ* thickness (includes saturating resin) will be different and should not be used as a basis for inspection or acceptance. The terminations of multiple plies should be staggered at least $20t_f \geq 1$ in. This is shown in Figure 34. Finally, a compatible putty filler is used to fill the existing region of section loss so that the surface to which the CFRP is applied has an amplitude variation less than 1/16 in.

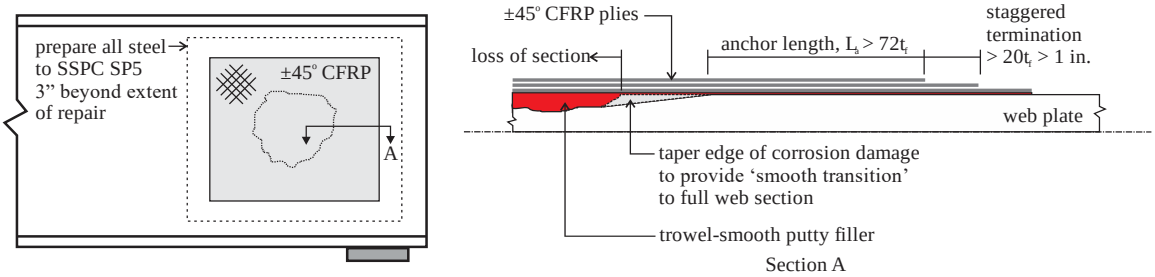

Figure 34 Details of wet lay-up CFRP web patch.

[22] *SikaWrap Hex 103C* (18 oz unidirectional CFRP) and *SikaWrap 600 ±45* (18 oz ±45° CFRP) products are selected. This is not an endorsement of Sika; there are other similar products available in the United States (e.g., Aegion's Fyfe/Tyfo products; Master Builders' MasterBrace products; Structural Technologies' V-Wrap)

2.3.8.4 Adhesively Bonded Steel Plate

Although FRP materials are more commonly considered for adhesively-bonded applications today, steel plate bonding has been extensively used in concrete infrastructure repair. It is the Research Team's opinion that steel plate bonding provides no benefit over FRP plate bonding and would be harder to execute. Nonetheless, in the interest of completeness, this approach is acknowledged here.

2.3.8.5 Selection of Adhesive, Surface Preparation and Details for Adhesive Bonding

Adhesive bonding to non-uniform steel substrates – as will be the case for cleaned, previously corroded surfaces – has one very distinct advantage: the adhesive is able to fill in the amplitude variations of the steel surface without meaningful loss of capacity. Indeed, a sound adhesive bond *requires* a roughened surface. Additionally, the adhesive will fill in existing holes (100% section loss) resulting in a more homogeneous final product.

Nonetheless, as described at length in Sections 1.11.6 and 1.11.7, there a number of considerations in terms of steel surface preparation and adhesive selection and detailing that require attention.

Sound adhesion to previously corroded steel likely requires SSPC-SP5 surface preparation: "blasting to white steel". This is the same degree of preparation required for repainting corroded steel. Additional care needs to be taken to protect the blasted surface from the reformation of oxides in the time between cleaning and adhesive application. A conventional organosilane primer has been shown to be effective in this regard.

There are a number of commercially available structural adhesives intended for steel substrates. The selection of an appropriate adhesive must include consideration of the viscosity or the addition of fillers to increase viscosity. An appropriate adhesive should self-support the adherands without the need for external clamping. This is unlikely possible for adhesively bonded steel applications.

Edge conditions and the shape of fillet can significantly impact performance of adhesively bonded patches. Assuming precured (shop-fabricated) patches can be used, providing an edge chamfer to permit a reverse taper fillet to be used is desirable (see Table 12). Providing an additional fillet to ensure that water cannot accumulate along the adhesive edge is also good practice. FRP sections can be pultruded with UV inhibitors and do not need additional environmental protection, although cut edges should be sealed.

2.3.9 Embedded Bearing Repair

Embedded bearing regions (Case III) require a different repair approach. In this case the corrosion damage is at the face of the embedment and (typically) not directly impacting the bearing region. The corrosion has resulted in a loss of section inboard of the bearing. In severe cases, the girder is entirely unsupported (see Figures 7d-f and 8a). The repair requirement is therefore more analogous to splicing the girder back to its support region than strengthening and stabilizing the support region.

Any repair will require removal of enough existing concrete to fully expose the existing bearing. The girder will then be 'spliced'. New concrete encasement is then provided and will typically extend beyond the original embedment face (Figure 35a).

An alternative approach is to extend the bearing of the existing embedment outward, essentially creating a corbel and supporting the beam over a shorter length. This is the approach used in Bridge I (see Figure 9); the detail used in this instance is shown in Figure 35b. Bridge I also illustrated a variation of this approach, in which a steel splice plate is anchored into the existing diaphragm; this is shown in Figure 35c.

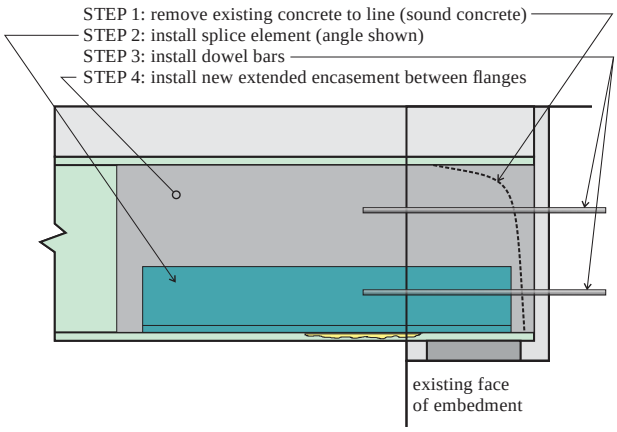

a) schematic representation of spliced region of embedded bearing

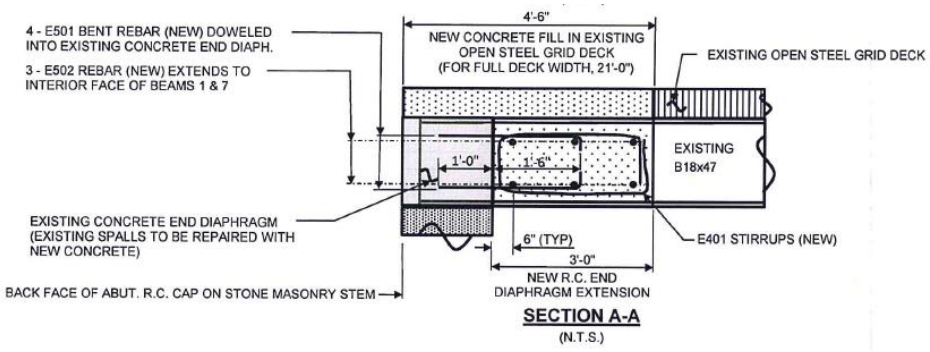

b) detail of steel-formed encasement (PennDOT 2020)

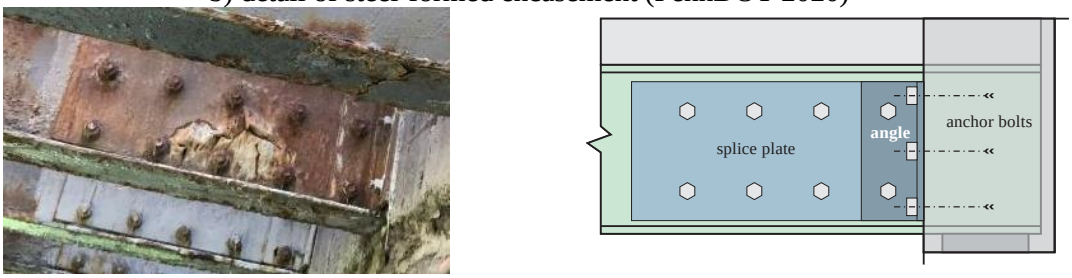

c) bolted steel 'splice' anchored to existing end diaphragm

Figure 35 Repair approaches for embedded bearing regions.

2.3.9.1 Corbel Repair of Embedded W18x60 (Case III)

The corbel is shifting the beam support further into the span, by-passing the damaged region and providing a continuous load path to the existing bearing. Conceptually, the corbel is supporting the girder from beneath its [typically undamaged] top flange and carrying this load as a strut to the bearing. By providing shear studs, the forces transmitted to the corbel can be distributed over its depth.

A beam-wide corbel can be developed in the same manner as shown in Section 2.3.6. However, for shallower members the area of concrete that can be formed within the flange width, *b*, is limited affecting the ability to locate shear reinforcement and dowl tie-backs.

A larger corbel may be affected as shown in Figure 36a by extending the end diaphragm into the beam span a dimension *e*. In doing so, the area of concrete that may be engaged to resist shear is $(b+e) \times h$ (*h* is the depth of the web; $h = d - 2t_f$ for rolled shapes). Shear reinforcement and dowel reinforcement located within the region $b+2e$ may be assumed to contribute to the corbel capacity, thereby mitigating the issues associated with the small dimension *b*. For Case III, the calculations are as follows.

The required shear capacity is 184 kips. The maximum permitted shear stress (AASHTO LRFD) in concrete is $0.25\sqrt{f_c'}$ [ksi][23]. Assuming f_c' = 5 ksi and knowing b = 7.5 in. and h = 16.8 in. for a W18x60, the required diaphragm extension e > 12 in. In this case, the concrete component of corbel resistance is $0.06\sqrt{f_c'}h(b+e)$ = 44 kips. The required 140 kip steel component requires 2.6 in^2 shear reinforcement distributed across the width $b+2e$ – this is 13 #4 bars.

The corbel must be doweled into the existing diaphragm. Using hairpin reinforcement as shown in Figure 36b, the dowel area is twice the shear reinforcement area and will therefore easily satisfy the interface reinforcement using a friction coefficient of μ = 1 (AASHTO LRFD §5.8.4). Fully developing the dowels provides a moment resistance of approximately 14 x 0.20 x 60 x 12 = 2016 kip-in. Assuming a lever arm of $e/2$, the moment at this interface is 184 x 12/2 = 1100 kip-in.

Finally, the hairpin reinforcement shown in Figure 36b must be developed into the existing diaphragm; hence the use of smaller bars. There a number of commercially available adhesive anchor products that can fully develop 60 Grade reinforcing steel. For the example considered, an 8 in. embedment is adequate to develop the capacity of the bar[24].

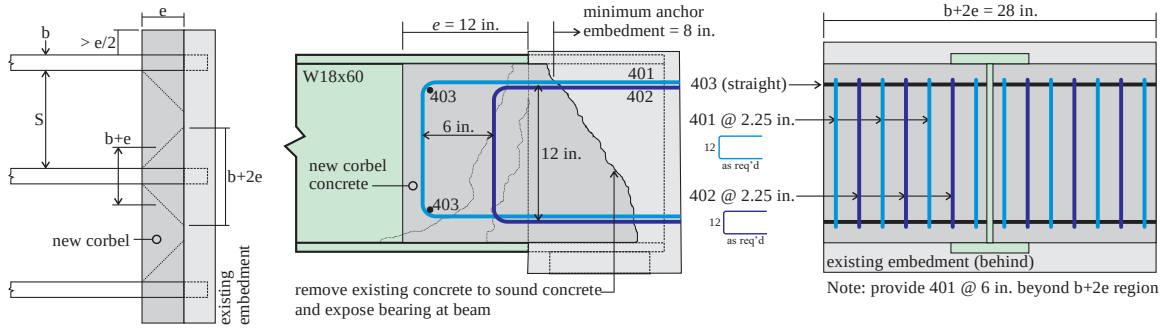

a) plan view of three girders

b) side and end elevations of b+2e region at embedment

Figure 36 Conceptual representation of corbel repair.

2.3.9.2 Embedded Splice Repair of Embedded W18x60 (Case III)

For embedded girders having more significant loss of section, and particularly loss of the bottom flange, a bolted steel or adhesive bonded pultruded GFRP may be embedded in the concrete corbel described in the previous section. This is shown schematically in Figure 37a. In this case, the embedded section may carry a portion or all of the load. The corbel may share in the load resistance or simply provide the confinement necessary to mitigate web yield and crippling behaviors. The corbel/concrete embedment should be provided with minimum reinforcement to control temperature and shrinkage cracks in all instances.

2.3.9.3 Steel Splice Repair of Embedded W18x60 (Case III)

This retrofit, shown in Figure 35c, will be limited by the capacity of the anchors that can be installed into the abutment. These anchor the cleat angles that provide a new support location for the beam inboard of the section loss at the face of the abutment (e in Figure 37). The anchors are subject to combined shear ($V = V_{cr}/n$; where n is the number of anchors used) and tension resulting from moment associated with the out-of-plane eccentricity of the load. For a three anchor arrangement as shown in Figure 37, the anchor tension force is $N = V_{cr}e/2s$. The anchor capacity is a function of anchor type, depth and size and single anchor capacity is reduced due to proximity of other anchors (ACI 319-19).

[23] AASHTO LRFD (2020) Eq. 5.7.3.3-2
[24] Hilti HIT-HY 200 or HIT-RE 500 V3 (the latter is listed in Bulletin 15)

The following is a hypothetical calculation of the shear force that could be developed by a steel splice repair of Case III archetypal damage. Abutment concrete is assumed to be sound but with some [potentially unknown] distress and have a strength, f_c'= 4 ksi. For the sake of calculation, a ¾-in. undercut anchor bolt having a 10-in. embedment is assumed[25]. The assumed geometry using a 10 in. angle is shown in Figure 37a as having e = 8 in. and s = 6 in.; n = *6* for each angle. As seen in Figure 37b, the *in situ* tension capacity of a single anchor, φN = 18 kips. In this case, the maximum moment that may be resisted by each cleat is 2 x 20 x 12 = 480 kip-in. and the corresponding shear force is 480/8 = 60 kips. Thus the total beam shear capacity that could be restored using this approach is 120 kips. The angle is then selected considering the prying limit state at the anchor bolts and the connection to the beam is designed. In the example shown, a pair of L10x10x7/8 can be made to work and the beam connection is easily made with 3 – 1-in. bolts.

This example demonstrates that this type of retrofit will typically be governed by anchor design and is therefore limited in the capacities it can develop.

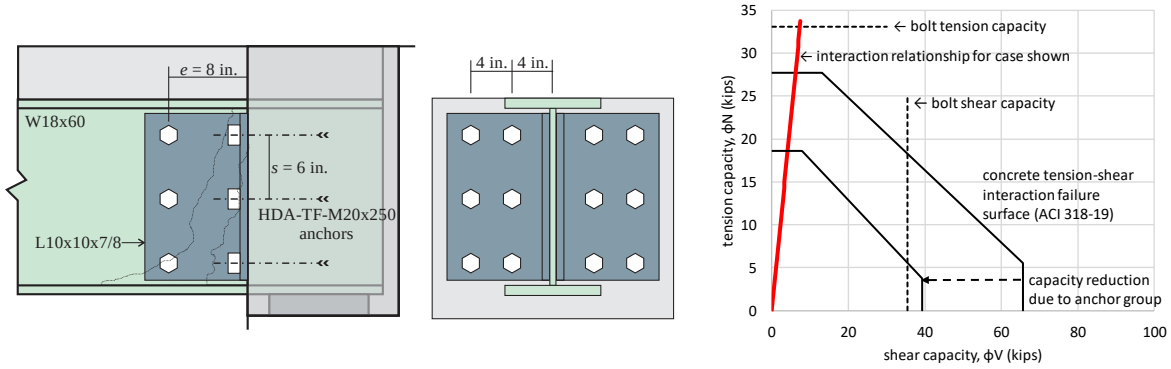

a) splice and anchor geometry considered

b) shear-tension interaction (see ACI 318-19 §17.8.3)

Figure 37 Conceptual representation of anchored steel splice repair

2.3.10 Section Replacement

Significant end region damage – particularly that resulting in significant section distortion – will typically require end region replacement such as shown in Figure 11. A variation of complete beam end replacement that might permit a simpler construction process is to provide a dapped girder in lieu of a full depth girder end replacement. In some cases, such a repair might be feasibly made with the girder in place and only jacked and lifted to transfer load from the deteriorated bearing region to the newly built dapped end. Figure 38 shows a schematic of a dapped steel girder. Dapped steel plate girders were studied by the Texas DOT (Fry et al. 2005). Due to their reduced depth, tension fields can be better developed, in many cases improving the shear capacity of the dapped end. Due to the potential for fatigue issues arising, only tapered dapped ends (Figure 38) are recommended.

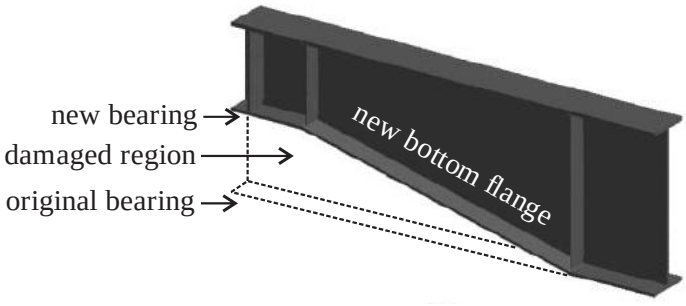

Figure 38 Dapped-end replacement (based on Fry et al. 2005).

[25] Hilti HDA-TF-M20x250

2.3.11 Hybrid Techniques

Many of the approaches proposed may be combined. Some examples are described in 2.3.9; others may include adhesive-bonded FRP tubes filled with concrete in order to affect more efficient and compact bearing stiffeners.

2.4 Jacking Requirements

Most beam end repairs will likely include bearing replacement and therefore require 'jacking' the beam to relieve the load on the bearing for replacement. Beam end repairs will also typically require jacking at some stage.

The objective of not requiring temporary support has an inherent implication that the existing structure is adequate to resist whatever loads are present during the repair (and subsequent curing, if applicable) procedure. Without pre-loading, prestressing or post-tensioning of some kind, any repair scheme is only able to partially resist loads applied after its installation. Repairs that are called upon to resist any portion of the bridge self-weight, for instance, must have this load relieved during installation. Preloading during repair installation may be effectively used on continuous structures but is not an available option for simple spans. The research team is unaware of any post-tensioning technology suitable for beam end repairs. While some potentially applicable prestressed technology has been proposed, none has been demonstrated at full scale and none – to the authors' knowledge – in any application similar to the repair of deteriorated beam ends. Thus, jacking and temporary support of the beam is a necessary step for repairs of significant damage. Once again, jacking is likely required for concurrent bearing replacement.

Jacking may be done from below the girder or above – through the deck. Jacking may react against the ground, the bridge foundation or adjacent superstructure elements. Methods of jacking themselves are beyond the scope of the present study. Nonetheless, the method of jacking must be considered in so far as its impact on the proposed repair technique and whether the repair must be made while the girder load is relieved, or the repair can be carried out and load 'transferred to it" via jacking.

2.5 Restoring Beam Support

Many instances of existing damage may be sufficiently severe that the beam is no longer resisting load at its bearing. Examples of such damage are shown in Figures 5, 7 and 8. In such cases, load resisted by the girder is redistributed transversely across the bridge to adjacent bearings. Redistribution may be through the composite slab and end diaphragms when present. In these instances, the capacity of the beam end can be restored – likely without the need of jacking. Following repair, the beam can be safely lifted off its old bearing and replaced allowing restoration of load bearing at the beam end. Due to likely distortion, the new bearing may need to accommodate a marginally different top-of-bearing height in order to restore the uniform transverse distribution of bearing forces. To better ensure uniform distribution of bearing forces, new end diaphragms may be considered.

3 Experimental Program

3.1 Experimental Specimens in Literature

As reported in Chapter 1, there are relatively few similar studies reported in the literature. The dimensions of these are summarised in Table 15. This summary reinforces the selection in this project of a 54 in. deep archetype (Figure 29, Case I) and the approximately 50% scale experimental specimens described in this chapter.

Table 15 Experimental specimens reported in literature.

citation	section (in.)				D/t_w	*a/d*	
	D	t_w	b	t_f		test span	back span
Ahn et al. 2013 Kim et al. 2013	31.5	0.24	7.9	0.63	131	1.5	1.5
Liu et al. 2011	49.2	0.24	7.9	0.47	205	2.0	2.0
Gerasimidis and Brena 2019	33WF125 21WF73				56 45	1.8 2.9	7.3 8.6
McMullen and Zaghi 2020	52	0.38	18	1.5 1.0	139	1.2	2.7
Wakabayashi et al. 2013	51.2	0.32	13.8	0.87	160	1.0	1.0
Zmerta et al. 2017	W21x55				53	1.5	5.3
this study (see below)…							
plate girder archetype	54	0.38	12	1.0	142		
reduced section W24x55	22.6	0.20	7	0.50	113	1.5	6.75

3.2 Experimental Specimen Selection

The 54 in. deep plate girder with a stiffened web, reported as Case I in Figure 29 was selected as the archetype for the experimental program. The plate girder end region capacity will be controlled by web shear and will require bearing stiffeners to have adequate capacity against web yield and crippling failure modes. The as-built and as-is capacities (see Section 1.3) of the archetype are summarized in Table 16.

3.2.1 Constraints on Experimental Specimen Selection

In order to optimize the available resources, double-ended specimens were used. These were tested in a simple span arrangement shown in Figure 39. End A was tested as shown with End B cantilevered beyond the back span support. The beam was then rotated and End B tested in the same manner. In this case, the back span support for End A becomes the loading location for End B. In order to ensure constructability and to ensure budget constraints were met, the Research Team engaged a steel fabricator[26] to assist with specimen design. The following constraints were considered in selecting the experimental specimen design.

1. Achieve end region behavior similar to 54 in. plate girder archetype;
2. Provide test span-to-depth ratio, $a/d = 1.5$;
3. To mitigate damage at load point, a bearing stiffener is provided at this location;
4. To minimize damage at back span bearing, provide back span $a/d > 5$;
5. Static test capacity < 108 kips (two 60 kip rams operating at 75%);
6. Fatigue test capacity < 33 kips (50 kip actuator operating at 66%); and,
7. Based on fabricator recommendation and constraints for rotating specimens in lab, the overall specimen length is limited to 20 feet.

Since flexural behavior of the back span is not of interest in this study and these spans are effectively tested twice, behavior must remain elastic in flexure, specifically ensuring:

[26] High Steel Structures in Lancaster PA

8. Top flange stability (flange local buckling)
9. Lateral stability (lateral torsional buckling)

Typically, such behavior is ensured by the presence of a deck. In this study (and all similar previous studies reported in Table 15), in order to clearly investigate steel behavior, specimens were tested without a deck.

3.2.2 As-received Test Specimens

As quantified in Section 3.3.2, the fabricator was unable to meet the web thickness reduction requested. This had several effects on the design constraints.

The shear capacity of the experimental specimens exceeds that anticipated, requiring an increase in the test frame capacity (constraints 5 and 6, above). In order to test the as-received beams, the static test capacity was increased to 280 kips (4 – 70 kip capacity hydraulic rams).

The fatigue actuator will be run to 90% capacity, providing a maximum capacity of 45 kips.

The unintentionally stronger specimens will provide a more robust demonstration of the repair techniques considered.

A summary of all predicted capacities – intended and as-delivered – for various test contingencies is provided in Table 16. Based on the spans used, the shear in the test span, and moment applied to the specimen are:

$$V = 162P/198 = 0.82P \quad \text{[kips]} \qquad [17]$$

$$M = (162 \times 36)P/198 = 29.4P \quad \text{[k-in]} \qquad [18]$$

Where P is the applied load in kips.

3.3 Test Specimen Design

It was desired to have the largest test specimen possible within the constraints identified. Multiple trial designs were considered. Ultimately, in consultation with the fabricator, a W24x55 was selected. This section, as rolled, is one of few with a non-compact web. As a result, the experimental specimen is approximately one-half scale the Case I archetype shown in Figure 29.

Despite having a non-compact web, in order to better model the behavior of the 54 in. deep plate girder archetype, the web in the test region (from the load point to the bearing) was intended to be further reduced from the as-rolled t_w = 0.395 in. to t_w = 0.20 in. Although not achieving the very slender D/t_w = 144 of the archetype, a web slenderness of 113 results (104 if the fillet region is considered). An advantage of using such a reduced section rolled specimen is that gross section can be maintained at the loading point and over the back span helping to address constraints 8 and 9 and ensuring elastic behavior outside the test span. In this test Program, despite the unanticipated additional capacity (Section 3.2.2), this approach worked well, allowing the double-ended specimens to be tested as intended.

A summary of the test specimen design is presented in Figure 39. Details transmitted to the fabricator are provided in Appendix B. Both end regions on a single beam are identical.

3.3.1 Bearing and Lateral Support Details

Full width steel bearing pads 5 in. (i.e., N = 5 in.) long were provided for all bearing locations and the application of load. The bearing was centered 3 in. from the test span end as shown in Figure 39.

Table 16 Summary of specimen design checks for W24x55.

capacity	note		54 in. archetype		W24x55 test specimen			
			as built	as is	as-rolled gross section	as-designed reduced section	as-received reduced section[b]	damaged section
F_y		ksi	36	36	50	50	57	50
					test span (*a/d = 1.5*)			
t_w		in.	0.375	0.28	0.395	0.20	0.326	0.167
t_{wc}	Eq. 5	in.	0.375	0.21	0.395	0.20	0.326	≈0.030
t_f		in.	1.0	0.75	0.505	0.505	0.505	0.375
V_{cr}	Eq. 1	kips	186	80	270	64	237	37
N		in.	10	10	5	5	5	5
R_{nyield}	Eq. 5	kips	177	99	149	75	140	11
R_{ncrip}	Eq. 6	kips	106	37	123	36	91	1.6
bearing stiffeners (F_y = 36 ksi)		in.	7 x 0.625	1.75 x 0.47	not required	3 x 0.5	3 x 0.5	-
R_{sb}	Eq. 8	kips	394	47		126	175	-
P_{sb}	Eq. 9	kips	315	59		108	150	-
R_{yield} at applied load		kips	-	-	226	226	258	226
					back span (*a/d = 6.75*)			
$M_y = SF_y$	gross section	k-in	-	-	5700	shear critical test region	potential for flexural inelasticity	shear critical test region
M_y	flanges only[a]	k-in	-	-	4180			
$M_p = ZF_y$	gross section	k-in	-	-	6700			
M_p	flanges only[a]	k-in	-	-	4267			
M_n	L_b = 13.5 ft C_b = 1.67	k-in	-	-	M_p			

[a] neglecting contribution of web results in conservative capacity suitable for ensuring elastic behavior
[b] Girder End 1A

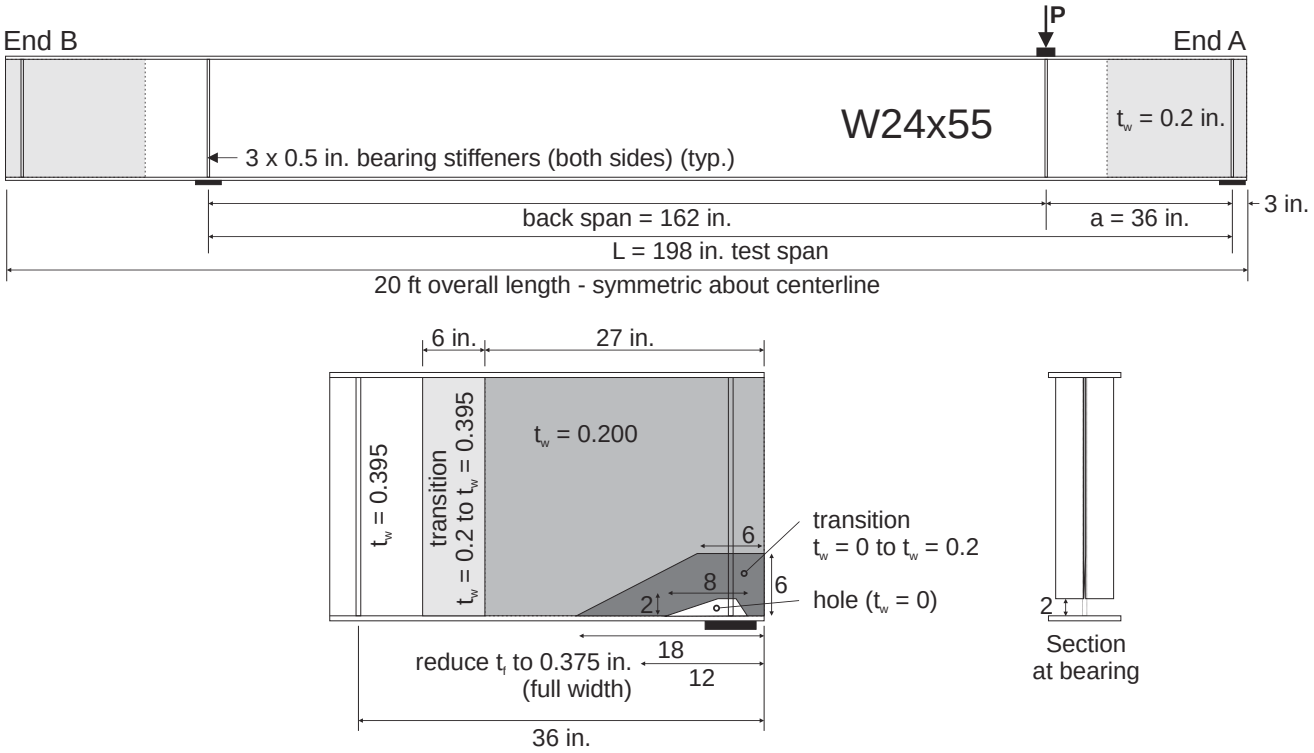

Figure 39 As-designed W24x55 specimen.

3.3.2 'Corroded' Girder Geometry

As shown in Figure 39, artificial 'corrosion damage' was machined into each girder end. All damage was marginally different and is quantified in Table 17. Girders 7 and 8, while not tested in this Program, are included in Table 17 as an archival record. These girders remain available and may be used in future study.

Web and flange thickness was determined using an ultrasonic thickness gage (Seesii model S-WT100A) across the reduced area shear span. Readings were taken on a 2 in. grid near the bearing and on a 3 in. spacing further into the span as shown in Appendix C. Average thicknesses reported are determined over this region excluding the 'corroded' hole and are adopted as web thickness, t_w, for subsequent calculations. Figure 40 also shows images of the region of 100% section loss at the bearing locations (the hole); the area of this region, A_{hole} obtained from image analysis (accurately measuring area of hole from photograph using image software) is also reported. Complete thickness reading matrices are provided in Appendix C.

A second issue associated with the method of reducing the web thickness used was that by 'thinning' the web from only one side, residual stresses were released resulting in the web distorting into a 'buckled' shape. Temporary stiffeners were used to mitigate this effect although some specimens still exhibited web distortion prior to repair. Figure 40 shows four beams during fabrication. In Figure 40, girder (b) is a W24 x 55 prior to web machining. Girder 8 (a) was fabricated without a temporary stiffener and severe web distortion is apparent. While the Girder 8 geometry was partially restored using heat-straightening, this girder was not used in this study. Although the web of Girder 1 (d) is machined, the full depth, intact bearing stiffeners controlled section distortion. Girder 2 (c) shows the limited distortion that resulted when only partial height stiffeners were provided. Once again, this issue with fabrication will require a more robust response from the repair techniques considered.

The web distortion was measured as the deviation of the web from straight at the midheight of each girder end at the location of the bearing (i.e., 3 in. from the girder end). The values are reported as a_{max} in Table 17.

a) Girder 8; fabricated without a stiffener

b) W24 x 55 prior to machining

c) Girder 2

d) Girder 1

Figure 40 Section distortion of girder specimens.
(photo: High Steel Structures)

Table 17 'Corrosion damage' and web thickness.

Girder	End A		End B	
1		t_w = 0.326 in. (COV = 0.030) A_{hole} = n.a. a_{max} = stiffened	t_w = = 0.340 in. (0.022) A_{hole} = n.a. a_{max} = stiffened	
2		t_w = 0.324 in. (0.032) A_{hole} = 10.38 in^2 a_{max} = 0.11 in.	t_w = = 0.312 in. (0.031) A_{hole} = 11.90 in^2 a_{max} ≈ 0 in.	
3[a]		t_w = 0.305 in. (0.029) A_{hole} = 11.58 in^2 a_{max} = 0.06 in.	t_w = = 0.298 in. (0.034) A_{hole} = 13.57 in^2 a_{max} = 0.07 in.	
4	 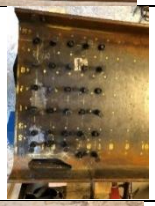	t_w = 0.317 in. (0.028) A_{hole} = 12.61 in^2 a_{max} = 0.03 in.	t_w = = 0.265 in. (0.055) A_{hole} = 16.19 in^2 a_{max} = ≈ 0 in.	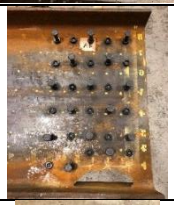
5	 	t_w = 0.281 in. (0.031) A_{hole} = 16.02 in^2 a_{max} = 0.90 in.	t_w = = 0.287 in. (0.033) A_{hole} = 18.44 in^2 a_{max} = 0.19 in.	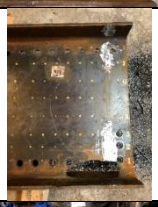
6		t_w = 0.298 in. (0.037) A_{hole} = 14.39 in^2 a_{max} ≈ 0 in.	t_w = = 0.315 in. (0.052) A_{hole} = 10.82 in^2 a_{max} ≈ 0 in.	
7		t_w = 0.288 in. (0.025) A_{hole} = 16.46 in^2 a_{max} = not measured	t_w = = 0.288 in. (0.027) A_{hole} = 16.07 in^2 a_{max} = not measured	
8		t_w = 0.266 in. (0.061) A_{hole} = 8.71 in^2 a_{max} = not measured	t_w = = 0.299 in. (0.035) A_{hole} = 9.93 in^2 a_{max} = not measured	

[a] The image of Girder End 3B was taken following testing.
Girder labelling was revised following delivery; disregard small paper labels in images.
Some images have been mirrored to affect the same orientation throughout table.

3.4 Test Program

Eight girders (16 test specimens) were fabricated as summarized in Table 18. Reserve Girders 7 and 8[27] remain uncommitted and untested but are reported here for archival integrity. In each girder, End A was tested under static load conditions to failure (i.e. a slow monotonically increasing load to failure). End B was a companion fatigue conditioned test.

Table 18 Test matrix.

Girder	repair technique	End A	End B	fabrication detail
1	no damage control	monotonic	fatigue	Appendix C Detail A
2	no repair control	monotonic	fatigue	Appendix C Detail B (also Figure 39)
3	conventional bolted steel[a]	monotonic	fatigue	Appendix C Detail C
4	UHPC	monotonic	fatigue	
5	conventional RC	monotonic	fatigue	
6	adhesive bonded pGFRP	monotonic	fatigue	
7	reserve specimen	monotonic	fatigue	
8	reserve specimen	monotonic	fatigue	

3.4.1 Specimen Material Properties

All girders came from the same heat and mill certifications indicated yield and tensile strengths of 55 ksi and 73 ksi, respectively. Ten tension coupons were obtained from the web of Girder 1 following testing – five specimens in each of the longitudinal and vertical directions. There was no statistical difference in results for each coupon orientation. The measured yield strength of the girders was F_y = 57.5 ksi (COV = 0.06); the tensile strength was F_u = 77.5 ksi (COV = 0.01) and elongation at ultimate was ε_u = 0.34 (COV = 0.06).

3.5 Test Set-up

All tests are conducted in simple span flexure over a test span of 198 inches and a shear span of 36 inches (Figure 39). Tests are conducted in a 400 kip capacity self-reacting steel frame as shown in Figure 41.

a) Monotonic tests of girder Ends A and B using four 70 kip capacity hydraulic cylinders

b) Fatigue conditioning of girder Ends B using 50 kip capacity servo-hydraulic actuator

Figure 41 Overall views of test set-ups
(Girder 3 shown in both cases).

[27] Girder labelling 1-8 was revised following quantification of web thickness. All captions and identification in this report are correct; disregard the small paper labels that appear in some images.

3.5.1 Monotonic Tests to Failure

Monotonic (or 'static') tests to failure are conducted using four 70 kip capacity hydraulic cylinders (Figure 41a). The cylinders have a compression area of 7.22 in^2 and are driven with a 10000 psi electric pump. Load is applied gradually using a regulator valve and pressure is recorded using a precision transducer. The transducer precision is 0.001 over full scale, resulting in the precision of the reported applied load being 0.29 kips[28].

Test are conducted monotonically to failure. Considering the need to record data and monitor the specimens for damage, each test takes approximately one hour – a load rate on the order of 4 to 5 kips/minute.

3.5.2 Fatigue Conditioning

End B of each girder was tested using the following fatigue conditioning protocol. The intent is *not* to affect a fatigue failure, but to replicate years of service – fatigue *conditioning* – after which the girder end was tested monotonically to failure as described in the previous section. The static capacity of Ends A and B are then compared and differences attributed to the effects of fatigue conditioning. Because of the poor brittle performance of 6A (Section 3.7.6), fatigue conditioning of 6B was not undertaken.

Fatigue loads are applied using a 50 kip capacity servo-controlled hydraulic actuator (Figure 41b). Load and displacement are obtained from the integrated actuator load cell (Figure 41b) and LVDT. The reported load and displacement precision is 0.01 kips and 0.001 in., respectively.

The fatigue conditioning protocol involves 1 million cycles of applied load, $P_{fatigue}$, cycling between 4 kips and 44 kips. Thus the average or baseline applied load is 24 kips and the full cycle amplitude is 40 kips: that is the fatigue loading is 24 ± 20 kips. Fatigue load was applied at a frequency of 1.2 Hz, resulting in a test rate of 100,000 cycles per day (including time for instrumented cycles).

The ratio of fatigue load to design load is a function of bridge geometry and loading and will vary to some extent. Two well-established 'design examples' – 1 and 2A from the *Steel Bridge Design Handbook* (Barth 2015; Grubb and Schmidt 2015, respectively) were used as the basis for establishing the fatigue load due to shear as a proportion of the design load. In Example 1, the ratio of shear demand under FATIGUE I load condition to that under STRENGTH I, $V_{FATIGUE}/V_{STRENGTH\ I}$ = 0.167; the same ratio is 0.165 for Example 2A.

For Girder 1A, the experimentally observed shear capacity was V = 213 kips. In consideration of the variation of as-received girder capacities and the limitations of the fatigue actuator, the amplitude of the fatigue load was selected to be 40 kips, resulting in a shear of 32.8 kips and ratio of $V_{FATIGUE}/V_{STRENGTH\ I}$ = 0.154 based on Girder 1A. This ratio is marginally greater for the other girders which all have thinner webs.

It is not practical to provide continuous instrumentation for fatigue conditioning. Applied load, deflections and strain gage-measured strains were monitored during 'instrumented cycles' as follows. Fatigue loading is paused. Data is reported at the baseline load of P = 24 kips and at a single load cycle to P = 44 kips. Instrumented cycles are conducted on a logarithmic schedule at cycles 1, 2, 5, 10, 20, 50, 100, 200, 500, 1000, 2000, 5000, 10,000, 20,000, 50,000, 100,000 and every 100,000 cycles thereafter to the end of conditioning at 1 million cycles.

3.5.3 Instrumentation

Figure 42 summarizes the instrumentation layout, described as follows. Acquisition of the applied load, P, is described in the previous sections. Vertical girder displacements (δ_1 and δ_2) were obtained in the monotonic tests using draw-wire transducers (Figure 42b) having a precision of 0.004 in.

[28] 0.001 x 10,000 psi x 7.22 in^2 x 4 cylinders = 289 lbs

Displacement δ_1 during fatigue tests was obtained directly from the actuator transducer with a precision of 0.001 in.

A triaxial electrical resistance strain gage (i.e.; shear gage shown in Figure 42c) was installed in the middle of the 36 in. shear span at the girder middepth (neutral axis). Using a triaxial gage, the oriented shears, maximum shear strain and orientation of the maximum strain can be obtained as shown in Figure 42d. All strains are recorded with a precision of 1 microstrain using a Micromeasurements P3500 strain indicator box.

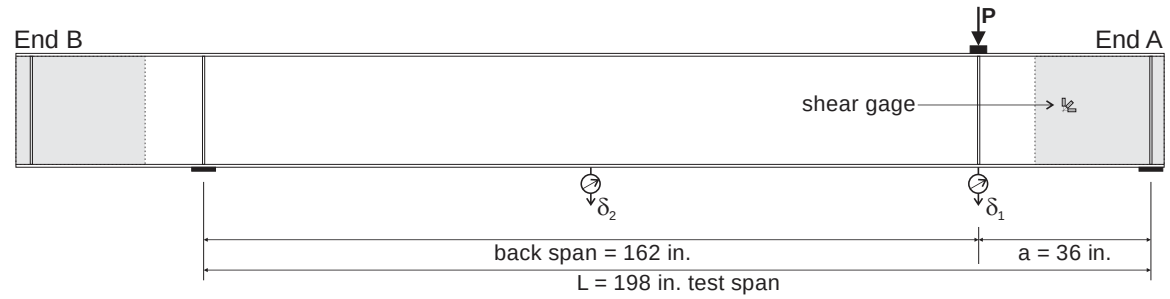

a) overall span instrumentation

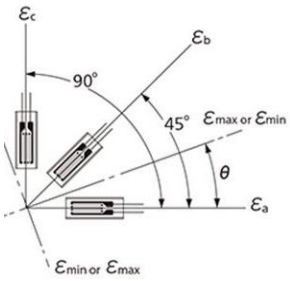

maximum and minimum principal strains:

$$\varepsilon_{max} = 0.5\left[\varepsilon_a + \varepsilon_c + \sqrt{2[(\varepsilon_a - \varepsilon_b)^2 + (\varepsilon_b - \varepsilon_c)^2]}\right]$$

$$\varepsilon_{min} = 0.5\left[\varepsilon_a + \varepsilon_c - \sqrt{2[(\varepsilon_a - \varepsilon_b)^2 + (\varepsilon_b - \varepsilon_c)^2]}\right]$$

maximum shear strain:

$$\gamma_{max} = \sqrt{2[(\varepsilon_a - \varepsilon_b)^2 + (\varepsilon_b - \varepsilon_c)^2]}$$

direction of principal strain

$$\theta = 0.5\tan^{-1}\left[\frac{2\varepsilon_b - \varepsilon_a - \varepsilon_c}{\varepsilon_a - \varepsilon_c}\right]$$

b) draw wire transducers

c) shear gage

d) shear gage calculations (image: Kyowa-ei.com)

Figure 42 Instrumentation.

3.6 Repair Designs

Girder 1 is an undamaged control girder and Girder 2 is a corrosion-damaged control girder; neither are repaired. Girder 1 provides the baseline 'target' capacity for restoring the capacity of the damaged girders. Girder 2 provides the baseline residual capacity available without repair. Initial designs and discussion of each repair technique were presented in Chapter 2.

3.6.1 Girder 3 – Conventional Bolted Steel Repair

Girder 3 is a 'control' specimen of sorts. The bolted steel repair is intended to match as closely as possible current practice. The bolted steel repair of Girder 3 – shown in Figure 43 – is essentially the same as that used to repair the archetypical damaged girder from Bridge D (Figures 29 and 30). Research Team member Jason Mash – in his role as a consulting engineer – prepared the bolted steel repair design for Bridge D. The Girder 3 repair consists of replacing the damaged 3 x 0.5 in. bearing stiffeners with 3 x 3 x 1/2 SLBB angles. An additional bent 0.25 in. plate is used along both sides of the lower web-to-flange interface.

9/16 in. diameter holes were drilled into the web and flanges to accommodate the 0.5 in. diameter Grade 8 bolts used[29]. All bolts were torqued to 110 ft-lbs which provides a pretension of 13.2 kips.

The material properties of the repair components were not determined.

[29] SAE Grade 8 is equivalent to ASTM F3125 Grade A490. Grade 8 are more readily available at this smaller bolt diameter. Both grades have minimum yield and tensile strengths of 120 and 150 ksi, respectively.

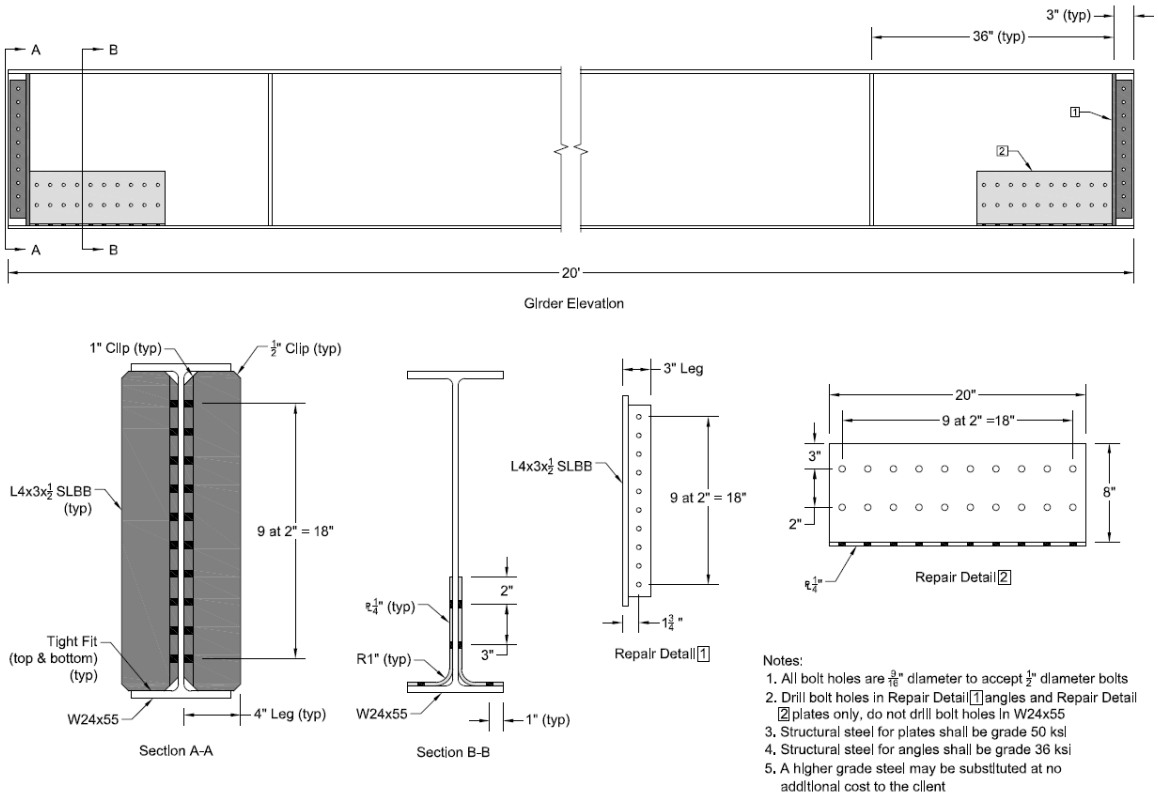

Figure 43 Bolted steel repair detail for Girder 3.

3.6.2 Girder 4 – UHPC Repair

Girder 4 was repaired using a full-girder depth UHPC repair located over the bearing and corrosion-damaged region as shown in Figure 44. A total of 30 – 0.5 in. Grade 8 bolts were used as shear studs at each girder end. These were installed as shown in Figure 44 in an alternating arrangement. The use of bolts, rather than welded studs, was described in Section 1.10.1. Given the thin and irregular web surface, it would not have been practical [or not possible] to weld studs to the test girder. It is noted that no shear connectors were provided on the beam flanges.

The full-depth UHPC was placed into closed forms through a 6 in. PVC elbow (Figure 44) as has been demonstrated in the field (Hain and Zaghi 2021). Because of the toughness of the UHPC, the filled PVC was not easily removed and was left in place during testing.

LaFarge Ductal® 130 UHPC was used. This proprietary mix consists of a bagged premix, liquid admixture and 2% steel fibers by weight. The UHPC was prepared in a single 4.1 ft^3 batch using a 12 ft^3 capacity mortar mixer. The mix proportions and mixing protocol used are given in Table 19. The mix protocol was prescribed by the LaFarge and the temperature and flow at placement were within specifications. The manufacture-reported compression strength for this material is 14 ksi and 21 ksi at 4 and 28 days, respectively. As seen in Table 19, these specifications were achieved.

Girder 4A was tested at an age of 28 days. The fatigue conditioning of Girder 4B took place between days 62 and 72 and the final monotonic test of 4B took place at an age of 90 days.

PennDOT indicated that due to the high forces involved, 2 in. cube tests are sometimes used for UHPC. Although the data is limited, the cube compressive strength obtained in this study was markedly less than that from the specified 3 in. cylinder tests. Further research is required to determine an appropriate relationship between cylinder and cube tests. Nonetheless, to adequately test 3 in. UHPC cylinders, a test machine having a capacity of at least 150 kips is necessary whereas cube tests may require only 100 kips. Cylinders also require that their ends be ground parallel; conventional cylinder capping techniques are inadequate for UHPC.

Table 19 UHPC mix protocol and measured material properties.

	Girders 4A and 4B	mix procedure
date UHPC placed	4 August 2021	
batch size	4.1 ft^3	
UFTEC L premix	550 lbs	dry mixed for 2m
Ductal F4 admixture	5.5 lbs	added and mixed for 6m 15s
water	24 lbs	
ice	15 lbs	
steel fiber	40.7 lbs	added over 1m 35s and mixed for 2m
ambient temperature during mixing	74.3 ºF	
mix temperature at removal from mixer	79.7 ºF	
flow table (2 min.)	9 in.	
3 in. cylinder compressive strength at 53h	14.3 and 14.1 ksi	
3 in. cylinder compressive strength at 168 h	19.4 and 17.5 ksi	
3 in. cylinder compressive strength at 28 days	21.8 and 20.9 ksi	
3 in. cylinder compressive strength at 90 days	17.1[a] and 22.7 ksi	
2 in. cube compressive strength at 28 days	16.9 and 13.1 ksi	
2 in. cube compressive strength at 90 days	18.9 and 20.6 ksi	
[a] nonsymmetric failure attributed to poor end-grinding		

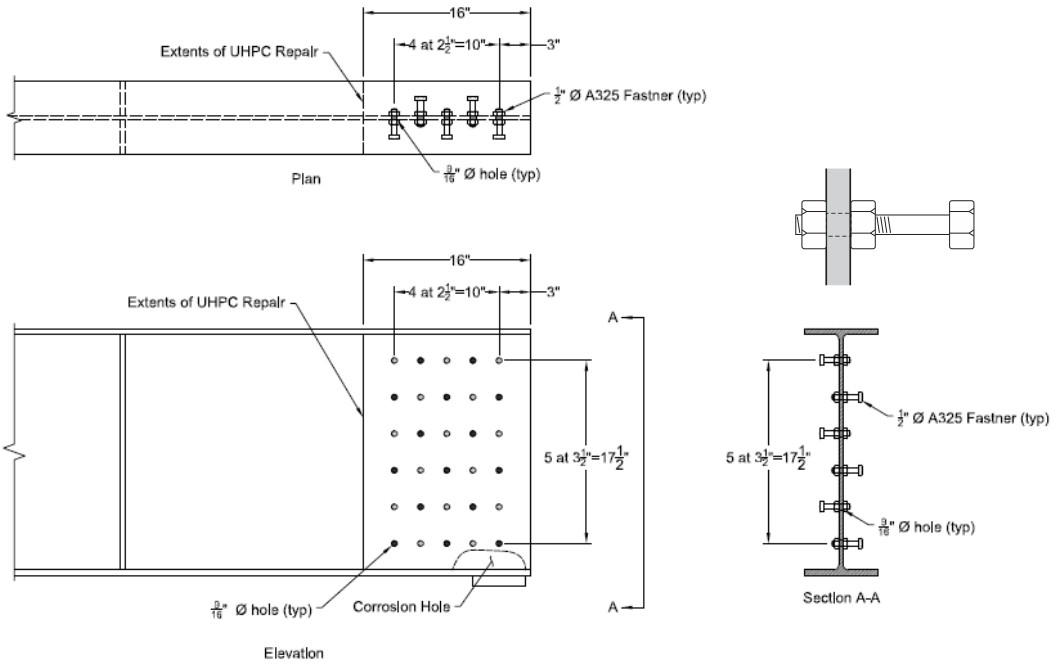


shear connectors


UHPC encasement


6 in. PVC used to place UHPC

Figure 44 UHPC repair detail for Girder 4.

3.6.3 Girder 5 – Reinforced Concrete (RC) Repair

Girder 5 was repaired using a full-girder depth conventional RC repair located over the bearing, corrosion-damaged region and extending the length of the shear span to the point of load application; this is shown in Figure 45. To provide confinement, vertically oriented #3 hairpins were placed through 1 in. diameter holes in the web to effectively create closed tie reinforcement. Three additional horizontally oriented ties were located above the bearing region to better confine this highly-stressed region and potentially provide some anchorage for a diagonal compression strut in this region. The measured yield and tensile strengths of the #3 bars were f_y = 74.1 ksi and f_u = 111.7 ksi, respectively.

At the request of PennDOT, a relatively low strength concrete having a target strength of 4000 psi was used. Sakrete 5000 premixed concrete was used. This mix reports a cement (Type I/II) content of 10-30%. For the purposes of calculation, 20% cement content was assumed. The concrete was mixed and placed in the same manner – mixed in a 12 ft^3 mortar mixer and placed into closed forms through a 6 in. PVC elbow – as the UHPC. The concrete was internally vibrated using a conventional wand vibrator. Girder end 5B was placed first and the mix was barely workable for the application. Additional water was added for 5A, resulting in a lower strength. The mix proportion and material properties of the concrete used are given in Table 20.

Girder 5A was tested at an age of 28 days. The fatigue conditioning of Girder 5B took place between days 77 and 87 and the final monotonic test of 5B took place at an age of 91 days.

Table 20 RC mix and measured material properties.

	Girder 5A	Girder 5B
date of concrete placement	3 August 2021	3 August 2021
batch size	4 ft^3	4 ft^3
Sakrete 5000 premix	660 lbs	660 lbs
water	10 gal	8.3 gal
assumed *w/c*	0.63	0.52
28 day compression strength (ASTM C39)	3161 psi (0.034)	4560 psi (0.072)
28 day split cylinder strength (ASTM C496)	291 psi (0.060); $5.2\sqrt{f_c'}$	393 psi (0.032); $5.8\sqrt{f_c'}$
91 day compression strength (ASTM C39)	-	4920 psi (0.014)

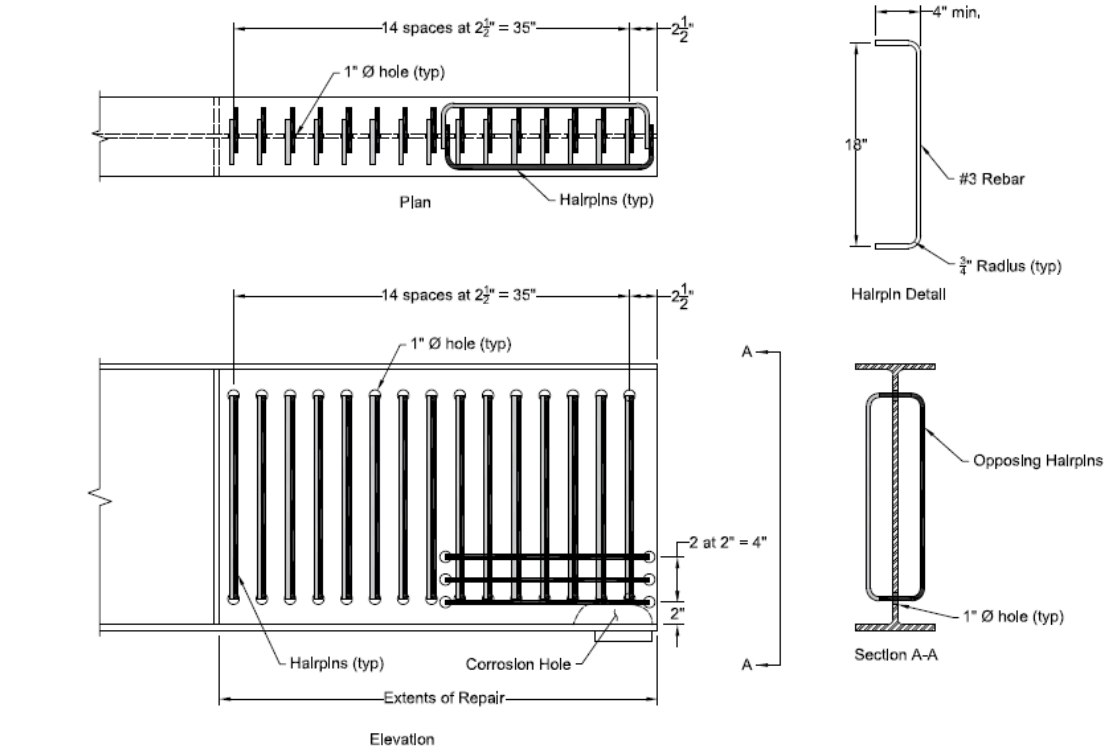

holes for steel hairpins steel hairpins in place completed concrete encasement

Figure 45 Reinforced concrete repair detail for Girder 5.

3.6.4 Girder 6 – Glass Fiber Reinforced Polymer (GFRP) Repair

Girder 6 was repaired using adhesively-bonded GFRP plates and pultruded I-sections. The steel surface to which the GFRP was bonded was first cleaned to an SSPC SP5 specification (Figure 46): blasting to white steel. A portable sand blasting unit was used. The GFRP surface to be bonded was lightly sand blasted to scar the resin-rich surface in order to enhance bond. Prior to adhesive installation, the steel and GFRP bonding surfaces were cleaned using compressed air and a primer consisting of 0.5% γ-GPS[30] silane in aqueous solution (Sigma Aldrich 440167) was applied and allowed to dry (about 1.5 hours). Unthickened SikaDur 32 epoxy adhesive was used and is applied in a thin layer to both faces to be bonded. Due to the relatively short potlife of SikaDur 32 (under 30 minutes), only one end of the beam was repaired at a time.

First, 0.5 in. GFRP plates were adhered to the entire web depth; the plates are fabricated such that their 'longitudinal' or strong direction is oriented vertically. Following installation of the plate, WF 3 x 3 x ¼ bearing stiffener sections are immediately applied on top of the 0.5 in. plate. Once installed, a clamping force was applied sufficient to bring all edges of the GFRP and steel web into contact. The entire assembly was left in place overnight. Although the outermost flange of the WF extends beyond the flange width, the presence of the WF flange provides support to the GFRP web resulting in a greater bearing capacity than if a WT were used.

Material properties of the GFRP and adhesive are given in Table 21. The GFRP used in this study was commercially-available (Bedford Plastics 2012) stock left over from previous studies. Measured material properties are those reported in these earlier studies.

Table 21 Material properties of pultruded GFRP and adhesive.

shape	0.5 in. plate		WF 3 x 3 x ¼		SikaDur 32
source of measured properties	manufacturer-reported (Bedford Plastics 2012)	measured (Cunningham et al. 2015)	manufacturer-reported (Bedford Plastics 2012)	measured (Cardoso 2014)	manufacturer-reported (Sika 2020)
resin type	polyester		vinyl ester		100% epoxy
d	-		3 in.	3.02 in.	-
b	-		3 in.	2.94 in.	-
t	0.5 in.		0.25 in.	0.25 in.	-
E_{Lt}	2000 ksi	3160 ksi	2500 ksi	3180 ksi	540 ksi (14d)
F_{Lt}	24 ksi	54.2 ksi	30 ksi	-	6.9 ksi (7d)
E_{Tt}	1400 ksi	1000 ksi	800 ksi	1770 ksi	-
F_{Tt}	10.0 ksi	11.4 ksi	7 ksi	-	-
E_{Lc}	-	-	2500 ksi	3710 ksi	210 ksi (7d)
F_{Lc}	-	-	30 ksi	62.4 ksi	12.2 ksi (14d)
G_{LT}	-	-	450 ksi	685 ksi	-
shear strength	-	-	-	-	6.2 ksi (14d)
bond strength to steel	-	-	-	-	2.0 ksi (14d)
elongation	F_{Lt}/E_{Lt} = 1.2%	F_{Lt}/E_{Lt} = 1.7%	F_{Lt}/E_{Lt} = 1.2%	-	1.9% (7d)
viscosity	-	-	-	-	4500 cps
pot life	-	-	-	-	30 min

E_{Lt} and F_{Lt} = modulus and strength in longitudinal direction determined from tension tests
E_{Tt} and F_{Tt} = modulus and strength in transverse direction determined from tension tests
E_{Lc} and F_{Lc} = modulus and strength in longitudinal direction determined from compression tests
G_{LT} = in-plane shear modulus

[30] γ-glycidoxypropyltrimethoxy = $CH_2OCHCH_2O(CH_2)3Si(OCH_3)_3$

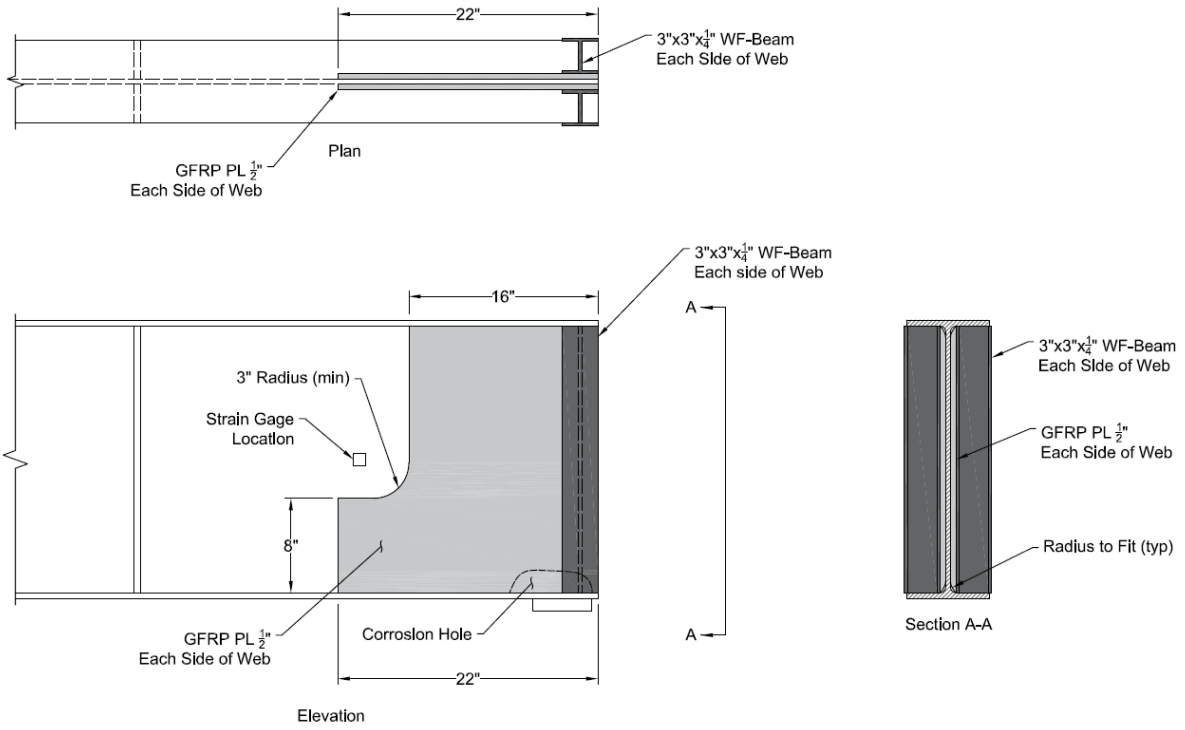

SSPC SP5 surface preparation

installation of FRP

completed FRP repair

Figure 46 GFRP repair detail for Girder 6.

3.7 Girder End A Monotonic Test Results

In the following discussion of test results, girder shear, V, is reported; that is the value of the reaction force at the bearing nearest the applied load, P. In all cases, $P = 1.22V$. The resulting applied moment at the point of application of load, $M = 3V$ (kip-ft). Additionally, due to the variation in web thickness (Section 3.3.2), it is convenient to report shear in terms of shear *stress*, $v = V/dt_w$; where $d = 23.6$ in. is the depth of the W24x55 section and t_w is the average measured web thickness in the reduced-thickness portion of the shear span (Table 17; repeated for clarity in Table 22).

A summary of key parameters of all End A tests is provided in Table 22. The values in parentheses are the ratios of the reported value to those for the control Girder 1A. The initial stiffness of the beam, K is determined from a straight line fit of the demonstrably linear portion of the shear-deflection curves shown in Figure 47 (straight line fits are shown in dashed lines). The deflection used is that under the load point (δ_1). This value is also reported in terms of shear stress as k. The values of V_{max} and v_{max} are determined at the maximum shear force observed in the test. The maximum shear strain,

γ_{max} is calculated from strain gage data as given in Figure 42d. The shear stress at theoretical shear yield strain, "v at γ = 1900 $\mu\varepsilon$", is also reported as a point of comparison between girders. Finally, because the beams were much stronger than intended (Section 3.2.2), observation of girder yield at the point of application of load is also made. This latter phenomenon was fully supported by full depth bearing stiffeners and is not believed to have significantly affected the shear span or bearing behavior of interest in this study.

Figure 47 shows the applied shear stress (V/dt_w) versus deflection (δ_1) curves obtained for all specimens. Control Girders 1A and 2A are repeated on all plots and each plot shows one of 3A to 6A. Without repair, all girders would exhibit a behavior similar to that shown for 2A. The initial stiffness of all repaired girders is similar to that of the undamaged control girder. With the exception of 6A, the load resisting behavior and ultimate capacities were also similar. Repairs demonstrated in Girders 3, 4 and 5 effectively restored the capacity of the corrosion-damaged girder end regions.

Table 22 Summary of key parameters of monotonic End A tests.

Girder		**1A**	**2A**	**3A**	**4A**	**5A**	**6A**
		undamaged control	corroded control	steel repair	UHPC repair	RC repair	GFRP repair
t_w	in	0.326	0.324 (0.99)	0.305 (0.94)	0.317 (0.97)	0.281 (0.86)	0.288 (0.88)
$K = V/\delta_1$	k/in	332	65 (0.20)	280 (0.84)	285 (0.86)	280 0.84)	292 (0.88)
$k = v/\delta_1$	ksi/ in	42.9	8.6 (0.20)	38.2 (0.89)	38.5 (0.90)	42.2 (0.98)	41.5 (0.97)
V_{max}	kips	213.1	15.1 (0.07)	196.6 (0.92)	202.9 (0.95)	199.3 (0.94)	81.8 (0.38)
$v_{max} = V_{max}/dt_w$	ksi	27.7	2.0 (0.07)	27.3 (0.98)	27.1 (0.98)	30.1 (1.09)	11.6 (0.42)
δ_1 at V_{max}	in.	0.78	0.28	0.71	0.76	0.76	0.28
failure at V_{max}		web buckling	bearing	web buckling	web buckling	concrete crushing at bearing	catastrophic GFRP debonding
γ_{max} at V_{max}	με	2730	256	3946	4852	2158	1174
v at $\varepsilon = \varepsilon_y$ = 1900 $\mu\varepsilon$	ksi	27.7	no yield	18.2	26.2	no yield	no yield
v at γ = 1900 $\mu\varepsilon$	ksi	20.0	-	18.2	21.9	27.6	-
V at initial yield at load point	kips	164 theoretical	no yield	147	not clearly observed	no yield; concrete contributes to bearing	no yield

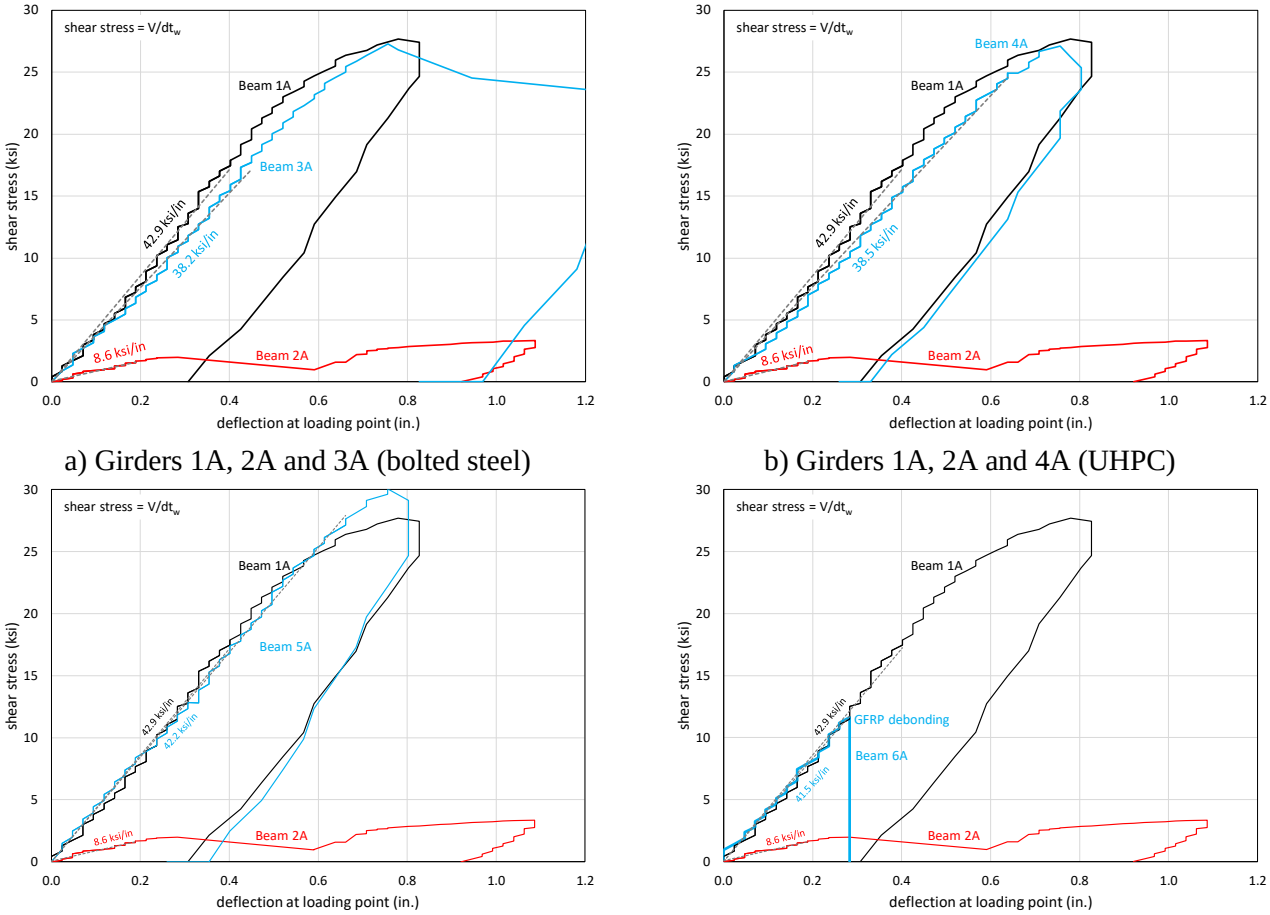

a) Girders 1A, 2A and 3A (bolted steel)

b) Girders 1A, 2A and 4A (UHPC)

c) Girders 1A, 2A and 5A (RC)

d) Girders 1A, 2A and 6A (GFRP)

Figure 47 Shear stress versus displacement curves from monotonic tests.

Maximum principal shear strains, γ_{max} and the angle of maximum shear, θ, (see Figure 42d for calculation of both) are shown in Figure 48. Initiation[31] of buckling was observed in Girders 1A, 3A and 4A. These girders had repair measures over only part of the shear span; the web region beyond the repair region was observed to buckle in each case. The web of Girder 5A, on the other hand, was entirely encased in well confined concrete and no evidence of web buckling – despite the initial out of straightness (see Table 17) – was observed. The concrete effectively braced the web against buckling. This is shown dramatically in Figure 53d, in which the initial distortion of the embedded web of 5A is shown at the end of testing (concrete was forcibly removed to obtain this image). This significant degree of distortion did not affect the ultimate capacity of this girder end.

The orientation of maximum shear (Figure 48b) for all specimens (except 2A) is in the vicinity of 45° to 50° as assumed by Bernoulli beam theory. 2A exhibited a very steep angle since the stress trajectories had to redistribute to accommodate the loss of bearing capacity. In 2A, bearing capacity of the beam end was provided mostly by bending of the bottom flange (see Section 3.7.2).

The steel web of Girder 5A resisted a smaller portion of the shear since it was entirely encased in concrete which was therefore able to resist most of the shear stress. Thus the shear stress shown in Figure 48a for 5A is not that carried by the web but that which *would* be carried by the web in the absence of the surrounding concrete. A discussion of the composite behavior of Girder 5 is provided in Section 3.10.

[31] For the End A tests, loading was stopped when buckling became evident in order to protect the girder from distorting so much that End B tests would be affected.

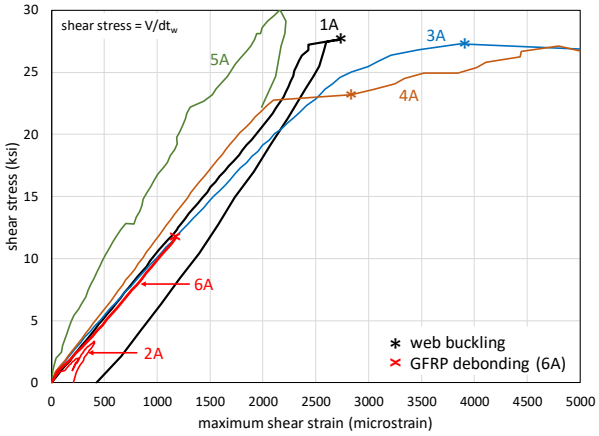

a) maximum shear strains, γ_{max}

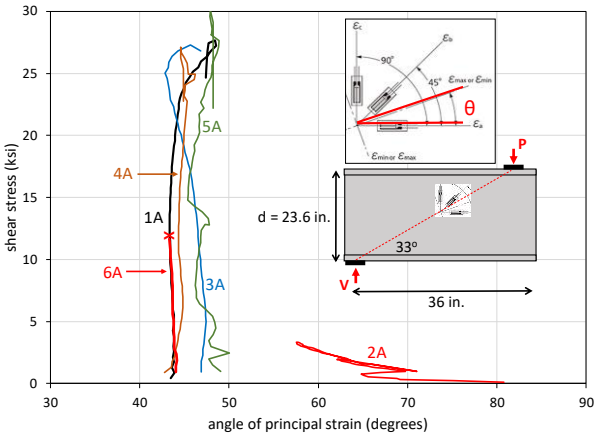

b) orientation of maximum strain, θ

Figure 48 Principal shear strains and orientation of maximum shear for monotonic End A tests.

3.7.1 Girder End 1A

Undamaged control Girder 1A behaved essentially as predicted, achieving a maximum shear capacity V = 213 kips (v = 27.7 ksi). This capacity corresponded to web yield beneath the applied load (260 kips applied over a 5 in. length of flange); this is shown in Figure 49. The predicted capacity based on this limit state was an applied load of 256 kips or shear of 210 kips. Nonetheless, strain data (Figure 48) indicated that web buckling had also just initiated at this capacity.

a) yield lines expressed in mill scale under point of application of load

b) distortion of top flange associated with web yield under point of application of load

Figure 49 Girder 1A following testing.

3.7.2 Girder End 2A

Unrepaired corroded Girder 2A exhibited little capacity, achieving a shear resistance of barely 7% of 1A: V = 15.1 kips (v = 2.0 ksi). In this girder, shown in Figure 50, the bearing capacity was provided almost entirely by the bottom flange bending about its weak axis. The web collapsed and some residual capacity was observed at displacements exceeding 0.75 in. (Figure 47) as the hole in the web physically closed and began to bear again on the flange.

a) bearing region during testing

b) residual distortion of bearing region after testing

c) complete collapse of the web

Figure 50 Girder 2A during and after testing.

3.7.3 Girder End 3A

Girder 3A demonstrated a conventional bolted steel repair. The girder capacity was effectively restored to approximately that of 1A: V = 197 kips (v = 27.3 ksi). 3A exhibited very clear web buckling in the unstrengthened region of shear span as shown in Figure 51. Following testing, the bolted stiffeners were removed (Figure 51d); no web distortion or collapse was observed although a few of the bolt holes appear to show evidence of bolt-bearing distortion ('ploughing').

a) bearing region following testing

b) web distortion following testing and removal of stiffeners

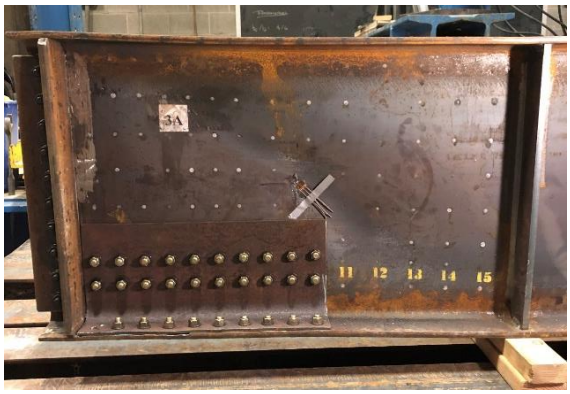

c) web buckling

d) bearing region following testing and removal of stiffeners

Figure 51 Girder 3A following testing.

3.7.4 Girder End 4A

UHPC-encased repair 4A achieved a capacity of V = 203 kips (v = 27.1 ksi), effectively restoring the capacity of 1A. Failure was predicated by buckling of the unencased portion of the web. As seen in Figure 52 there was essentially no discernible damage to the UHPC itself. Separation between the top and bottom flanges and the UHPC was noted at shear of V = 42 kips, approximately 21% of the ultimate capacity (Figure 52b). This crack, once formed did not appear to vary through the remainder of the test. The presence of the crack at relatively low (service) load levels does indicate the potential for crevice corrosion at these interfaces. The assumed strains at which this crack appeared suggests that it would not be mitigated by providing shear connectors along the flange.

a) bearing region following testing

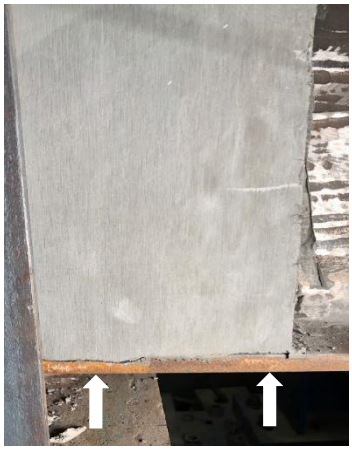

b) separation along flange-UHPC interface was observed at V = 42.5 kips

Figure 52 Girder 4A following testing.

3.7.5 Girder End 5A

The reinforced concrete-encased repair 5A extended along the entire shear span and effectively mitigated web instability. Despite the quite low concrete strength (3.2 ksi; see Table 20), the girder capacity, V = 199 kips (v = 30.1 ksi), marginally exceeded that of 1A. The web thickness of 5A was only 86% of that of 1A while the maximum shear stress was 109% that of 1A.

The concrete encasement was well confined and appeared to behave as a concrete beam in shear. Concrete cracking initiated at a shear of V = 42.5 kips (Figure 53a). The concrete crack pattern developed as the test progressed (Figure 53b) although all crack widths remained well controlled and the concrete remained sound.

Cracking and minor spalling was observed at the back of the bearing region from a shear of V = 59 kips. Concrete crushing at the bearing represented the ultimate failure of this Girder end (Figure 53c). The low concrete strength clearly contributed to this behavior. The horizontal reinforcement provided above the bearing (Figure 45) appeared to control spalling to some extent although due to the corrosion damage, this reinforcement is difficult to anchor in the bearing region – right where it is needed most.

As the bearing began to crush, the cracking along the shear span became flatter: initial cracking was observed at an angle of about 45^o (Figure 53a) while later cracks transitioned to an angle of about 30^o (Figure 53b) [measured from horizontal as indicated in Figure 42d].

Figure 53d shows the web distortion inside the concrete. This distortion is that around which the concrete was placed; the distortion was unaffected during testing. Thus the confined concrete effectively restrained the damaged web. Shear strain data (Figure 48a) indicates that this web did not resist as great a proportion of the load as in other specimens: there was load sharing between the

concrete and steel web. This observation is supported by the nature of the concrete cracking and is discussed further in Section 3.10.

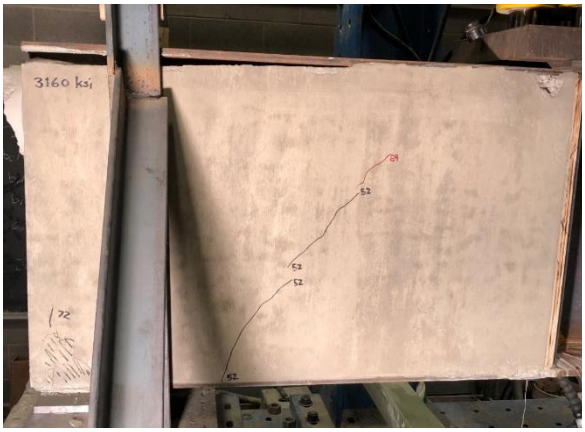

a) initial cracking at V = 42.6 kips; crack angle ≈ 45°

b) final crack pattern after completion of tests; late-forming crack angle ≈ 30°

c) concrete bearing failure

d) encased concrete mitigated further distortion of web (distortion seen was present at concrete placement); concrete intentionally removed to show web

Figure 53 Girder 5A during and following testing.

3.7.6 Girder End 6A

As seen in Figures 47d and 48, Girder 6A initially behaved quite well, matching the stiffness of the Girder 1 and the other repaired girders. At V = 81.8 kips (v = 11.6 ksi), about 40% of the capacity of Girder 1, Girder 6A exhibited catastrophic debonding of the GFRP plate. Immediately upon debonding, the now-overloaded web collapsed at the bearing as seen in Figure 54c. Although the final failure was quite brittle, debonding was progressive: some evidence (popping sounds) occurred at V = 42.5 kips and progressed until the test ended. A delamination crack was evident above the bearing region at V = 68.7 kips (Figure 54b). Because of the poor, brittle performance of 6A, fatigue conditioning and testing of 6B was not undertaken.

Bond between the steel and GFRP plate was quite good on the smooth web surface (Figure 54f) while evidence of voids in the adhesive line are evident on the 'corroded' side which had greater amplitude of small flaws (see Figure 46). In both cases, debonding occurred primarily as an adhesive failure at the GFRP plate interface (Figures 54e and f). The bond of the GFRP W3 stiffener to the GFRP plate was excellent. While the debonding still occurred primarily as an adhesive failure at the GFRP plate interface, some evidence of cohesive failure penetrating the plate was seen (Figure 54d).

a) bearing at beginning of test

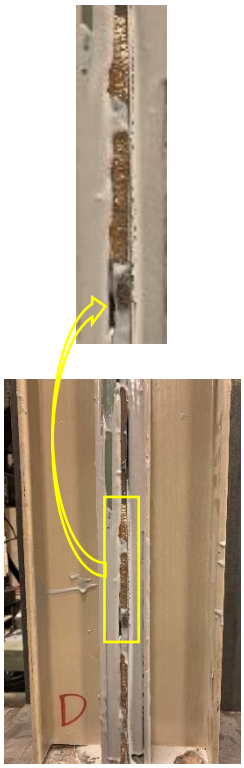

b) initial debonding at V = 68.7 kips

after removal of GFRP

c) catastrophic debonding at V = 81.8 kips

d) debonded surface of W3 and GFRP plate

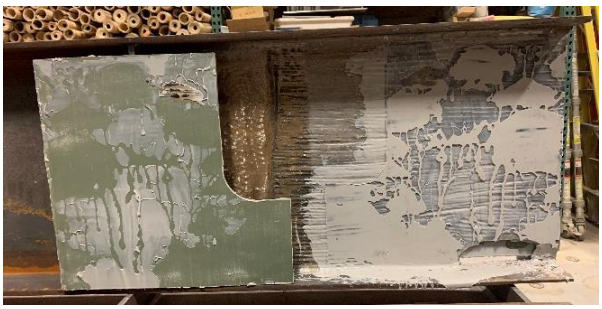

e) debonding of West side GFRP plate (affixed to 'corroded' steel)

f) debonding of East side GFRP plate (affixed to smooth steel)

Figure 54 Girder 6A following testing.

3.8 Fatigue Conditioning (Girder Ends B)

Fatigue conditioning was undertaken for Girders 3, 4 and 5. Because of the poor brittle performance of 6A, fatigue conditioning of 6B was not undertaken. Girder 1 has no damage and should not be expected to exhibit any deterioration under the fatigue conditioning used and was therefore not tested[32]. Girder 2 exhibited a static capacity below the fatigue loads (P = 24 ± 20 kips) and was therefore also not tested. Fatigue conditioning to 1 million cycles was not expected to result in any significant deterioration of the specimens. Indeed, very little was observed.

In order to quantify deterioration, the history of the maximum shear strain, γ_{max}, (see calculation shown in Figure 42d) and displacement of the load point, δ_1, with cycling for all specimens is reported in Figure 55. Data is reported at the peak shear force, V = 36 kips (P = 44 kips) and mean shear, V =

[32] based on AASHTO LRFD fatigue life calculations, the fatigue life of Girder 1 subject to the conditioning protocol used in this study is N = 125,000,000 cycles

19.7 kips (P = 24 kips). Only initial and final cycle data is reported at the minimum shear, V = 3.3 kips (P = 4 kips). Any deterioration would result in an increase in these values as the apparent stiffness of the girder fell. Although displacement data is shown in Figure 55, this is not directly comparable with that reported in the monotonic tests: displacement during fatigue conditioning is determined from the actuator LVDT and therefore includes compliance of the actuator and test frame.

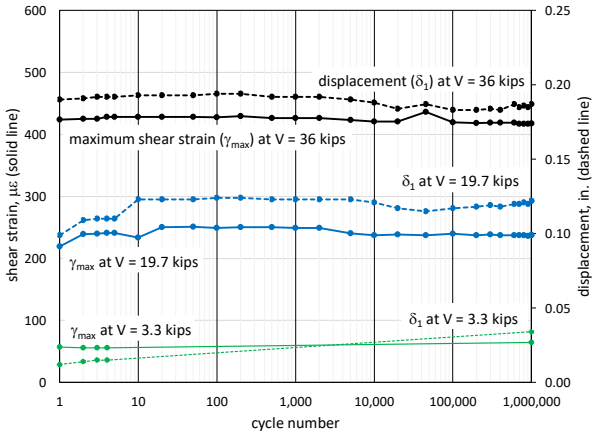

a) Girder 3B

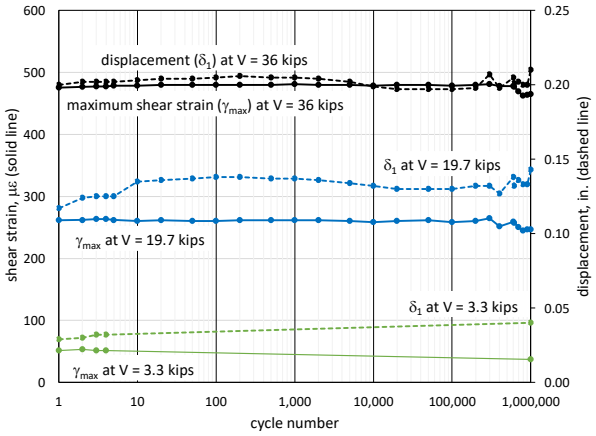

b) Girder 4B

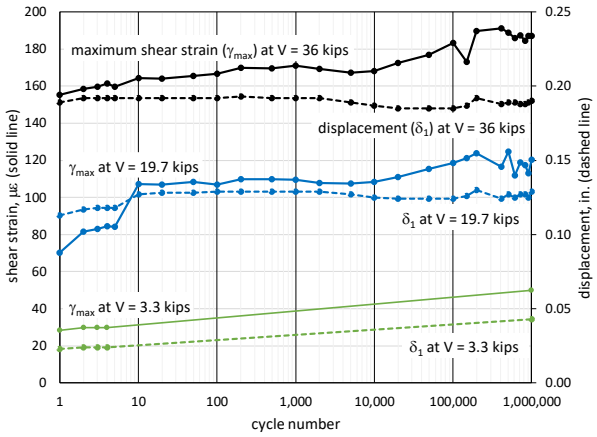

c) Girder 5B (note different scale for strain axis)

Figure 55 Shear strain and displacement histories during fatigue conditioning.

3.8.1 Girder End 3B

The source of the 0.013 in. increase at V = 19.7 kips between the fifth and tenth cycle (Figure 55a) is unknown although may be related to the test protocol: the first five individual cycles were conducted "manually" at a rate on the order of 0.1 Hz whereas, beginning with cycles 6 to 10 cycling at 1.2 Hz was initiated. The increase was evident in other specimens as well. Since the step is not seen at V = 36 kips or in the strain data, this is not interpreted as any damage to the girder. Peak shear strains at V = 36 kips remained in the range 417 με – 436 με whereas γ_{max} = 455 με at V = 36 kips in End A. No distress in Girder 3B was evident following one million cycles fatigue conditioning.

3.8.2 Girder End 4B

Separation of the UHPC and bottom and top flanges, similar to that shown in Figure 52b, was evident from the initial cycle although this was not observed to progress through one million cycles of fatigue conditioning. Small variations in measured displacements (variation less than 0.02 in.) and strains (variation less than 20 με) for N > 200,000 was observed; these are not interpreted as representing any significant damage initiation or progression. Peak shear strains at V = 36 kips remained in the range 462 με – 481 με whereas γ_{max} = 397 με at V = 36 kips in End A. Recognizing that the steel web thickness of 4B was only 84% of that of 4A, these strains are essentially equivalent.

3.8.3 Girder End 5B

No cracking of the reinforced concrete was observed in initial cycles. Distress in the form of concrete cracks (see Figure 56) was first observed at N ≈ 49,000 cycles. The cracking propagated somewhat through N = 200,000 cycles. After N = 200,000 cycles, apart from a short crack extension observed in one crack at N ≈ 340,000 cycles, no additional distress was observed through 1,000,000 cycles. Such fatigue damage progression in reinforced concrete is relatively typical (ACI 215R-22). All cracks were 'hairline' and only observable (i.e. open) when the beam was subject to the maximum shear, V = 36 kips indicating that they were being well controlled by the internal reinforcement.

a) East side (support bearing at right)

b) support region

c) West side (support bearing at left); vertical crack (dotted lines) appeared prior to testing

Figure 56 Cracking observed during fatigue conditioning of Girder 5B.

Unlike Girders 3B and 4B, a steady increase in web strain was observed with fatigue conditioning (Figure 55c). Due to the concrete encasing the entire shear span – and sharing in the shear resistance, the steel web strains in Girder 5 are lower than those in the other girders (note different vertical strain scale in Figure 55). The peak shear strain at V = 36 kips in End A was 206 με. The peak shear strain during fatigue conditioning progressed from 155 με at N = 1 to 191 με at N ≈ 400,000, falling marginally to 187 με at N = 1,000,000. A similar progression is seen at V = 19.7 kips and V = 3.3 kips. This progression was not accompanied by a meaningful change in displacement and therefore can be attributed to a minor degradation of the composite behavior of the reinforced concrete encasement resulting in shear being redistributed from the concrete back into the steel web.

3.9 Girder End B Post Fatigue Conditioning Monotonic Test Results

These tests are the same as the End A tests except that they are conducted following the one million cycles of fatigue conditioning described in the previous sections. A summary of key parameters of all End B tests is provided in Table 23. The End A data (reported in Table 22) is repeated in Table 23 for clarity and the values in parentheses are the ratios of the reported value to those for End A of the same girder. Figure 57 shows the applied shear stress (V/dt_w) versus deflection (δ_1) curves obtained for all specimens. Control Girder 1A is repeated on all plots and each plot shows one set of comparable girder ends. Figure 58 shows a comparison of the maximum shear strains for each fatigue conditioned girder.

Each of the End B tests performed essentially the same as the End A tests. Because the End B tests were the last conducted, these could be 'pushed' to larger deformations than End A tests.

Each of the End B tests exhibited an initially stiffer response and resisted greater capacity than the comparable End A. This may have resulted from the 'shakedown' effect from the fatigue conditioning. This result confirms that the fatigue conditioning protocol used had no deleterious effect on the girders' performance.

When interpreting results, it should be noted that strain data is generally unreliable at gage readings exceeding 10,000 με (0.1%) and that the gage [embedded in concrete] of Girder 5B failed during testing at essentially the peak load attained.

Table 23 Summary of key parameters of monotonic End B tests.

Girder		**3A**	**3B**	**4A**	**4B**	**5A**	**5B**
		steel repair		UHPC repair		RC repair	
t_w	in	0.305	0.298 (0.98)	0.317	0.265 (0.87)	0.281	0.287 (1.02)
f_c at time of test	psi	-	-	21,400	22,700 (1.06)	3160	4920 (1.56)
$K = V/\delta_1$	k/in	280	297 (1.06)	285	301 (1.06)	280	335 (1.20)
$k = v/\delta_1$	ksi/in	38.2	41.3 (1.08)	38.5	48.1 (1.25)	42.2	49.5 (1.17)
V_{max}	kips	196.6	216.0 (1.10)	202.9	199.0 (0.98)	199.3	232.7 (1.17)
$v_{max} = V_{max}/dt_w$	ksi	27.3	30.7 (1.12)	27.1	31.8 (1.17)	30.1	34.4 (1.14)
δ_1 at V_{max}	in.	0.71	0.87 (1.22)	0.76	0.83 (1.09)	0.76	0.99 (0.30)
failure at V_{max}		web buckling	stiffener bearing and web buckling	web buckling	web buckling	concrete crushing at bearing	web yield
γ_{max} at V_{max}	με	3946	>10,000	4852	>10,000	2158	4008
v at $\varepsilon = \varepsilon_y$ = 1900 $\mu\varepsilon$	ksi	18.2	28.0	26.2	27.7	no yield	34.4
v at γ = 1900 $\mu\varepsilon$	ksi	18.2	21.9	21.9	17.8	27.6	27.5
V at initial yield at load point	kips	147	not clearly observed	not clearly observed	not clearly observed	no yield	no yield

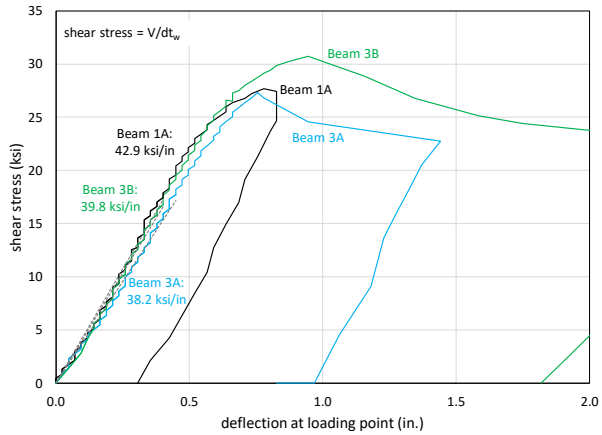

a) Girders 1A, 3A and 3B

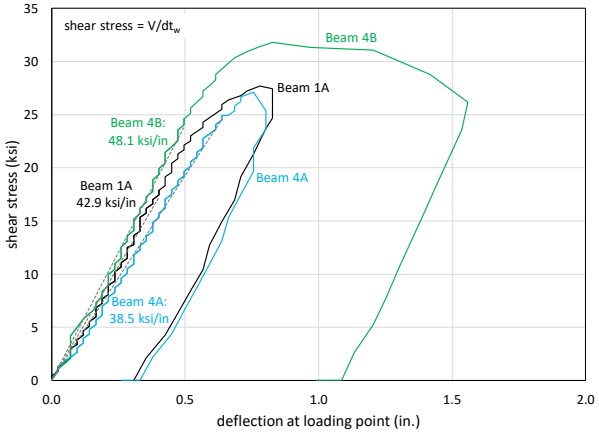

b) Girders 1A, 4A and 4B

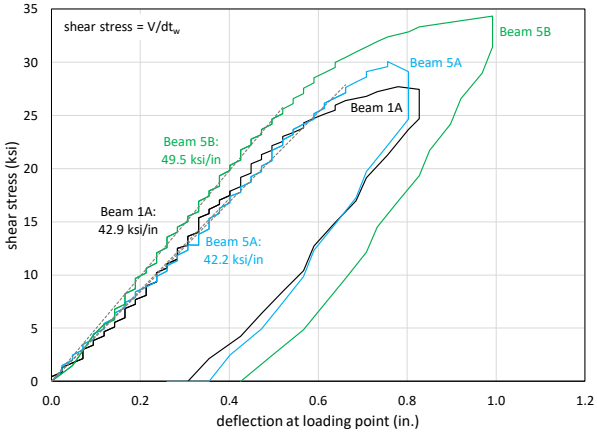

c) Girders 1A, 5A and 5B

Figure 57 Shear stress versus displacement curves from monotonic tests.

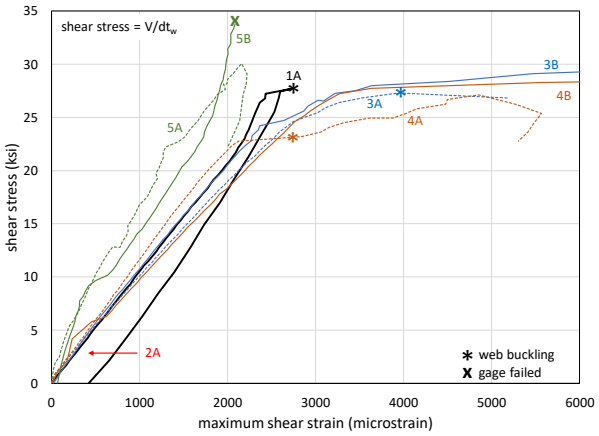

a) maximum shear strains, γ_{max}

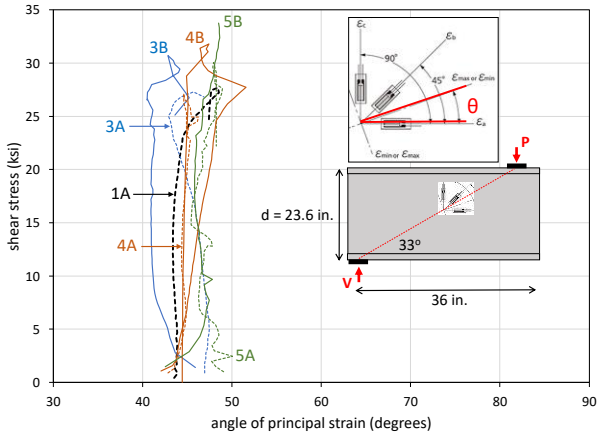

b) orientation of maximum strain, θ

Figure 58 Principal shear strains and orientation of maximum shear for monotonic End A tests.

3.9.1 Girder End 3B

Girder End 3B behaved in a manner comparable to End 3A (Table 23), achieving a marginally greater ultimate capacity of V = 216 kips. Web buckling dominated ultimate behavior (Figure 59a) although it was also noted that the bearing stiffener exhibited yield (Figure 59b). The AASHTO-prescribed (Eq. 8) design capacity of the fitted end of the bearing corresponds to $V = 1.4A_{pn}F_y$ = 140 kips

whereas the nominal capacity is best estimated to be $V = 1.8A_{pn}F_y$ = 180 kips (ANSI/AISC 360 2016 §J.7(a)).

During testing of End 3B, some instances of 'bolt banging' were heard beginning at V = 147 kips. Like Girder End 3A, upon removal of the repair plates, a few holes along the bearing stiffener showed evidence of bearing induced distortion ('ploughing'). No evidence of fatigue-induced damage (fretting, fraying, etc.) at bolted interfaces was apparent and the faying surfaces had clearly remained in full frictional contact throughout fatigue conditioning (V < 36 kips).

a) Girder 3B following testing

b) evidence of yield of the bearing stiffener – imprint of stiffeners on bottom flange (arrows)

Figure 59 Girder 3B following testing.

3.9.2 Girder End 4B

Girder End 4B achieved a capacity of V = 199 kips, comparable to that of End A (Table 23) and the ultimate behavior was controlled by buckling of the unencased portion of the web (Figure 60). Flange distortion at the ultimate load (Figure 60) indicates that the UHPC effectively created a 23 in. long shear panel between the applied load and edge of the UHPC. There was no apparent distress in the UHPC apart from minor separation along the flanges as also observed for End A (Section 3.7.4).

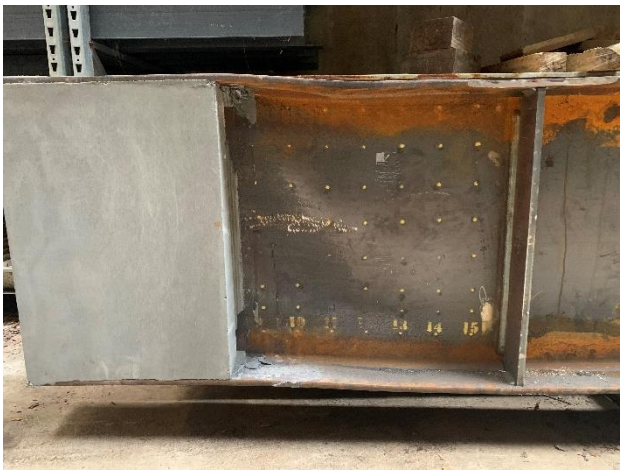

Figure 60 Girder 4B following testing showing panel buckling of the unencased portion of the web.

3.9.3 Girder End 5B

The capacity achieved by Girder End 5B was V = 233 kips, exceeding that of 5A (199 kips) despite the web thickness being essentially the same (Table 23). The concrete strength in End 5B was greater

(Table 20) resulting in an improved overall response. The cracks that had formed during fatigue conditioning opened with increased loading and new cracks appeared at a V = 72 kips. Like End 5A, the angle of the cracks was approximately 45° at lower loads and flattened to about 30° as the applied shear increased (see Figure 61).

The concrete remained in good shape and effectively resisted steel web buckling throughout the test. Following testing, concrete was removed and the web was found to have remained entirely plane, as expected.

a) East side (support bearing at right) b) West side (support bearing to left)

Figure 61 Girder 5B following testing.

3.10 Composite Behavior of Reinforced Concrete Encased Girder 5

The analysis described in this section is approximate, requiring a fitting curve for the section shear stress ($v = V/dt_w$) versus measured steel web shear strain (γ_{max}) to be established. A cubic relationship having excellent fit characteristics ($R^2 > 0.99$ in all cases) was used, although this 'forces' the proportion shown to also be cubic. The fitting curves determined from experimental data are as follows, with τ_{max} expressed in microstrain.

Girder 1A: $\gamma_{max} = -0.047v^3 + 1.404v^2 + 86.48v$ [19]

Girder 5A: $\gamma_{max} = -0.106v^3 + 1.469v^2 + 36.99v$ [20]

Girder 5B: $\gamma_{max} = -0.102v^3 + 4.483v^2 + 24.73v$ [21]

In all girders except Girder 5, the strain recorded from the web captures 100% of the shear resisted at the location of the strain gage located at the center of the shear span. In Girder 5, the web is encased by reinforced concrete at this location and therefore shear is expected to be resisted in a composite manner. Using the web stress strain behavior of Girder 1A as a benchmark, the proportion of total shear resisted by the steel girder web can be estimated as the ratio of steel web shear strain in Girder 5 to that observed in Girder 1 (i.e, the ratios of Eq. 20/Eq. 19 and Eq. 21/Eq. 19 for 5A and 5B, respectively).

Based on a simple transformed sections analysis, the steel webs are expected to resist 35% and 31% of the total applied shear for Ends 5A and 5B, respectively. As seen in Figure 62, the initial proportion of shear resisted by the web of End 5A is 44% and that for 5B is 33%. During fatigue conditioning of End 5B, the proportion began at 30% and progressed to 38% over 1 million cycles. In both Ends 5A and 5B, as the load increases, a greater proportion of shear is resisted by the steel web. This indicates that there is a deterioration of the composite behavior present and shear is being redistributed from the concrete to the steel web.

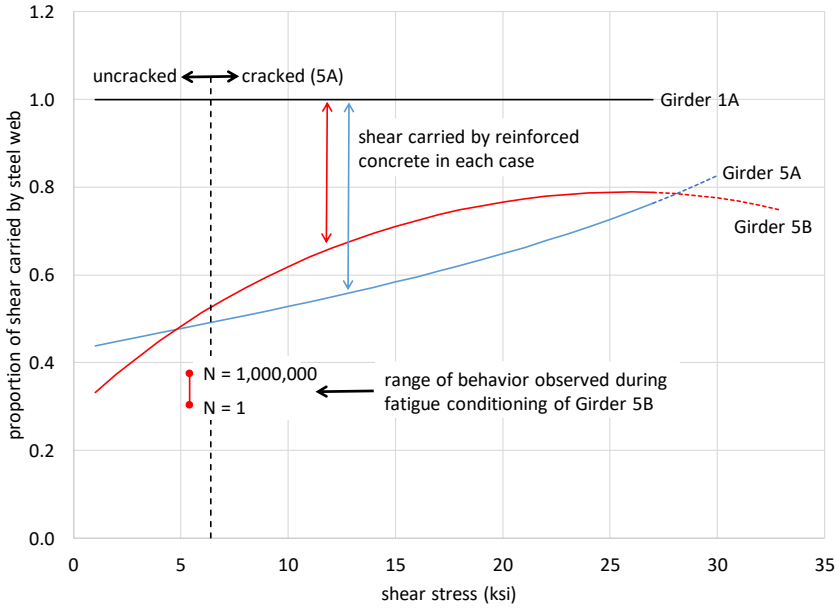

Figure 62 Proportion of shear resisted by steel web in Girder 5.

3.11 Interpretation of Test Results and Correlation with In Situ Conditions

All of the experimental results must be interpreted in the context of their load history. None of the beams were subject to load during the repair process. This situation is similar to that in the field in which the member being repaired is entirely relieved of load through jacking (or similar). This is the condition necessary during a bearing replacement, for instance. Thus, all tests begin at a true 'zero load' condition in which the repair and substrate girder are behaving in a composite manner immediately upon application of load. This is implied, for instance, in the discussion of Section 3.10. Strain data (Figures 48, 55 and 58), are also 'zeroed': residual strains in the member are not captured. In the field, even if the load is entirely relieved, residual deformations/strains may be present.

A second consideration in interpreting the results of this study is that the objective of the repair was to restore the full as built bearing and shear capacity of the girders. This may not always be strictly necessary. Especially when rolled shapes are used, shear capacity is rarely an issue and "rating factors" for shear may be on the order of 3 or greater. Long prismatic bridge girders will typically be flexure critical and may also have reserve shear capacity. Thus the repair objective of restoring full as built shear capacity may be unnecessary – the objective is to restore adequate capacity to ensure an inventory rating greater than unity.

3.12 Summary of Experimental Results

The AASHTO-prescribed shear capacity of uncorroded control Girder 1A is V_{cr} = 257 kips, corresponding to v_{cr} = 30.8 ksi. The crippling (R_{crip} = 91 kips (v = 11.8 ksi)) and yield (R_{yield} = 140 kips (v = 18.2 ksi)) capacities at the bearing are lower than this although both can be mitigated by providing bearing stiffeners. The AASHTO-prescribed capacity of the bearing stiffeners provided at 1A is P_{sb} = 150 kips (v =19.5 ksi) and the bearing capacity is R_{sb} = 175 kips (v = 22.7 ksi). Thus the *in situ* as-built AASHTO-prescribed capacity is 150 kips (v =19.5 ksi). The experimentally observed capacity exceeded this and approached the critical buckling capacity; indeed, evidence of initial buckling of the girder web of 1A was observed.

Table 24 provides a summary of key experimental results from this test Program. Data shown is normalized in terms of equivalent shear stress, $v = V/dt_w$. The following conclusions are drawn:

1. Corrosion-damaged 2A exhibited a load bearing capacity of only 7% of that of undamaged girder 1A. Initial stiffness of 2A was 20% that of 1A.

2. Each of repairs 3A (steel), 4A (UHPC) and 5A (RC) effectively restored the load bearing capacity of corrosion-damaged 2A to that of the undamaged girder 1A. Tests were stopped before the ultimate capacity could be achieved in each case to permit testing of End B.
3. Each of 3A, 4A and 5A also achieved comparable (although marginally reduced) stiffness to 1A. The loss of stiffness may be associated with the fact that the monotonic tests are also 'shakedown cycles' for the installed strengthening.
4. Each of the repairs 3B (steel), 4B (UHPC) and 5B (RC) exhibited little deterioration associated with the one million cycles fatigue conditioning performed. 5B exhibited minor cracking.
5. Following fatigue conditioning, each of 3B, 4B and 5B, exceeded the load bearing capacity of 1A.
6. The stiffness of 3B, 4B and 5B exceeded that of the End A tests and 4B and 5B exceeded that of 1A. This confirms the 'shakedown' effect of the fatigue conditioning.
7. GFRP-repaired 6A exhibited a catastrophic debonding failure at 42% of the load bearing capacity of 1A. Up to this debonding, behavior was comparable to 1A. Subsequently, 6B was not tested.

Table 24 Summary of key parameters and experimental results.

Monotonic Load Test (normalized to 1A)		**1A**	**2A**	**3A**	**4A**	**5A**	**6A**
		undamaged control	corroded control	steel repair	UHPC repair	RC repair	GFRP repair
t_w	in	0.326	0.324 (0.99)	0.305 (0.94)	0.317 (0.97)	0.281 (0.86)	0.288 (0.88)
$k = v/\delta_1$	ksi/in	42.9	8.6 (0.20)	38.2 (0.89)	38.5 (0.90)	42.2 (0.98)	41.5 (0.97)
$v_{max} = V_{max}/dt_w$	ksi	27.7	2.0 (0.07)	27.3 (0.98)	27.1 (0.98)	30.1 (1.09)	11.6 (0.42)
failure at V_{max}		web buckling	bearing	web buckling	web buckling	concrete crushing at bearing	catastrophic GFRP debonding
γ_{36kips}	με	446	-	455	397	206	524
γ_{max} at V_{max}	με	2730	256	3946	4852	2158	1174
Fatigue Conditioning		**1B**	**2B**	**3B**	**4B**	**5B**	**6B**
t_w	in	no expected effects of fatigue on 1A	2A did not have sufficient monotonic capacity to carry fatigue loads	0.298	0.265	0.287	6A exhibited catastrophic bond failure – further testing not warranted
v	ksi			5.11	5.76	5.31	
γ_{36kips}	με			436	481	191	
Post Fatigue Monotonic Load Test (normalised to 3A-5A)				**3B**	**4B**	**5B**	
$k = v/\delta_1$	ksi/in			41.3 (1.08)	48.1 (1.25)	49.5 (1.17)	
$v_{max} = V_{max}/dt_w$	ksi			30.7 (1.12)	31.8 (1.17)	34.4 (1.14)	
failure at V_{max}				stiffener bearing and web buckling	web buckling	web yield	
γ_{max} at V_{max}	με			>10,000	>10,000	4008	

3.13 Qualitative Assessment of Repair Techniques

Table 25 provides a qualitative assessment of the repair techniques tested. The assessment reflects the best judgement of the Research Team, has been informed by sample designs attempted (Chapter 2) and test results and observations (Chapter 3). Ranking (color coding) is subjective and intended only to guide the reader. Red entries, however, should be viewed as impediments to the repair system described.

Table 25 Quantitative assessment of repair techniques.

row		consideration/parameter	Repair technique			
			bolted steel	UHPC encasement	concrete encasement	bonded FRP
1	Performance	structural performance	excellent	excellent	very good	inadequate
2		performance concerns	corrosion	none	cracking/corrosion	debonding
3		practical limitation on capacity restored	no	no	high shear may exceed capacity	bond-limited behavior
4		develop tension field capacity of end web panel	yes	yes	yes	no
5		load sharing between beam and repair	possible	no	yes	no
6		restore or provide bearing stiffener	yes	yes	yes	marginal
7		***potentially*** fatigue sensitive details	unlikely	no yes if welded studs used	no yes if welded studs used	adhesive bond line
8		globally susceptible to further corrosion	yes	no	no	no
9		susceptible to crevice corrosion around edges of repair	yes	yes	yes	no with good detail
10	Design	design type	quantitative	prescriptive	semi prescriptive	quantitative
11		design complexity	easy	easy	easy	moderate
12		existing design standards applicable or adaptable to technique	AASHTO	no (McMullen 2019)	partially AASHTO	no (FCAPS and C595)
13		potential for BC/BD standard development	good	very good	very good	good
14		new Bulletin 15 approvals needed	no	yes	no	yes
15		practical limitations on beam depth	no	d > 18”	d > 18”	no
16		address ***large areas*** of 100% section loss	yes	yes	yes	yes
17	Fabrication/Installation	shop prefabrication of components	yes	no	no	yes
18		bespoke adjustment on site	limited	yes	yes	yes
19		jacking ***during*** repair if designed to carry portion of existing load[a]	bolted: no welded: yes	yes	yes	yes
20		SSPC surface preparation required	SP3	SP3	SP3	SP5
21		additional surface treatment required	no	no	no	silane treatment
22		permitted surface amplitude variation	≈ 1/16”	any[b]	any[b]	≈ 1/8”
23		minimum web thickness	none	none[b]	none[b]	none
24		hot work required	bolted: no welded: yes	no yes if welded studs used	no yes if welded studs used	no
25		drilling or machining of existing web (in addition to surface treatment)	yes	no yes if bolted studs used	yes	no/perhaps
26		power tools larger than ‘hand tools’ required	no	no except concrete mixer	no except concrete mixer	no
27		handling equipment under deck	yes	no	no	perhaps
28		possible interference handling materials in confined area including jacking	yes	not likely	not likely	not likely
29		concrete placement access required	no	yes	yes	no
30		formwork required	no	yes	yes	no
31		sensitivity to temperature and RH during application	no	requires special handling outside range 50ºF < T < 85ºF	>38ºF	>≈50ºF > dew point
32		estimated time on site for one beam end	bolted: 1d welded: multiple d	multiple days	multiple days	one day
33		cure time	none	12h	3-7d	24h
34		***possible*** OSHA regulated activities ***not typical*** of bridge repair	no	particulate	no	inhalant particulate
35	Contractor	specialized contractor required	no	yes	no	possibly
36		proprietary materials required	no	yes	no	no
37		contractor familiarity	high	moderate	high	low
38		need for special contractor certification or oversight	no	yes	no	maybe (adhesive handling)
39	Inspection	construction inspectability	good	specialist	good	good
40		special QC/QA requirements	no	yes	no	yes
41		in service inspectability	good	good	good	good
42		special/unfamiliar inspection techniques required	no	no	no	yes
43	Maintenance	frequency of preventative maintenance	as steel	none	none	similar to steel
44		compatible with future painting and maintenance	yes	yes	yes	possible painting issues
45		compatible with future bearing replacement	yes	possible issues	possible issues	yes
46		estimated design life	50 yr	50+ yr	50 yr	25-50 yr
47	General	demonstration projects available	yes	yes	none known	none known
48		overall perceived complexity	easy	moderate/ difficult	easy/ moderate	moderate
49		perceived relative cost	$	$$-$$$	$-$$	$-$$
notes		[a] jacking required as final stage of retrofit if any portion of existing load is to be carried; this operation would likely coincide with bearing replacement. [b] use of welded studs will limit surface amplitude variation and web thickness				

4 Numeric Modelling Program

4.1 Summary of Previous Numerical Studies

As described in Chapter 1, several studies have reported finite element (FE) simulations of the behavior of girders subject to beam end corrosion. All studies report quasi-static nonlinear analyses and focus on web buckling behavior. In general, the models reported in the literature provide details (or restraints/constraints) that will mitigate local bearing effects. The latter, however, are critical to corroded end region behavior, resulting in most extant studies having little relevance to the present study. Gerasimidis and Brena (2019), however, report an extensive validation and parametric study focused on local effects, neglecting buckling. The development and details of this model are most relevant to the present study. The modeling reported here leverages the extensive validation provided by Gerasimidis and Brena with the following adopted for this study:

1. Quasi-static analysis using ABAQUS. ABAQUS is well suited to modeling repair materials.
2. Mid-surface shell elements (SR4) having thickness based on corrosion mapping and 100% section loss modeled by removing elements, not setting the thickness = 0. Most previous studies take this approach.
3. Mesh size in bearing region equal to 0.5 in. transitioning to 2 in. in the span. Gerasimidis and Brena report a convergence study having these recommendations for similar beam dimensions and corrosion damage.
4. 'Hard contact' interaction in normal direction permitting holes/gaps to close and transmit load upon doing so.
5. 'Softened contact' in the normal direction at bearings. Gerasimidis and Brena calibrate a stiffness of 20 kips/in for this contact stiffness.
6. Friction coefficient in the transverse direction at bearings equal to 0.74. Gerasimidis and Brena recommend this value based on experimental validation and note that model results are not terribly sensitive to this parameter.

4.2 Finite Element Model Parameters

4.2.1 Modeling Steel Girders

In this study, ABAQUS 2020 (version 6.22) is used. All steel elements are S4R elements: 4-node general-purpose quadrilateral shell elements having reduced integration (one point) with hourglass control. These elements are conventional stress/displacement elements and are commonly used for steel sections. Uniform 0.5 in. mesh size is applied to the web and flanges at the bearing end of the girder. Mesh size is increased to 2 in. away from the end region as seen in Figure 63a. This mesh generation allows detailed modeling in the damaged region to capture local response while reducing computational time.

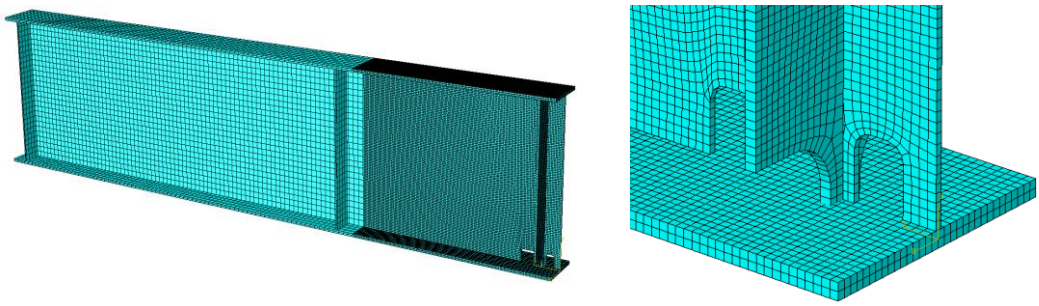

a) girder mesh b) 100% section loss modeled by removing elements

Figure 63 Mesh geometry.

4.2.2 Modeling Section Loss

Partial section loss is achieved by reducing the S4R shell thickness. In regions of 100% section loss the shell elements were removed altogether (Figure 63b).

4.2.3 Steel Material Properties

For the test specimens, measured yield strength of the girders was F_y = 57.5 ksi, and tensile strength was F_u = 77.5 ksi (see Section 3.4.1). For the 54" deep archetypal girders, existing plans for Bridge D indicate that ASTM A36 steel was used. For benchmark modeling, yield and tensile strength are assumed to be F_y = 36 ksi and F_u = 58 ksi, respectively. The modulus of elasticity is taken as E = 29,000 ksi.

For an isotropic material exhibiting ductile behavior, ABAQUS requires the true stress- strain relationship (rather than engineering stress-strain) as input. This is a monotonically increasing function, given by Equations 22 and 23, over the entire strain range and is valid only to the ultimate tensile stress.

$$\sigma_{true} = \sigma_{engineering}\,(1 + \varepsilon_{engineering}) \quad \text{for } \sigma_{engineering} \leq F_u \qquad [22]$$

$$\varepsilon_{true} = ln(1 + \varepsilon_{engineering}) \qquad [23]$$

To model plasticity, the true stress (Eq. 22) versus true plastic strain is required.

$$\varepsilon_{true}^{plastic} = ln(1 + \varepsilon_{engineering}) - \sigma_{true}/E \qquad [24]$$

Using Equations 22-24, any experimentally determined steel stress strain relationship can be used. For modeling the 54" deep girders, a generic A36 Grade 36 stress-strain relationship is adopted (F_y = 36 ksi; F_u = 65 ksi) as shown in Figure 64. A similar relationship using measured properties is adopted for modeling the test specimens. The same material model is also used for other steel components including concrete reinforcing bars.

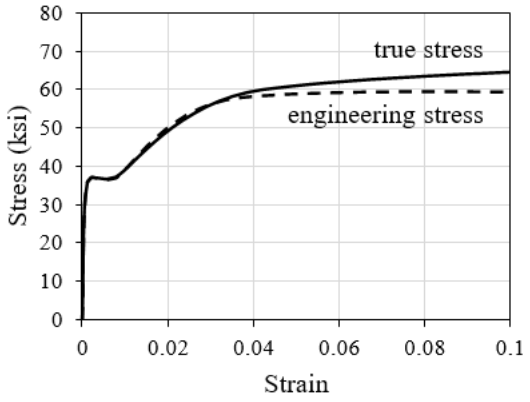

Figure 64 Engineering (experimental) and true stress strain relationship for ASTM A36 steel.

4.2.4 Concrete Material Model

Concrete encasement, whether ultra-high-performance concrete (UHPC) or normal-strength concrete (NSC), is modelled using ABAQUS C3D8 elements: 8-node general purpose solid (brick) elements. These elements are conventional continuum stress/displacement elements and are commonly used for modelling concrete.

4.2.5 Concrete Material Properties

The ABAQUS 'smeared crack' concrete model is adopted.

"*The smeared crack concrete model in ABAQUS provides a general capability for modeling concrete in all types of structures. As a 'smeared' model, it does not track individual 'macro' cracks. Constitutive calculations are performed independently at each integration point of the finite element model. The presence of cracks enters into these calculations by the way in which the cracks affect the stress and material stiffness associated with the integration point. Cracking is assumed to occur when the stress of the element reaches the 'crack detection surface' which is a linear relationship between the equivalent pressure stress and the von Mises equivalent deviatoric stress. As soon as the crack detection surface has been activated, the crack direction is taken to be the direction of that part of the maximum principal plastic strain. Following the crack detection, the crack affects the response of the model because a damage elasticity model is used*" (ABAQUS 2011).

To affect a smeared crack model, nonlinear compression and tension constitutive models and a failure surface interaction are defined in the following sections.

4.2.5.1 Concrete Compression

The complete concrete compression stress-strain curve is derived using the experimentally verified numerical model proposed by Hsu and Hsu (1994). Shown in Figure 65a, this model can be used to develop the stress-strain relationship under uni-axial compression through $0.3\sigma_{cu}$ on the descending portion using only the maximum compressive strength, σ_{cu}. The model assumes linear behavior having stiffness E_c through $0.5\sigma_{cu}$ beyond which, the stress-strain relationship through $0.3\sigma_{cu}$ (at ε_d) is defined as:

$$\sigma_c = \left(\frac{\bar{\beta}\left(\frac{\varepsilon_c}{\varepsilon_o}\right)}{\bar{\beta} - 1 + \left(\frac{\varepsilon_c}{\varepsilon_o}\right)^{\bar{\beta}}} \right) \sigma_{cu} \qquad [25]$$

Where, the parameter $\bar{\beta}$ which depends on the shape of the stress-strain diagram, is calculated as:

$$\bar{\beta} = \frac{1}{1 - \left[\frac{\sigma_{cu}}{\varepsilon_o E_0}\right]} \qquad [26]$$

For the generic model, Hsu and Hsu prescribe the strain at peak stress as:

$$\varepsilon_0 = 8.9 \times 10^{-5} \sigma_{cu} + 0.00211 \qquad [27]$$

4.2.5.2 Concrete Tension

Tension stiffening is the ability of concrete to carry tension between cracks in reinforced concrete members and is known to control the deformation calculation particularly at serviceability stress levels (Bischoff 2003). The concrete tensile stress-strain model proposed by Nayal and Rasheed (2006), shown in Figure 65b, is integrated into ABAQUS. Like compression, this is a two-parameter model, requiring cracking stress, σ_{to} and concrete elastic modulus. All other control parameters for the tension stiffening stress-strain model are shown in Figure 65. The values reported previously in Table 7 are adopted; these are repeated here in Table 26 for clarity.

Table 26 Typical properties of UHPC, HPC, and NSC.

	UHPC	NSC
primary citation	Russell and Graybeal (2013)	AASHTO LRFD
density, ρ_c	150 to 156 pcf	≈ 145 pcf
compressive strength, σ_{cu}	20 to 30 ksi	4 to 8 ksi
direct tensile strength	$\sigma_{ct} \approx 0.25(\sigma_{cu})^{0.5}$	$\sigma_{ct} \approx 0.23(\sigma_{cu})^{0.5}$
elastic modulus	$E_c = 1460(\sigma_{cu})^{0.5}$	$E_c = 1820(\sigma_{cu})^{0.5}$

4.2.5.3 Failure Surface

The plane stress smeared crack concrete failure surface adopted in ABAQUS is that described by Kupfer and Gerstle (1973) and is shown in Figure 65c. Four failure ratios are required:

1. The ratio of the ultimate biaxial compressive stress to the ultimate uniaxial compressive stress, σ_2/σ_{cu}; the ABAQUS default value is $\sigma_2/\sigma_{cu} = 1.16$.
2. The absolute value of the ratio of the uniaxial tensile stress at failure to the ultimate uniaxial compressive stress, σ_{ct}/σ_{cu} (see Table 26).
3. The ratio of the magnitude of a principal component of plastic strain at ultimate stress in biaxial compression to the plastic strain at ultimate stress in uniaxial compression; the ABAQUS default value is 1.28.
4. The ratio of the tensile principal stress at cracking in plane stress when the other principal stress is at the ultimate compressive value to the tensile cracking stress under uniaxial tension; the ABAQUS default value is 0.33.

4.2.5.4 Shear Retention

The ABAQUS smeared crack model also permits shear retention. That is the degree of shear capacity retained in the cracked concrete model. The ABAQUS default is full shear retention. This assumption typically has little impact on results and does not affect the behavior of the repairs modeled in this study.

The smeared crack model is well established for normal (NSC) and high-strength concretes (HSC). Less validation is available for UHPC. However, with the higher cracking stresses inherent in UHPC and no cracking observed during testing, the material will remain essentially elastic.

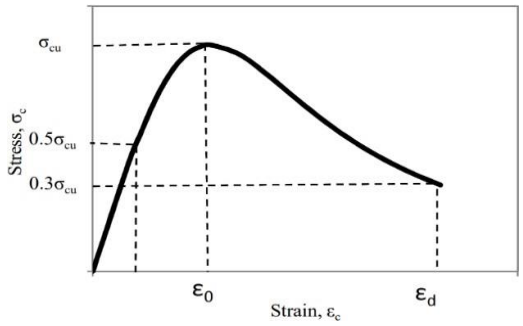

a) compressive constitutive relationship (shown positive)

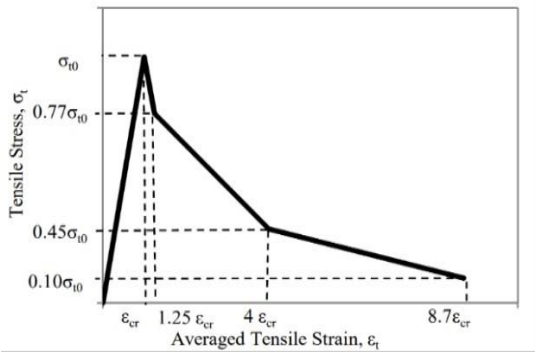

b) tensile constitutive relationship

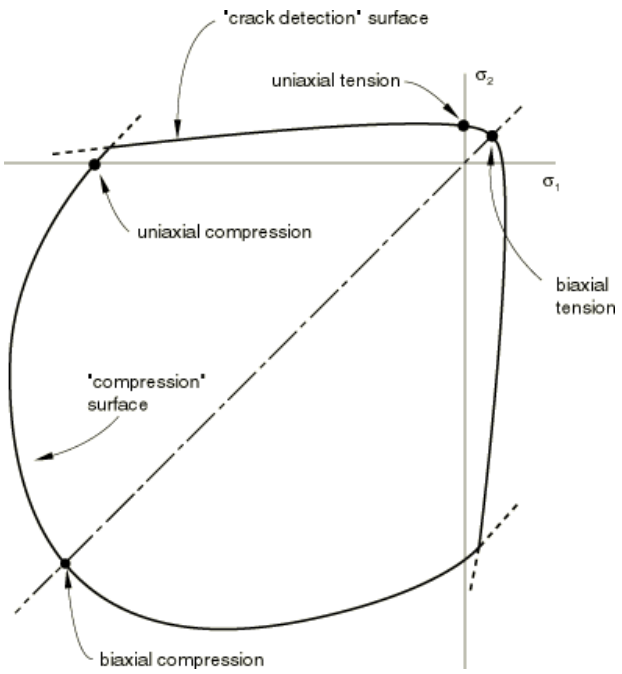

c) concrete failure surface

Figure 65 ABAQUS smerared crack concrete model.

4.2.6 Internal Reinforcing Steel

ABAQUS supports the discrete modeling of internal reinforcing steel. T3D2, two node linear displacement truss, elements are used to model conventional 60 ksi steel reinforcement (Figure 66). The reinforcement is embedded in the concrete using an embedment constraint. Initially this constraint is rigid, implying 'perfect bond' although it can be calibrated for experimentally

determined reinforcing bar bond-slip relationships. Typically, perfect bond is a suitable assumption for uncracked concrete and remains reasonable for reinforcing bar stresses below yield.

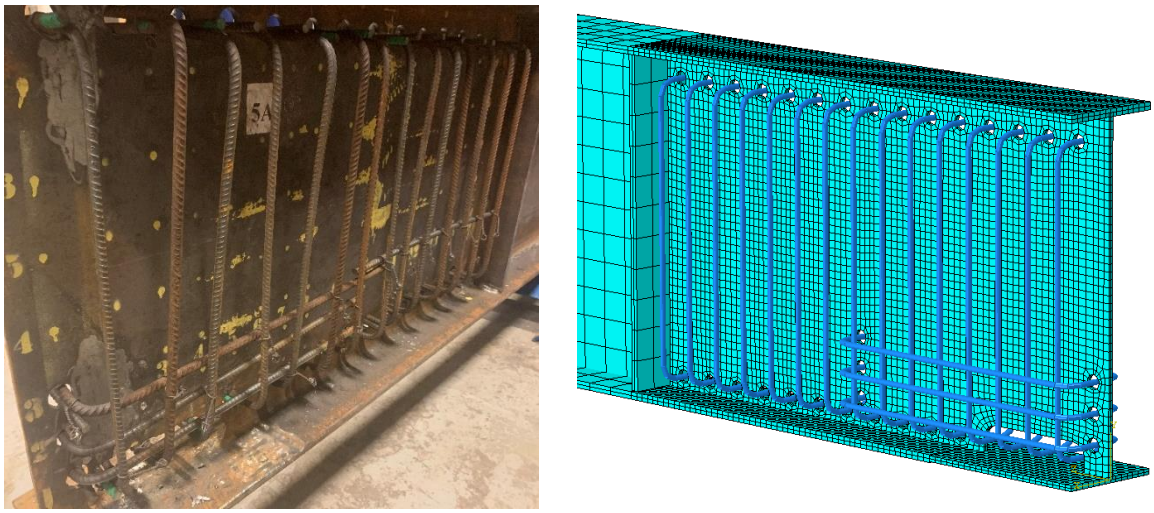

a) Girder 5A b) ABAQUS model with concrete hidden

Figure 66 Modeling internal reinforcing steel of Girder 5A.

4.2.7 Boundary Conditions

Boundary conditions, shown in Figure 67, are modeled to match the laboratory testing. The top flange is braced against lateral displacement, mimicking the lateral support of a composite deck slab.

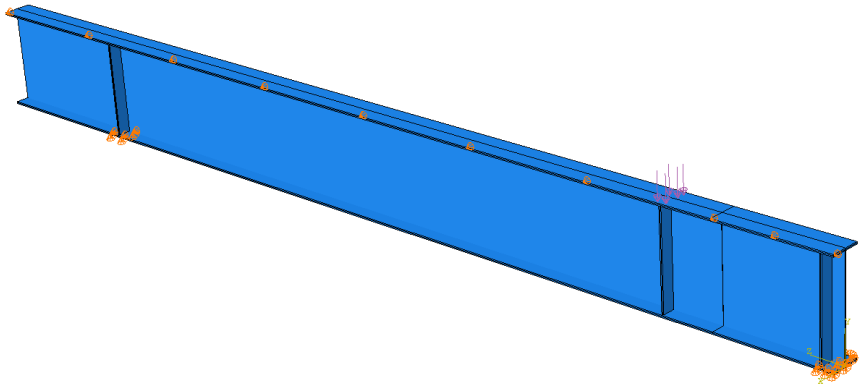

Figure 67 Numerical model boundary conditions

4.2.7.1 Interaction with Bearing Plate

At each end of the simple span, the girder bearing is a 1 in. thick steel plate 5 in. long and wide enough to support the entire width of the bottom flange. Based on the recommendation of Gerasimidis and Brena (2019), the interaction between the bottom flange and bearing plate was defined using a linear ‘softened contact’ having stiffness k = 20 kip/in. in the normal direction. This factor was calibrated using experimental data and defines the contact pressure-over closure relationship at the contact interface. In the directions orthogonal to the interface surface, a contact friction coefficient equal to 0.74 was defined. Once again, Gerasimidis and Brena recommend this value based on experimental validation and note that model results are not sensitive to this parameter. The bottom surface of the bearing plate is fixed.

4.2.7.2 Applied Load

Static analysis is conducted by applying a monotonic load ramp to a region of the top flange. Load is applied gradually until an instability occurs. The reaction at the girder end represents the shear capacity of the girder. The load is applied across the full width of the flange over a length of 5 in. centered on the bearing stiffener; i.e., the same condition as the bearing plates (Figure 67).

4.2.8 Contact Interfaces Around 100% Section Loss

'Hard contact' is defined at the edges of all holes. In this way, as the girder deforms and edges of holes come into contact, no over closure is permitted in the model and load may be transmitted.

4.2.9 Geometric Imperfections

ABAQUS can be used to determine the critical buckling (bifurcation) load using an eigenvalue buckling analysis. This process is a linear perturbation procedure. Such analysis is well established as a means of providing geometric imperfections or to investigate sensitivity to imperfections (Ellobody 2014). This approach is preferred over arbitrarily assigning imperfections based on design guides or standard tolerance (e.g., Latif and White 2021).

Buckling loads are calculated based on the original state of the structure, therefore, the girders were first modeled having no geometric imperfections when performing the eigenvalue buckling analysis. The same boundary conditions and loading are applied to the structure although the magnitude of the load is not relevant since it is scaled by the load multipliers that are predicted during the eigenvalue buckling analysis. The lowest mode (mode 1) is used since this is the most likely buckling mode of the girder. Following buckling analysis, the imperfections calculated (Figure 68) were incorporated into the model and the monotonic load was applied.

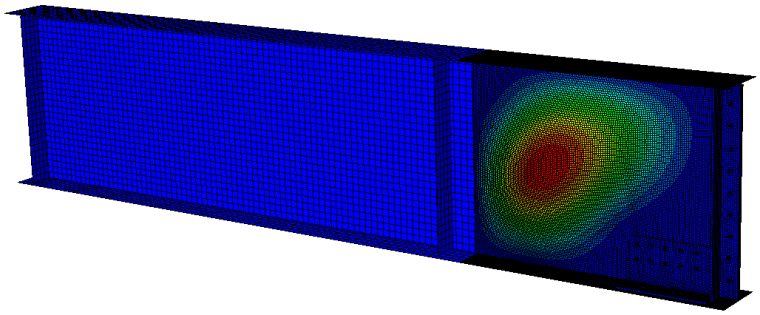

Figure 68 Girder imperfections based on eigenvalue buckling analysis (deflection amplified).

4.3 Modeling Test Specimens

The experimental girders reported in Chapter 3 were modeled as they were tested. Measured material properties were used. Each model is summarized in the following sections and a summary of model results is provided in Table 27. The models are shown to be relatively robust, capturing limit states and experimental capacities well.

Table 27 Summary of Predicted Capacities for Test Specimen Modeling

model	FE-predicted		laboratory testing	
	capacity (kips)	limit state	capacity (kips)	limit state
Girder 1A (undamaged steel)	215	web shear	213	web shear
Girder 2A (damaged steel without bearing stiffener)	16	web crippling	15.1	web crippling
Girder 3A (bolted steel repair)	200	tension field	197	tension field
Girder 4A (UHPC repair)	200	tension field	203	tension field
Girder 5A (RC repair)	200	concrete crushing	199	concrete crushing

4.3.1 Girder 1A

Girder 1A was modeled as tested. The FE-predicted shear capacity was 215 kips in shear (determined as reaction at bearing) with failure by web shear. Testing resulted in 213 kips. As seen in Figure 69, tension field behavior was observed at maximum capacity.

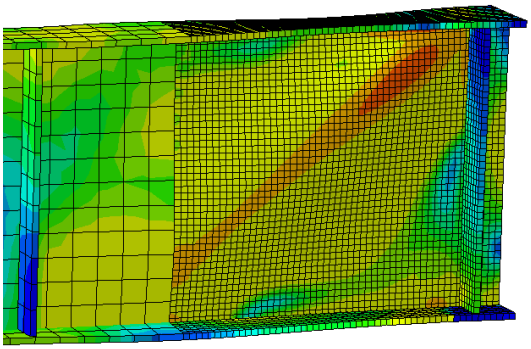

Figure 69 Girder 1A loaded end elevation with maximum (von Mises) stresses plotted.

4.3.2 Girder 2A

Girder 2A was modeled based on the archetypal damage. The FE-predicted capacity was 16 kips and failure, shown in Figure 70 was characterized as web yield, followed by crippling. Without the bearing stiffener present, the shear capacity observed during testing was 15.1 kips.

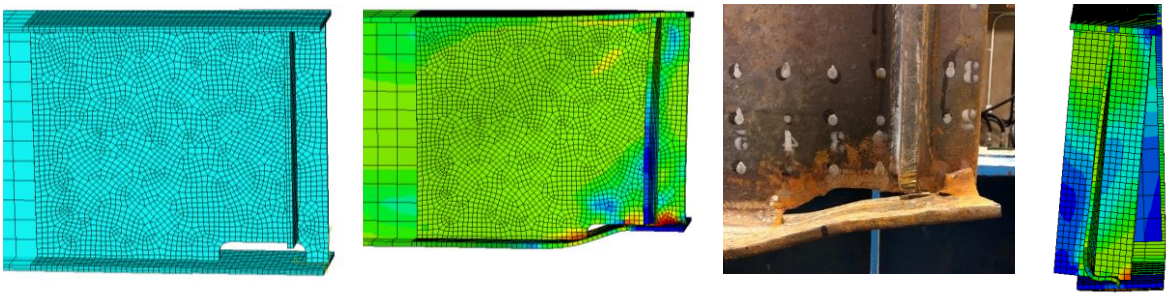

a) girder end prior to loading

b) girder end at maximum loading

c) observed behavior following testing (photograph mirrored)

Figure 70 Bearing region failure of Girder 2A.

4.3.3 Girder 3A

Bolted steel repairs are modeled in the same manner as the substrate steel using actual geometry, S4R elements, and the same isotropic material model. Mesh size matches the substrate steel and bolts are modelled using tie constraints. Bolts holes were included in the model that matched the pattern of the test specimen. Normal compression is transferred through ‘hard contact’. The FE-predicted shear capacity was 200 kips as compared to an experimental capacity of 197 kips. As seen in Figure 71, tension field behavior was predicted.

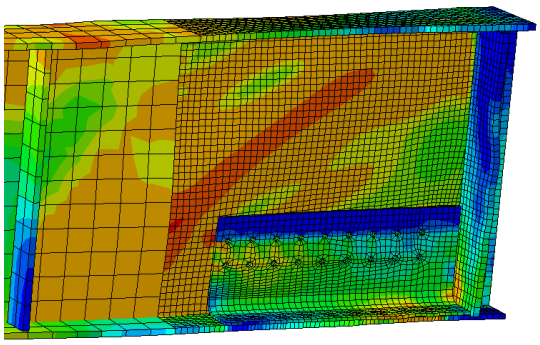

a) girder end view with tension field action evident

b) observed behavior following testing (image mirrored)

Figure 71 Bolted steel repair.

4.3.4 Girder 4A

Girder 4A was modeled as tested. The FE-predicted shear capacity was 200 kips as compared to a test capacity of 203 kips. As seen in Figure 72, tension field behavior was observed over the shortened shear panel between the UHPC encasement and bearing stiffener at the applied load.

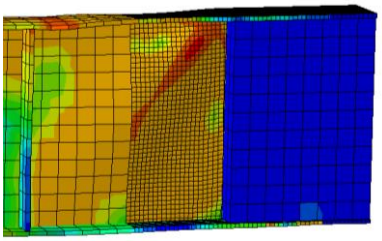

a) failure of UHPC encasement repair with tension field action evident

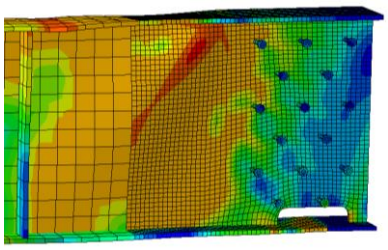

b) bolted shear studs (UHPC hidden)

c) observed web buckling behavior (image mirrored)

Figure 72 UHPC encasement repair.

4.3.5 Girder 5A

Girder 5A was modeled as tested. The FE-predicted shear capacity was 200 kips and the tested capacity was 199 kips. The specimen failed by concrete crushing (Figure 73). The steel web and internal reinforcing bars remained elastic.

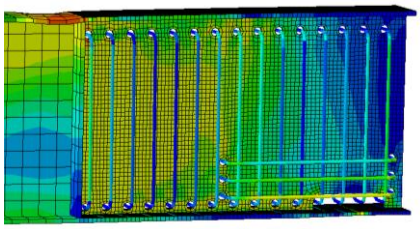

a) bearing region shown with concrete elements hidden

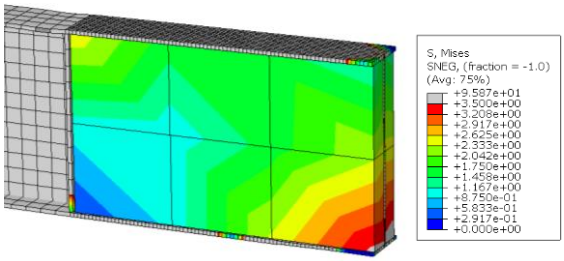

b) concrete crushing (f_c' = 3,161 psi) stress over 3,500 psi grayed out

Figure 73 NSC encasement repair.

4.4 Modelling Archetypal Plate Girders

The modelling campaign was extended to consider the archetypal 54 in. deep plate girder described in Section 2.1. The model results are compared against AASHTO capacity predictions and are

summarized in Table 28. As with the test specimen modeling, the models are shown to be relatively robust, capturing limit states and capacities well.

Table 28 Summary of predicted capacities for plate girder modeling.

model	FE-predicted		AASHTO-predicted	
	capacity (kips)	limit state	capacity (kips)	limit state
undamaged steel	183	web shear	186	web shear
damaged with bearing stiffener	100	web yield	99	web yield
damaged without bearing stiffener	45	web crippling	80	web shear
			37	web crippling
			99	web yield
conventional steel repair	297	tension field	296	tension field[a]
HPC repair	244	tension field	226	web shear
NWC repair	250	web yield	253	web shear

[a] AASHTO does not address tension field action in an end panel

The unrepaired models highlight the complexity of interactions between limit states not captured in standard design equations. In particular, the constraining effects of undamaged regions on the corrosion-damaged regions appears to be captured in the FE models. The models indicate that the repair techniques considered are able to restore the undamaged capacity of the steel plate girders.

4.4.1 Undamaged Plate Girder

The undamaged plate girder was modeled with the load applied 1.5D = 81 in. from the centerline of the bearing (*a/d* = 1.5). The FE-predicted shear capacity was 183 kips in shear (measured as the reaction at the bearing). As seen in Figure 74, local web yield is evident at the bearing although the bearing stiffener remains mostly elastic. The predicted failure is web shear of the panel. The AASHTO-predicted capacity of this section is 186 kips.

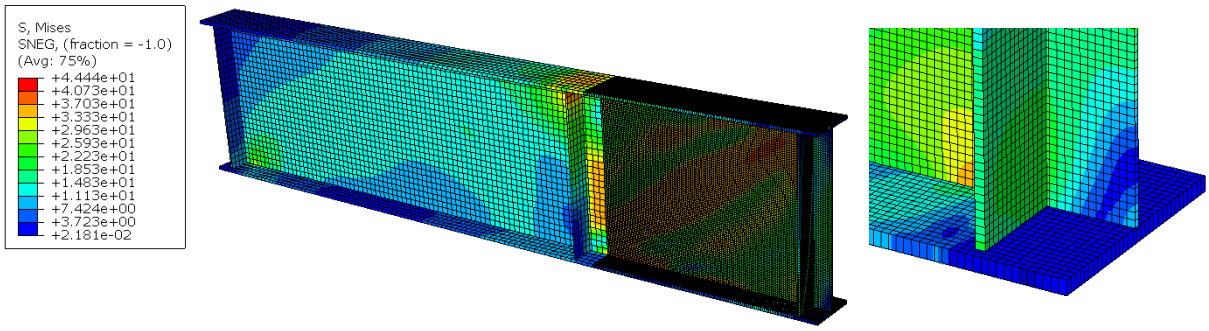

a) girder elevation with maximum (von Mises) stresses plotted; development of tension field is evident

b) bearing region detail

Figure 74 Undamaged girder predicted behavior at failure.

4.4.2 Case I Archetypal Damage

The damaged plate girder was modeled based on the archetypal damage described in Figure 29. The FE-predicted capacity was 100 kips and failure, shown in Figure 75a was characterized as web yield, followed by crippling. Without the bearing stiffener present, the AASHTO-predicted web yield capacity for this case is 99 kips.

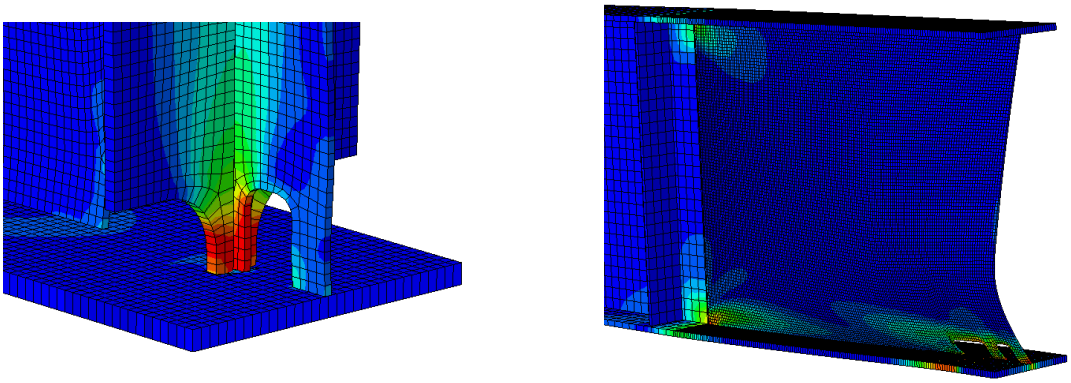

a) with bearing stiffener b) without bearing stiffener

Figure 75 Bearing region failure of Case I archetypical damage
(stress plots on deformed model)

Repeating this analysis without the bearing stiffener, the FE-predicated capacity falls to 45 kips and web instability is clearly evident (Figure 75b). For this case, without a stiffener, the AASHTO-predicted web crippling capacity is 37 kips, the web yield capacity is 99 kips while the web shear capacity is approximately 80 kips.

4.4.3 Conventional Bolted Steel Repair

Bolted steel repairs are modeled in the same manner as described in Section 4.3.3. The repair details, shown in Figure 76a are those used to repair Bridge D in the field[33]. The 7 x 5/8 in. bearing stiffeners are replaced with considerably stiffer L9.5x5x3/4 SLBB angles. Section loss to the lower region of the 3/8 in. web is repaired with 0.5 in. bent plates, extending 12 in. up the web and across the full width of the flange, on both sides of the web.

Not surprisingly, considering the significant stiffening effect of the repair, the FE-predicted capacity increased to 297 kips. At 297 kips, a tension field has clearly developed in the shear panel as can be seen in Figure 76b. The conservatively designed repair plates have mitigated web yield and crippling.

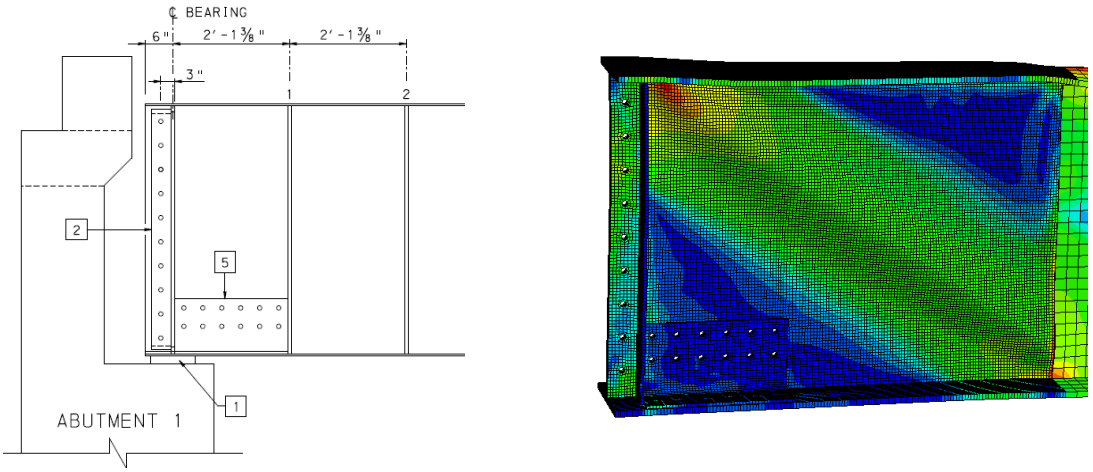

a) Bridge D repair (intermediate stiffeners are not modeled) b) stresses at girder end (tension field is evident)

Figure 76 Bolted steel repair.

[33] Jason Mash executed this design in his role as a consulting engineer.

4.4.4 UHPC Encasement

The UHPC encasement modeled is similar to the full height repairs proposed and tested by McMullen and Zaghi (2020) and shown in Figure 77c. In this model, 19 ksi UHPC was modeled. The UHPC columns extend the full height of the web, the full breadth of the flanges, and 16 in. along the length of the beam. Four vertical rows of bolted studs are used in the undamaged region of the web (Figure 77b). The stud spacing is 8 inches vertically and 4 inches horizontally.

The FE-predicted capacity was 244 kips, exceeding the 183 kip capacity of the undamaged girder. As reported in McMullen and Zaghi, the model shows evidence that tension field action was being developed over the shorter shear panel bounded by the UHPC and bearing stiffener at the load point (Figure 77a).

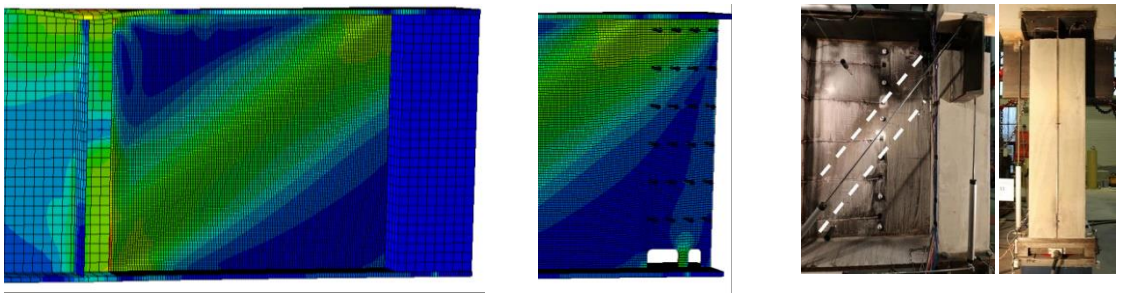

a) Failure of UHPC encasement repair (stress plot on deformed model)

b) UHPC hidden

c) full height UHPC repair McMullen and Zaghi (2020)

Figure 77 UHPC encasement repair.

4.4.5 NSC Encasement

In this model, shown in Figure 78, the loaded girder end region was encased in 5 ksi normal strength concrete. The reinforcement detail includes conventional 60 ksi hairpins passing through the web. This detail provides reinforcement development, continuity through the web, and eliminates the need for shear studs.

The FE-predicted capacity was 250 kips. The concrete encasement provided adequate lateral support to the damaged web. The web remained stable over its entire depth. Figure 78a shows the stress in the embedded reinforcement and indicates that this steel remained elastic (f_s < 34.8 ksi).

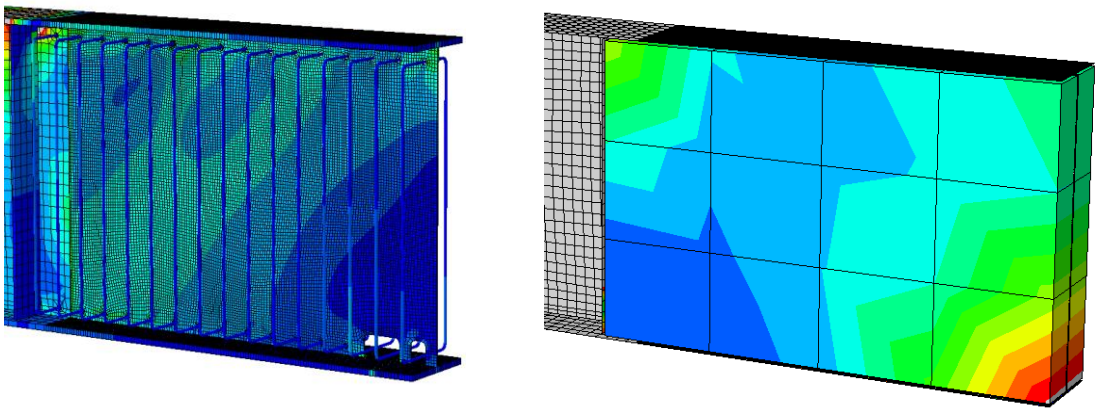

a) hairpin details used as internal reinforcement and steel stresses; concrete hidden

b) bearing region with maximum stress set to f_c'

Figure 78 NSC encasement repair.

4.5 Tension Field Action

AASHTO LRFD (2020) does not recognize the potential increase in strength afforded by the development of tension field action in the end panel of a steel girder. Typically, the bearing stiffener is not sufficiently stiff to permit the full development of tension field action since there is little or no inherent resistance to the out-of-balance horizontal force developed at the top flange-web-stiffener junction. In the case of a very stiff bearing stiffener replacement, however, greater tension field action can be developed.

The conventional bolted steel repair is likely overdesigned (an actual field design was modelled in Section 4.4.3) and was stiff enough to permit the development of full tension field action in the girder end panel and to mitigate local yield and crippling. Based on AISC (2016) calculations[34], the capacity of the modeled girder including the effects of tension field action is 296 kips. The FE modelled predicted a capacity of 297 kips.

Although AASHTO does not permit tension field action to be considered in design, the numerical analyses presented here are able to capture this behavior and, therefore, illustrate the degree of conservativeness in actual repair designs. The tension field develops because the bearing stiffener is sufficiently stiff about an axis perpendicular to the plane of the web to anchor the unbalanced force imparted by the tension field at the top flange-web-stiffener junction. Additionally, the stiffener must have sufficient flexural stiffness about an axis in the plane of the web to restrain web buckling. Table 29 compares the effective flexural stiffnesses (*EI/D*) of the bearing stiffeners provided in the conventional steel repair model. The calculations shown in Table 29 reinforce the fact that web buckling can be mitigated with relatively small amounts of lateral support. Furthermore, the results suggest additional design criteria for repairs that may be appropriate for engaging tension field action.

Table 29 Bearing stiffener stiffness and oberserved behavior

	as built	bolted steel
stiffener	7 x 5/8 both sides	L9.5x5x3/4 SLBB
D, in.	54	
E, ksi	29,000	
I_x (in plane of web), in^4	143	457
EI_x/D, k-in	76,800	245,000
adequate to resist web buckling at web shear capacity	yes	yes
I_y (perpendicular to web), in^4	0.35	37.8
EI_y/D, k-in	188	20,300
adequate to develop tension field behavior	no	full tension field developed
FE-predicted shear capacity, kips	183	297
nominal design shear capacity, kips	186	296

4.6 Concrete Encasement

Concrete encasement provided lateral restraint to the slender web and permitting continuity of force flow through the damaged region. The behavior observed manifests as an increase in shear capacity. This increase in capacity results from a combination of controlling web buckling and the reduction in the length of the shear panel. Essentially, the encasement acts as a wide bearing stiffener. Table 30 summarizes the effective shear panel length and corresponding shear strength of the remaining exposed steel web for the 54 in. deep plate girder model. The beam capacity is easily restored, and the

[34] In this calculation, the AASHTO-prescribed shear capacity, $0.58F_y$ was used rather than $0.6F_y$ prescribed by AISC 360.

concrete remains largely undamaged. The reinforcing bars remained elastic indicating the likelihood of good crack control.

Table 30 Web shear capacity

	as built	UHPC encased	NWC encased
shear panel length, *a*, in.	81	74	51
a/h	1.50	1.37	0.94
V_{cr}, kips	186	198	273
FE-predicted shear capacity, kips	183	244	250

5 Conclusions and Recommendations

5.1 Summary of States-of-the-Art and -of-Practice

The objective of this project was to investigate practical repair methods using high performance and traditional materials which can be applied to corroded and/or damaged steel girder ends in their *in-situ* state. Observed corrosion damage follows well known patterns: beam end corrosion is associated with leaking expansion joints and is most prevalent at bottom flange-to-web interfaces where debris accumulates, trapping moisture.

5.1.1 Existing Conditions

A review of damage studies from the literature and of a non-random sample of Pennsylvania bridges illustrated the proliferation of such beam end damage. In most cases, damage was dominated by patterns W1 and W2 (see Table 1) and the extent of the damage generally confined to the lower third of the web. Many beam ends were reported to have 100% section loss at some locations and girder section distortion resulting from this was identified in some Pennsylvania structures.

Having established relatively consistent patterns of beam end corrosion damage, the residual capacity of the bearing region must be established. Web shear (Eq. 1), web yield due to bearing (Eq. 5), and web crippling (Eq. 6) are the primary limit states of concern. The residual capacities in each case are found using the AASHTO-prescribed equations and the existing (reduced) web plate thickness, t_w, or t_{wc} as defined for Eq. 1 or Eq 5 (and 6), respectively. Other limit states identified in the review – in particular flange distortion – result from the loss of web bearing capacity and are therefore not primary limit states.

There is limited experimental and some analytical study of the behavior of corroded beam end regions. Due to the nature of corrosion damage, the utility of studies that assume essentially uniform [machined] damage is limited and difficult to generalize. Nevertheless, the existing studies largely validate the AASHTO-prescribed limit state equations described above. Given the typical damage being more severe at the lower web-flange junction, web yield (Eq. 5) tends to dominate behavior. Such behavior, if extreme, can result in distortion of the girder as described in relation to Figures 5 and 6 and will result in the affected bearing region carrying essentially no load. The key to a good prediction is a good record of section loss.

5.1.2 Analytical Modeling Beam End Regions

A number of studies have reported finite element (FE) simulations of beam end corrosion behavior. All studies report quasi-static nonlinear analyses and focus on web buckling behavior. In general, the models reported in the literature provide details (or restraints/constraints) that will mitigate local bearing effects. The latter, however, are critical to corroded end region behavior, resulting in most extant studies having little relevance to the present study. Gerasimidis and Brena (2019), on the other hand, report an extensive validation and parametric study focused on local effects, neglecting buckling (Section 1.5.1). The development and details of this model are most relevant to the present study. The modeling effort conducted for the present study (Chapter 4) leveraged this earlier validation.

5.1.3 Conventional Repair of Beam End Corrosion Damage

The current state of practice for structural repair of beam ends is the complete replacement of the affected region as shown schematically in Figure 11. For localized damage, bolted or welded steel patches and/or doubler plates, as shown in Figure 12, are used. Extended encasement of beam end regions in conventional concrete has also been observed for beams having embedded bearings. This latter approach is analogous to adding a corbel although confined within the depth of the beam.

5.1.4 Partial Encasement of Beam End Corrosion Damage

Reported in Section 1.8, an extensive study, demonstrated the efficacy of partially encasing damaged beam ends in ultra-high performance concrete (UHPC). McMullen (2019) proposed recommendations

for such UHPC encasement; although in some cases, provides no justification for the details proposed. There are two significant limitations of this series of studies: a) conclusions are limited to ultimate limit state (overload) performance; and b) the study makes no comparison with other methods of repair or other encasement materials.

Section 1.9 summarizes other materials that may be equally as efficient as UHPC in partial encasement applications including a) high strength concrete (HSC); b) fiber reinforced concrete (FRC); c) fabric-reinforced cementitious matrix (FRCM); and d) latex-modified concrete (LMC). EVA, SBR and PVA latex polymers at varying dosages in LMC have shown promise by enhancing the bond between the concrete and steel plate. Such adhesion will be critical for the long term durability of encasement repairs.

Encasement relies on transfer of beam forces to the encasing concrete using shear connectors. Considering the confined region over which this transfer takes place and the necessary use of small stud diameters, the recommendations of Provines et al (2019) are very relevant to beam end region repair. In particular, adoption of Eq. 12, limiting the capacity of individual shear connectors (studs), is recommended. Consideration of non-welded shear connectors should be made to avoid the need for applying welded studs in a relatively confined space to varying and thin substrate surfaces.

5.1.5 Fiber Reinforced Polymer Repair of Beam End Corrosion Damage

The use of fiber reinforced polymer (FRP) materials to address various aspects of steel degradation have been demonstrated (Section 1.11). In terms of beam end repair, using adhesively bonded FRP plates or sections (see Figure 25) is analogous to welded or bolted patch repairs. Such repairs can strengthen and provide stability to a deteriorated steel web. Despite some advantages and one successful laboratory installation (Wakabayashi et al. 2013), the difficulty in developing and maintaining an adequate bond was demonstrated in the present study and the use of FRP is not advised as a means of repairing beam end damage.

5.1.6 Effect of Existing Load

The objective of providing a repair without requiring temporary support has an inherent implication that the existing structure is adequate to resist whatever loads are present during the repair (and subsequent curing, if applicable) procedure. Without pre-loading, prestressing or post-tensioning of some kind, any repair scheme is only able to partially resist loads applied after its installation. Repairs that are called upon to resist any portion of the bridge self-weight, for instance, must have this load relieved during installation.

5.2 Summary of Experimental Program

An experimental study involving static tests of corrosion-damaged beam ends to failure is reported in Chapter 3. End A tests were conducted without conditioning and End B tests were conducted following one million cycles of fatigue conditioning. Two control (undamaged Girder 1A and corrosion damaged Girder 2A) and four repair techniques (Girders 3-6) were tested: 3) conventional bolted steel repair; 4) ultra-high performance concrete (UHPC) encasement; 5) normal strength reinforced concrete (RC) encasement; and 6) adhesively bonded glass fiber reinforced polymer (GFRP) plates, respectively.

The *in-situ* AASHTO-prescribed shear capacity of uncorroded control Girder 1A was 150 kips (web shear stress, $v = V/dt_w = 19.5$ ksi). The experimentally observed capacity exceeded this ($v = 27.7$ ksi) and approached the critical buckling capacity ($v_{cr} = 30.8$ ksi); indeed, evidence of initial buckling of the girder web of 1A was observed. Corrosion-damaged control 2A exhibited a load bearing capacity of only 7% of that of undamaged girder 1A. Initial stiffness of 2A was 20% that of 1A. Table 24 provides a summary of key experimental results from this test Program. The following conclusions are drawn:

7. Each of repairs 3A (steel), 4A (UHPC) and 5A (RC) effectively restored the load bearing capacity of corrosion-damaged 2A to that of the undamaged girder 1A.

8. Each of 3A, 4A and 5A also achieved comparable (although marginally reduced) stiffness to 1A. The loss of stiffness may be associated with the fact that the monotonic tests are also ‘shakedown cycles’ for the installed strengthening.
9. Each of the repairs 3B (steel), 4B (UHPC) and 5B (RC) exhibited little deterioration associated with the one million cycles fatigue conditioning performed. 5B exhibited minor cracking.
10. Following fatigue conditioning, each of 3B, 4B and 5B, exceeded the load bearing capacity of 1A.
11. The stiffness of 3B, 4B and 5B exceeded that of the End A tests and 4B and 5B exceeded that of 1A, confirming the ‘shakedown’ effect of the fatigue conditioning.
12. GFRP-repaired 6A exhibited a catastrophic debonding failure at 42% of the load bearing capacity of 1A. Up to this debonding, behavior was comparable to 1A. Subsequently, 6B was not tested.

5.3 Summary of Numerical Program

An extensive finite element modeling campaign was conducted and validated based on the experimental program. The modeling of the test specimens proved to be robust and captured observed behavior well. Once the test specimen modeling was “benchmarked” against the observed behavior, the models were expanded to archetypal plate girders to verify the validity of the repair methods. The following conclusions are drawn from the numerical modeling:

5. The modeling approach was sufficiently robust to capture behaviors of interest. Apart from the need for good geometric modeling of section loss, the FE models demonstrated required little special calibration.
6. The models additionally confirmed the validity of adopting AASHTO prescribed equations (described in Section 1.3) for estimating residual capacity of damaged girder ends.
7. Development of tension field action was observed in the steel repair and UHPC repair. Such behavior requires stiff end bearings as summarized in Section 5.5.
8. Stability of the steel web through encasement was achieved in the UHPC and reinforced concrete repairs as summarized in Section 5.6.

5.4 Tension Field Action in End Panel of Girder

AASHTO LRFD (2020) does not recognize the potential increase in strength afforded by the development of tension field action in the end panel of a steel girder. Typically, the bearing stiffener is not sufficiently stiff to permit the full development of tension field action since there is little or no inherent resistance to the out-of-balance horizontal force developed at the top flange-web-stiffener junction. Additionally, the stiffener must have sufficient flexural stiffness about an axis in the plane of the web to restrain web buckling. In the case of a very stiff bearing stiffener replacement, however, greater tension field action can be developed.

The conventional bolted steel repair is likely overdesigned (an actual field design was modelled in Section 4.4.3) and was stiff enough to permit the development of full tension field action in the girder end panel and to mitigate local yield and crippling. Based on AISC (2016) end panel tension field calculations, the capacity of the modeled girder including the effects of tension field action is 296 kips. The FE modelled predicted a capacity of 297 kips.

The numerical analyses presented in Chapter 4 are able to capture tension field behavior and, therefore, illustrate the degree of conservativeness – under ultimate loading conditions – in actual repair designs. The calculations shown in Table 29 reinforce the fact that web buckling can be mitigated – allowing tension field behavior to develop – with relatively small amounts of lateral support. Furthermore, the results suggest additional design criteria for repairs that may be appropriate for engaging tension field action.

5.5 Concrete Encasement

Concrete encasement provided lateral restraint to the slender web and permitted continuity of force flow through the damaged region. The behavior observed manifests as an increase in shear capacity. This increase in capacity results from a combination of controlling web buckling and the reduction in the length of the shear panel. Essentially, the encasement acts as a wide bearing stiffener. By shortening the end panel length, beam capacity is restored, and the concrete remains largely undamaged. This was observed both experimentally and demonstrated analytically for both UHPC and RC encasement. In RC encasement, the reinforcing bars remained elastic indicating the likelihood of good crack control.

5.6 Recommendations of Practical Means of Repairing Corrosion-damaged Girder Ends

Table 25 provides a qualitative assessment of the repair techniques tested. The assessment reflects the best judgement of the Research Team, has been informed by sample designs attempted (Chapter 2) and test results and observations (Chapter 3). Ranking (color coding) is subjective and intended only to guide the reader. Red entries, however, should be viewed as impediments to the repair system described. Recommendations are based partially on this summary assessment.

The following section present the recommendations stemming from this study. Proposed revisions to PennDOT DM-4 based on these are proved in Appendix D.

5.6.1 Prior to Strengthening Repair

As specified by PennDOT DM-4 §5.5.2.6b, “deteriorated steel beam ends shall be cleaned, [strengthened if needed,] painted and protected from future deterioration by providing continuity or leakproof joints.”

If the damage has progressed to the degree in which distortion of the girder has occurred, the distortion should be corrected prior to repair installation or as a result of repair installation.

5.6.2 Conventional Bolted Steel Repairs

Conventional bolted steel repairs are preferable to other repair methods considered.

Conventional steel repairs work and their design and implementation is well established. Much of the preparatory work can be undertaken with the bridge open to traffic. While subject to deterioration (further corrosion), inspection of steel repairs will follow the same protocols as inspection of adjacent steel regions and represents no impediment to long term maintenance.

5.6.2.1 Recommended Details for Bolted Steel Repairs – Bearing Stiffeners

Complete replacement of damaged bearing stiffeners is often required; assuming that this is the case:

i. Verify capacity of the unstiffened web prior to removal of bearing stiffeners (see Figure 75b) and provide temporary support as required.

ii. Replacement bearing stiffeners shall be applied to both sides of the girder web.

iii. Bolted replacement stiffeners shall be steel angles whose out-stand leg dimensions are at least those of the bearing stiffener being replaced or required based on AASHTO LRFD requirements.

iv. The leg bolted to the web shall be sufficient to accommodate a single vertical row of bolts.

As a result, typically such double angle bearing stiffeners will be arranged in the ‘short leg back-to-back’ (SLBB) arrangement, sandwiching the girder web. The resulting stiffener detail has the effect of significantly increasing both the area of the bearing stiffener and its flexural stiffness in both principal axes. Conservatively designed replacement bearing stiffeners are able to develop tension field behavior in the end panel of a girder.

v. Bolted connection of stiffener to the web shall be sufficient to transmit the design bearing force as a slip critical connection. Consideration of section loss shall be accounted for.

In some instances, a reduction in the AASHTO surface condition factor, K_s, may be justified. Only bolts penetrating regions of relatively undamaged web can be counted to contribute to the connection capacity.

vi. Regardless of bolts required, bolts shall be spaced vertically at no less than 6 in.

vii. If replacement bearing stiffeners are also used to realign distorted flanges or webs, the additional forces associated with jacking the stiffeners into place and the potential residual stress in the stiffeners and their connection shall be accounted for.

viii. Welded connection of replacement bearing stiffeners shall be permitted with consideration of appropriate web surface preparation and amplitude.

5.6.2.2 Recommended Details for Bolted Steel Repairs – Web Patches

Most significant corrosion-induced damage occurs near the bottom of the section affecting both the web and bottom flange.

i. The total thickness of repair plates will typically be at least the thickness of the existing beam web; double sided repairs are permitted although plate thickness requirements of AASHTO §6.7.3 shall be respected.

ii. Repair plates should be designed to provide continuity between the web and flange; machine-bent plates are permitted.

iii. Repair plates shall be anchored to sound portions of the web and flange such that the shear the plate is expected to resist is anchored.

iv. Anchorage of the plate shall be designed to transmit the shear to be resisted by the plate in a slip-critical manner.

v. Shear buckling of large repair plates shall be considered and may be addressed by providing through-bolts intermittently in the area of repair to engage a double-sided repair plate (if present) and the existing web.

vi. Welded connections shall be permitted with consideration of appropriate web surface preparation and amplitude.

5.6.3 UHPC Encasement

UHPC encasement is a viable means of repairing corrosion-damaged girder ends.

UHPC is expensive and requires specialized equipment for mixing and monitoring the batch sizes needed for beam end repairs. If UHPC is already being deployed on a project, its use for girder end repair may be found to be appropriate. It is unclear that UHPC provides any improvement in performance or long-term behavior over conventional methods of repair. A potential advantage of UHPC is that it achieves a high strength quite rapidly, allowing traffic re-opening within 12 hours of placement.

Formwork for UHPC needs to be watertight, nonabsorbent where in contact with UHPC and be designed to ensure it may be filled completely; that is, appropriate venting is required and internal details should have no potential air traps.

5.6.3.1 Recommended Details for UHPC Encasement

i. Existing bearing stiffeners should be removed verifying the capacity of the unstiffened web prior to removal of bearing stiffeners and providing temporary support that does not encroach upon the UHPC placement as required.

ii. UHPC encasement shall extend the full height of the web, be cast against each flange, and may replace the presence of a steel bearing stiffener.

iii. UHPC encasement shall extend to the flange tips when used as a bearing stiffener.

iv. UHPC shall conform to an approved, commercially available UHPC product and all storage, batching, mixing, and quality control requirements recommended by the manufacturer.

Only LaFarge Ductal® was used in the present study. This product is appropriate. Its use typically requires oversight by LaFarge technicians and the use of special mixing equipment rented from LaFarge. There are other UHPC products on the market in addition to some "open source" mixes available. These need to be evaluated for inclusion into PennDOT Bulletin 15, but most should be adequate for girder end repairs.

v. Strength evaluation of UHPC shall use the method recommended by the manufacturer including requirements for finishing cylinder ends.

LaFarge prescribes the use of 3 in. diameter x 6 in. tall cylinders having their ends ground smooth and parallel. End preparation requires specialized equipment and test machine capacity is a consideration. Further study is required to establish strength-correction factors for 2 in. mortar cube specimens; these should not be used for UHPC.

vi. Shear connections are required between the steel web and UHPC sufficient to transfer the design shear. Shear connector details and recommendations are presented in Section 5.6.5.

vii. Shear connectors are recommended between the flanges and UHPC for lengths of UHPC encasement exceeding the depth of the steel girder web, *D.*

viii. The effectively reduced length of shear panel resulting from UHPC encasement should be considered.

Typically, the reduced shear panel length will result in increased capacity.

5.6.4 *RC Encasement*

RC encasement is a viable means of repairing corrosion-damaged girder ends especially in cases were large shear stresses are not anticipated.

5.6.4.1 Recommended Details for RC Encasement

i. Existing bearing stiffeners should be removed verifying the capacity of the unstiffened web prior to removal of bearing stiffeners and providing temporary support that does not encroach upon the RC placement as required.

ii. RC encasement shall extend the full height of the web and may replace the presence of a steel bearing stiffener.

iii. RC confinement shall extend to the flange tips at all locations.

iv. The RC used shall conform to a mix approved for non-prestressed superstructure applications.

RC encasement will typically extend the entire length of the end panel of the girder in which case the following apply:

v. Shear capacity of the end panel shall be replaced by the RC element. The shear capacity of the RC element shall be determined as the sum of concrete (V_c) and internal reinforcing steel components (V_s) as follows (AASHTO LRFD (2020) Eq. 5.7.3.3-1):

$$V_n = V_c + V_s = 0.06\sqrt{f_c'}b_f D + A_s f_y d'/s \quad \text{[ksi units]} \quad [28]$$

Where D is the depth of the steel web; b_f is the flange width; A_s is the area of shear reinforcement provided at a section; d' is the height of the shear reinforcement within the girder depth; and s is the spacing of shear reinforcement.

vi. Shear reinforcement may take either of the following forms.

   a. closed ties located on both sides of the web; the ties shall fit within the steel cross section and have adequate cover. [maximum tie width is therefore $b_f/2$ – *concrete cover*].

   b. Hairpin ties anchored through the web with a lap splice adequate to develop the tie.

vii. If closed ties not penetrating the web are used (case a, above), shear connections are required between the steel web and RC sufficient to transfer V_n (Eq. 28). Shear connector details and recommendations are presented in Section 5.6.5.

5.6.5 Shear Connections for Encasement Repairs

For structural repair associated with active structures and corrosion damage, the use of welded shear studs will often not be practical. To avoid burn-through and distortion, welded studs require a minimum substrate thickness exceeding 1/3 the stud diameter and a smooth, uncontaminated surface to which to weld.

i. The use of high strength structural bolts is a practical alternative to welded shear studs.

ii. High strength bolts used as shear studs shall meet or exceed the requirements of ASTM F3125 Grade A325 bolts.

iii. The capacity of a high strength bolt-type shear stud shall be taken as:

$$Q_n = 0.5A_{sc}\sqrt{f_c'E_c} \leq 0.7A_{sc}F_u \quad [29]$$

Where A_{sc} is taken as the nominal area of the bolt and F_u is taken as 75 ksi.

iv. Bolts shall be installed into holes have the ***same nominal diameter*** as the bolt.

v. Bolts shall be nutted on both sides of the web and installed with a pretension according to AASHTO LRFD Table 6.13.2.8-1.

vi. Bolts shall be installed in a grid pattern with the bolt head (stud) protruding on alternating sides of the steel web.

The combination of limiting F_u to 75 ksi and recommendation iv is intended to limit the slip inherent in such bolted stud connections.

There is a commercially available product marketed as a bolt-on shear stud manufactured by TCB. This is a promising product for repair; review for inclusion into PennDOT Bulletin 15 is recommended.

5.6.6 Durability of Repairs

All repairs present an interface between the repair material and existing steel girder. This interface is a potential location for the initiation of crevice corrosion ('pack rust'). Design can provide some relief to water, moisture and moisture-trapping debris accumulating at these new interfaces in some instances. Correctly painted surfaces extending under the repair is paramount – no recommended repair relies on bond to the web. Sloped edges and 'drip strips' on encasement repairs can also help to eliminate water ingress at the concrete-steel interface. Joints between the repair material and steel should be caulked and maintained to prevent water ingress.

Finally, repairs shall be inspected during routine bridge inspection and maintenance items identified should be addressed to ensure adequate repair life.

6 References

AASHTO (2020) *LRFD Bridge Design Specifications*, 9th edition.

ABAQUS (2011) ABAQUS Analysis User's Manual, Volume III: Materials. 22.6.1-2 pp

ABAQUS (2020) ABAQUS User's Manual. https://help.3ds.com/2020/English/DSSIMULIA_Established/SIMULIA_Established_FrontmatterMap/sim-r-DSDocAbaqus.htm?ContextScope=all [login/license required]

ACI Committee 215, (2022). ACI PRC 215R-22 *Considerations for Design of Concrete Structures Subjected to Fatigue Loading*

ACI Committee 318 (2019). *Building Code Requirements for Structural Concrete (ACI 318-19) and Commentary (ACI 318R-19)*, American Concrete Institute.

ACI Committee 363 (2010). *ACI 363R-10 Report on High Strength Concrete*, American Concrete Institute.

ACI Committee 440 (2017). *ACI 440.2R-17 Guide for the Design and Construction of Externally Bonded FRP Systems for Strengthening Concrete Structures*, American Concrete Institute.

ACI Committee 544 (2010). *ACI 544.5R-10 Report on the Physical Properties and Durability of Fiber-Reinforced Concrete*, American Concrete Institute.

ACI Committee 548 (2009). *ACI 548.3R-09 Report on Polymer-Modified Concrete*, American Concrete Institute.

ACI Committee 548 (2011). *ACI 548.4-11 Specification for Latex-Modified Concrete Overlays*, American Concrete Institute.

ACI Committee 549 (2020). *ACI 549.4R-20 Guide to Design and Construction of Externally Bonded Fabric-Reinforced Cementitious Matrix and Steel-Reinforced Grout Systems for Repair and Strengthening of Concrete Structures*, American Concrete Institute.

Ahn, J-H, Kim, I-T, Kainuma, S. and Lee, M-J (2013) Residual shear strength of steel plate girder due to web local corrosion, *Journal of Constructional Steel Research*, **89**, 198-212.

Al Badran, M.S. (2013) Structural Reliability Analysis of Corroded Steel Girder Bridge, *MS Thesis*, University of Nebraska-Lincoln, 93 pp.

Al-Saidy, A.H., Klaiber, F.W., and Wipf, T.J. (2004) Repair of Steel Composite beams with carbon fiber-reinforced polymer plates, *ASCE Journal of Composites for Construction* **8**(2), 163-171.

Al-Shawaf, A., Al-Mahaidi, R. and Zhao, X.L. (2006) Study on Bond Characteristics of CFRP/Steel Double-Lap Shear Joints at Subzero Temperature Exposure. *The Third International Conference on FRP Composites in Civil Engineering (CICE 2006)* 13-15 December 2006, Miami, Florida, USA.

American Welding Society (AWS) (2015) *AWS D1.1 Structural Welding Code - Steel*.

ANSI/AISC 360-16 (2016) *Specifications for Structural Steel Buildings*, American Institute of Steel Construction.

ASCE Fiber Composites and Polymers Standards (FCAPS) Committee. Forthcoming *LRFD Standard for Pultruded GFRP Members*. Harries serves on FCAPS

Australian Standard. (2004). *Bridge Design. Part 6: Steel and Composite Construction*.

Balapour, M., Joshaghani, A. and Althoey, F. (2018) Nano-SiO_2 contribution to mechanical, durability, fresh and microstructural characteristics of concrete: a review. *Construction and Building Materials* **181**, 27-41.

Bao, A., Gulasey, M., Guillaume, C., Levitova, N., Moraes, A. and Satter, C. (2018) Structural Capacity Analysis of Corroded Steel Girder Bridges, *Proceedings of the 3rd International Conference on Civil, Structural and Transportation Engineering (ICCSTE'18)*, Niagara Falls, Canada – June 10 – 12, 2018, Paper No. 118.

Barth, K. (2015) Steel Bridge Design Handbook Design Example 2A: Two-Span Continuous Straight Composite Steel I-Girder Bridge, *FHWA-HIF-16-002-Vol 21*.

Batikha M., Chen J., Rotter J. and Teng J. (2009) Strengthening metallic cylindrical shells against elephant's foot buckling with FRP, *Thin-Walled Structures* **47**(10), 1078–91.

Bedford Reinforced Plastics (2012) *Design Guide*. https://bedfordreinforced.com/app/uploads/2017/07/BRP_Design-Guide.pdf

Bedford Reinforced Plastics (2020) *ProForms Structural Shapes*. https://bedfordreinforced.com/app/uploads/2017/07/Bedford_PROForms-v05042020.pdf

Bertrand, J. (2012) Performance of latex-modified bridge overlays after 20+ years of service. *Preservation Engineering – Stone, Masonry and Concrete*. ICRI Spring Convention, Quebec City. April 2012.

Bertrand, J. and Sprinkel, M. (2009) *History and case studies of latex modified concrete (LMC) in USA and Quebec*. American Concrete Institute. Section du Québec et de l'est de l'Ontario. Progress in concrete seminar, December 2009, Montreal.

Bhetwal K.K. and Yamada S. (2012) Effects of CFRP reinforcements on the buckling behavior of thin-walled steel cylinders under compression. *International Journal of Structural Stability and Dynamics* **12**(1), 131–51.

Bischoff, P. H. (2003) Tension stiffening and cracking of steel fiber reinforced concrete, *ASCE Journal of Materials in Civil Engineering*, **15**(2), 174–182.

Black, C. J., Makris, N., and I. D. Aiken. (2004) Component Testing, Seismic Evaluation and Characterization of Buckling-Restrained Braces. *ASCE Journal of Structural Engineering*, **130**(6), 880-894.

Bourban, P.E., McKnight, S.H., Shulley, S.B., Karbhari, V.M. and Gillespie, J.W. (1994) Durability of Steel/Composites Bonds for Rehabilitation of Structural Components, *Infrastructure: New Materials and Methods of Repair – Proceedings of the Third Material Engineering Conference*. 295-303.

Brown. A.R.G. (1974) The corrosion of CFRP-to-metal couples in saline environments. *Carbon Fibres, proceedings of the 2nd International Conference*, Feb. 18-20, 1974, London England, 230-241.

Bruneau, M., Uang, C. M., and Whittaker, A. (1998) *Ductile Design of Steel Structures*, McGraw-Hill, Boston, MA.

Burg, R. G., and Ost, B. W. (1994) Engineering Properties of Commercially Available High-Strength Concretes (Including Three-Year Data), *Research and Development Bulletin RD104*, Portland Cement Association.

Cadei, J.M.C., Stratford, T.J., Hollaway, L.C. and Duckett, W.G. (2004) *Strengthening Metallic Structures Using Externally Bonded Fibre-Reinforced Polymers*. CIRIA Pub. No. C595. 233 pp.

Cardoso, D. (2014) *Compressive Strength of Pultruded Glass-Fiber Reinforced Polymer (GFRP) Columns*, PhD Dissertation, Universidade Federal do Rio de Janeiro.

Cardoso, D., Harries, K.A. and Batista, E. (2014) Closed-Form Equations for Local Buckling of Pultruded Thin-Walled Sections, Thin-walled Structures, **79**, 16-22.

Chacon, A., Chajes, M., Swinehart, M., Richardson, D. and Wenczel, G. (2004) Applications of Advanced Composites to Steel Bridges: A Case Study on the Ashland Bridge. *Proceedings of the 4th Advanced Composites for Bridges and Structures Conference*, Calgary.

CEN (2015) *EN 14399-1:2015 High-strength structural bolting assemblies for preloading - Part 1: General requirements.*

CNR (Italian National Research Council) (2007) *Guidelines for the design and construction of externally bonded FRP systems for strengthening existing structures: Metallic structures*. Rome.

Colombi, P. Fanesi, E., Fava, G. and Poggi, C. (2005) Durability of steel elements strengthened by FRP plates subjected to mechanical and environmental loads. *Composites in Construction, 2005 – Third international conference*, Lyon, France, July 11 – 13, 2005.

Colombi, P., Poggi, C. (2006) An Experimental, Analytical and Numerical Study of the Static Behavior of Steel Beams Reinforced by Pultruded CFRP Strips. *Composites Part B*, **37**. 64-73.

Crasto, A.S. and Kim, R.Y. (1996) Environmental durability of a composite-to-composite adhesive bond in infrastructure applications. *28th international SAMPE technical conference*, November, 4-7, 1996, 837-849.

Cunningham, D., Harries, K.A. and Bell, A.J., (2015) Open-Hole Tension Capacity of Pultruded GFRP Having Staggered Hole Arrangement, *Engineering Structures*, **95**, 8-15.

Curtis, P.T. (1989) Fatigue Behavior of Fibrous Composite Materials, *Strain Analysis* **24**(4) 235-244.

Dawood, M. and Rizkalla, S. (2010) Environmental durability of a CFRP system for strengthening steel structures, *Construction and Building Materials* **24**(9) 1682-1689.

Dawood, M., Rizkalla, S., and Sumner, E. (2007) Fatigue and overloading behavior of steel-concrete composite flexural members strengthened with high modulus CFRP materials. *ASCE Journal of Composites for Construction*, **11**(6), 659-669.

Dawood, M.; Guddati, M.; Rizkalla, S. (2009) Effective splices for a carbon fiber-reinforced polymer: Strengthening system for steel bridges and structures. *Transportation Research Record*, **2131**, 125-133.

De Nève B., and Shanahan, M.E.R. (1992) Effects of humidity on an epoxy adhesive. *International Journal of Adhesion and Adhesives*, **12**(3), 191-196.

Ekiz, E. and El-Tawil, S. (2008) Restraining Steel Brace Buckling Using a Carbon Fiber-Reinforced Polymer Composite System: Experiments and Computational Simulation. *ASCE Journal of Composites for Construction*, **12**(5), 562-569.

Ellobody, E. (2014) Finite Element Analysis and Design of Steel and Steel-Concrete Composite Bridges, Elsevier Science and Technology, 522-525.

El-Tawil, S., Ekiz, E., Goel, S. and Chao, S-H. (2011) Restraining local and global buckling behavior of steel plastic hinges using CFRP, *Journal of Constructional Steel Research*, **67**, 261-269.

El-Tawil, S., Fortney, P., Harries, K.A., Shahrooz, B.M., Kurama, Y., Hassan, M. and Tong, X. (2009) *Recommendations for Seismic Design of Hybrid Coupled Wall Systems*, ASCE/SEI, 80 pp.

Eurocode 4 (EC4) (2005). *1994-2:2005 Design of Composite Steel and Concrete Structures, Part 2 – General Rules and Rules for Bridges*

Federal Highway Administration (FHWA) (1978) Styrene-Butasiene Latex Modifiers for Bridge Deck Overlay Concrete, *Report No. FHWA-RD-78-35*.

Federal Highway Administration (FHWA) (2019) https://highways.dot.gov/research/structures/ultra-high-performance-concrete/ultra-high-performance-concrete accessed 6.19.20.

Federal Highway Administration (FHWA) (2021) https://www.fhwa.dot.gov/innovation/everydaycounts/edc_6/uhpc_bridge_preservation.cfm accessed 4.15.21.

Fernando D., Yu T., Teng J.G. and Zhao X-L (2009) CFRP strengthening of rectangular steel tubes subjected to end bearing loads: effect of adhesive properties and finite element modelling. *Thin-Walled Structures*, **47**(10), 1020–8.

Francis, R. (2000) *Bimetallic Corrosion: Guide to good practice in corrosion control*. Teddington, Middlesex: National Physical Laboratory. http://www.npl.co.uk/upload/pdf/bimetallic_20071105114556.pdf [accessed 6.14.20]

Fry, G.T., Bailey, B.M., Farr, J.L., Elliott, J.E. and Keating, P.B. (2005) Behavior and design of dapped steel plate girders. *Report FHWA/TX-05/0-2102-1*, Texas Transportation Institute, Texas A&M University. 174 pp.

Garden, H.N. (2001) Use of Composites in Civil Engineering Infrastructure, *Reinforced Plastics*, **45**(7/8) 44-50.

Gerasimidis, S. and Brena, S. (2019) Development of Load Rating Procedures for Deteriorated Steel Beam Ends, *massDOT Report 19-008*, 278 pp.

Gettings, M. and Kinloch, A.J. (1977) Surface analysis of polysiloxane/metal oxide interfaces. *Journal of Material Science*, **12**, 2511-2518.

Gledhill, R.A., Shaw, S.J. and Tod. D.A. (1990) Durability of adhesive-bonded joints employing organosilane coupling agents. *International Journal of Adhesion & Adhesives*, **10**(3), 192-198.

Graybeal, B.A. (2014) *Design and Construction of Field-Cast UHPC Connections*. FHWA-HRT-14-084.

Grubb, M.A. and Schmidt, R.E. (2015) Steel Bridge Design Handbook Design Example 1: Three-Span Continuous Straight Composite Steel I-Girder Bridge, *FHWA-HIF-16-002-Vol 20.*

Haber, Z.B., De La Varga, I., Graybeal, B.A., Nakashoji, B. and El-Helou, R. (2018) *Properties and Behavior of UHPC-Class Materials*, FHWA-HRT-18-036

Haedir J, and Zhao X-L (2011) Design of short CFRP-reinforced steel tubular columns. *Journal of Constructional Steel Research* **67**, 497–509.

Hain, A. and Zaghi, A.E. (2021) Learnings from the Field Implementation of a Novel UHPC Beam End Repair on a Corroded Steel Girder Bridge in Connecticut, *TRB Annual Meeting Presentation*, https://www.youtube.com/watch?v=wIU9CgIlTmI, accessed 4.15.21.

Hand, H.M., Arah, C.O., McNamara, D.K. and Mecklenburg, M.F. (1991) Effects of environmental exposure on adhesively bonded joints. *International Journal of Adhesion and Adhesives*, **11**(1), 15-23.

Hanshin Expressway (2020) https://hanshin-exp.co.jp/english/businessdomain/renewal/syuzen/syuzen03.html, accessed 6.12.20

Harries, K.A. (2005) Deterioration of FRP-to-Concrete Bond Under Fatigue Loading. *Proceedings of the International Symposium on Bond Behaviour of FRP in Structures*, Hong Kong.

Harries, K.A. (2014) Chapter 5: Enhancing Stability of Steel Structural Sections using FRP Composites in *Rehabilitation of Metallic Civil Infrastructure Using Fibre Reinforced Polymer Composites*, V. Karbhari, editor. Woodhead Publishing Series in Civil and Structural Engineering No. 51, pp 117-139.

Harries, K.A. and Dawood, M., (2012) Behavior and Performance of FRP-to-Steel Bond, *Transportation Research Record: Journal of the Transportation Research Board* **2313**/2012, 181-188.

Harries, K.A. and El-Tawil, S. (2008) Review of Steel-FRP Composite Structural Systems, *Proceedings of the 5th International Conference on Composite Construction*, Colorado, July 2008

Harries, K.A., McCabe, M. and Sweriduk, M. (2013) Structural Evaluation of Slab Rehabilitation by the Method of Hydrodemolition and Latex Modified Overlay, *FHWA-PA-2013-006-PIT WO 01*, 118 pp.

Harries, K.A., Peck, A. and Abraham, E.J. (2009) Enhancing Stability of Structural Steel Sections Using FRP, *Thin Walled Structures*, **47**(10), 1092-1101.

Harries, K.A., Richard, M.J. and Kim, Y. (2010) Fatigue Behaviour of CFRP Retrofitted Damaged Steel Beams, *Proceedings of 13th International Conference on Structural Faults and Repair* Edinburgh, June 2010.

Hsu, L.S. and Hsu, C.-T.T. (1994). Complete stress-strain behaviour of high-strength concrete under compression. *Magazine of Concrete Research*, **46** (169), 301-312.

Ismael, r., Silva, J.V., Carmo, R.N.F., Soldado, E., Lourenco, C., Costa, H. and Julio, E. (2016) Influence of nano-SiO_2 and nano-Al_2O_3 additions on steel-to-concrete bonding, *Construction and Building Materials* **125**, 1080-1092.

Jia, L, Zhao, F., Guo, J. and Yao, K. (2019) Properties and Reaction Mechanisms of Magnesium Phosphate Cement Mixed with Ferroaluminate Cement, *Materials (Basel)* **12**(16), 2561.

Jones, S.C. and Civjan, S.A. (2003) Application of Fiber Reinforced Polymer Overlays to Extend Steel Fatigue Life, *ASCE Journal of Composites for Construction* **7**(4) 331-338.

Karbhari, V.M. and Shulley, S.B. (1995) Use of Composites for Rehabilitation of Steel Structures – Determination of Bond Durability, *ASCE Journal of materials in Civil Engineering*, **7**(4) 239-245.

Khurram, N., Sasaki, E., Katsuchi, H. and Yamada, H. (2014) Experimental and Numerical Evaluation of Bearing Capacity of Steel Plate Girder Affected by End Panel Corrosion, *International Journal of Steel Structures*, **14**(3), 659-676.

Kim, I-T., Lee, M-J. Ahn, J-H. and Kaiuma, S. (2013) Experimental evaluation of shear buckling behaviors and strength of locally corroded web, *Journal of Constructional Steel Research*, **83**, 75-89.

Kinloch, A.J. (1983) *Durability of structural adhesives*. London: Applied Science Publishers.

Knox, E.M., and Cowling, M.J. (2000) Durability aspects of adhesively bonded thick adherend lap shear joints. *International Journal of Adhesion and Adhesives*, **20**, 323-331.

Kruszewski, D. (2018) Performance Evaluation of Shear Connectors Embedded in Ultra-High Performance Concrete as Part of a Bridge Repair Method. *PhD Dissertation*, University of Connecticut, 281 pp.

Kulicki, J.M., Prucz, Z., Sorgenfrei, D.F., Mertz, D.R. and Young, W.T. (1990) Guidelines for evaluating corrosion effects in existing steel bridges, *NCHRP Report 333*, Transportation Research Board.

Kupfer, H. B. and K. H. Gerstle (1973) Behavior of Concrete under Biaxial Stresses, *ASCE Journal of Engineering Mechanics Division*, **99,** 853.

Lapique, F., and Redford, K. (2002) Curing effects on viscosity and mechanical properties of a commercial epoxy resin adhesive. *International Journal of Adhesion and Adhesives*, **22**, 337-346.

Latif, W., White, D. (2021) Flange Local Buckling Resistance and Local-Global Buckling Interactions in Slender-Flange Welded I-Section Beams, *AISC Engineering Journal*, 59, 121.

Lenwari, A., Thepchatri, T., Albrecht, P. (2005) Flexural Response of Steel Beams Strengthened with Partial-Length CFRP Plates. *ASCE Journal of Composites for Construction* **9**(4), 296-303.

Lenwari, A., Thepchatri, T., Albrecht, P. (2006) Debonding Strength of Steel Beams Strengthened with CFRP Plates. ASCE *ASCE Journal of Composites for Construction* **10**(1), 69-78.

Liu, C., Miyahita, T. and Nagai, M. (2011) Analytical Study on Shear Capacity of Steel I-Girders with Local Corrosion nearby Supports, *Procedia Engineering*, **14**, 2276-2284.

Liu, H.B., Zhao, X.L. and Al-Mahaidi, R. (2006) The Effect of Fatigue Loading on Bond Strength of CFRP Bonded Steel Plate Joints, *Proceedings of the International Symposium on Bond Behaviour of FRP in Structures*, Hong Kong.

McKnight, S.H., Bourban, P.E., Gillespie, J.W. and Karbhari, V.M. (1994) Surface Preparation of Steel for Adhesive Bonding in Rehabilitation Applications, *Infrastructure: New Materials and Methods of Repair – Proceedings of the Third Material Engineering Conference*. 1148-1155.

McMullen, K.F. (2019) Full-Scale Evaluation of a Novel Repair for Corroded Plate Girders with UHPC, *PhD Dissertation*, University of Connecticut, 288 pp.

McMullen, K.F. and Zaghi, A.E. (2020) Experimental Evaluation of Full-Scale Corroded Steel Plate Girders Repaired with UHPC, *ASCE Journal of bridge Engineering*, **25**(4): 04020011

Mertz, D.R. and Gillespie, J.W. (1996) *Rehabilitation of Steel Bridge Girders Through the Application of Advanced Composite Materials* NCHRP-IDEA Project 11, 30 pp.

Mertz, D.R., Gillespie, J.W., Chajes, M.J. and Sabol, S.A. (2002) *The Rehabilitation of Steel Bridge Girders Using Advanced Composite Materials* NCHRP-IDEA Project 51, 25 pp.

Miller, T.C., Chajes, M.J., Mertz, D.R. and Hastings, J.N. (2002) Strengthening of a Steel Bridge Girder Using CFRP Plates. *ASCE Journal of Bridge Engineering* **6**(6) 514-522.

Nakayama, M. and Beaudoin, J.J. (1987) Bond strength development between latex-modified cement paste and steel, *Cement and Concrete Research*, **17**(4), 562-572.

Nayal, R. and Rasheed, H.A. (2006) Tension Stiffening Model for Concrete Beams Reinforced with Steel and FRP Bars. *ASCE Journal of Materials in Civil Engineering*, **18**(6), 831-841.

Nguyen-tri, P. and Nguyen, T.A. (2020) Chapter 1: Smart nanoconcretes: an introduction, in *Smart Nanoconcretes and Cement-Based Materials*, Elsevier.

Nishino T, and Furukawa T. (2004) Strength and deformation capacities of circular hollow section steel member reinforced with carbon fiber. *Proceedings of the Seventh Pacific Structural Steel Conference*. American Institute of Steel Construction, March 2004.

Nozaka, K., Shield, C. K., Hajjar, J. F. (2005) Effective Bond Length of Carbon-Fiber-Reinforced Polymer Strips Bonded to Fatigued Steel Bridge I-Girders. *ASCE Journal of Composites for Construction* **9**(4) 304-312.

O'Neill, A., Harries, K.A. and Minnaugh, P. (2007) Fatigue Behavior of Adhesive Systems used for Externally-bonded FRP Applications, *Proceedings of the 3rd International Conference on Durability and Sustainability of FRP Composites for Construction*. Quebec City.

Okeil, A., Bingol, Y., and Ferdous, M. (2009) Novel Technique for Inhibiting Buckling of Thin-Walled Steel Structures Using Pultruded Glass FRP Sections. *ASCE Journal of Composites for Construction*, **13**(6), 547–557.

Owens, D.K. (1970) Some thermodynamic aspects of polymer adhesion. *Journal of applied polymer science*, **14**, 1725-1730.

Patnaik, A.K. and Bauer, C.L. (2004) Strengthening of Steel Beams with Carbon FRP Laminates. *Proceedings of the 4th Advanced Composites for Bridges and Structures Conference*, Calgary.

Pavlovic, M., Markovic, Z., Veljkovic, M, and Budevac, D. (2013) Bolted shear connectors vs. headed studs behaviour in push-out tests, *Journal of Constructional Steel Research*, **88**, 134-149.

PennDOT (2010) *Bridge Maintenance Manual*, PennDOT Publication No. 55.

PennDOT (2019) *Design Manual Part 4*, PennDOT Publication 15M.

PennDOT (2020) *personal correspondence with research team*

Photiou, N. K., Hollaway, L. C., Chryssanthopoulos, M. K. (2006) Strengthening of an Artificially Degraded Steel Beam Utilizing a Carbon/Glass Composite System. construction and Building Materials. **20** 11-21.

Provines, J.T., Ocel, J.M. and Zmerta, K. (2019) *Strength and Fatigue Resistance of Clustered Shear Stud Connectors in Composite Steel Girders*, FHWA-HRT-20-005.

Ringelstetter, T.E., Bank, L.C., Oliva, M.G., Russell, J.S., Matta, F. and Nanni, A. (2006) Cost-Effective, Structural Stay-in-Place Formwork System of Fiber-Reinforced Polymer for Accelerated and Durable Bridge Deck Construction, *Transportation Research Record: Journal of the Transportation Research Board* **1976**, 182-189.

Rupasinghe, M., Nicolas, R.S., Mendis, P., Sofi, M., and Ngo, T. (2017) Investigation of strength and hydration characteristics in nano-silica incorporated cement paste. *Cement and Concrete Composites* **80**, 17-30.

Russell, H.G. and Graybeal, B.A. (2013) *Ultra-High Performance Concrete: A State-of-the-Art Report for the Bridge Community*, FHWA-HRT-13-060.

Schnerch, D., Dawood, M., Rizkalla, S., and Sumner, E. (2007) Proposed design guidelines for strengthening of steel bridges with FRP materials. *Construction and Building Ma*terials, **21**(5), 1001-1010.

Schnerch, D., Stanford, K., Sumner, E., and Rizkalla, S. (2004) Strengthening Steel Structures and Bridges with High Modulus Carbon Fiber Reinforced Polymers: Resin Selection and Scaled Monopole Behavior, *Proceedings of the 83rd Transportation Research Board Meeting*, Washington D.C.

Schnerch, D.A. (2005) Strengthening of Steel Structures with High Modulus Carbon Fiber Reinforced Polymer (CFRP) Materials. *PhD Dissertation*, North Carolina State University.

Sen, R. Liby, L. and Mullins, G. (2001) Strengthening Steel Bridge Sections Using CFRP Laminates, *Composite: Part B*, **32** 309-322.

Shaat, A. and Fam, A. (2006) Axial Loading Test on Short and Long Hollow Structural Steel Columns Retrofitted Using Carbon Fibre Reinforced Polymers. *Canadian Journal of Civil Engineering*, **33**(4), 458-470.

Sika (2020) *SikaDur 32 Product Data Sheet*, https://usa.sika.com/en/construction/repair-protection/multi-purpose-epoxies/adhesives/sikadur-32-hi-mod.html, accessed 11.17.21.

Sizemore, J., Aidoo, J., Harries, K.A. and Monnell, J. (2011) Use of Silane Adhesion Promoter to Enhance FRP-to-Steel Bond Performance, *Proceedings of the 4th International Conference on Durability and Sustainability of FRP Composites for Construction*. Quebec City.

Sloan, F.E., and Talbot, J.B. (1992) Corrosion of graphite-fiber reinforced composites I – Galvanic coupling damage. *Corrosion Engineering*, **48**(10), 830-839.

Society for Protective Coatings (SSPC) (2006) *NACE No. 1/SSPC-SP 5-2006 White Metal Blast Cleaning*, SSPC, Pittsburgh, PA, 5 pp.

Society for Protective Coatings (SSPC) (2018) *NACE No. 1/SSPC-SP 2-2018 Hand Tool Cleaning*, SSPC, Pittsburgh, PA, 3 pp.

Society for Protective Coatings (SSPC) (2018) *NACE No. 1/SSPC-SP 3-2018 Power Tool Cleaning*, SSPC, Pittsburgh, PA, 5 pp.

Sprinkel, M. (2003) High Performance Concrete Overlays for Bridges, *Proceedings of the Prestressed Institute Convention/National Bridge Conference/Federal Highways Administration Symposium on High Performance Concrete*, Orlando FL, October 2003.

Sprinkel, M. (2009) *A Short History of Latex Modified Concrete for Bridge Repairs*, American Concrete Institute. Section du Québec et de l'est de l'Ontario. Progress in concrete seminar, December 2009, Montreal.

Stratford, T., and Cadei, J. (2006) Elastic analysis of adhesion stresses for the design of a strengthening plate bonded to a beam. *Construction and Building Materials*, **20**, 34-45.

Stratford, T.J. and Chen, J.F. (2005) Designing for Tapers and Defects in FRP-Strengthened Metallic Structures, *Proceedings of the International Symposium on Bond Behaviour of FRP in Structures*, Hong Kong.

Stratton, J., Smith, K. and Lloyd, J.B. (2021) Lasting Longer, *Modern Steel Construction*, March 2021, 16-18.

Tavakkolizadeh, M. and Saadatmanesh, H. (2001) Galvanic Corrosion of Carbon and Steel in Aggressive Environments. *ASCE Journal of Composites for Construction*, **5**(3) 200-210.

Tavakkolizadeh, M. and Saadatmanesh, H. (2003a) Strengthening of Steel-Concrete Composite Girders using Carbon Fiber Reinforced Polymers Sheets, *ASCE Journal of Structural Engineering* **129**(1) 30-40.

Tavakkolizadeh, M. and Saadatmanesh, H. (2003b) Fatigue Strength of Steel Girders Strengthened with Carbon Fiber Reinforced Polymer Patch. *ASCE Journal of Structural Engineering* **129**(1) 186-196.

Taylor A.C. (2011) Adhesives with Nanoparticles. In *Handbook of Adhesion Technology* (da Silva L.F.M., Öchsner A. and Adams R.D. (editors)). Springer.

Teng J.G. and Hu Y.M. (2007) Behaviour of FRP-jacketed circular steel tubes and cylindrical shells under axial compression. *Construction and Building Materials* **21**(4), 827–38.

Teng, J.G., Yu, T. and Fernando, D. (2012) Strengthening of steel structures with fiber-reinforced polymer composites, *Journal of Constructional Steel Research*, **78**, 131-143.

Teng, L.G., Chen, J.F., Smith, S.T. and Lam, L. (2002) *FRP-strengthened RC Structures*. Wiley.

Tension Control Bolts (2022) TCB Shear Stud Data Sheet, https://www.tcbolts.com/en/products/tcb-shear-stud, accessed 02.10.22

TxDOT (2021) Ultra-High Performance Concrete for Bridge Preservation and Repair, *EDC News, April 8, 2021*.

Tzortzinis, G., Knickle, B.T., Gerasimidis, S., Bardow, A. and Brena, S.F. (2019) Experiments and computations on steel bridge corroded beam ends, *Proceedings of the Annual Stability Conference Structural Stability Research Council*, St. Louis, Missouri, April 2019.

Wakabayashi, D., Miyashita, T., Okuyama, Y., Kobayashi, A., Hidekuma, Y., Horimoto, W., Koide, N. and Nagai, M. (2013) Repair method using CFRP for corroded steel girder ends, *Proceedings of Fourth Asia-Pacific Conference on FRP in Structures (APFIS 2013)*, Melbourne, December 2013.

Walker, P. (1991) Organosilanes as adhesion promoters. *Journal of Adhesion Science and Technology*, **5**(4), 279-305.

West, T.D. (2001) Enhancement to the bond between advanced composite materials and steel for bridge rehabilitation. *Master's Thesis*, University of Delaware.

Xia, S.H. and Teng, J.G. (2005) Behaviour of FRP-to-Steel Bonded Joints, *Proceedings of the International Symposium on Bond Behaviour of FRP in Structures*, Hong Kong.

Xie, Q. (2004) State of the art of buckling-restrained braces in Asia, *Journal of Constructional Steel Research*, **61**, 727-748.

Yamaguchi, E., Akagi, T. and Tsuji, H. (2014) Influence of corrosion on load-carrying capacities of steel I-section main-girder end and steel end cross-girder, *International Journal of Steel Structures*, **14**, 831–841.

Yang, J., Teng, J.G. and Chen, J.F. (2004) Interfacial stresses in soffit-plated reinforced concrete beams, *ICE: Structures and buildings*, **157**(1), 77-89.

Yu, R., Spiesz, P. and Brouwers, H.J.H. (2014) Effect of nano-silica on the hydration and micro-structure development of Ultra-High Performance Concrete (UHPC) with a low binder amount, *Construction and Building Materials* **65**, 140-150.

Zhao X-L, Fernando D. and Al-Mahaidi R. (2006) CFRP strengthened RHS subjected to transverse end bearing force. *Engineering Structures*, **28**(11),1555–65.

Zmerta, K.M. (2015) Repair of Corrosion Damaged Steel Bridge Girder Ends by Encasement in Ultra-High Strength Concrete, *PhD Dissertation*, University of Connecticut, 349 pp.

Zmerta, K.M., McMullen, K.F., Zaghi, A.E. and Wille, K. (2017) Experimental Study of UHPC Repair for Corrosion-Damaged Steel Girder Ends, *ASCE Journal of Bridge Engineering*, **22**(8), 04017037.

6.1 Uncited References

Stevens, M.T., Gleeson, B., Mash, J. and Li, B. (2019) Steel Bridge Corrosion Prevention and Mitigation Strategies: Literature Review, Report *IRISE-19-P19-01-01*, University of Pittsburgh.

van de Lindt, J.W. and Ahlborn, T.M. (2005) Development of Steel Beam End Deterioration Guidelines, *Research Report RC-1454*, Michigan Technological University

Wipf, T.J., Fabous, F.S., Klaiber, F.W. and Eapen, A.S. (2003) Evaluation of Appropriate Maintenance, Repair and Rehabilitation Methods for Iowa Bridges, *Iowa DOT Report TR-429*.

Appendix A – Review of Bridge Inspection Reports

All data is obtained from bridge inspection records provided to research team. Where research team has had to interpret data or images provided do not appear to match data, research team has made appropriate inferences. These are noted in *blue italic font*.

Damage patterns reported are based on those shown in Table 1. All dimensions are reported in inches. In cases where bearing is embedded in concrete diaphragm, dimensions are based on face of diaphragm rather than end of beam.

Inspection Report Summary **Bridge A**

BMS: 09 4027 0190 0000

District: 6

Inspection date: 3/17/20

Condition: 3 (Superstructure)

Posting: 15 ton

Span: 23 ft simple non-composite

Width: 32 ft

Beams: 9 – *W18x60 @ 4 ft* AISC data base: *historic B18 ref 2 or 5*

d =	17 + t_f	b =	7.56	t_f =	0.56	t_w =	0.44

Bearing: unknown; beam encased in end diaphragm

Beam end conditions: [all patterns are outside embedded end diaphragm]

Beam end have timber flange shim installed as seen in all images

Near end	Beam	Far end
no report damage	1	no reported damage
no report damage	2	**E-W1**: C_L = 4; C_H = 1.75; $t_{w\ min}$ = 0.375 (85%)
E-M3: b = 5; **E-M4**: b = 10; and associated web thinning adjacent holes 50% loss of flange over 5 in.	3	***E-M4**: b = 12; a = 3.5* **E-W3**: C_{L3} = 17; C_{L1} = 2; C_{H1} = 3.5; C_{H2} = H_o; $t_{w\ min}$ = 0.125 (28%) >50% loss of flange over 17 in. 
***E-M4**: b = 1; a = 1* **E-W3**: C_{L3} = 24; C_{L1} = 5; C_{H1} = 2; C_{H2} = H_o; $t_{w\ min}$ = 0.125 (28%) >50% loss of flange over 17 in. 	4	***E-M4**: b = 3; a = 1.5* **E-W3**: C_{L3} = 17; C_{L1} = 2; C_{H1} = 3.5; C_{H2} = H_o; $t_{w\ min}$ = 0.125 (28%) (away from M4) 100% loss of flange over 4 in. 

Near end	Beam	Far end
E-W1: C_{L1} = 12; C_H = 1; t_w = 0.125 (28%)	5	***E-M4**: b = 2; a = 2* **E-W3**: C_{L3} = 12; C_{L1} = 2; C_{H1} = 2; C_{H2} = H_o; $t_{w\ min}$ = 0.19 (43%) (away from M4) 100% loss of flange over 4 in. 
E-W3: C_{L3} = 5; C_{L1} = 2; C_{H1} = 3; C_{H2} = H_o $t_{w\ min}$ = 0.06 (14%) 12% loss of flange over 6 in.	6	**E-W3**: C_{L3} = 12; C_{L1} = 1; C_{H1} = 2; C_{H2} = H_o; $t_{w\ min}$ = 0.125 (28%) 85% loss of flange over 4.5 in. 
E-W3: C_{L3} = 8; C_{L1} = 3; C_{H1} = 3; C_{H2} = H_o $t_{w\ min}$ = 0.25 (57%) 100% loss of flange over 6 in.	7	***E-M4**: b = 12; a = 2* **E-W3**: C_{L3} = 20; C_{L1} = 1.5; C_{H1} = 3; C_{H2} = H_o; $t_{w\ min}$ = 0.125 (28%) (away from M4) 85% loss of flange over 4.5 in. 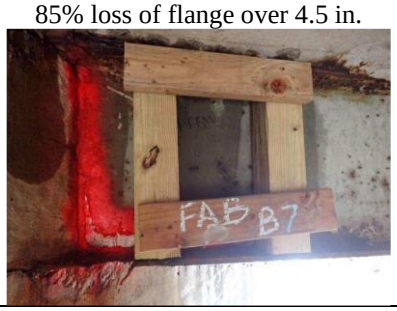
***E-M4**: b = 12; a = 1* **E-W1**: C_{L1} = 23; C_H = 3; t_w = 0.25 (57%) 85% loss of flange over 7 in. 	8	***E-M4**: 19 = 12; a = 3* **E-W3**: C_{L3} = 26; C_{L1} = 6; C_{H1} = 3; C_{H2} = H_o; $t_{w\ min}$ = 0.125 (28%) (away from M4) 75% loss of flange over 10 in. 

Near end	Beam	Far end
***E-M4**: 1 = 12; a = 2* **E-W3**: C_{L3} = 6; C_{L1} = 3; C_{H1} = 2; C_{H2} = 12; $t_{w\ min}$ = 0.19 (43%) (away from M4) 100% loss of flange over 3.5 in.  	9	no reported damage

Inspection Report Summary **Bridge B**

BMS: 25 0020 0520 2114

District: 1

Inspection date: 9.4.19

Condition: 3 (Superstructure)

Posting: none

Span: four span: simple-continuous-continuous-simple; all noncomposite

Width: 40 ft

Beams: rolled sections not reported

Bearing: steel plate bearings

Beam end conditions:

Pier 3 Span 4 Beam 1	**M1**: b = 17; a = 1.5 cut(?) through entire exterior bottom flange lateral distortion of web	  
Pier 3 Span 4 Beam 2	**M1**: b = 4; a = 0.5; inboard of bearing CL **M1**: b = 3; a = 3; end of beam	
Pier 3 Span 4 Beam 3	**M1**: b = 3.5; a = 2.5 span 3 girder end seen on left	
Pier 3 Span 3 Beam 1	**W1**: $C_L \approx B_L$; $C_H \approx B_L/2$	

Inspection Report Summary **Bridge C**

BMS: 17 2021 0010 3023

District: 2

Inspection date: 1.25.18 (Problem area inspection)

Condition: 4 (Superstructure)

Posting: none

Span: *12 ft* simple non-composite

Width: 17 ft

Beams: 5 – S12x31.8 @ *4.25 ft* ; top 2.5 in. embedded in concrete deck

Bearing: steel plate bearings

Beam end conditions:

Considerable pack rust and debris at all bearings

Near end	Beam	Far end
no measurable section loss 	2	**W5**: $C_L \approx 2B_L$; $C_H \approx 8$; $t_w = 0.32$ (83%) 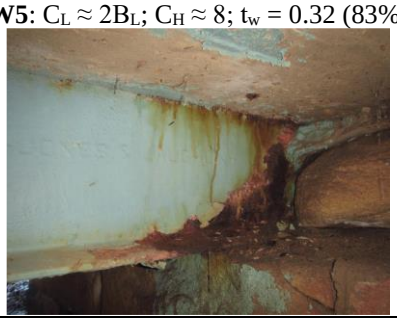
no measurable section loss 	3	no measurable section loss 
W2: $C_{L1} \approx C_{L2} \approx B_L$; $C_H \approx 3.5$; $t_w = 0.32$ (83%) 100% loss of bottom flange at end of beam 	4	**W3**: $C_{L1} \approx B_L$; $C_{L2} \approx B_L/2$; $C_{H1} \approx 3.5$; $C_{H2} = 9$; $t_w = 0.32$ (83%) >50% loss of bottom flange at end of beam 
steel angle bolted to bottom flange steel plate bolted to web (no photo available) exterior of fascia beams embedded in concrete (girder five shown at right)	1 & 5 both ends	

Inspection Report Summary **Bridge D**

BMS: 02 3039 0030 0682

District: 11

Inspection date: 6.10.19 (Interim)

Condition: 4 (Superstructure)

Posting: none

Span: four span: spans 1-3 are continuous, span 4 is simple; all composite

Width: 44 ft

Beams: plate girders

Bearing: steel sliding plates at both abutments, rocker bearings at pier 2, bronze sliding plates at pier 3

Beam end conditions:

Span 1 Girder 1 Near Abutment	**M1**: b = 5; a = 2; bearing stiffener **W1**: $C_L \approx 24$; $C_H \approx 6$		
Span 1 Girder 2 Near Abutment	**M3**: b ≈ 2; a ≈ 12; behind CL bearing **W1**:$C_L \approx 12$; $C_H \approx 56$		
Span 1 Girder 6 Near Abutment	**M1**: b = 3; a = 3 **W4**: $C_{L1} \approx 20$; $C_{L2} \approx 40$; $C_{L3} \approx 12$; $C_{H1} \approx 6$; $C_{H2} \approx 56$;		
Pier 3 Span 3/4 Girder 6	**Span 3** **M1**: b = 6; a = 4 (web) **M1**: b = 6; a = 6; (bearing stiffener) **W4**: $C_{L1} \approx 24$; $C_{L2} \approx 36$; $C_{L3} \approx 6$; $C_{H1} \approx 12$; $C_{H2} \approx 56$		**Span 4** **M1**: b = 6; a = 4 **W1**: $C_L \approx 24$; $C_H \approx 56$
Pier 3 Span 3 Girder 1	**M1**: b = 5; a = 5 bearing stiffener		

Inspection Report Summary **Bridge E**

BMS: 02 1015 0080 0375

District: 11

Inspection date: 1.27.20 (Interim)

Condition: 4 (Superstructure)

Posting: none

Span: single span; non-composite

Width: 27.5 ft

Beams: rolled sections not reported

Bearing: rocker bearings (fixed) at near abutment, rocker bearings (expansion) at far abutment

Beam end conditions:

Near end	Beam	Far end
no report damage	1	no reported damage
no report damage	2	no reported damage
W1: $C_L = 84$; $C_H = 4$ $t_{w\ min} = 0.518$ (83%) $t_{bf\ min} = 0.625$ (70%) 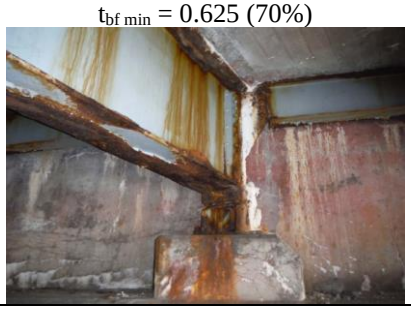	3	no reported damage
W1: $C_L \approx 36$; $C_H \approx 12$ no section loss noted 	4	no reported damage
W1: $C_L \approx 144$; $C_H \approx 24$ $t_{w\ min} = 0.505$ (81%) $t_{bf\ min} = 0.279$ (31%) 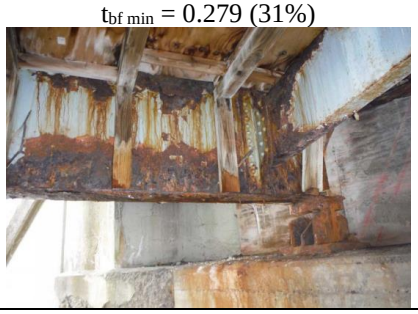	5	**W1**: $C_L = 48$; $C_H = 35.5$ $t_{w\ min} = 0.378$ (60%) $t_{bf\ min} = 0.250$ (28%)

Inspection Report Summary **Bridge F**

BMS: 26 1052 0010 0267

District: 12

Inspection date: 2.20.19 (Routine)

Condition: 4 (Superstructure)

Posting: none

Span: single span; non-composite

Width: 24.0 ft

Beams: 12 - W14x38

Bearing: unknown; beam encased in end diaphragm

Beam end conditions:

Near end	Beam	Far end
E-W1: C_L = 6; C_H = 12 $t_{w\ min}$ = 0.195 (63%)  	1	**M1**: b = 4; a = 6 **E-W5**: C_L = 20; C_H = 14 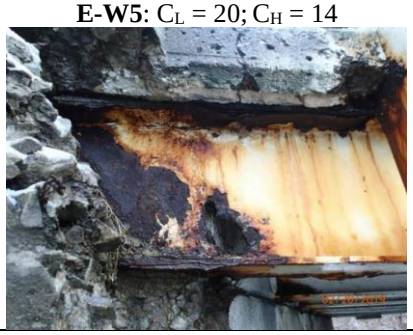
no report damage	6	2” of 100% loss along the right bottom flange 

Inspection Report Summary **Bridge G**

BMS: 48 4007 0020 2524

District: 5

Inspection date: 3.26.20 (Routine)

Condition: 2 (Superstructure)

Posting: closed

Span: single span; non-composite

Width: 19.7 ft

Beams: rolled sections not reported

Bearing: unknown; beam encased in end diaphragm

Beam end conditions:

Girders in this bridge has slots (long slotted holes from previous use?) in all webs at supports

Near end	Beam	Far end
E-W1: C_L = 4.5; C_H = 14 beam reported to be 'twisted' 	1	**E-W1**: C_L = 3; C_H = 14
E-W1: C_L = 5; C_H = 14	2	**E-W1**: C_L = 1; C_H = 9 significant flange loss (reduced to 7.5 in. wide)  
E-W1: C_L = 3.5; C_H = 14 	3	**E-W1**: C_L = 3.5; C_H = 14
E-W1: C_L = 3.5; C_H = 14 	4	**E-W1**: C_L = 3.5; C_H = 14

E-W1: C_L = 5; C_H = 14	5	**E-W1**: C_L = 3.5; C_H = 14
E-W1: C_L = 5; C_H = 14	6	**E-W1**: C_L = 3.5; C_H = 14 
E-W1: C_L = unknown; C_H = 14 **M1**: b = unknown; a = unknown 	7	**E-W1**: C_L = 3.5; C_H = 14 section loss of bottom flange (reduced to 9 in.) 
E-W1: C_L = 4.5; C_H = 14	8	**E-W1**: C_L = 3.5; C_H = 14

Inspection Report Summary **Bridge H**

BMS: 48 4007 0030 0953

District: 5

Inspection date: 6.11.18 (Routine)

Condition: 5 (Superstructure)

Posting: closed (inspected and closed June 2020, inspection report unavailable to research team)

Span: single span; non-composite

Width: 19.5 ft

Beams: rolled sections not reported

Bearing: unknown; beam encased in end diaphragm

Beam end conditions:

Near end	Beam	Far end
M1: b = 6; a = 1.5 right side of bottom flange has 100% section loss; 8.5” remain of original 10.5”	3	1/8” web thickness remaining; dimensions and original section not reported 
9” of 100% section loss to bottom flange 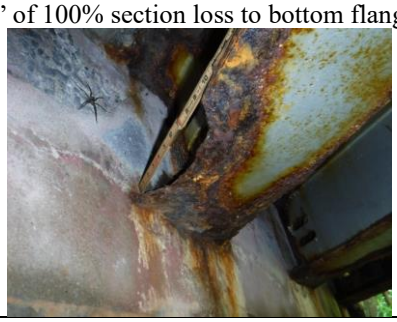	5	no reported damage

Inspection Report Summary **Bridge I**

BMS: 15 0896 0260 0000

District: 6

Inspection date: 4.11.18 and 4.22.20 (Routine)

Condition: 5 (Superstructure)

Posting: none

Span: two 32 foot spans, non-composite (steel grid deck)

Width: 16.7 ft

Beams: 7 – B18x47

Bearing: beams set directly on stone masonry at abutments, beams set directly on pier

This bridge has a steel grid deck – primary damage to girders is flange loss along span as can be seem below in images from 2020 report.

The beam ends at the far abutment are encased in steel forms and concrete placed from above (see before (2018) and after (2020) images below). The 2018 report identifies the significant damage at the near abutment (see below); but reports no specific damage at the far abutment. However, in 2020, the far abutment has been encased as shown. The encasement is associated with significant abutment and deck deterioration, rather than the beams themeslves.

2018 report	
2020 report	 

Beam end conditions:

Near Abutment Span 1 Girder 3	$t_{bf\ min}$ = 3/8” (86%) no section loss to web noted	
Near Abutment Span 1 Girder 4	**E-W1**: C_L = 6; C_H = 3 **E-M3**: a = 12; b = 2+ girders 4-7 shown at right	 

Near Abutment Span 1 Girder 5	**E-W1**: $C_L = 6$, $C_H = 3$ **E-M3**: a = 6; b = 1	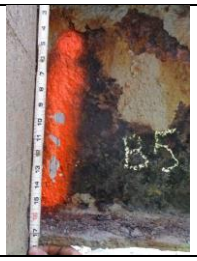
Pier 1 Span 1 Girders 2-5	$t_{bf\ min}$ = 1/4" (67%) no section loss to web noted	
Pier 1 Span 2 Girders 2-5	$t_{bf\ min}$ = 5/16" (71%) no section loss to web noted beam 4 shown at right	
Far Abutment Span 2 Girder 5	$t_{bf\ min}$ = 3/8" (86%) no section loss to web noted	

Inspection Report Summary **Bridge J**

BMS: 22 8003 0760 0760

District: 8

Inspection date: 4.29.19 and 10.31.19 (Problem Area)

Condition: 5 (Superstructure)

Posting: none

Span: 13 spans, composite

Width: 31.0 ft

Beams: 5 plate girders

Bearing: steel sliding plates

Beam end conditions:

Pier 4 Span 4 Girder 1	**M1**: b = 10; a = 1.625 (shown in photo) **M3**: b = 2; a = 1.375 (not shown in photo) **M3**: b = 1.5; a = 1.5 (not shown in photo) **W2**: C_{L1} = 12; C_{L2} = 12; C_H = 4 bottom flange distortion	 
Pier 4 Span 5 Girder 1	**W1**: C_L = 15; C_H = 2.5 $t_{w\ min}$ = 0.813” (81%)	
Pier 6 Span 6 Girder 1	**M3**: b = 5; a = 3 **M3**: b = 0.375; a = 0.375 **W1**: C_L = 10; C_H = full height minor section loss noted	
Pier 6 Span 7 Girder 1	**M3**: b = 1.5; a = 1.5 **W1**: C_L = 6; C_H = full height	
Pier 9 Span 9 Girder 1	**W1**: C_L = 24; C_H = 5 $t_{w\ min}$ = 3/4” (75%) $t_{stiffener,min}$ = 1/4” (67%)	
Pier 9 Span 10 Girder 1	**W1**: C_L = 6; C_H = 4 minor section loss noted	
Pier 11 Span 11 Girder 1	**W1**: C_L = 9; C_H = full height $t_{w\ min}$ = 0.813” (81%) $t_{stiffener,min}$ = 0.189” (50%)	
Pier 13 Span 13 Girder 1	**W1**: C_L = 15; C_H = 2 $t_{w\ min}$ = 7/8” (88%)	

Pier 13 Span 14 Girder 1	**W1**: $C_L = 52; C_H = 5.5$ $t_{w\ min} = 0.813$” (81%)	
Pier 13 Span 13 Girder 2	**W1**: $C_L = 15; C_H = 2$ $t_{w\ min} = 7/8$” (88%)	
Pier 4 Span 4 Girder 3	**W1**: $C_L = 30; C_H = 4$ $t_{w\ min} = 0.813$” (81%) $t_{bf\ min} = 0.65$” (80%)	
Pier 6 Span 6 Girder 3	**W1**: $C_L = 6; C_H = 2$	
Pier 6 Span 6 Girder 5	**W1**: $C_L = 10; C_H = 3$	
Far Abutment Span 16 Girder 5	**W1**: $C_L = 6, C_H = 2$	

Inspection Report Summary **Bridge K**

BMS: 36 3006 0030 0000

District: 8

Inspection date: 4.22.20 (Routine)

Condition: 5 (Superstructure)

Posting: none

Span: 3 spans, non-composite

Width: 31.5 ft

Beams: 5 plate girders

Bearing: steel rocker bearings

Beam end conditions:

No photos of the defect areas are available because there was no access to the underside of the bridge during the inspection. Abutment regions appear to be newly painted (visible at right of both images). No other inspection reports provided to the research team.

Near Abutment	Beam	Far Abutment
M1: b = 7; a = 3.5 **M1**: b = 5; a = 4 no other details provided	1	beam end corrosion noted, no other details provided
beam end corrosion and section loss noted, no other details provided	2	**M1**: b = 9; a = 3 **M1**: b = 9; a = 4 no other details provided
M1: b = 5; a = 1.5 **M1**: b = 3.5; a = 1.5 **M1**: b = 9; a = 4 $t_{w\ min}$ = 0.113” (15%) $t_{bf\ min}$ = 0.528” (70%) no other details provided	3	**M1**: b = 10.5; a = 2 **M1**: b = 9; a = 7 no other details provided
$t_{w\ min}$ = 0.299” (40%) $t_{bf\ min}$ = 0.528” (70%) no other details provided	4	**M1**: b = 7; a = 2 no other details provided
beam end corrosion and section loss noted, no other details provided	5	beam end corrosion noted, no other details provided

Inspection Report Summary **Bridge L**

BMS: 66 0083 0024 1285

District: 8

Inspection date: 7.29.19 (Routine)

Condition: 5 (Superstructure)

Posting: none

Span: 3 spans, composite

Width: 84.0 ft

Beams: 14 rolled sections not reported, top flange is encased

Bearing: steel rocker bearings

Beam end conditions:

Near Abutment Span 1 Girder 1	**W2**: C_{L1} = 132; C_{L2} = 12; C_H = 9 $t_{w\ min}$ = 0.493” (72%) $t_{bf\ min}$ = 0.975” (89%)	
Near Abutment Span 1 Girder 8	**W1**: C_L = 84; C_H = 6 $t_{w\ min}$ = 0.375” (55%) $t_{bf\ min}$ = 0.538” (49%)	
Pier 1 Span 2 Girder 1	**W1**: C_L = 96; C_H = 5 $t_{w\ min}$ = 0.493” (72%)	
Pier 2 Span 2 Girder 14	**W1**: C_L = 120; C_H = 3 $t_{w\ min}$ = 0.493” (72%) $t_{bf\ min}$ = 0.913” (83%)	 
Far Abutment Span 3 Girder 1	**W1**: C_L = 36; C_H = 3	
Far Abutment Span 3 Girder 7	**W1**: C_L = 132; C_H = 3	
Far Abutment Span 3 Girder 14	**W3**: C_{L1} = 12; C_{L2} = 120; C_{L3} = 132; C_{H1} = 9; C_{H2} = 34; C_{H3} = 9 $t_{w\ min}$ = 0.493” (72%)	

Inspection Report Summary **Bridge M**

BMS: 66 0083 0094 0585

District: 8

Inspection date: 3.25.20 (Routine)

Condition: 5 (Superstructure)

Posting: none

Span: 3 spans, composite

Width: 82.6 ft

Beams: 14 – W24x76

Bearing: steel plates at abutments and steel rocker bearings on piers

Beam end conditions:

Near Abutment Span 1 Girder 14	**M3**: b = 4; a = 5 **M1**: b = 8; a = 5 **M1**: b = 0.5; a = 0.5 $t_{w\ min}$ = 0.13" (30%)	looking from girder 2 →  from outside →  

Inspection Report Summary **Bridge N**

BMS: 66 0083 0190 0630

District: 8

Inspection date: 9.12.19 (Routine)

Condition: 5 (Superstructure)

Posting: none

Span: 4 spans, composite

Width: 71.5 ft

Beams: 12 - 33 WF 130, partial length bottom flange cover plates

Bearing: steel sliding plates

Beam end conditions:

Near Abutment Span 1 Girder 6	**M3**: b = 6; a = 6 (bearing stiffener) **W5**: C_L = 78; C_H = 12 $t_{w\ min}$ = 0.28" (48%) $t_{bf\ min}$ = 7/16" (51%)	 
Near Abutment Span 1 Girder 7	beam end corrosion noted, no other details provided	
Pier 1 Span 1 Girders 6/7	beam end corrosion noted, no other details provided	
Pier 2 Span 2/3 Girder 6	**M1**: b = 4; a = 2 (bearing stiffener) **M1**: b = 2; a = 1.5 (web) **W1**: C_L = 48; C_H = 30	 
Far Abutment Span 4 Girder 6	**M1**: b = 5; a = 2 (bearing stiffener) **W5**: C_L = 60; C_H = 24	 
Far Abutment Span 4 Girder 7	beam end corrosion with minor section loss noted, no other details provided	

Inspection Report Summary **Bridge O**

BMS: 55 2013 0090 0000

District: 9

Inspection date: 2.4.19 (Routine)

Condition: 4 (Superstructure)

Posting: none

Span: 1 span, non-composite

Width: 22.0 ft

Beams: 10 - rolled sections not reported

Bearing: unknown; beam encased in end diaphragm

Beam end conditions:

Near Abutment	Beam	Far Abutment
$t_{w\ min}$ = 0.188” no other details provided	1	$t_{w\ min}$ = 0.197” no other details provided 
$t_{w\ min}$ = 0.322” no other details provided	2	$t_{w\ min}$ = 0.437” no other details provided
no report damage	3	no report damage
no other details provided 	4	$t_{w\ min}$ = 0.437” no other details provided 
$t_{w\ min}$ = 0.315” no other details provided	5	no other details provided 
$t_{w\ min}$ = 0.333” no other details provided	6	no other details provided 

$t_{w\ min}$ = 0.266” area of bottom flange with 100% section loss no other details provided 	7	no report damage
$t_{w\ min}$ = 0.322” no other details provided	8	no report damage
$t_{w\ min}$ = 0.330” area of bottom flange with 100% section loss no other details provided 	9	$t_{w\ min}$ = 0.322” no other details provided
$t_{w\ min}$ = 0.207” no other details provided	10	area of web with 100% section loss no other details provided 

Appendix B – Test Specimen Fabrication Drawings Transmitted to Fabricator

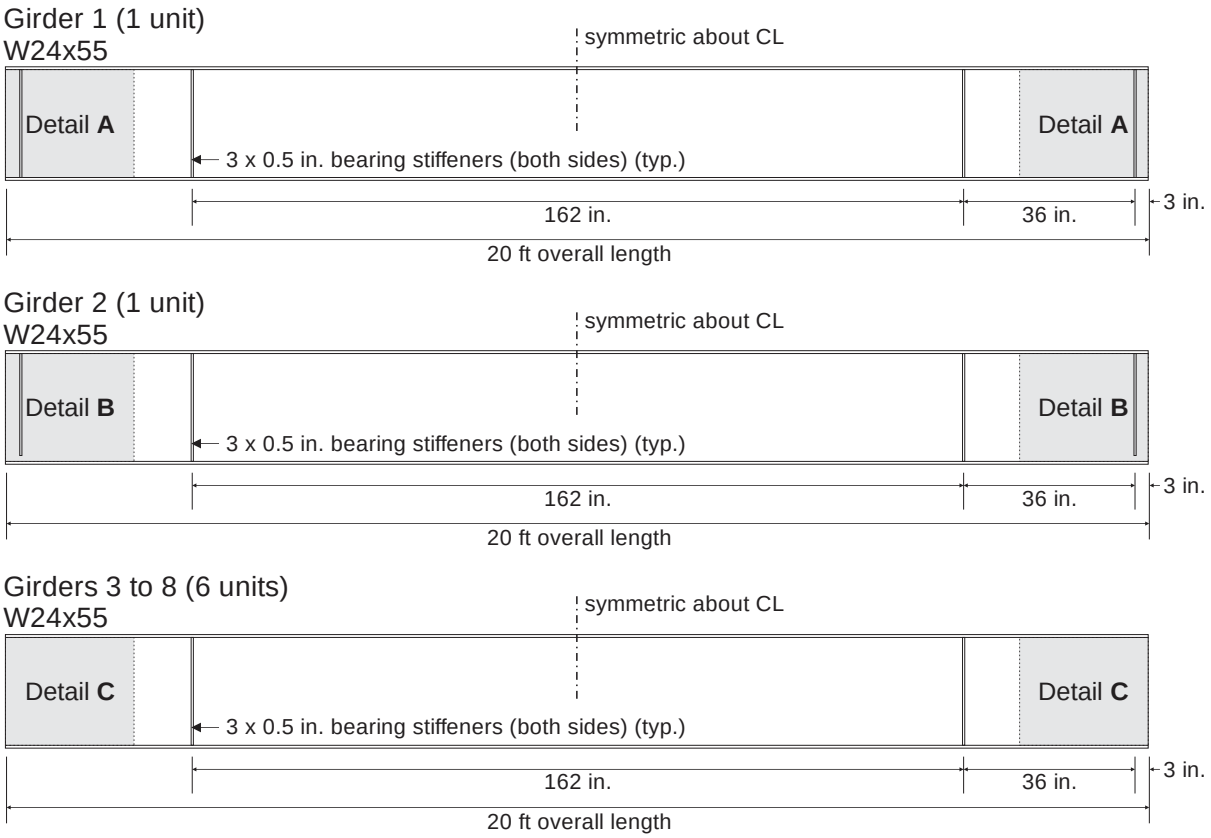

Figure C1

Figure 79 Specimen elevations.

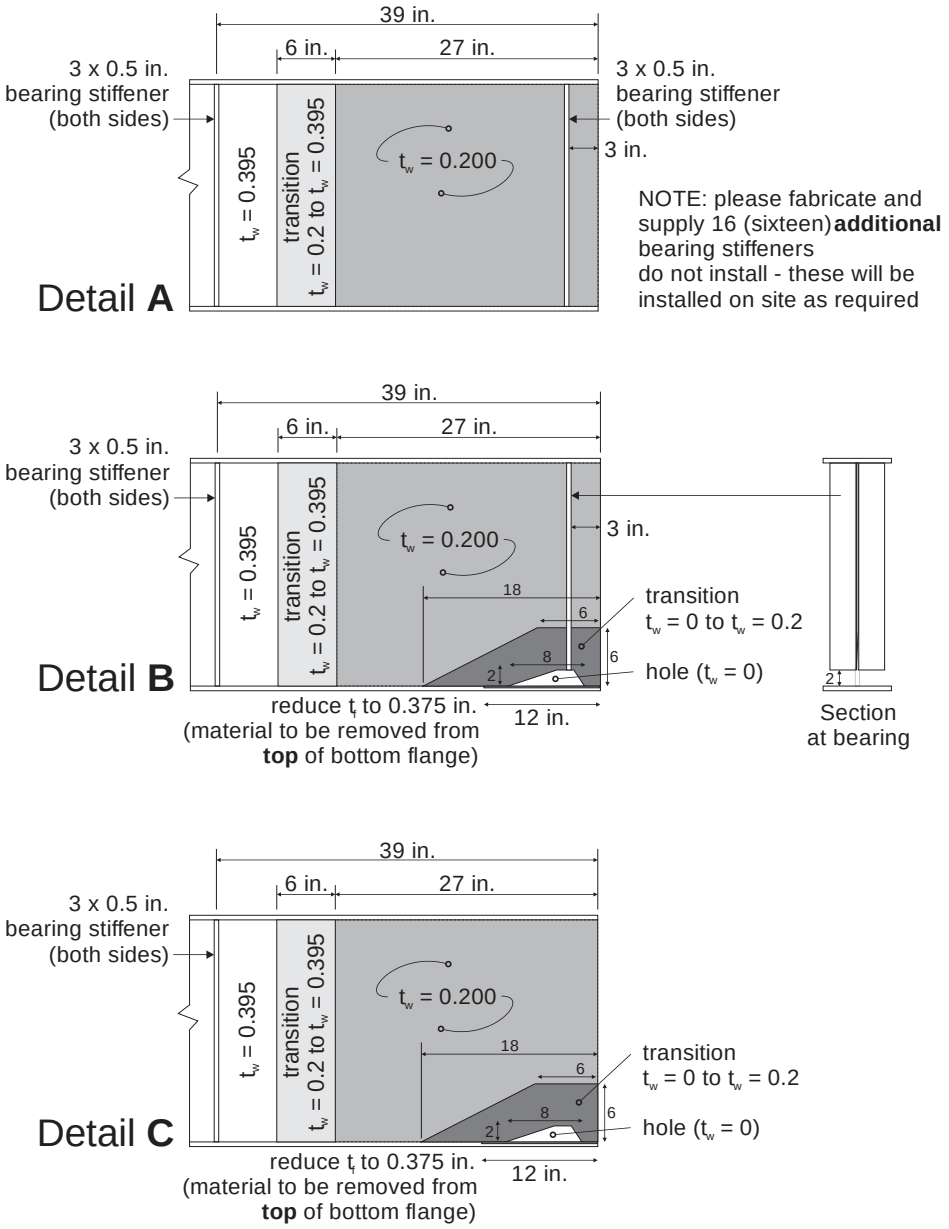

Figure C2

Figure 80 Specimen end region details.

Appendix C – Test Specimen Web Thickness Measurements

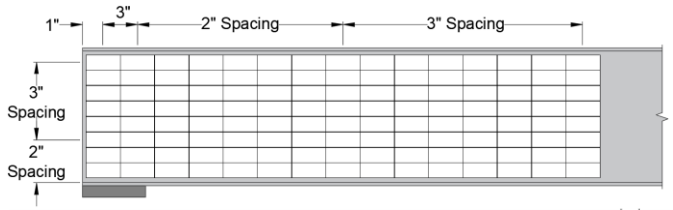

D-Meter Reading Locations
(typical; both girder ends)

0.34 0.31 0.35 0.29 0.32 0.32 0.29 0.25 0.25 0.34 0.33 0.39 0.39 0.39 0.34 0.31 0.31 0.34 0.32 0.37 0.30 0.35 0.31 0.33 0.34 0.35 0.39 0.39 0.40 0.40 0.34 0.36 0.33 0.32 0.32 0.34 0.33 0.33 0.33 0.34 0.36 0.39 0.39 0.39 0.40 0.33 0.37 0.30 0.30 0.33 0.34 0.34 0.33 0.32 0.34 0.34 0.39 0.40 0.39 0.40 0.32 0.34 0.36 0.36 0.36 0.36 0.33 0.35 0.32 0.36 0.34 0.39 0.39 0.40 0.34 0.33 0.34 0.31 0.31 0.33 0.32 0.34 0.31 0.34 0.35 0.34 0.38 0.39 0.40 0.39 0.28 0.28 0.31 0.34 0.32 0.20 0.24 0.33 0.34 0.36 0.36 0.40 0.39 0.39 0.32 0.32 0.22 0.32 0.32 0.35 0.34 0.34 0.35 0.34 0.33 0.31 0.39 0.38 0.39 0.39	0.40 0.39 0.38 0.38 0.35 0.36 0.35 0.32 0.32 0.35 0.33 0.35 0.38 0.31 0.30 0.40 0.40 0.39 0.38 0.30 0.31 0.33 0.32 0.29 0.27 0.29 0.36 0.34 0.34 0.32 0.40 0.40 0.39 0.39 0.34 0.37 0.36 0.36 0.33 0.33 0.35 0.33 0.30 0.37 0.34 0.40 0.40 0.39 0.39 0.36 0.35 0.37 0.34 0.35 0.37 0.37 0.34 0.34 0.30 0.34 0.41 0.40 0.40 0.38 0.35 0.31 0.37 0.36 0.36 0.32 0.33 0.32 0.33 0.34 0.35 0.40 0.40 0.39 0.39 0.34 0.35 0.36 0.33 0.31 0.31 0.32 0.34 0.34 0.33 0.33 0.40 0.40 0.39 0.38 0.32 0.35 0.34 0.35 0.36 0.36 0.37 0.36 0.36 0.35 0.35 0.40 0.40 0.38 0.37 0.32 0.34 0.37 0.37 0.36 0.34 0.35 0.37 0.37 0.35 0.34
Girder 1A	Girder 1B
0.31 0.30 0.33 0.35 0.35 0.32 0.32 0.31 0.30 0.31 0.30 0.32 0.34 0.38 0.33 0.31 0.32 0.34 0.32 0.40 0.32 0.34 0.34 0.34 0.34 0.31 0.31 0.32 0.39 0.39 0.34 0.36 0.34 0.35 0.35 0.35 0.34 0.31 0.35 0.36 0.33 0.34 0.32 0.40 0.40 0.31 0.31 0.33 0.34 0.35 0.35 0.34 0.33 0.32 0.33 0.32 0.33 0.29 0.39 0.40 0.26 0.31 0.34 0.34 0.34 0.32 0.34 0.30 0.34 0.32 0.34 0.33 0.26 0.40 0.40 0.33 0.35 0.36 0.36 0.34 0.34 0.33 0.31 0.36 0.35 0.33 0.33 0.29 0.38 0.39 0.31 0.22 0.34 0.31 0.33 0.36 0.30 0.32 0.33 0.35 0.35 0.35 0.29 0.37 0.40 0.27 0.17 0.24 0.26 0.28 0.30 0.32 0.31 0.32 0.34 0.35 0.33 0.27 0.35 0.39	0.33 0.38 0.37 0.31 0.36 0.33 0.36 0.35 0.31 0.32 0.30 0.29 0.29 0.30 0.31 0.39 0.39 0.37 0.32 0.32 0.35 0.33 0.33 0.33 0.33 0.34 0.35 0.33 0.32 0.39 0.40 0.39 0.28 0.34 0.34 0.34 0.33 0.29 0.31 0.30 0.30 0.31 0.31 0.30 0.40 0.40 0.38 0.32 0.34 0.35 0.34 0.30 0.34 0.32 0.29 0.28 0.27 0.31 0.26 0.40 0.40 0.37 0.32 0.34 0.33 0.33 0.35 0.34 0.34 0.32 0.32 0.31 0.33 0.31 0.40 0.39 0.37 0.32 0.33 0.33 0.29 0.34 0.32 0.32 0.32 0.35 0.29 0.29 0.28 0.39 0.39 0.38 0.32 0.31 0.32 0.29 0.31 0.32 0.29 0.30 0.32 0.29 0.28 0.31 0.39 0.39 0.38 0.39 0.31 0.30 0.31 0.30 0.27 0.29 0.29 0.27 0.19 0.16 0.30
Girder 2A	Girder 2B
0.34 0.36 0.35 0.32 0.33 0.37 0.32 0.34 0.28 0.33 0.33 0.42 0.38 0.38 0.39 0.33 0.29 0.32 0.29 0.27 0.26 0.26 0.28 0.29 0.30 0.30 0.36 0.37 0.39 0.40 0.32 0.32 0.32 0.32 0.35 0.35 0.33 0.30 0.26 0.26 0.29 0.36 0.39 0.40 0.41 0.31 0.33 0.33 0.32 0.28 0.28 0.29 0.31 0.27 0.30 0.29 0.36 0.40 0.42 0.41 0.30 0.32 0.33 0.32 0.27 0.27 0.31 0.31 0.26 0.30 0.30 0.33 0.40 0.40 0.40 0.34 0.33 0.35 0.36 0.27 0.30 0.29 0.32 0.25 0.28 0.30 0.32 0.39 0.39 0.40 0.30 0.37 0.29 0.31 0.28 0.29 0.30 0.32 0.31 0.27 0.28 0.35 0.39 0.39 0.39 0.35 0.31 0.27 0.26 0.34 0.31 0.28 0.32 0.29 0.25 0.29 0.25 0.39 0.35 0.39	0.40 0.38 0.38 0.38 0.31 0.36 0.30 0.39 0.28 0.26 0.28 0.27 0.27 0.29 0.25 0.39 0.39 0.38 0.38 0.29 0.27 0.25 0.33 0.34 0.33 0.32 0.34 0.33 0.34 0.24 0.39 0.39 0.39 0.39 0.28 0.25 0.26 0.29 0.30 0.31 0.31 0.32 0.31 0.32 0.39 0.39 0.39 0.39 0.38 0.30 0.30 0.27 0.33 0.30 0.31 0.31 0.33 0.29 0.29 0.28 0.40 0.39 0.39 0.39 0.28 0.31 0.26 0.24 0.30 0.33 0.31 0.30 0.37 0.31 0.35 0.39 0.39 0.39 0.38 0.29 0.29 0.27 0.33 0.31 0.30 0.28 0.34 0.31 0.32 0.30 0.39 0.39 0.38 0.38 0.28 0.23 0.25 0.29 0.30 0.30 0.27 0.32 0.32 0.33 0.31 0.39 0.39 0.38 0.38 0.24 0.21 0.21 0.31 0.30 0.30 0.28 0.31 0.29 0.31 0.31
Girder 3A	Girder 3B
0.33 0.38 0.34 0.33 0.30 0.34 0.32 0.38 0.35 0.35 0.35 0.38 0.36 0.39 0.40 0.33 0.35 0.35 0.33 0.33 0.30 0.30 0.31 0.32 0.32 0.30 0.24 0.34 0.35 0.40 0.33 0.35 0.31 0.34 0.31 0.31 0.26 0.30 0.31 0.33 0.31 0.32 0.35 0.36 0.39 0.35 0.41 0.36 0.35 0.34 0.29 0.31 0.30 0.33 0.30 0.32 0.34 0.35 0.35 0.39 0.34 0.33 0.31 0.32 0.29 0.31 0.33 0.34 0.33 0.32 0.32 0.32 0.33 0.35 0.39 0.29 0.33 0.34 0.31 0.30 0.32 0.31 0.29 0.31 0.32 0.28 0.33 0.35 0.32 0.39 0.28 0.29 0.33 0.32 0.29 0.33 0.31 0.33 0.34 0.30 0.27 0.32 0.33 0.34 0.39 0.24 0.23 0.32 0.26 0.33 0.30 0.30 0.28 0.30 0.30 0.32 0.32 0.32 0.42 0.38	0.38 0.39 0.39 0.40 0.37 0.33 0.32 0.35 0.33 0.34 0.31 0.35 0.29 0.31 0.26 0.39 0.39 0.34 0.34 0.29 0.26 0.31 0.31 0.36 0.36 0.30 0.28 0.28 0.31 0.36 0.39 0.39 0.38 0.35 0.27 0.27 0.27 0.27 0.32 0.29 0.28 0.28 0.29 0.29 0.29 0.40 0.41 0.38 0.28 0.20 0.28 0.28 0.28 0.28 0.35 0.25 0.28 0.27 0.22 0.29 0.39 0.39 0.38 0.23 0.23 0.21 0.23 0.23 0.24 0.24 0.23 0.30 0.20 0.22 0.17 0.39 0.39 0.38 0.19 0.23 0.23 0.26 0.26 0.26 0.24 0.25 0.25 0.26 0.28 0.23 0.38 0.39 0.39 0.22 0.24 0.24 0.22 0.22 0.26 0.40 0.25 0.27 0.27 0.26 0.26 0.43 0.40 0.39 0.24 0.22 0.28 0.21 0.21 0.23 0.37 0.14 0.14 0.12 0.13 0.16
Girder 4A	Girder 4B
0.32 0.26 0.28 0.30 0.29 0.31 0.25 0.18 0.26 0.29 0.24 0.38 0.38 0.38 0.39 0.35 0.28 0.28 0.24 0.24 0.36 0.28 0.25 0.22 0.30 0.28 0.39 0.39 0.39 0.41 0.31 0.34 0.32 0.29 0.29 0.30 0.31 0.22 0.26 0.29 0.27 0.39 0.39 0.40 0.40 0.31 0.32 0.33 0.27 0.30 0.29 0.25 0.26 0.26 0.29 0.30 0.39 0.38 0.40 0.40 0.21 0.29 0.25 0.26 0.27 0.29 0.32 0.26 0.28 0.32 0.30 0.39 0.39 0.40 0.40 0.29 0.29 0.31 0.29 0.26 0.23 0.27 0.28 0.28 0.26 0.24 0.40 0.39 0.40 0.40 0.30 0.30 0.29 0.30 0.26 0.27 0.27 0.28 0.30 0.28 0.28 0.39 0.39 0.39 0.39 0.26 0.29 0.28 0.26 0.22 0.34 0.34 0.31 0.28 0.28 0.28 0.39 0.39 0.39 0.35	0.39 0.38 0.41 0.40 0.29 0.30 0.27 0.32 0.32 0.32 0.33 0.34 0.30 0.32 0.24 0.40 0.39 0.38 0.39 0.25 0.30 0.30 0.24 0.25 0.27 0.25 0.32 0.30 0.30 0.29 0.39 0.39 0.39 0.39 0.31 0.30 0.30 0.26 0.30 0.30 0.28 0.26 0.27 0.34 0.23 0.39 0.39 0.39 0.38 0.27 0.26 0.27 0.33 0.29 0.27 0.30 0.27 0.26 0.26 0.28 0.40 0.40 0.39 0.37 0.28 0.29 0.26 0.29 0.33 0.32 0.30 0.29 0.29 0.27 0.25 0.40 0.40 0.39 0.37 0.31 0.31 0.29 0.33 0.30 0.28 0.26 0.26 0.24 0.24 0.24 0.39 0.39 0.38 0.41 0.38 0.30 0.31 0.27 0.24 0.29 0.29 0.32 0.25 0.28 0.29 0.40 0.39 0.39 0.38 0.35 0.29 0.27 0.25 0.22 0.27 0.23 0.29 0.35 0.38 0.27
Girder 5A	Girder 5B
--- 0.284 0.28 0.267 0.312 0.322 0.381 0.328 0.335 0.37 0.353 0.384 0.383 0.374 0.387 --- 0.298 0.332 0.321 0.309 0.338 0.335 0.286 0.294 0.288 0.303 0.377 0.378 0.384 0.392 --- 0.314 0.312 0.288 0.327 0.322 0.33 0.324 0.327 0.321 0.298 0.388 0.386 0.391 0.387 --- 0.345 0.324 0.343 0.33 0.302 0.257 0.276 0.298 0.324 0.277 0.387 0.389 0.394 0.39 --- 0.351 0.338 0.377 0.291 0.299 0.269 0.294 0.314 0.284 0.283 0.384 0.387 0.388 0.391 --- 0.276 0.34 0.338 0.298 0.294 0.34 0.227 0.214 0.244 0.261 0.373 0.381 0.383 0.387 --- 0.33 0.306 0.267 0.325 0.249 0.256 0.261 0.256 0.264 0.292 0.374 0.377 0.384 0.391 --- 0.225 0.285 0.249 0.261 0.284 0.237 0.234 0.251 0.256 0.276 0.376 0.396 0.392 0.39	0.41 0.38 0.38 0.38 0.38 0.29 0.33 --- --- --- --- --- --- --- 0.39 0.38 0.38 0.38 0.38 0.27 0.26 0.28 0.28 0.33 0.27 0.32 0.30 0.27 0.28 0.25 0.38 0.38 0.39 0.39 0.27 0.28 0.29 0.25 0.28 0.25 0.29 0.29 0.28 0.25 0.27 0.39 0.38 0.37 0.38 0.27 0.27 0.26 0.27 0.29 0.31 0.31 0.29 0.26 0.25 0.28 0.39 0.39 0.39 0.38 0.32 0.28 0.25 0.28 0.25 0.30 0.30 0.32 0.34 0.29 0.29 0.39 0.39 0.39 0.38 0.29 0.28 0.26 0.25 0.25 0.27 0.27 0.28 0.32 0.32 0.34 0.39 0.39 0.38 0.38 0.32 0.25 0.26 0.21 0.17 0.34 0.33 0.29 0.32 0.31 0.34 0.39 0.38 0.38 0.39 0.30 0.30 0.27 0.30 0.29 0.35 0.30 0.30 0.31 0.30 0.31
Girder 6A	Girder 6B
--- 0.30 0.29 0.32 0.28 0.29 0.27 0.27 0.29 0.29 0.28 0.29 0.38 0.41 0.39 --- 0.32 0.34 0.32 0.31 0.31 0.28 0.26 0.28 0.27 0.29 0.39 0.39 0.39 0.39 --- 0.30 0.25 0.30 0.26 0.23 0.26 0.29 0.33 0.31 0.33 0.40 0.39 0.40 0.40 --- 0.30 0.29 0.30 0.27 0.27 0.28 0.29 0.29 0.31 0.34 0.40 0.39 0.39 0.39 --- 0.28 0.29 0.27 0.24 0.23 0.29 0.31 0.30 0.31 0.31 0.40 0.39 0.40 0.39 --- 0.32 0.32 0.33 0.29 0.26 0.26 0.28 0.29 0.29 0.29 0.39 0.41 0.40 0.41 --- 0.28 0.27 0.32 0.31 0.26 0.26 0.29 0.23 0.28 0.30 0.39 0.32 0.39 0.39 --- 0.32 0.32 0.30 0.27 0.28 0.26 0.33 0.28 0.25 0.30 0.38 0.38 0.38 0.40	0.39 0.42 0.392 0.38 0.34 0.32 0.29 0.27 0.28 0.29 0.25 0.35 0.27 0.32 0.34 0.39 0.39 0.386 0.38 0.3 0.28 0.27 0.25 0.25 0.23 0.24 0.3 0.3 0.33 0.31 0.4 0.39 0.4 0.38 0.31 0.3 0.29 0.28 0.26 0.25 0.26 0.27 0.27 0.28 0.29 0.4 0.39 0.39 0.38 0.3 0.28 0.26 0.3 0.31 0.26 0.28 0.3 0.31 0.24 0.3 0.39 0.43 0.386 0.38 0.3 0.25 0.23 0.3 0.3 0.28 0.28 0.29 0.31 0.32 0.33 0.39 0.39 0.387 0.39 0.27 0.27 0.25 0.32 0.33 0.31 0.27 0.32 0.29 0.31 0.31 0.39 0.38 0.384 0.38 0.27 0.29 0.24 0.31 0.31 0.28 0.28 0.27 0.27 0.31 0.25 0.39 0.39 0.386 0.38 0.31 0.28 0.31 0.27 0.29 0.28 0.3 0.31 0.33 0.27 0.27
Girder 7A	Girder 7B
0.31 0.34 0.32 0.33 0.31 0.33 0.32 0.31 0.32 0.32 0.32 0.32 0.37 0.38 0.40 0.23 0.29 0.30 0.31 0.30 0.30 0.31 0.29 0.32 0.35 0.32 0.35 0.31 0.41 0.40 0.26 0.30 0.30 0.32 0.34 0.34 0.21 0.25 0.26 0.27 0.30 0.30 0.29 0.32 0.38 0.30 0.29 0.28 0.28 0.28 0.30 0.17 0.23 0.23 0.25 0.24 0.23 0.25 0.34 0.39 0.31 0.34 0.28 0.30 0.29 0.24 0.22 0.20 0.18 0.16 0.18 0.19 0.20 0.35 0.39 0.35 0.33 0.29 0.35 0.31 0.26 0.22 0.18 0.18 0.18 0.20 0.20 0.20 0.35 0.40 0.26 0.26 0.30 0.31 0.31 0.28 0.19 0.14 0.14 0.14 0.16 0.17 0.17 0.32 0.39 0.32 0.22 0.34 0.27 0.25 0.18 0.11 0.19 0.22 0.19 0.17 0.20 0.19 0.38 0.39	0.39 0.38 0.38 0.39 0.30 0.29 0.35 0.34 0.36 0.30 0.29 0.29 0.28 0.29 0.32 0.39 0.38 0.37 0.37 0.30 0.30 0.32 0.31 0.33 0.25 0.22 0.21 0.26 0.31 0.28 0.40 0.39 0.38 0.38 0.27 0.29 0.32 0.31 0.28 0.31 0.32 0.33 0.33 0.31 0.31 0.39 0.39 0.39 0.38 0.25 0.32 0.33 0.29 0.31 0.32 0.30 0.32 0.26 0.27 0.30 0.39 0.39 0.38 0.39 0.31 0.32 0.30 0.30 0.30 0.31 0.32 0.34 0.33 0.33 0.33 0.39 0.39 0.39 0.38 0.39 0.29 0.31 0.29 0.27 0.35 0.31 0.31 0.32 0.30 0.31 0.39 0.39 0.38 0.38 0.34 0.35 0.31 0.29 0.27 0.31 0.30 0.30 0.23 0.27 0.23 0.39 0.39 0.38 0.38 0.33 0.34 0.34 0.28 0.27 0.28 0.31 0.29 0.18 0.20 0.29
Girder 8A	Girder 8B

Appendix D – Proposed Revisions to PennDOT DM-4

Revisions based on DM4 December 2019 version (Strike-Off Letter Revisions through 12/11/2020)

DM4 was searched for the terms “beam ends” (14 instances) and “beam end” (11 instances). The only instances relevant to the present study occur in Part A §5.5.2.6. References to beam end repair/rehabilitation in Part A §5.5.4 and §5.6.1 require no revision. There are no references in Part B that require attention. The following notation is used:

black text – existing DM4 text unchanged
green text – existing DM4 text moved to new location with text otherwise unchanged
blue underlined text – proposed new text
~~red strikeout – deleted existing DM4 text~~

5.5.2.6 Deteriorated Beam Ends

(a) Deteriorated Concrete Beam Ends

Deteriorated concrete beam ends shall be cleaned, repaired for structural integrity and protected from future deterioration either by deck continuity, encasing in concrete (diaphragm), or providing leakproof joints, and applying a breathable coating.

(b) Deteriorated Steel Beam Ends

Deteriorated steel beam ends shall be cleaned, strengthened in accordance with 5.5.2.6.1 if needed, painted and protected from future deterioration by providing continuity or leakproof joints.

To determine cost effectiveness, compare the remaining fatigue life, load carrying capacity, steel repair costs, cleaning and painting costs and other associated costs for the existing bridge, to the longer life and relatively minimal maintenance costs associated with a new superstructure. In borderline cases, permit a Contractor's alternate for a new superstructure.

Where needed, spot and zone or total bridge painting shall be incorporated in the rehabilitation project to achieve the targeted life specified in PP5.5.4, unless a special painting contract is to follow very shortly after the rehabilitation project. Either the contract plans or special provisions must indicate whether or not the existing paint contains lead and other toxic materials such as cadmium, chromium, arsenic, etc., in order to alert the contractor. Paint coating coupons from different bridge members must be laboratory tested for lead content and other toxic materials such as cadmium, chromium, arsenic, etc. To determine cleaning and painting strategy, evaluate the thickness of the paint to be retained, adhesiveness and compatibility of the existing paint to the proposed paint system. For small span steel bridges with lead base paint, it may be cost effective to replace the superstructure.

5.5.2.6.1 Strengthening Deteriorated Steel Beam Ends

If damage to the beam end has progressed to the degree in which distortion of the girder has occurred, the distortion should be corrected prior to repair installation or as a result of repair installation.

Existing capacity of an un-distorted girder shall be assessed using appropriate design equations from Part B Section 6 using existing measured steel plate thicknesses. Effects of increased slenderness resulting from loss of plate thickness shall also be considered. Beam end bearing capacity is often found to have deteriorated to the point that it is negligible.

Typically, removal and replacement of existing bearing stiffeners is required for beam end strengthening. Capacity of the unstiffened web prior to removal of bearing stiffeners shall be verified and temporary support provided as required. Temporary support shall not impinge upon the repair installation.

(a) Bolted Steel Repairs

Conventional bolted steel repairs are preferable to other repair methods considered. Welded connection of replacement bearing stiffeners shall be permitted with consideration of appropriate web surface preparation and amplitude.

Bolted connections shall be slip-critical. Only bolts penetrating regions of relatively undamaged regions of existing steel shall be counted on to contribute to the connection capacity. Based on surface condition, a reduction in the surface condition factor, K_s, may be justified.

(1) Bearing Stiffeners

Complete replacement of damaged bearing stiffeners is often required and ultimately easier to affect.

Replacement bearing stiffeners shall be applied to both sides of the girder web.

Bolted replacement stiffeners shall be steel angles whose out-stand leg dimensions are at least those of the bearing stiffener being replaced or required based on requirements of A6.10.11.2.

Typically, such double angle bearing stiffeners will be arranged in the ‘short leg back-to-back’ (SLBB) arrangement, sandwiching the girder web and having a single of row of bolts securing both stiffeners.

The bolted connection of stiffener to the web shall be sufficient to transmit the design bearing force.
Bolts shall have a maximum spacing of 6 in. vertically.

If replacement bearing stiffeners are also used to realign distorted flanges or webs, the additional forces associated with jacking the stiffeners into place and potential residual stress in the stiffeners and their connection shall be accounted for.

(2) Web Patches

Most significant corrosion-induced damage occurs near the bottom of the section affecting both the web and bottom flange.

The total thickness of repair plates shall be at least the thickness of the existing uncorroded beam web; double sided repairs are permitted respecting plate thickness requirements of A6.7.3.

Repair plates shall be designed to restore deteriorated continuity between the beam web and flange; machine-bent or cold-bent plates are permitted.

Anchorage of the plate shall be designed to transmit the shear to be resisted by the plate.

Shear buckling of large repair plates shall be considered and may be addressed by providing through-bolts intermittently over the area of repair to engage a double-sided repair plate (if present) and the existing web.

(b) Concrete Encasement

Concrete encasement shall extend the full height of the web, be cast against each flange, and may replace the presence of a steel bearing stiffener.

Concrete encasement shall extend to the flange tips when used as a bearing stiffener.

(1) Ultra-High-Performance Concrete (UHPC) Encasement

UHPC requires specialized equipment for mixing and monitoring the batch sizes needed for beam end repairs. A potential advantage of UHPC is that it achieves a high strength quite rapidly, allowing traffic re-opening within as little as 12 hours of placement.

Formwork for UHPC needs to be watertight, nonabsorbent where in contact with UHPC and be designed to ensure it may be filled completely; that is, appropriate venting is required, and internal details should have no potential air traps.

UHPC shall conform to an approved, commercially-available (i.e. premixed) UHPC product and all storage, batching, mixing, and quality control requirements recommended by the manufacturer.

Shear connections in accordance with 5.5.2.6.1(c) sufficient to transfer the design shear between the steel web and UHPC shall be provided.

Shear connections in accordance with 5.5.2.6.1(c) are recommended along the flanges when UHPC encasement length along the girder exceeds the depth of the steel girder web.

(2) Reinforced Concrete (RC) Encasement

RC encasement is a viable means of repairing corrosion-damaged girder ends, especially in cases where large shear stresses are not anticipated. Shear capacity of the end panel shall be replaced by the RC element.

The concrete used shall be an approved AA mix. A higher strength concrete may be substituted at no additional cost to the Department.

RC encasement shall extend the entire length of the end panel of the girder.

The shear capacity of the RC element shall be determined as the sum of concrete (V_c) and internal reinforcing steel components (V_s) in accordance with A5.7.3.3-1).

Shear reinforcement shall conform to (i) or (ii):

(i) closed ties located on both sides of the web; the ties shall fit within the width of the steel cross section and have adequate cover.

Shear connections in accordance with 5.5.2.6.1(c) sufficient to transfer the design shear between the steel web and UHPC shall be provided.

(ii)Hairpin ties anchored through the web with a lap splice adequate to develop the tie.

(c) Shear Connections for Concrete Encasement Repairs

For repairs associated with structures having corrosion damage, the use of welded shear studs will often not be practical. To avoid burn-through and distortion, welded studs require a minimum substrate thickness exceeding 1/3 the stud diameter and a smooth, uncontaminated surface to which to weld.

The use of ASTM F3125 Grade A325 bolts shall be an acceptable alternative to welded shear studs.

The capacity of a high strength bolt-type shear stud shall be taken as:

$$Q_n = 0.5A_{sc}\sqrt{f_c'E_c} \leq 0.7A_{sc}F_u \qquad (5.5.2.6.1c)$$

Where A_{sc} is taken as the nominal area of the bolt and F_u is taken as 75 ksi.

Bolts shall be installed into holes that have the ***same nominal diameter*** as the bolt (i.e., no oversize).

Bolts shall be nutted on both sides of the web and installed with a pretension according to AASHTO LRFD Table 6.13.2.8-1.

Bolts shall be installed in a grid pattern with the bolt head (stud) protruding on alternating sides of the steel web.

d) Durability of Repairs

All repairs present an interface between the repair material and existing steel girder. This interface is a potential location for the initiation of crevice corrosion ('pack rust'). Design shall provide some relief to water, moisture and moisture-trapping debris accumulating at these new interfaces.

Paint all steel surfaces under and around the repair area. Sloped edges and drip notches on encasement repairs can also help to eliminate water ingress as the concrete-steel interface. Joints between the repair material and steel shall be caulked and maintained to prevent water ingress.

Repairs shall be inspected during routine bridge inspection and maintenance items identified should be addressed to ensure adequate repair life.

5.5.2.~~6~~7 Other Superstructure Elements and Fatigue

Establish material parameters based upon existing plans or previous testing. If data is not available, samples may be taken and tested to establish needed parameters. All construction details must be inspectable and maintainable.

(a) Redundancy

For non-redundant superstructure, ensure that all elements are structurally sound and will provide prescribed service life as specified in PP5.5.4. Where possible, an alternate load path should be provided if economically feasible. All pin-hanger connections shall be removed and replaced with continuity when replacing the deck as specified inPP5.5.2.4, item (a).

For redundant superstructures, the pin-hanger connections shall also be replaced when replacing the deck.

~~(b) Deteriorated Beam Ends and Painting~~

~~Deteriorated concrete beam ends shall be cleaned, repaired for structural integrity and protected from future deterioration either by deck continuity, encasing in concrete (diaphragm), or providing leakproof joints, and applying a breathable coating.~~

~~Deteriorated steel beam ends shall be cleaned, strengthened if needed, painted and protected from future deterioration by providing continuity or leakproof joints.~~

~~Where needed, spot and zone or total bridge painting shall be incorporated in the rehabilitation project to achieve the targeted life specified in PP5.5.4, unless a special painting contract is to follow very shortly after the rehabilitation project. Either the contract plans or special provisions must indicate whether or not the existing paint contains lead and other toxic materials such as cadmium, chromium, arsenic, etc., in order to alert the contractor. Paint coating coupons from different bridge members must be laboratory tested for lead content and other toxic materials such as cadmium, chromium, arsenic, etc. To determine cleaning and painting strategy, evaluate the thickness of the paint to be retained, adhesiveness and compatibility of the existing paint to the proposed paint system. For small span steel bridges with lead base paint, it may be cost effective to replace the superstructure.~~

~~To determine cost effectiveness, compare the remaining fatigue life, load carrying capacity, steel repair costs, cleaning and painting costs and other associated costs for the existing bridge, to the longer life and relatively minimal maintenance costs associated with a new superstructure. In borderline cases, permit a Contractor's alternate for a new superstructure.~~

(~~c~~b) Cable Bridges

For cable-stayed and suspension bridges, cable condition must be thoroughly evaluated to ensure the targeted service life. Cables in the anchoring zone and splash zone are the most vulnerable. Deteriorated cables shall be replaced or reconstructed.

etc…

[renumber all subsequent sections as required]

Proposed Additions to PennDOT Bulletin 15

Bulletin 15 Page 797 of 6/14/22 version

MISC Ultra High Performance Concrete (UHPC)
Per *Special Provision a10303 Ultra High Performance Concrete*

LaFarge Ductal® was used in the present study. This product is appropriate for use for steel beam end repairs. Its use typically requires oversight by LaFarge technicians and the use of special mixing equipment rented from LaFarge.

LaFarge Ductal® should be considered for addition to Bulletin 15 for steel beam end repairs.

There are other UHPC products on the market in addition to some "open source" mixes available. These should be evaluated for inclusion into PennDOT Bulletin 15 and Bulletin 42 as applicable; most should be adequate for girder end repairs.

Bulletin 15 Page 720 of 6/14/22 version

A new classification of product should be considered for inclusion in Bulletin 15: Bolted Shear Studs. These should be restricted to repair and rehabilitation applications until a study of their performance in new-built structures can be conducted.

Consider adding new designation [conveniently this section jumps from (e) to (j)]

1105.02(f) Bolted Stud Shear Connectors
For concrete encasement repairs only

ASTM F3125 Grade A325 bolts shall be permitted for this use. Grade A490 shall not be permitted.
See **1105.02(d) High Strength Bolt Assemblies**
Bolts - ASTM F3125, Grades A325

Bolt-on shear stud manufactured by TCB are marketed for this use and appear to meet European and UK specifications for high strength bolts. Review for inclusion into PennDOT Bulletin 15 is recommended. See: https://www.tcbolts.com/en/products/tcb-shear-stud. It is unclear whether this product is marketed in the US and whether it would be meet Buy America acceptance criteria for use on PennDOT projects.